A STUDY OF SOME FREE RADICALS BY ELECTRON SPIN RESONANCE

David Rorke

A Thesis Submitted for the Degree of PhD
at the
University of St Andrews

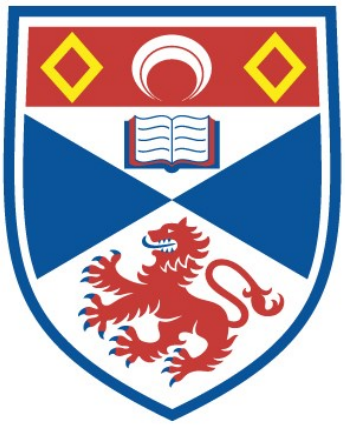

1965

A STUDY OF SOME FREE RADICALS BY ELECTRON SPIN RESONANCE

A Thesis

presented by

David Rorke, B.Sc.

to the

University of St. Andrews

in application for the Degree

of Doctor of Philosophy

ProQuest LLC.
789 East Eisenhower Parkway
P.O. Box 1346
Ann Arbor, MI 48106 – 1346

DECLARATION

I hereby declare that the following Thesis is based on the results of experiments carried out by me, that the Thesis is my own composition, and that it has not previously been presented for a Higher Degree.

CERTIFICATE

I certify that David Rorke, B.Sc., has spent nine terms as a research student in the Physical Laboratory of the United College of St. Salvator and St. Leonard in the University of St. Andrews, that he has fulfilled the conditions of Ordinance No. 16 of the University Court of St. Andrews and that he is qualified to submit the accompanying Thesis in application for the Degree of Doctor of Philosophy.

Research Supervisor.

CAREER

I matriculated in the United College of St. Salvator and St. Leonard in the University of St. Andrews in October 1957 and followed a course leading to graduation in June 1961 with the Degree of Bachelor of Science with Honours in Natural Philosophy. In October 1961 I was admitted by the Senatus Academicus of the same University as a research student in the Department of Natural Philosophy in the same College and have since then been engaged in the work which is the subject of this Thesis.

TABLE OF CONTENTS

LIST OF ILLUSTRATIONS

CHAPTER 1

INTRODUCTION

§ 1.1 Free Radicals

As a consequence of the Pauli Exclusion Principle, electrons in atomic and molecular orbitals, normally occur in pairs, with their spins antiparallel. There exists, however, a type of molecule which has the property of containing at least one unpaired valence electron. Molecules of this type are known as free radicals.

Many free radicals exist only as unstable and short lived intermediate products of a reaction. These may be examined either by trapping them, for example in a glass, or by observing them shortly after the beginning of the reaction by a method similar to the one described in § 3.18.

Some radicals, however, are stable and do not show this high reactivity. This stability arises from a resonance involving two or more mesomeric structures of the molecule and results in the unpaired electron occupying a delocalised molecular orbital.

As the molecules of free radicals contain unpaired electrons, they are paramagnetic and may be detected by E.S.R.

§ 1.2 Electron Spin Resonance (E.S.R.)

Since it was discovered in 1945 by Zavoisky [Z1], E.S.R. has become increasingly widely used for a variety of problems in Physics, Chemistry, Biology and Medicine. In the last few years, in particular,

since the advent of commercially available E.S.R. spectrometers, the number of workers in this field has risen considerably.

E.S.R. experiments on free radicals and other paramagnetic samples, normally concern the determination of the following quantities.

(a) The g-value or spectroscopic splitting factor which may be anisotropic as g is a tensor.

(b) Hyperfine splitting produced by the interaction of the unpaired electron with nuclear magnetic moments in the molecule. The hyperfine splitting parameters are also tensors.

(c) Line width resulting from one of the processes which will be discussed in § 2.3. Anisotropies in line width also are important and will be considered further in § 2.3 and § 4.10.

Hyperfine splittings and linewidths are normally expressed in gauss but it is conventional to refer to magnetic field rather than magnetic induction. This slight anomaly in terminology will be adhered to in this thesis also.

Free radicals are normally studied in polycrystalline form, as single crystals or in dilute solution.

§ 1.3 General and spin Hamiltonians for a Paramagnetic System

A paramagnetic crystal or a solution of paramagnetic molecules is a quantum mechanical system, and so it should be possible, in principle, to apply Schroedinger's equation to obtain the eigenvalues.

The ground state energy eigenvalue , E_o, is of particular interest and should be obtained from

$$\mathcal{H}\psi_o = E_o \psi_o \qquad (1.3.1)$$

where ψ_o is the eigenfunction of the ground state and $\mathcal{H}$ is the appropriate Hamiltonian. When dealing with the entire aggregation of paramagnetic molecules the complexity of the problem prevents the solution of (1.3.1). An approximate solution, may, however, be obtained by replacing the effect of neighbouring atoms by an electrostatic field potential (ϕ). Magnetic dipole-dipole interactions and exchange effects must also be taken into account. The Hamiltonian may then be represented by

$$\mathcal{H} = \frac{p_k^2}{2m} - \frac{Ze^2}{r_k} + \frac{e^2}{r_{jk}} + e_i\phi(r_i) + \mathcal{H}_s \qquad (1.3.2)$$

where the first four terms represent respectively the kinetic energy of the electrons, coulomb attractions of electrons and nuclei, mutual repulsion of the electrons, the interaction of the electrons with the electrostatic field. Finally, $\mathcal{H}_s$ contains the terms which involve the spin operators. The energy levels of $\mathcal{H}_s$ may be described in terms of an effective spin and $\mathcal{H}_s$ is referred to as the Effective Spin Hamiltonian.

Thus the Spin Hamiltonian deals with only those terms with which E.S.R. is concerned, and was introduced [A1], [P1], [B1], [B2], to standardize and simplify the previously rather cumbersome methods of expressing E.S.R. results. The values obtained experimentally of the

quantities of § 1.2 (a), (b) and (c) determine the constants in $\mathcal{H}_s$ and from these it is possible to calculate energy levels and orbitals of the paramagnetic centre.

In (1.3.2) the pattern of the lowest lying energy levels may normally be obtained by considering $\mathcal{H}_s$ as a perturbing term in the ground state manifold of the first four terms of (1.3.2). This conception is normally valid except when the electrons responsible for paramagnetism occupy low lying shells and are screened from the electrostatic fields as, for example, in the rare earth group. With this exception the orbital angular momenta are "quenched" owing to the removal of orbital degeneracy by a Stark splitting which aligns the orbits with the crystal field. In solutions of free radicals the intramolecular electric field arising from the distribution of atoms within the molecule replaces the crystal field. The delocalised molecular orbitals are aligned by this field to such an extent that "quenching" is almost complete, and the behaviour of the spins approaches that of free spins.

The form of the Spin Hamiltonian will be considered in § 2.1

§ 1.4 Experimental Technique

Essentially an E.S.R. spectrometer consists of a microwave oscillator which feeds power into a resonant cavity in which the paramagnetic sample is located in the region of maximum microwave magnetic field. The D.C. magnetic field at the sample can be adjusted to the

resonance value and the change in cavity Q caused by E.S.R. absorption or dispersion will produce a voltage change which is subsequently detected and displayed.

The spectrometer used for this research is a superhetrodyne reflection cavity spectrometer the klystrons of which are stabilised by a system based on the Pound scheme [P2]. A detailed description of the design, construction and performance of this spectrometer is given in Chapter 3.

§ 1.5 Scope of Thesis

The object of this research was to investigate the E.S.R. characteristics of some molecular complexes which involve free radicals and also radical cations and anions.

The results are divided into two main sections -

(a) Chapter 4 contains a discussion of the E.S.R. properties of phenothiazine complexes with acceptors and also of the phenothiazine positive ion in sulphuric acid solution. The unpaired spin densities calculated from the hyperfine splitting parameters are compared to those predicted by the Hückel molecular orbital theory in Chapter 6. This chapter also contains molecular orbital calculations on various substituted phenothiazines whose E.S.R. properties are considered in Chapter 5.

(b) The complexes of s-Trinitrobenzene with various donors, mainly aliphatic and aromatic amines are examined in Chapter 7 and an attempt is made to relate their E.S.R. properties to the optical absorption

measurements of Miller and Wynne-Jones [M2].

In addition the results of several other E.S.R. experiments are reported in Chapter 8.

CHAPTER 2

E.S.R. HYPERFINE SPLITTINGS AND LINE WIDTHS

§ 2.1 The Spin Hamiltonian

As was mentioned in § 1.3, the Spin Hamiltonian provides a useful means of expressing E.S.R. results and for a collection of paramagnetic molecules, takes the form [B1], [B2]

$$\mathcal{H}_S = \mathcal{H}_Z + \mathcal{H}_E + \mathcal{H}_I + \mathcal{H}_Q + \mathcal{H}_{NZ} + \mathcal{H}_D + \mathcal{H}_X \quad (2.1.1)$$

where
$$\mathcal{H}_Z = \beta(g_x S_x H_x + g_y S_y H_y + g_z S_z H_z) \quad (2.1.2)$$

is the Zeeman term between the levels of which E.S.R. transitions take place. x, y, z refer to the axis in laboratory coordinates. H_x S_x and g_x are the components of the external magnetic field, electron spin and spectroscopic splitting tensor respectively in the x direction.

$$\mathcal{H}_E = D(S_z^2 - \tfrac{1}{3} S(S+1)) + E(S_x^2 - S_y^2) \quad (2.1.3)$$

represents the fine structure splitting of the magnetic levels in an electric field through the spin orbit coupling. If the symmetry is axial, the term in E vanishes and if $S = \frac{1}{2}$, $\mathcal{H}_E$ vanishes as this term refers to a Kramers doublet.

$$\mathcal{H}_I = A_x S_x I_x + A_y S_y I_y + A_z S_z I_z \quad (2.1.4)$$

is the term which determines the hyperfine splitting of the levels by the interaction of the electron spin with the nuclear spin, I.

$\mathcal{H}_Q$ and $\mathcal{H}_{NZ}$ are the operators for the interactions of the nuclear

quadrupole moment with the electric field gradient and the direct interaction of the nuclear spins with the magnetic field respectively. Both terms are usually negligible.

$\mathcal{H}_D$ and $\mathcal{H}_x$ are the dipolar and exchange interactions which will be considered in § 2.3 (e) and 2.3 (f).

In the case of axial symmetry where the axis is parallel to the z axis and neglecting $\mathcal{H}_Q$ and $\mathcal{H}_{NZ}$, the Spin Hamiltonian becomes

$$\mathcal{H}_S = [g_{\parallel} H_z S_z + g_{\perp}(H_x S_x + H_y S_y)] + D[S_z^2 - \tfrac{1}{3} S(S+1)] + A I_z S_z + B(I_x S_x + I_y S_y) + \mathcal{H}_D + \mathcal{H}_X \qquad (2.1.5)$$

where $g_{\parallel} = g_z$, $g_{\perp} = g_x = g_y$

$A = A_z$

$B = A_x = A_y$

§ 2.2 The Microcrystalline Model

A paramagnetic molecule in solution may sometimes be surrounded by a sheath of solvent molecules. This would probably be more likely for a paramagnetic ion in a polar solvent, some molecules of which would tend to be polarised in the vicinity of the ion. This assembly may then act as a rigid entity, and has been regarded by McConnel [M1] as a "microcrystal" or "microcrystallite" which undergoes Brownian tumbling motion as a unit. The microcrystal is assumed to have an axis of symmetry, r, where the crystal axes are p, q, r. The Brownian motion causes a rapid variation of the orientations of p, q and r with respect

to the laboratory coordinates. If the ground state of the ion is taken to be a Kramer's doublet then (2.1.2) becomes

$$\mathcal{H}_S = \beta[g_{\parallel} H_r S_r + g_{\perp}(H_p S_p + H_q S_q)] + A I_r S_r + B(I_p S_p + I_q S_q). \qquad (2.2.1)$$

A transformation to the laboratory system is made, and the orientation of crystal axes expressed in spherical polar coordinates [P3]. $\mathcal{H}_S$ may be divided into two parts, one of which ($\mathcal{H}_o$) contains no angular functions and is therefore time independent, and a second which involves the polar and azimuthal angles θ and ϕ is therefore time dependent

$$\mathcal{H}_o = g\beta H S_z + a\underline{S}.\underline{I} \qquad (2.2.2)$$

$$\mathcal{H}_t = (\Delta g\beta H + bI_z)(\cos^2\theta - \tfrac{1}{3})S_z + \tfrac{1}{2}(\Delta g\beta H + bI_z)\sin\theta\cos\theta(S_+ e^{-i\phi} + S_- e^{i\phi}) - \tfrac{1}{4}b(\cos^2\theta - \tfrac{1}{3})(S_+ I_- + S_- I_+) + \tfrac{1}{4}b\sin^2\theta(I_+ S_+ e^{-2i\phi} + I_- S_- e^{2i\phi}) + \tfrac{1}{2}b\sin\theta\cos\theta(I_+ e^{-i\phi} + I_- e^{+i\phi}) \qquad (2.2.3)$$

where
$$\Delta g = g_{\parallel} - g_{\perp} \qquad a = \tfrac{1}{3}A + 2/3B$$
$$g = \tfrac{1}{3}g_{\parallel} + 2/3g_{\perp} \qquad b = A - B \qquad (2.2.4)$$

The operators $S_{\pm}$ and $I_{\pm}$ have the property of respectively raising and lowering the electron and nuclear spin eigenfunctions.

The time average of $\mathcal{H}_t$ vanishes, but taken over a short enough period of time τ_c the values of the angular functions involved have a fairly high probability of being correlated. This implies that if at $t = 0$, $f(\theta,t)$ has its maximum value, then at $t = \tau_c$, $f(\theta,t)$ is unlikely to have changed sign. τ_c is said to be the correlation time. Bloembergen,

Purcell and Pound [B3] considered a Debye model for a sphere radius a in a fluid of viscosity η, and took

$$\tau_c = \frac{4\pi\eta a^3}{3kT} \qquad (2.2.5)$$

The microcrystalline model will be referred to in discussions on relaxation mechanisms and isotropic and anisotropic line broadening (§ 2.3 (g) and § 4.10).

§ 2.3 Line widths

The mechanisms which may cause a broadening of E.S.R. lines will be briefly considered and an estimate quoted in each case of the magnitude of the effect. Since in E.S.R. the microwave frequency is kept constant while the magnetic field is varied, it is more convenient to express line widths in gauss. (1 c/s = 3.5×10^{-7} gauss)

(a) Natural Line Width

Owing to the possibility of spontaneous emission the molecules spends a finite time, T, in a given state and by the uncertainty principle this leads to an energy spread in the state and thus a line width [B4]

$$\delta H \doteq \frac{h}{g\beta T} \qquad (2.3.1)$$

This line width is of the order 10^{-10} gauss which is negligible compared with other effects.

(b) Doppler Broadening

In gaseous spectroscopy a significant broadening arises from the spread in molecular velocities. The corresponding line width is

$$\delta H = \frac{Hv}{c} \qquad (2.3.2)$$

where v is the mean velocity and c the velocity of light. In solution the molecular velocities are smaller and the line widths are of the order 10^{-5} - 10^{-6} gauss.

It would be expected that, even in crystals when the molecular velocities are zero, a broadening would arise from the velocity with which a molecule of mass M, recoils on emitting or absorbing a quantum

$$\delta H \doteqdot \frac{Hh\nu}{c^2 M}$$

This predicts a line width of the same order as the natural line width (2.3.1) for very low molecular weight and for x-band frequencies. If the recoil is absorbed by the entire crystal as in Mössbaur lines, H will be reduced by a factor 10^6 or more.

(c) Collision Broadening

During a collision between paramagnetic molecules an overlap of the unpaired electron wave function causes a spin coupling which interupts the Larmor precession and causes a line width of [V1]

$$\delta H = \frac{h}{2\pi\tau g\beta} \qquad (2.3.3)$$

where τ is the time between collisions the duration of which is assummed short compared with the Larmor frequency.

Considering a very simple model where the free radical molecules form an ideal gas in the absence of solvent then a molecular weight of 200 at 300°K would lead to an ideal gas RMS velocity $\sim 2 \times 10^4$ cms/sec. If a collision occurs when the centres of two free radical molecules

are 5A° apart then for a 10^{-3} M solution, from (2.3.3)

$$\delta H \doteq 5 \text{ gauss.}$$

Collision broadening in solution does not result in line widths of this magnitude and the ideal gas model is evidently over simplified.

In fact in a liquid a molecule of the solute may be considered to be contained in a "cage" of solvent molecules [N1] and many collisions with these nearest neighbours occur (with a frequency $\frac{1}{\tau_o}$, where $\tau_o \doteq 10^{-12} - 10^{-13}$ sec) before sufficient thermal energy is acquired to enable the "trapped" molecule to pass out of the first "cage" and into a second. The "encounter lifetime" of this process, $\tau_1 \doteq 10^{-10} - 10^{-8}$ sec.

Assuming that in each jump the trapped molecule moves about 10A° then the effective diffusion velocity is between 10 and 10^3 cms/sec and using these values in (2.3.3) instead of the RMS velocity gives

$$\delta H \doteq 0.004 - 0.4 \text{ gauss}$$

The values of τ_o, T_1 and the energy (W) required for a molecule to escape from a cage are related by

$$\tau_1 = \tau_o e^{W/kT} \qquad (2.3.4)$$

Since W will be lower at higher temperatures, as the viscosity falls, and also since kT will be greater, T_1 will decrease with increasing temperature and thus δH should increase with temperature.

The collision frequency between paramagnetic molecules will be much greater when a free radical forms part of the "cage" and in this case $\delta H \doteq 5 \times 10^4$ gauss. For 10^{-3} M solution, the probability of

this situation is only about 2×10^{-4} and this contribution to the hyperfine line is negligible.

If the solvent is polar, and a radical cation or anion is involved, it is possible to visualise a situation where $W \gg kT$ and the ion cannot escape from the "cage". The ion, which may no longer be considered to collide with the molecules of the "cage", is merely free to vibrate about some central position. The system of "cage" plus ion will then approximate to McConnel's microcrystalline model (§ 2.2).

(d) Spin-Lattice Relaxation

The Spin-Lattice or longitudinal relaxation time, T_1 determines the rate at which the spin system comes to equilibrium with the lattice. This can occur through the Spin-Orbit coupling or exchange as the orbital motion and the exchange interaction are both strongly coupled to the lattice. A quantum may be transferred either directly or by a Raman process in which a lattice quantum is scattered.

In solution the "lattice" is formed by thermal motions of the nuclei in the molecule. In Free Radicals the orbital motion is almost completely quenched and in dilute solution when the exchange is negligible the spin lattice relaxation time may be several seconds which leads to line widths of the order of 10^{-7} gauss [M4].

In viscous solutions another contribution to T_1 arises which will be discussed in § 2.3 (g).

Spin Lattice relaxation and collision broadening both give rise to line shapes corresponding to a collision damped oscillator. The macroscopic concept of a friction damped oscillator also predicts a similar line shape but it has been shown that, on increasing the damping, the resonant frequency shift occurs in opposite directions in the two cases [B5].

(e) Spin-Spin Broadening

Dipole-Dipole interactions (represented by $\mathcal{H}_D$ in (2.1.1)) between neighbouring electron spins enable the spin system to come to equilibrium in two separate ways at a rate determined by the spin-spin relaxation time T_2'.

(a) The local magnetic field at nearby spins is altered owing to the steady component of the precessing spin parallel to H.

(b) The component perpendicular to H causes a rotating magnetic field at the Larmor frequency which provides a resonance broadening. The RMS line width in gauss for $S = \frac{1}{2}$ is [B1]

$$\delta H = \frac{3}{4} g\beta \left[\sum_k \left(\frac{1 - 3\cos^2\theta_{jk}}{r_{jk}^3} \right)^2 \right]^{\frac{1}{2}} \qquad (2.3.5)$$

where r_{jk} is the separation of spins j and k and θ is the angle between the line joining them and H. In order that dipolar broadening should not obscure hyperfine splitting dilute solutions should be used to increase r_{jk}. A concentration of 10^{-3} M leads

to a line width of about 0.1 gauss [H1]. The contribution to T_2' of microcrystalline tumbling will be considered in § 2.3 (g).

(f) Intermolecular Exchange Narrowing

The isotropic exchange interaction $\mathcal{H}_x$ is given by [A2]

$$\mathcal{H}_x = \sum_{j,k} J_{jk}\, \underline{S}_j \cdot \underline{S}_k$$

where J is the exchange integral and the summation is taken over nearest neighbours. Although $\mathcal{H}_x$ commutes with $\mathcal{H}_z$ (2.1.2) and with S_x, it does not commute with the dipolar interaction $\mathcal{H}_D$ and the effect of $\mathcal{H}_x$ is to introduce a time dependence of $\mathcal{H}_D$ which is then reduced on time averaging. This narrows the line which then assumes a Lorentzian line shape. The effect of exchange on a spectrum containing hyperfine structure is to reduce the spacings between hyperfine components.

(g) Effect of Microcrystalline Tumbling on Relaxation

The time dependent microcrystalline Hamiltonian $\mathcal{H}_t$ (2.2.3) contains terms all of which involve Δg and b. These quantities represent the degree of anisotropy of g value and hyperfine splitting. If the correlation time, $\tau_c \ll \frac{1}{\nu}$ where ν is the frequency of the r.f. magnetic field, H_{rf}, then over one period of H_{rf}, $\mathcal{H}_t$ will average to zero and the line will not be broadened.

If, however, $\tau_c \doteq \frac{1}{\nu}$, the line will, in general, be broadened and McConnel has calculated the contributions to T_1 and T_2' from the 1st and 2nd terms of (2.2.3) [M1]

$$\frac{1}{T_1} \doteq \frac{2}{15\hbar^2} (\Delta g\beta H + bI_z)^2 \tau_c/(1 + 4\pi^2 \nu_o^2 \tau_c^2) \quad (2.3.6)$$

$$\frac{1}{T_2'} \doteq \frac{8}{45\pi\hbar^2} (\Delta g\beta H + bI_z) \tan^{-1} \left(\frac{2\tau_c}{T_2}\right) \quad (2.3.7)$$

In deriving these expressions S is taken to be $\frac{1}{2}$, i.e. zero field splitting terms do not appear, and also the last three terms of (2.2.3) are neglected i.e. b^2 is neglected in comparison with $(\Delta g\beta H)$ (b) and $(\Delta g\beta H)^2$.

(h) Variation of Line Width with I_z

(i) The expressions for the contributions to T_1 and T_2' by tumbling (2.3.6), (2.3.7) both involve I_z. Thus if either of these times is short enough to affect the line width then it is expected that the line width will vary with I_z. In this case shorter values of T_1 and T_2' are predicted for negative I_z than for positive I_z.

(ii) It was noted by Schreurs, Blomgren and Fraenkel [S1] in an accurate comparison of intensity ratios with theoretical values that the central components of hyperfine multiplets in the E.S.R. spectra of some free radicals are not as intense as expected. The line broadening mechanisms in the central components are not as strong as in the outer lines and saturation occurs.

A possible explanation involves the anisotropic intramolecular electron-nuclear dipolar interaction which can contribute to relaxation. If the total nuclear angular momentum

$$J = \sum I_i \quad (2.3.8)$$

then J^2 commutes with $\mathcal{H}_s$ and also, for a molecule with only equivalent nuclei, with the intramolecular dipolar interaction which therefore cannot induce transitions between states with different J. This implies that the central lines will not be so strongly relaxed as the outer ones.

(iii) In certain free radicals, for example the m-dinitro-benzene anion [F1] an alternation of broad and narrow hyperfine lines occurs. This is explained by the line width theory of Freed and Fraenkel [F2] in which the line widths are determined from the eigenvalues of a relaxation matrix. Degenerate hyperfine lines are predicted to consist of several superimposed Lorentzian lines which may not have equal line widths and therefore a variation from the expected peak to peak derivative intensity may occur (cf (ii) above). Also in this case the line shape will not, in general be Lorentzian.

(i) Variation of Line Width with Temperature and Viscosity

From the expression for the correlation time (2.2.5) it follows that, for a fall in temperature or an increase in viscosity of the solvent, τ_c will be increased and this will lead to broader hyperfine lines at lower temperatures. On raising the temperature the lines narrow as tumbling motion becomes more effective in averaging the anisotropies but at still higher temperatures the line width again increases [T1] owing to collision broadening (§ 2.3 (c)).

(j) Dissolved Oxygen

Hausser noted that on removing dissolved oxygen, the resolution of hyperfine spectra is sometimes improved [H1].

Evidently adsorption of oxygen shortens the spin lattice relaxation time T_1 under the influence of the magnetic moments of the O_2 molecules and this causes a line broadening [A3].

In addition the presence of paramagnetic oxygen molecules in solution leads to dipolar broadening.

(k) Electron Exchange Reactions

Ward and Weissman [W1], [W2] have shown that when naphthalene is added to solutions containing the naphthalene negative ion, a line broadening of the hyperfine components occurs as a result of an electron exchange reaction involving the anion and the free acceptor molecule -

$$A + A^- \rightleftharpoons A^- + A \qquad (2.3.9)$$

The line width produced by this process between the positions of maximum and minimum slope of the absorption line

$$\delta H = 6.5 \times 10^{-8} K [A] \qquad (2.3.10)$$

where K is the rate constant and [A] is the concentration of free acceptor.

Brown [B6] has observed this reaction for T.C.N.E. with T.C.N.E.$^-$ and calculated an approximate value for the rate constant.

§ 2.4 Apparatus Broadening

(a) Saturation Broadening

If T_1 is very long and the microwave magnetic field is appreciable, it may happen that the energy which is being fed into the spin system is not all transferred to the lattice, and an increase in spin temperature results. Thus a reduction in E.S.R. absorption is observed as the population difference has been reduced. This reduction occurs to a greater extent near the centre of the line where the transition probability is greatest.

(b) Inhomogeneity of magnetic field

The resolution of hyperfine splittings less than the field inhomogeneity over the sample will not be possible. Also if there is any mains ripple superimposed on the steady field then this also will inhibit any resolution less than the amplitude of the A.C. magnetic field.

(c) Modulation Broadening

Some detection schemes involve a magnetic field modulation often using 100 Kc/s. This causes a broadening of the same order as the modulation frequency. Modulation broadening does not apply, of course, to this spectrometer.

The phase sensitive detection scheme of § 3.13 requires a 280 c/s modulation of the magnetic field and this will inhibit resolution of splittings less than the amplitude of the 280 c/s modulation.

(d) Bandwidth Broadening

If the output time constant for a certain rate of magnetic field

sweep is too low to pass the higher frequency Fourier components in an E.S.R. line, a broadening can result, as well as an apparent shift in g value [R1].

§ 2.5 Hyperfine splitting and mechanisms involved

(a) Configuration Interaction

In solution the anisotropic part of the hyperfine interaction (2.1.4) averages to zero by tumbling motions or leads to a line broadening. The isotropic part is due to the Fermi contact term, [F3] which in a strong magnetic field, H, is given by,

$$\mathcal{H}_F = \frac{8\pi}{3} \mu_{nz} \sum_k \mu_{kz} \delta(\underline{r}_k - \underline{r}_n) \qquad (2.5.1)$$

where μ_{nz} and μ_{kz} are the components of the spin magnetic moments of the nucleus and the kth electron in the z direction and $\delta(\underline{r}_k - \underline{r}_n)$ is the Dirac delta function. (The second term in (2.2.2) is, in fact, $\mathcal{H}_F$.) The contribution of the filled orbitals is zero owing to the effect of the pairing of electrons and therefore the hyperfine splitting arises from the expectation value of $\mathcal{H}_F$ for the unpaired electron.

Considering a -CH fragment of an aromatic ring, to zero order, the ground state wave function Φ involves

$$(\text{filled orbitals}) \ (\sigma_b)^2 \ (\pi) \qquad (2.5.2)$$

where σ_b is a bonding σ orbital formed from the overlap of a hydrogen 1s and a carbon sp^2 orbital.

Now a π orbital has a node at the plane of the aromatic ring, and

thus the expectation value of $\mathcal{H}_F$ at the proton is zero. Weissman [W3] suggested that zero point vibrations of the proton might explain the observed splitting, but this is an order of magnitude too small [F6].

The explanation lies, in fact, in configuration interaction by which some σ character is imparted to the unpaired electron [W4] [M3] [J1]. In order for this to occur, there must be some admixture of an excited state wave function Ψ in which the unpaired electron has some character. Ψ must have the same symmetry about the aromatic plane as Φ. The orbital part of Ψ has the form

$$\sigma_b^{\pi} \sigma_a^{-} \tag{2.5.3}$$

where σ_a^{-} is an antibonding orbital. The ground state wave function is taken as

$$\chi = \Phi + \lambda\Psi \tag{2.5.4}$$

where $\lambda = \dfrac{\langle \Psi | \mathcal{H}_F | \Phi \rangle}{W_{\Psi} - W_{\Phi}} \ll 1$ and where W_{Ψ} and W_{Φ} are eigenvalues of Ψ and Φ. Jarrat [J1] obtained for a CH fragment, the hyperfine splitting

$$Q = \frac{16\pi}{3} \mu_h \mu_e \frac{[h^2(r_h) - \sigma^2(r_h)]\lambda}{1 - S_{\sigma h}^{\ 2}} \tag{2.5.5}$$

where $h^2(r_h)$ and $\sigma^2(r_h)$ are the squares of the magnitudes of the hydrogen and carbon σ wave functions, and $S_{\sigma h}^{\ 2}$ is the overlap integral. On evaluating the quantities involved he found

$$Q = -28 \text{ gauss} \tag{2.5.6}$$

which is in fairly good agreement experimentally with the splitting due to a ring proton.

In aromatic radicals the molecular orbital that contains the unpaired electron is in general delocalised and an unpaired electron density (ρ_i) may be associated with each nucleus (i). The ground state wave function for the i^{th} nucleus is now taken as

$$\chi_i = \Phi + \lambda_i \rho_i \Psi \qquad (2.5.7)$$

and the splitting a^h due to the proton attached to the i^{th} ring carbon atom, at which the unpaired electron density is ρ_i [M3], is

$$a^h = \rho_i Q \qquad (2.5.8)$$

This is known as the McConnel relation, and it is found experimentally that the magnitude of Q is fairly constant ($\fallingdotseq$ 28 gauss) for radical fragments, which consist of a ring carbon atom and a proton. In fact, Q is usually taken to be about -23.7 gauss rather than -28 gauss [M5]. It is thus possible using (2.5.8) to obtain information about the unpaired electron density at different sites in the molecule by measuring the hyperfine splittings. When there are several groups of non equivalent protons in an aromatic molecule it will not always be possible to assign an unpaired electron density to a particular atom. However, in this case, by substituting deuterons for protons, or C^{13} for C^{12} atoms, the ambiguity may be resolved.

(b) Hyperconjugation

A hyperfine splitting is produced by the protons of a methyl group bonded to an aromatic ring carbon atom. The π wave function does not extend as far as the methyl carbon atom and the splitting cannot be explained by configuration interaction.

In this case it is possible for a linear combination of the three hydrogen wave functions h_1, h_2, h_3 to result in a methyl group wave function (ψ_{me}), for example

$$\psi_{me} = h_1 - \tfrac{1}{2}(h_2 + h_3) \qquad (2.5.9)$$

which possesses a symmetry similar to that of the $2p_z$ orbital. This method of providing the required overlap which permits an interaction of the unpaired electron with the methyl protons is known as hyperconjugation. The hyperfine splitting which results is of the same order of magnitude as in configuration interaction for a similar unpaired electron density (ρ) on the ring carbon atom. The methyl proton splitting, a^h may be expressed in a form similar to that of the McConnel relation (2.5.8) [M8]

$$a^h = \rho Q' \qquad (2.5.10)$$

Q' is the value of a^h when the unpaired electron is localised on the associated ring carbon atom. Experimentally it is found that Q' is about 25-30 gauss.

(c) C^{13} and N^{14} splitting

C^{12} atoms can cause no hyperfine splitting as they have zero nuclear spin but the natural abundance of C^{13} ($I = \frac{1}{2}$) is about 1%, and hyperfine splitting by C^{13} has been observed [S2]. N^{14} has $I = 1$ and this also gives rise to a hyperfine splitting. This splitting arises similarly to that of ring protons from a non zero π electron density at the nucleus as a result of σ-π configuration interaction.

In the case of C^{13}, both 1s- and 2s-orbital mixing must be included, in order to estimate the hyperfine interaction, and separate perturbation treatments are performed for the 1s- and 2s-orbitals [K1].

The hyperfine interaction in gauss a^c has been calculated [K1] for various different radical fragments and the results are expressed in terms of Q symbols corresponding to the notation of (2.5.8). Here $Q_{ab}{}^b$ represents the splitting caused by the nucleus B, owing to the interaction with the π electron spin on nucleus A through the bond AB. In molecules the σ bonds are normally localised and thus the results of the Q values obtained for radical fragments may be used to calculate splittings. The contribution of the unpaired electron density in each π orbital is added in turn.

If a C^{13} atom is bonded to atoms X_1, X_2, X_3 in a molecule, where the unpaired spin density on X_i is ρ_i^{π} ($i = 1, 2, 3$) and on C is ρ^{π}, then the total hyperfine splitting is [K1]

$$a^c = S^c \rho^{\pi} + \sum_{i=1}^{3} Q_{cxi}{}^c \rho^{\pi} + \sum_{i=1}^{3} Q_{xic}{}^c \rho_i^{\pi} \qquad (2.5.11)$$

This expression is just an extension of the McConnel relation, (2.5.8) where the hyperfine splitting represented by the first term arises from the 1s contribution; the splitting represented by the second and third terms corresponds to the contributions of the C-X_i bonds, where the unpaired electron density is on the C^{13} atom (ρ^{π}) and on X_i (ρ_i^{π}) respectively. Thus (2.5.11) accounts for the possibility that the electron density may be different at different ends of the bond i.e.

$\left|Q_{cx}^{c}\right| \neq \left|Q_{xc}^{c}\right|$. This variation is normally small except for hetero-nuclear bonds.

A similar result may be expressed for N^{14} splittings. If the N^{14} atom is bonded to two carbon atoms and a hydrogen atom the hyperfine splitting (a^{n}) may be expressed [B8]

$$a^{n} = (S^{n} + 2Q_{nc}^{\ n} + Q_{nh}^{\ n})\rho_{n}^{\pi} + Q_{cn}^{\ n}(\rho_{c_1}^{\ \pi} + \rho_{c_2}^{\ \pi}) \quad (2.5.12)$$

where S^{n} is the 1s orbital contribution, ρ_{n}^{π} is the π electron density at the N^{14} atom and ρ_{ci}^{π} is the π density at the neighbouring carbon atom C_i.

When the N^{14} atom is part of a nitro-group which is bonded to a ring carbon the expression for the N^{14} hyperfine splitting becomes [R2]

$$a^{n} = (S^{n} + Q_{nc}^{\ n} + 2Q_{no}^{\ n})\rho_{n}^{\pi} + Q_{cn}^{\ n}\rho_{c}^{\pi} + 2Q_{on}^{\ n}\rho_{o}^{\pi} \quad (2.5.13)$$

The expressions (2.5.12) and (2.5.13) will be used in Chapters 6 and 7 where N^{14} splittings are considered.

CHAPTER 3

THE SPECTROMETER

§ 3.1 Introduction

The primary requirement of a spectrometer designed for the investigation of hyperfine structure of free radicals in dilute solution is high sensitivity. In order to obtain the high resolution necessary to study hyperfine splittings down to ~100 milligauss, the following requirements must be satisfied:-

(a) The concentration of free radicals should not be much greater than 10^{-3} molar or the resulting dipolar broadening will inhibit resolution of hyperfine splittings of the order 100mG [H1].

(b) Microwave power must not exceed the level at which saturation broadening occurs (§ 2.4 (a)).

(c) The amplitude of the magnetic field modulation must be kept below the hyperfine splitting to avoid magnetic field modulation broadening of the line (§ 2.4 (c)).

(d) The sample dimensions must be less than that necessary to produce broadening by inhomogeneity of the magnet (§ 2.4 (b)).

These four quantities must all be reduced to a level which does not inhibit resolution. This results in a proportional reduction in the E.S.R. absorption signal in cases (a), (c) and (d) and in a reduction proportional to the square root of the microwave power in case (b). Thus, if, owing to lack of spectrometer sensitivity, the

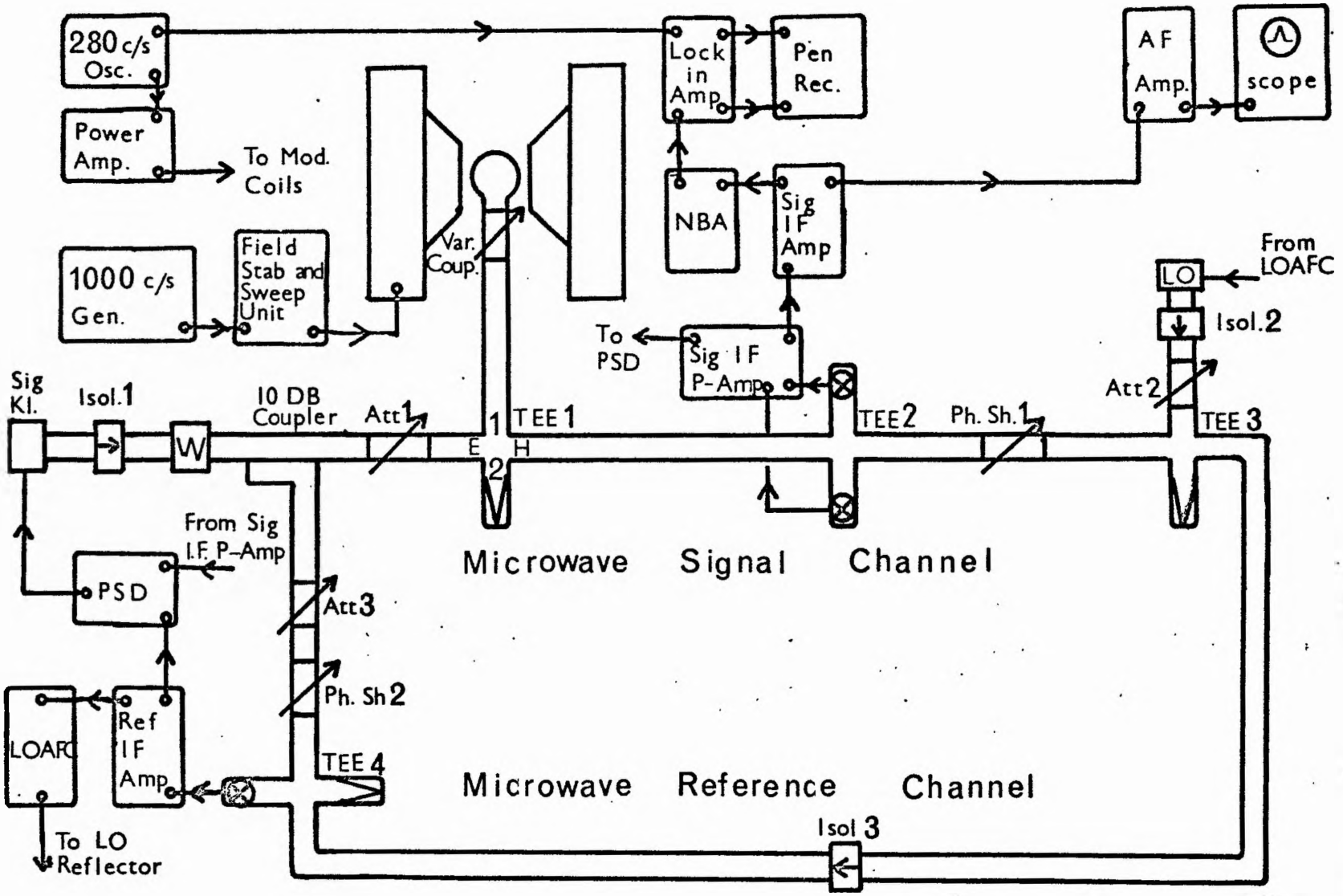

FIG 3·1 Block Diagram of Spectrometer

signal to noise ratio is too low, then one or more of the above quantities must be increased to a level which broadens the line excessively.

The system suggested by Feher [F4] and by Hausser [H1] as providing a high sensitivity without the disadvantages of high frequency modulation is a superhetrodyne spectrometer. The spectrometer used is based upon a design by Dr. I. M. Brown which was similar to the system used by Hirshon and Fraenkel [H2]. This employs separate stabilisation of both Local Oscillator and Signal Klystrons.

The microwave components and electronic units which were designed and built by the author are here described in detail. Reference is made to Brown's spectrometer for components which are identical to those employed by him [B6].

§ 3.2 Description of Spectrometer

The block diagram of the spectrometer is shown in Fig. 3.1. The microwave system, together with the I.F. amplifiers, consists of two distinct parts, the Signal Channel, and the Reference Channel or stabilisation loop.

The Signal Channel consists of the following components. Magic Tee (1) forms a microwave bridge and the power which is coupled back into the H arm of this is determined by the reflection coefficient of the cavity in arm 1. This signal in the H arm must be sufficiently small to allow a high gain to be used without causing saturation of the Signal I.F. Amplifiers. Thus the cavity arm must be close to

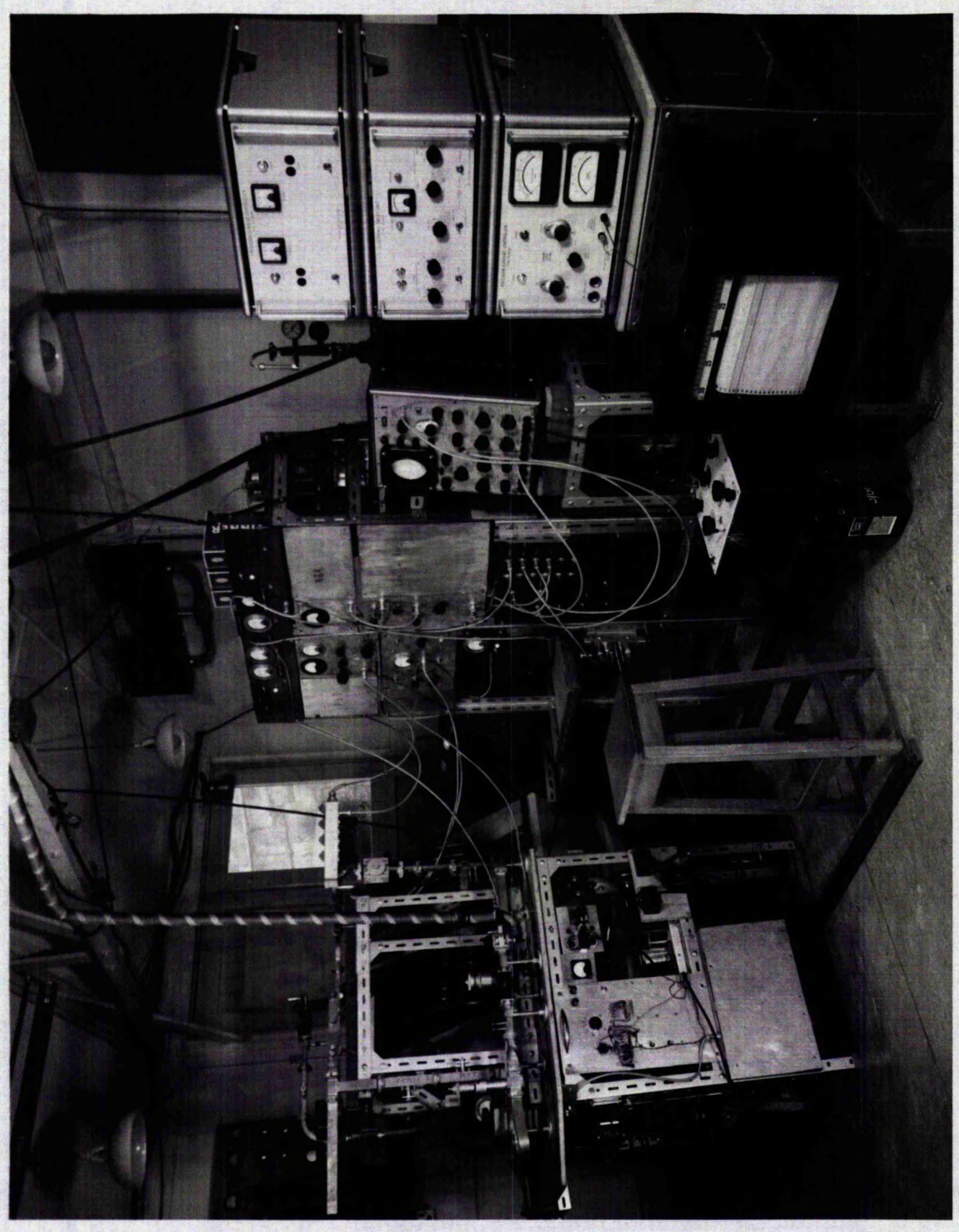

FIG 3.2 General View of Spectrometer.

match which requires the cavity coupling to be nearly critical. Local Oscillator (L.O.) power reaches the Signal Channel by way of the E arm of Tee (3). It then mixes with Signal Klystron power at the Balanced Mixer (Tee (2)). The resulting I.F. voltage from the crystals of the Balanced Mixer forms the input of the Signal I.F. Amplifiers. The output of these may be used to display E.S.R. absorption lines according to either the video or Phase Sensitive Detection schemes described in § 3.11 and § 3.13 respectively.

In the Reference Channel, L.O. power from the H arm of the L.O. Tee (Tee (3)) mixes at the crystal of the Reference Tee (Tee (4)) with Signal Klystron power which has been abstracted from the Signal Channel by a 10 db coupler. The resulting reference I.F. voltage which forms the input of the Reference I.F. Amplifier, is coherent with the Signal I.F. Pre-amplifier output but is independent of the cavity reflection coefficient.

The outputs of these two amplifiers provide the Reference and Signal voltages for the Phase Sensitive Detector. The phase of the signal voltage varies through the bandwidth of the cavity and by suitable choice of phase difference between the signal and reference inputs to the P.S.D., achieved by means of the Microwave Phase Shifters (1) and (2), it is possible to stabilise the Signal Klystron to the resonant frequency of the cavity by feeding the P.S.D. output back to the Signal Klystron reflector.

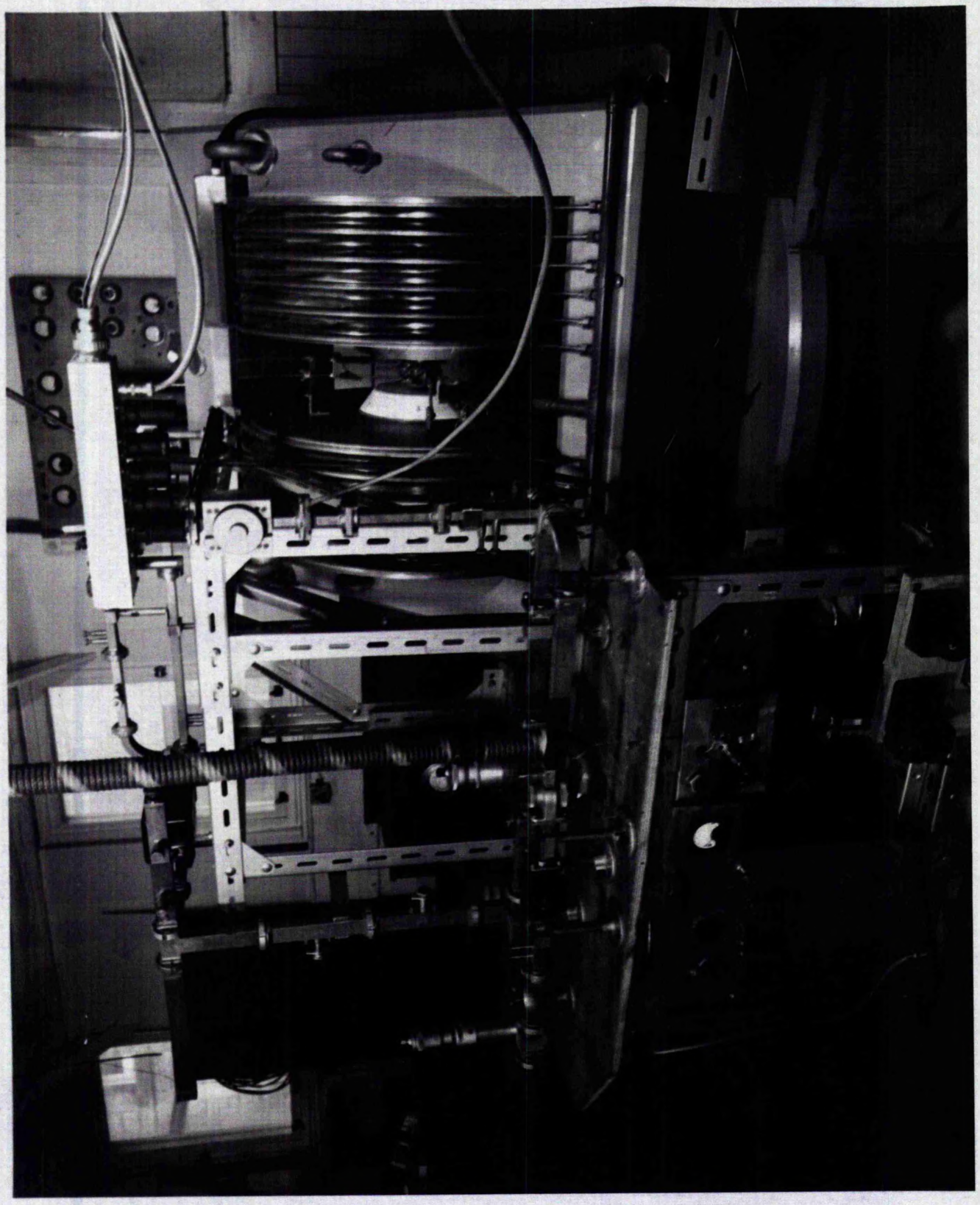

FIG 3.3 Microwave System and Mullard Magnet.

The Local Oscillator klystron is also stabilised. The output of the Reference I.F. Amplifier is fed into the Local Oscillator Automatic Frequency Control unit (L.O.A.F.C.). This produces an error signal which is fed back to the reflector of the L.O. and stabilises the L.O. frequency such that the I.F. is maintained at 30 mc/s.

Fig. 3.2 shows a general view of the spectrometer and Fig. 3.3 the microwave system and the Mullard magnet. The stabilisation and sweep units for this are seen to the right of Fig. 3.2.

§ 3.3 General Microwave Components

(a) Waveguide

The waveguide system employed consists of a hybrid of sizes 15 and 16, some components of each size being available. At the junctions of the two sizes, quarter wave transformer sections [B6], [R3] were included. Although these have V.S.W.R.s which are less than 1.05, in order to minimize reflections between Tees (1) and (2), no such junctions occur between Attenuator (1) and Phase Shifter (1) (Fig. 3.1). This part consists of W.G. size 16.

(b) Mounting

The waveguide system (Fig. 3.3) is clamped to a "Handy Angle" framework which is screwed to a table. The table is adjustable in height to allow the cavity to be centred between the magnet pole pieces, and is mounted on rubber blocks to obviate the effects of mechanical vibrations.

(c) Klystrons

The Signal Klystron is an E.M.I. R5222 which is capable of providing a microwave power of about 15-20mW at the cavity. This can be reduced by means of the calibrated Attenuator (1).

The L.O. Klystron is an English Electric K302 from which power at the Balanced Mixer was adjusted to give a crystal current of approximately 0.5mA.

(d) Isolators

Ferrite isolators (1) and (2) are included after the klystrons to prevent "pulling" of frequency caused by reflections. Isolator (3) prevents signal klystron power reaching the Balanced Mixer by way of the Reference Channel. The isolators have a forward loss ~ 2 db and a reverse loss ~ 30 db.

(e) Magic Tees

Tee (2) is a commercial component (Elliot type B) and, together with the Balanced Mixer and I.F. Signal Pre-amplifier, forms a rigid unit. Tees (1), (3) and (4) were made in the department [B6], the E and H arms including screws for fine adjustment of matching.

(f) Crystals

The crystals used in the Balanced Mixer are Mullard S1M 2 and S1M 5 matched to give optimum L.O. noise suppression. The reference crystal in Tee (4) is an A.E.I. C.S.3 B.

(g) Attenuators

These are of the movable vane type (Microwave Instruments). In Attenuator (1) the vane is moved by a micrometer screw and was calibrated in db using a Wayne Kerr Milliwattmeter (type U281). This calibration is accurate only over the first 10 db but it has never been found necessary to use greater attenuation than this.

(h) Phase Shifter

These also are of the Microwave Instruments movable vane type. The phase shift produced is slightly less than 360° and thus it was found useful to have two Phase Shifters.

(i) Sliding Stub Tuner (S.S.T.)

For the measurement of V.S.W.R. it was found convenient to calibrate the S.S.T. penetration in V.S.W.R. as follows. As shown in Fig. 3.4 a standing wave detector (S.W.D.) and the S.S.T. are included in Arm (2) of Tee (2). When a V.S.W.R. is introduced by the S.S.T., the S.W.D. is positioned with its probe at a standing wave minimum. With the probe now at a standing wave maximum, the Attenuator (1) is screwed in until the S.W.D. meter reading is equal to the previous reading at the minimum. Thus the V.S.W.R. may be obtained from the known attenuation. In this way it is not necessary to know the exact detector law of the S.W.D. crystal.

The S.S.T. may now be used to measure V.S.W.R. by adjusting the position and penetration of the probe until the unknown reflected

Calibration of S.S.T

FIG 3·4

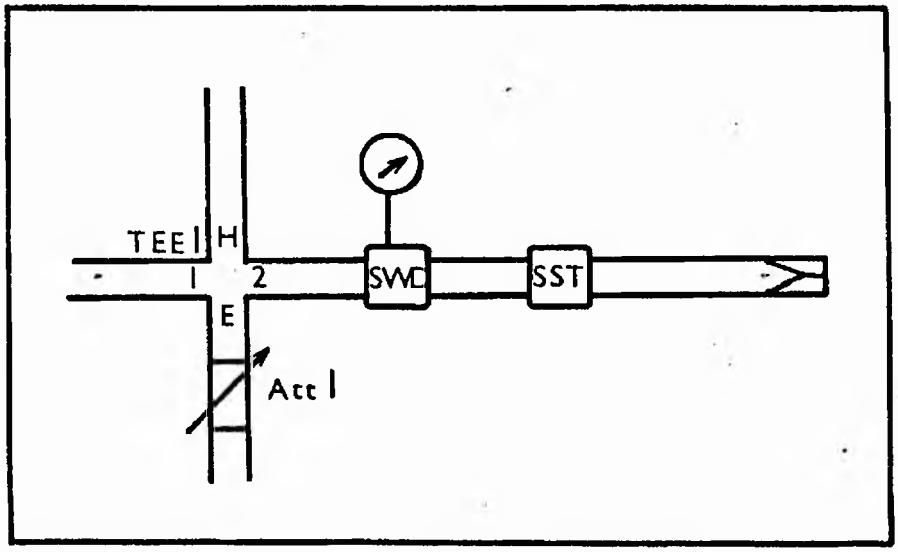

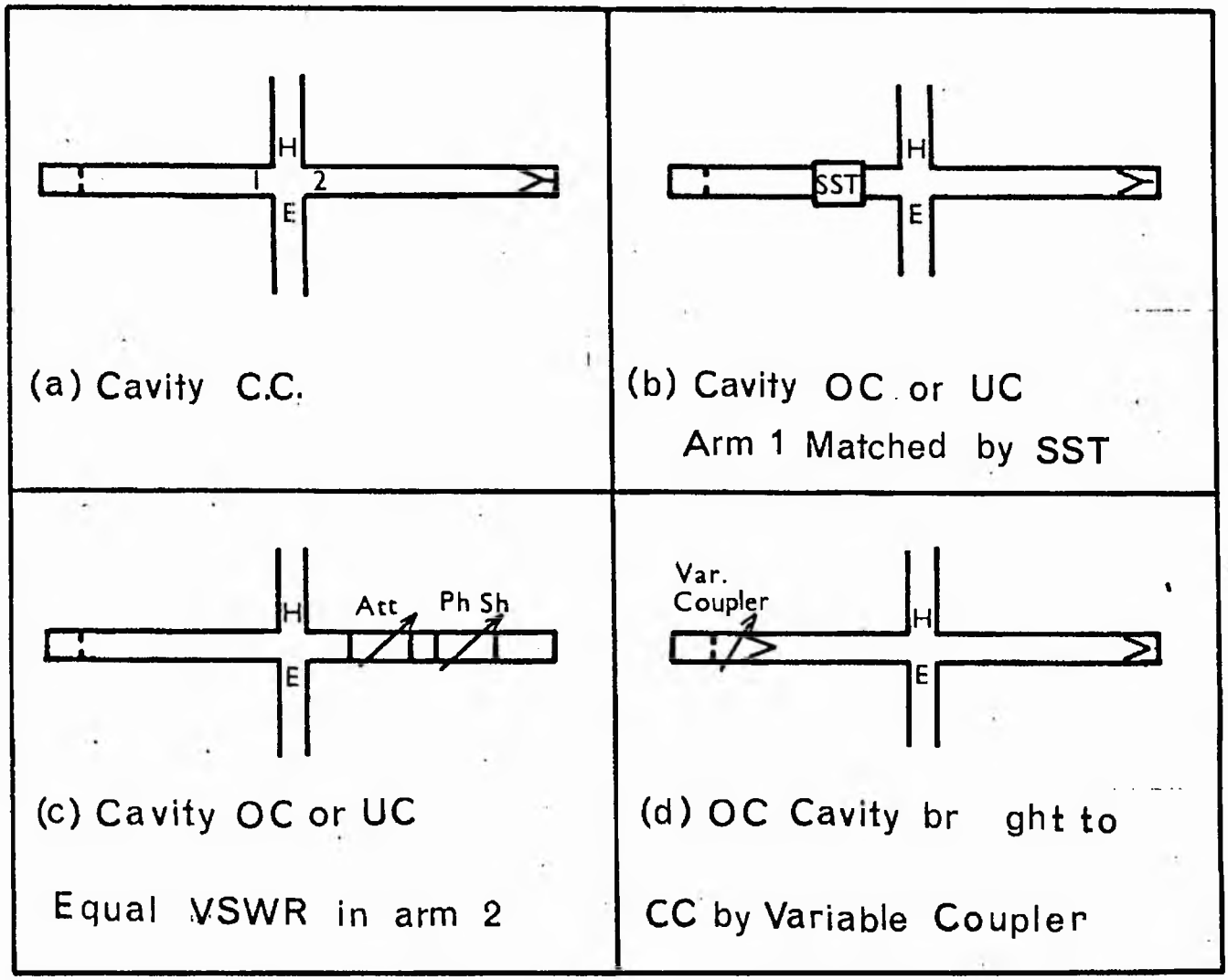

FIG 3·5 Balancing of Microwave Bridge (TEE 1)

voltage is balanced out by the S.S.T. The V.S.W.R. is then equal to that produced by the S.S.T. itself in a correctly terminated line [Y1].

The V.S.W.R. produced by a given S.S.T. penetration has been found to show little variation with frequency.

§ 3.4 Variable Coupler

(a) Balancing of the Microwave Bridge

In order that the optimum E.S.R. signal is observed, it is necessary to ensure that the microwave bridge (Tee (1)) should be almost exactly balanced in which case the signal in the H arm of Tee (1) is zero except when an E.S.R. signal is present. This situation corresponds to the four cases of Fig. 3.5 which are discussed below. In practice the functioning of the stabilisation system requires that a small amount of power should always be present in this arm.

In Fig. 3.5 (a), with the Signal Klystron oscillating at the cavity resonant frequency, the ideal situation exists where the cavity is critically coupled, arm (1), therefore, is correctly matched and the Tee balanced. The V.S.W.R.s in arms (1) and (2) are also unity.

Normally, although a range of irises is available, the cavity is not critically coupled and the cavity arm may then be matched by means of a Sliding Stub Tuner (S.S.T.) as in Fig. 3.5 (b). In this case a V.S.W.R. exists between the cavity and the S.S.T. in arm (1) and, as the stub is susceptible to vibration,this method leads to microphonics.

In Fig. 3.5 (c) the bridge is balanced by introducing an equal

V.S.W.R. of the appropriate phase in arm 2. This is done by the combination of Attenuator, Phase Shifter and Short Circuit, the Attenuator varying the amplitude and the Phase Shifter the phase of the voltage reflected from the short circuit [I2], [F4]. In this case the cavity arm is not matched. In practice, although it is not so susceptible to vibration as a S.S.T., this method has the disadvantage that the range of V.S.W.R. over which it is effective is limited to values fairly close to unity.

Fig. 3.5 (d) shows a cavity which was initially overcoupled but has been coupled critically by means of a variable coupler. In this case the conditions are again as in Fig. 3.5 (a), the V.S.W.R. in both arm (1) and arm (2) being unity.

(b) Principle of Operation

For a TE_{01} mode in a waveguide of inside dimensions of a and b ($a > b$), the guide wavelength λ_g is given by

$$\frac{1}{\lambda_g^2} = \frac{1}{\lambda^2} - \frac{1}{4a^2} \qquad (3.4.1)$$

For values of $a < \frac{\lambda}{2}$, the wave guide is cut off and the mode evanescent. A wavelength Λ may be defined for this evanescent mode where

$$\Lambda = i\,\lambda_g \qquad (3.4.2)$$

If a is reduced to below cut off by introducing brass strips into the section of guide adjacent to the cavity (Fig. 3.6), the cavity coupling will be changed by an amount determined by the magnitude of

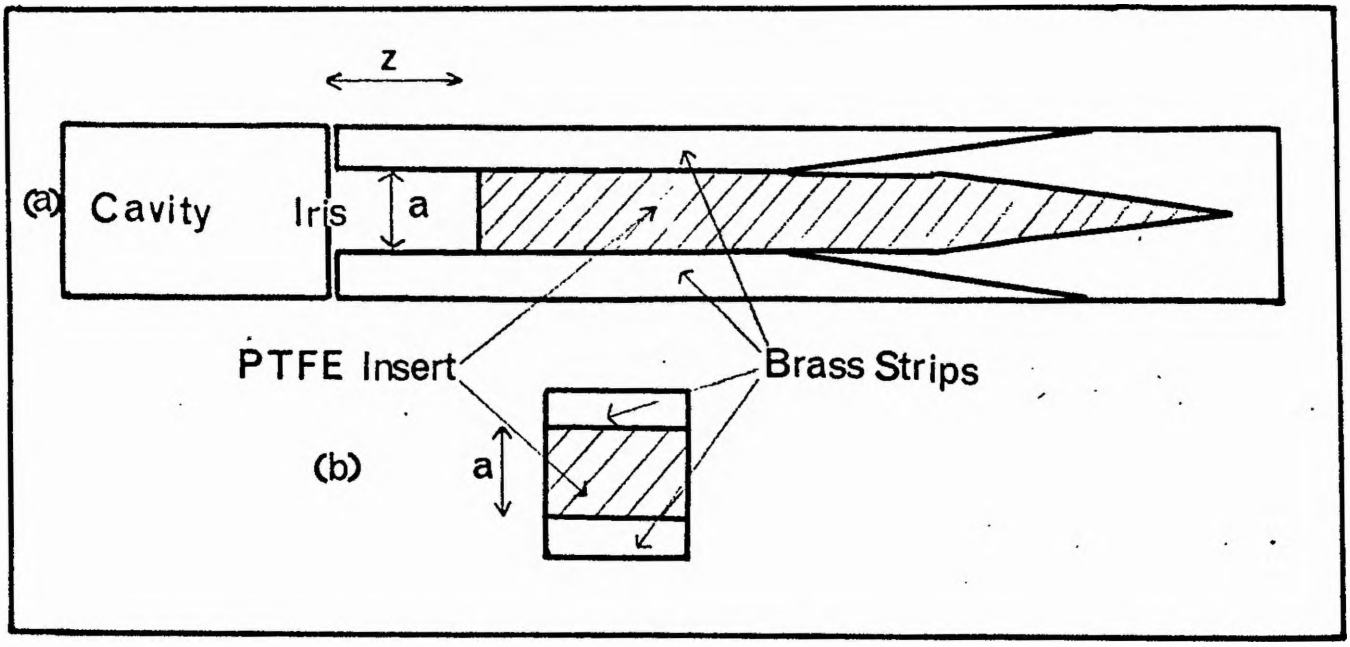

FIG 3·6 Variable Coupler (not to scale)

(a) Section through narrow side of waveguide

(b) Cross Section

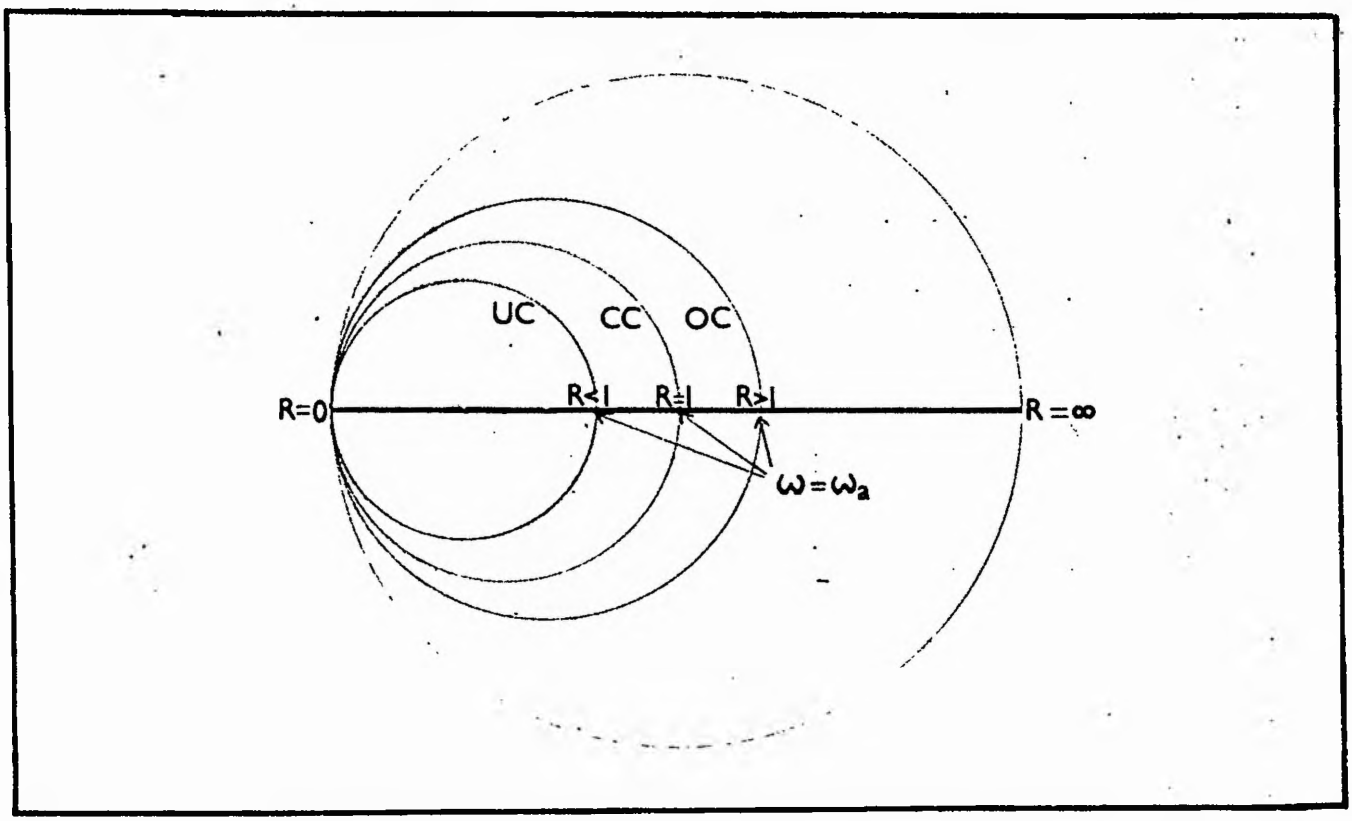

FIG 3·7 Smith Chart: variation with ω of complex input impedence (Z) for a U.C., C.C., and O.C. cavity $R = \frac{Z}{Z_0}$.

a and the length of cut off waveguide (z). This length may be varied by filling part of the cut off region with a material of dielectric constant such that in this region, the guide is no longer cut off. By slotting the waveguide to allow the position of the dielectric insert and thus z to be varied, it should be possible to vary continuously the coupling of the cavity.

The idea for producing such a device was obtained from Mr. V. W. Rampton at the British Radiospectroscopy Group Conference at Keele (April 1963). It was later found that a variable coupling cavity which works on a similar principle,has been described in the literature [G1].

(c) Construction

The details of construction are shown in Figs. 3.6 and 3.8. The brass strips are fixed in place by means of 4BA screws. This was preferred to soldering the strips in place which could lead to a being non-uniform. The brass strips and the dielectric insert were tapered for 5 cms and 7 cms respectively in order to minimize reflections. A P.T.F.E. plug mounted on a length of 4BA screwed rod passed through a slot in the waveguide and engaged in a hole in the insert which was movable over a distance of ~2 cms.

(d) Dielectric Insert

The original insert was cast from Araldite following the technique used for making plastic cavities (§ 3.5 (b)). Using this insert,the spectrometer sensitivity was found to be lower by approximately a

factor 5 than when the cavity arm was matched with a S.S.T.

The dielectric constant and loss tangent were measured by terminating arm (2) of Tee (2) with a short circuit next to which a slab of Araldite was placed. The V.S.W.R. in the arm and the position of the first electric field minimum were measured and the dielectric constant and loss tangent calculated [R4]. Values were found as follows:-

$$\epsilon' = 2.7 \pm 0.4 \quad ; \quad \tan\delta = 0.09 \pm 0.03$$

Thus the power absorbed in the Araldite will lead to a reduction in sensitivity of the order of that observed.

Inserts have been made of Polythene and P.T.F.E. which have loss tangents $\sim 4 \times 10^{-4}$ and as expected with these inserts no such reduction in sensitivity has been observed.

(e) Reflections from the Brass Strips

In order to estimate what reflections occur from the tapers in the brass strips, a cavity in arm (1) of Tee (1) was critically coupled by introducing dielectric losses, into the cavity in the absence of the Variable Coupler. With the Variable Coupler present but with z = 0, i.e. not affecting the coupling, the reflection from the brass strips was balanced out using the calibrated S.S.T. and the V.S.W.R. was found to be ~ 1.02.

(f) Theoretical Range of Coupling possible

The effect of introducing a length of cut off waveguide in front of the cavity is to reduce its input impedance, Z. The locus of Z/Z_o

(Z_o is the characteristic waveguide impedance) plotted on a Smith or hemisphere impedance chart against ω is a circle [G2] and, at the cavity resonant frequency ω_a, Z/Z_o is real. From Fig. 3.7 it is seen that if

$$R = Z/Z_o \text{ at } \omega_a$$

then

$R < 1$ for an undercoupled cavity

$R = 1$ for a critically coupled cavity

$R > 1$ for an overcoupled cavity

The reduction of the cavity input impedance due to the length of cut off guide will decrease the radius of the circle on the Smith chart. This will enable a cavity to be critically coupled only if it was originally overcoupled. Also a cavity originally overcoupled will become critically coupled and then increasingly undercoupled as the length of waveguide cut off (z) is increased.

(g) Operation

The Variable Coupler appears to function well according to the principles of § 3.4 (b). It has been found considerably more versatile than the S.S.T. in matching cavities for which the initial coupling is far from critical. This is only true provided that initially the cavity is O.C. as explained in §§ 3.4 (f).

Thus, by choosing a fairly large coupling iris, the cavity can be matched for a large number of different samples.

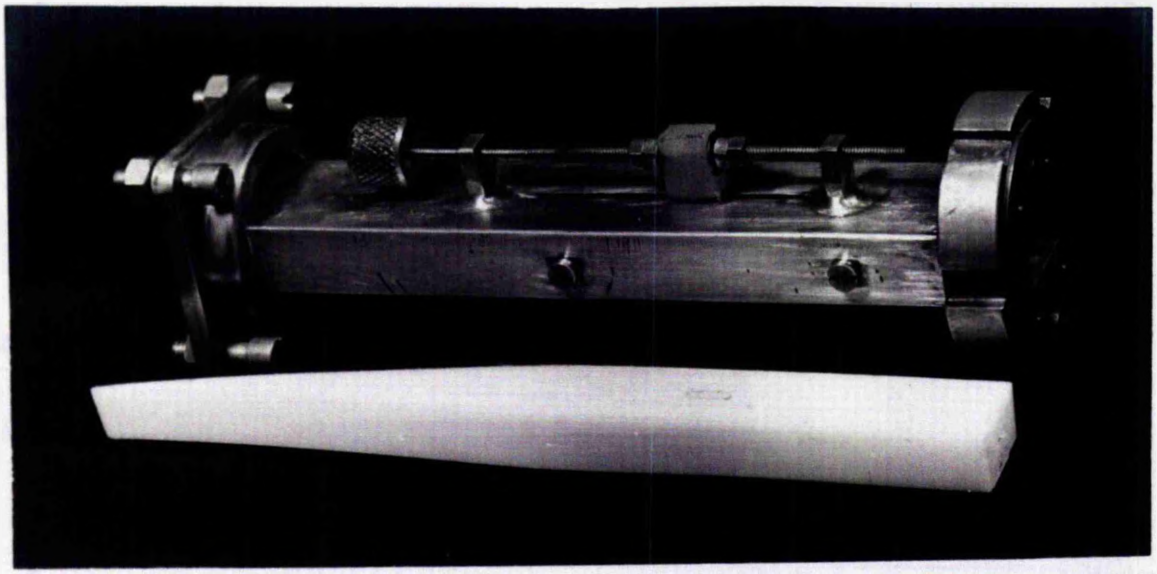

FIG 3.8 Variable Coupler.

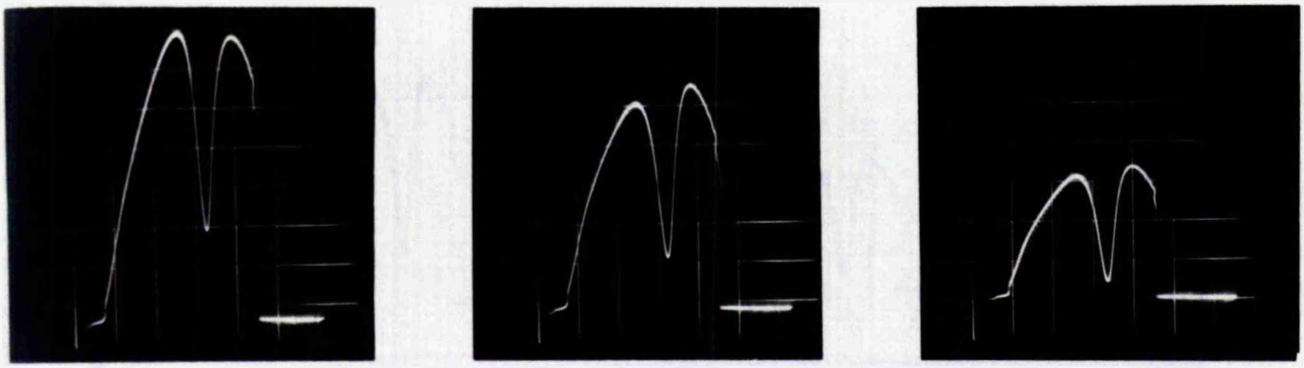

FIG 3.9 Response of U.C. Cavity.

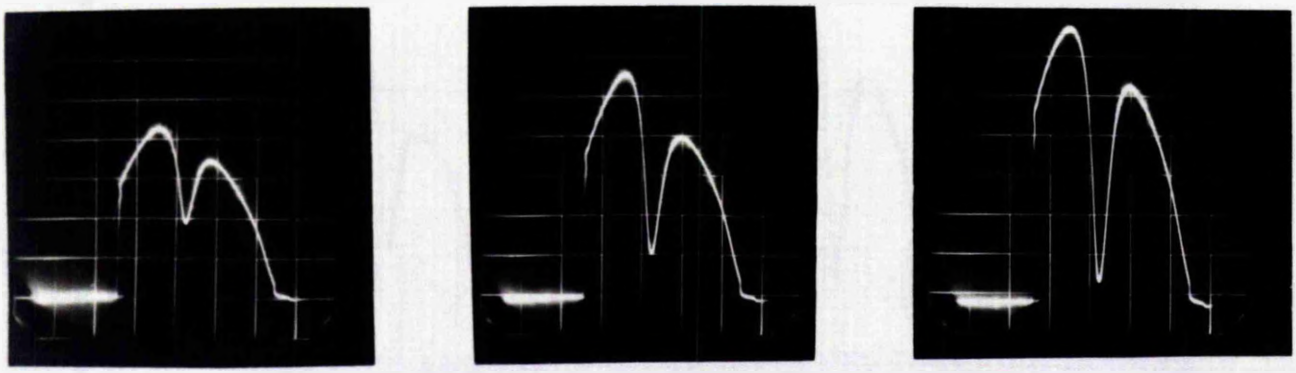

FIG 3.10 Response of O.C. Cavity.

The fact that, using such an iris, the cavity is O.C. for a small value of z and U.C. for a large value of z may be demonstrated as follows [Y1].

A small voltage is added to that reflected from the cavity by means of a S.S.T. in the cavity arm. The phase of this added voltage may be varied while keeping the amplitude constant by moving the S.S.T. probe position without altering its penetration.

The total reflected voltage is displayed on the oscilloscope as a function of frequency by observing the output of one of the Balanced Mixer crystals while sweeping the Signal Klystron frequency.

Fig. 3.9 shows this oscillogram for a large value of z when the added voltage in the three photographs has relative phase 0°, 90° and 180° respectively. The apparent vertical movement of the cavity dip and the adjacent "shoulders" without change of shape corresponds to the U.C. case when no change occurs in the size of the cavity reflection coefficient.

Fig. 3.10 shows the results of the addition of the same voltage for a small value of z. In this case, corresponding to an O.C. cavity and thus to a change in sign of reflection coefficient, the dip changes shape and moves in the opposite direction to the adjacent "shoulders".

(h) Estimation of Λ

Using an iris which is large enough to ensure that the H_{102} cavity (§ 3.5 (e)) was O.C. for z = 0, the V.S.W.R. in the cavity arm was

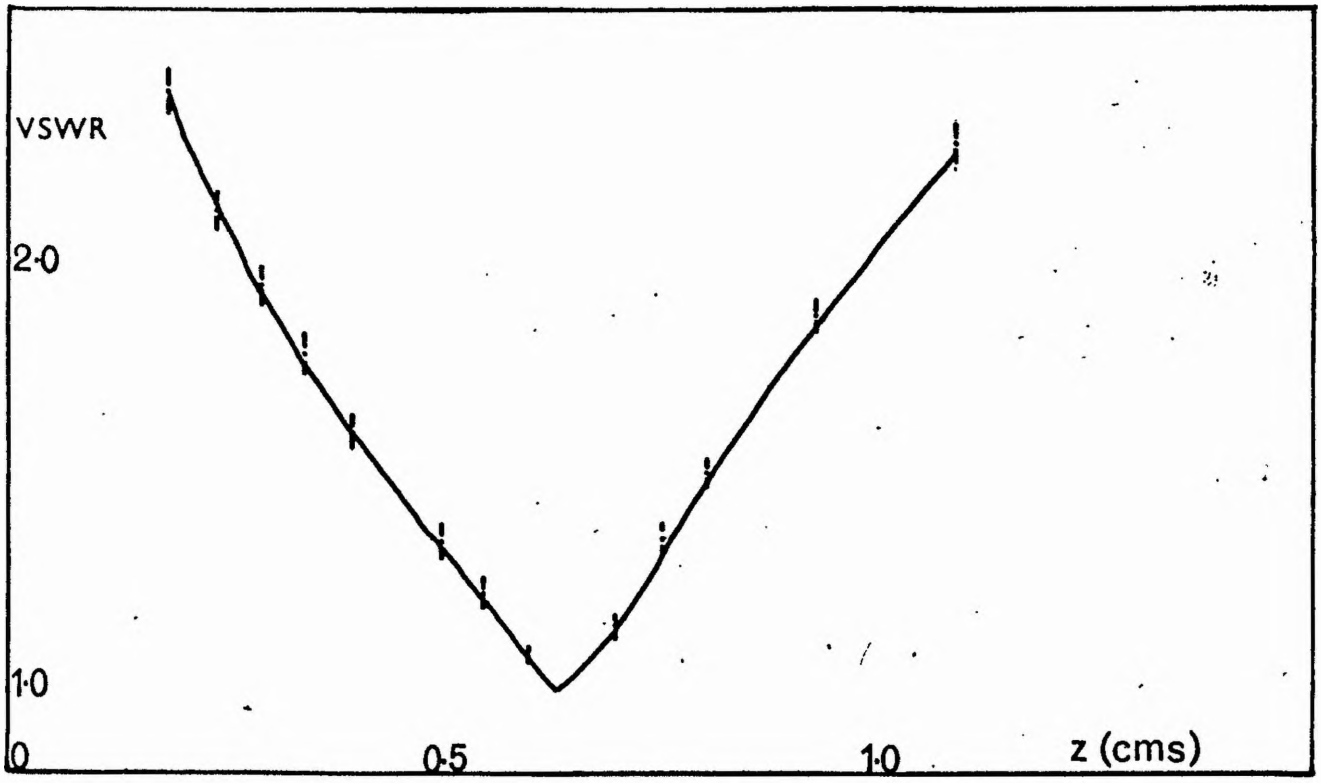

FIG 3·11 VSWR against z

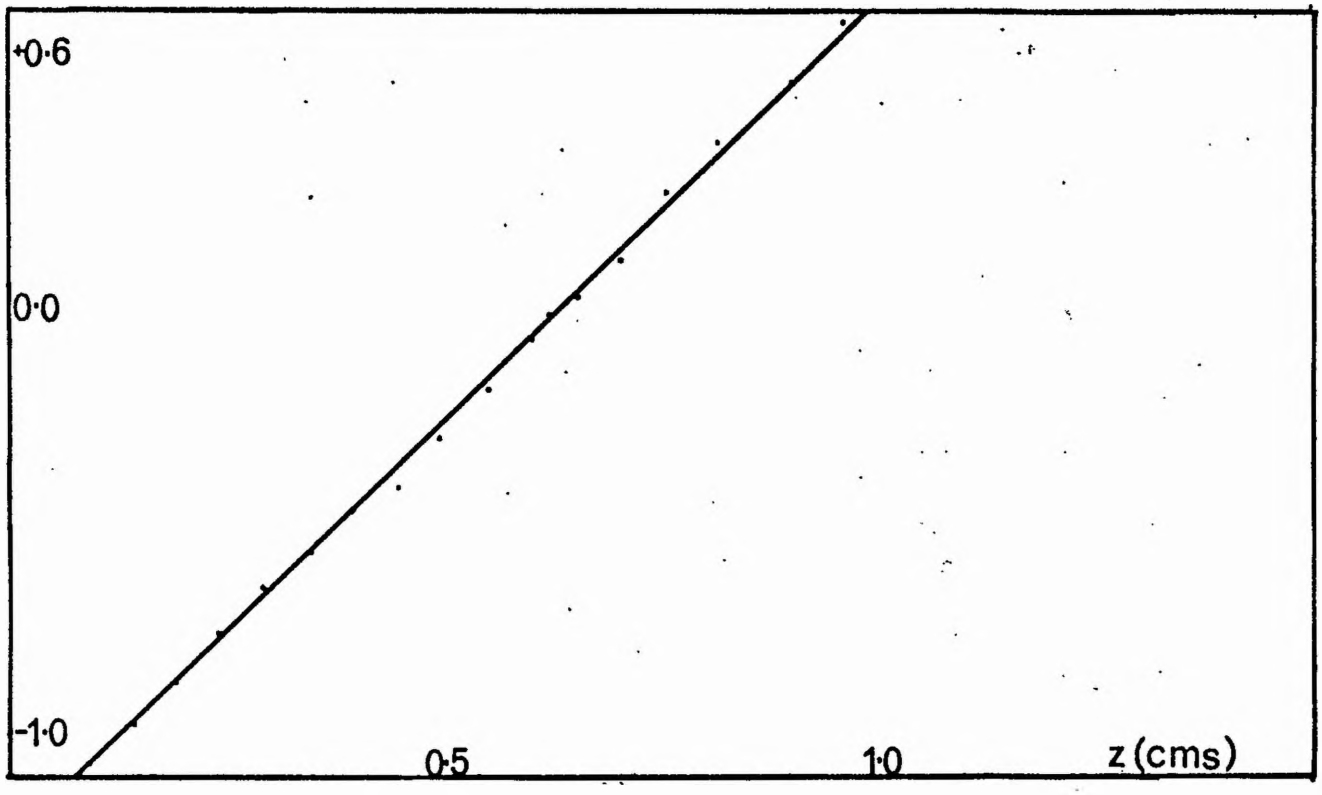

FIG 3·12 $\ln(Q_x/Q_a)_z$ vs z.

measured using the calibrated S.S.T. (§ 3.3 (h)) for different values of z. The V.S.W.R. is plotted against z in Fig. 3.11.

Over the first part of this curve, for which the cavity is O.C.

$$\text{V.S.W.R.} = \frac{Q_a}{Q_x}$$

where Q_a is the unloaded or cavity Q and Q_x is the external or coupling Q.

For the second part of the curve when the cavity becomes increasingly U.C.

$$\text{V.S.W.R.} = \frac{Q_x}{Q_a}$$

Now, for a small thin circular iris of radius r through which power is coupled from a waveguide in a dominant T.E. mode, the external Q is given by [S3]

$$\frac{1}{Q_x} = (\frac{4}{3}r^3)^2 \left|H_t\right|^2 \left|H_a\right|^2 \beta Z_o^2 \qquad (3.4.3)$$

where H_a and H_t are the magnitudes of the tangential magnetic field at the iris, within the cavity and in the waveguide, respectively, $\beta = \frac{2\pi}{\lambda_g}$ and Z_o is the wave impedance.

For the section of cut off waveguide, Λ is defined by

$$\frac{1}{\Lambda^2} = \frac{1}{4a^2} - \frac{1}{\lambda_{fs}^2} \qquad (3.4.4)$$

where a is the larger waveguide side and λ_{fs} the free space wavelength. Then, for a length z of variable coupler waveguide cut off,

$$\left|H_t\right| = \left|H_{t(o)}\right| \exp(-\frac{2\pi}{\Lambda} z)$$

$$|H_a| = |H_{a(o)}| \exp(-\frac{2\pi}{\lambda} z)$$

where $|H_{t(o)}|$ is the value of $|H_t|$ when z = 0.

Thus (3.4.3) becomes

$$\frac{1}{Q_x} = (\frac{4}{3}r^3)^2 |H_{t(o)}|^2 |H_{a(o)}|^2 \beta Z_o^2 \exp(-\frac{8\pi}{\lambda} z) \quad (3.4.5)$$

If the length of cut off waveguide required to couple the cavity critically is z_o and $(\frac{1}{Q_x})_z$ is the value of $\frac{1}{Q_x}$ for z cms cut off,

$$(\frac{1}{Q_x})_{z_o} = \frac{1}{Q_a}$$

Thus from (3.4.5)

$$(\frac{Q_x}{Q_a})_z = e^{\frac{8\pi}{\lambda}(z-z_o)} \quad (3.4.6)$$

$$\therefore \ln(\frac{Q_x}{Q_a})_z = \frac{8\pi}{\lambda}(z-z_o) \quad (3.4.7)$$

In Fig. 3.12 $\ln(\frac{Q_x}{Q_a})_z$ is plotted against z to give a fair approximation to the straight line predicted by (3.4.7). From the slope of this line,

$$\lambda = 12.8 \pm 0.8 \text{ cms}$$

for a frequency of 9325 mc/s.

From (3.4.4) with $\lambda = 12.8$ cms and f = 9325 mc/s

$$a = 1.560 \pm .005 \text{ cms} \quad (3.4.8)$$

The intention had been to make $\lambda \sim 5$ cms (i.e. $a \sim 1.40$ cms) but a slight misinterpretation of the workshop drawings led to $a = 1.60 \pm 0.01$ cms. This means that the guide should be cut off, only for

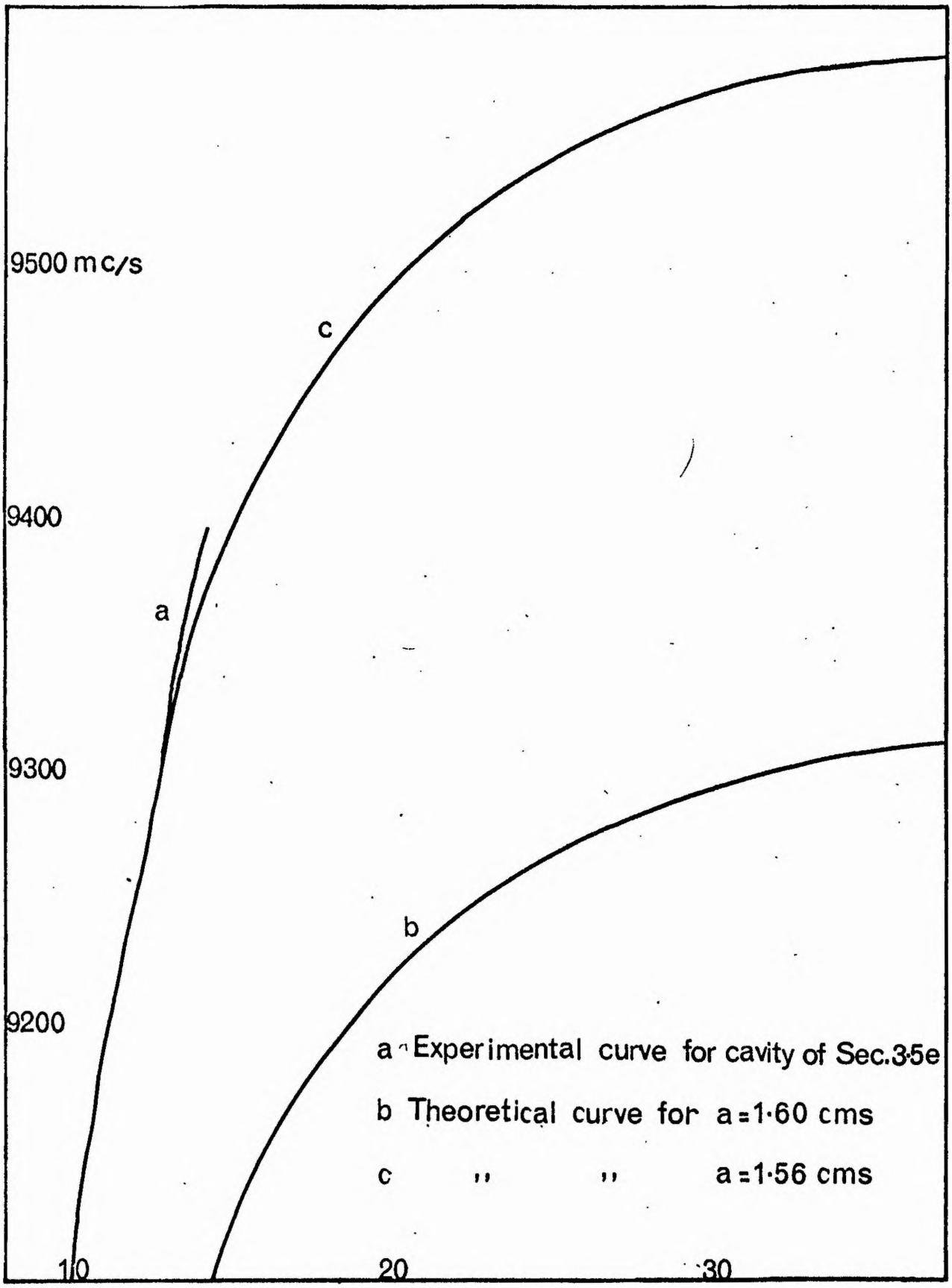

FIG 3·13 Variation of Λ with frequency

frequencies below 9350 mc/s.

The variation of Λ with frequency may be found experimentally as follows using the variable frequency cavity of § 3.5 (e). As the resonant frequency of the cavity is varied, z is adjusted to maintain critical coupling and therefore Q_x is kept constant. Over the tuning range of this cavity, the variation in frequency is less than 1% and thus changes in β can be neglected. From (3.4.5), therefore, it follows that $\Lambda \propto z$.

The measured variation in Λ with frequency for this cavity is shown in Fig. 3.13 curve (a). The curves (b) and (c) show the calculated variation in Λ for the actual value of a (1.60 cms) and the effective value (1.56 cms) respectively.

The finite conductivity of the waveguide reduces the sharpness of cut off [R5] and this is probably the reason for the discrepancy between the actual and effective values of a. This is supported by the fact that in curve (a), Λ is evidently tending to infinity more slowly than in curve (c).

The H_{011} cavity (§ 3.5 (c)) is tunable over a much wider range of frequencies but movement of the choke plunger effectively alters the position of the coupling iris relative to the axis of the cavity. It was not possible, therefore, to make quantitative measurements of using this cavity. However, the Variable Coupler continued to function up to the highest frequencies attainable by the Signal Klystron

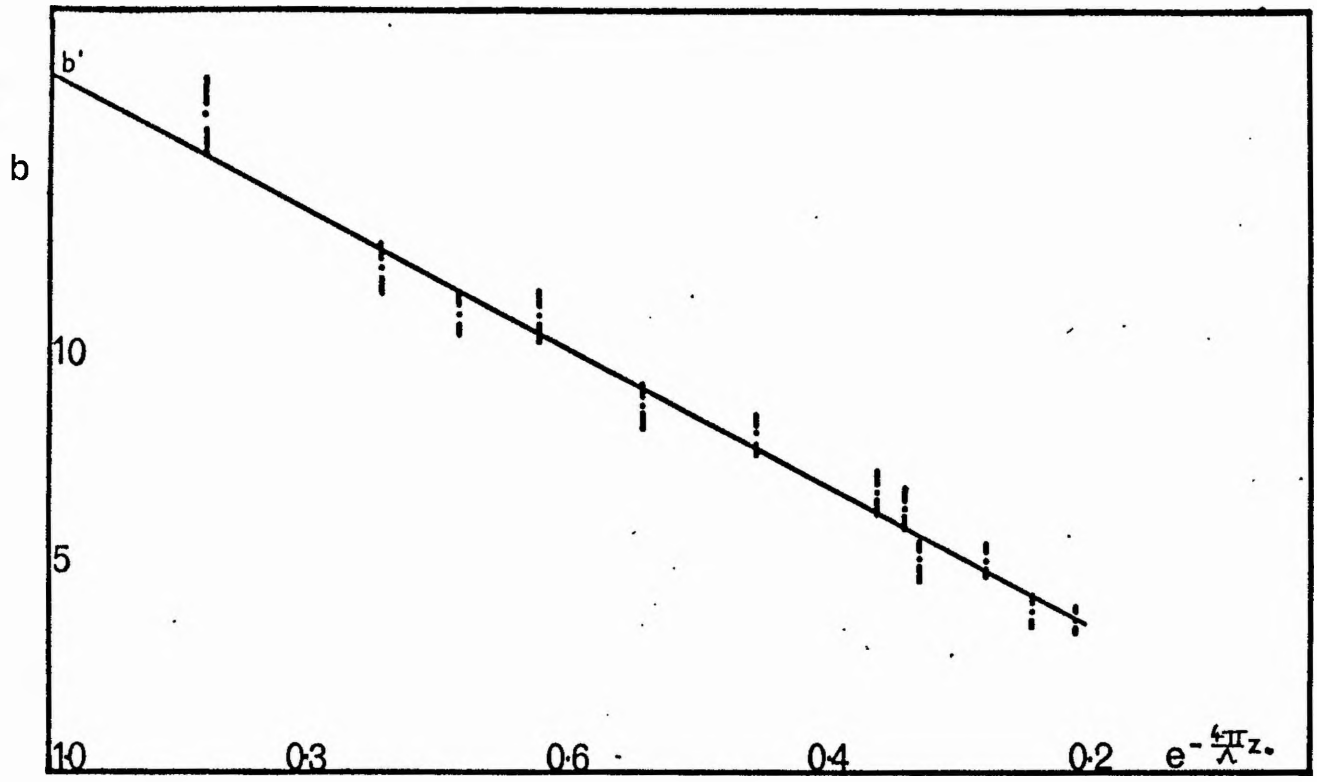

FIG 3·14 Variation of Normalised Iris Susceptance b with $e^{-\frac{4\pi}{\lambda}z}$. for a series of Irises.

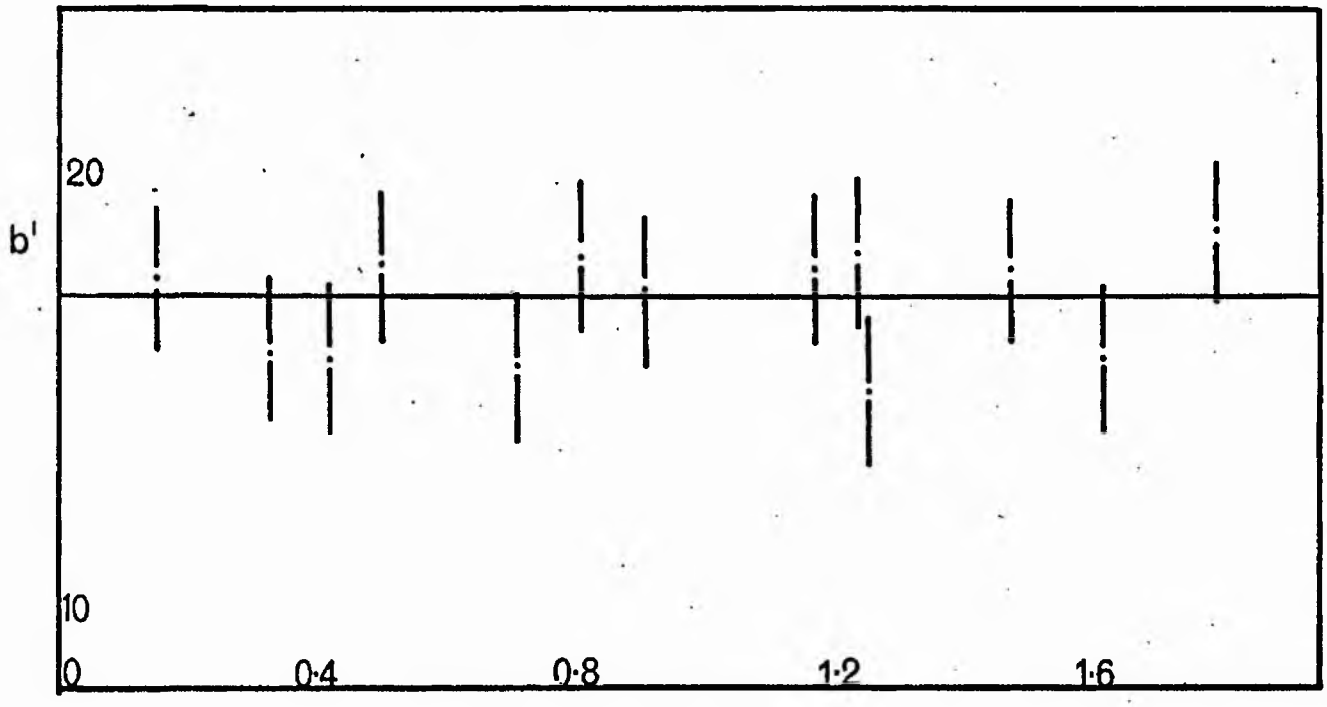

FIG 3·15 b' vs. z for a series of Irises.

(~9550 mc/s).

(i) Iris Susceptance

The normalised susceptance of a small circular iris of radius r is given by [M6], [S3]

$$b = -\frac{3}{4r^3}\,\frac{\int |H_t|^2\, da}{\beta\,|H_t|^2} \qquad (3.4.9)$$

where the integral is over the cross-section of the waveguide. When a length z of Variable Coupler waveguide is cut off, the tangential magnetic field of the iris becomes $|H_{t(o)}|\exp(-\frac{2\pi}{\lambda} z)$ and the susceptance (b'), with the Variable Coupler present, becomes

$$b' = b\exp(+\frac{4\pi}{\lambda} z) \qquad (3.4.10)$$

For each of a series of irises of different radius, b is calculated from (3.4.9), and plotted against $\exp(-\frac{4\pi}{\lambda} z_o)$ where z_o is the value of z required to produce critical coupling. This is shown in Fig. 3.14 in which the result is a fairly good approximation to a straight line, as expected from (3.4.10). The intercept corresponding to z = 0 yields b' = 17.2 from (3.4.10).

The linearity of Fig. 3.14 indicates that the correct value of λ has been used. The value of b' for each iris can be calculated from (3.4.9) and (3.4.10). A plot of b' against $\exp(-\frac{4\pi}{\lambda} z_o)$ is shown in Fig. 3.15. As the Variable Coupler has been adjusted to C.C. for each iris, the values of b' should be the same in each case, and should lie on the horizontal line in Fig. 3.15. The points in Fig. 3.15 appear

to be fairly uniformly distributed about this line which again indicates that Λ = 12.8 cms is the correct figure. When values of Λ differing by 20% from 12.8 cms were used in the calculations the points of Fig. 3.15 deviated noticeably from this line.

The fairly large scatter of points in Fig. 3.14 and particularly in 3.15 is due to difficulties in ensuring that the coupling holes were centred exactly, and to variations in Q_a owing to imperfect electrical contact with the copper foil containing the iris.

(j) Performance of Variable Coupler

The fact that the value of Λ is as high as 12.8 cms instead of the intended value of approximately 5 cms, has not proved to be a serious limitation on the range of coupling possible. The 2 cms of movement of the insert provides sufficient attenuation to increase the normalised susceptance from 3.5 to the value (17.2) for which the cavity is critically coupled.

This Variable Coupler has the advantage over one which has $\Lambda \sim$ 5 cms, that it provides a finer control in coupling. If Λ = 5 cms the above change in susceptance is produced by a movement of only 0.6 cms. Also if Λ = 5 cms the brass strips will be $\sim$ 50% thicker and reflection from the tapers is more likely to be serious. A Variable Coupler made by D. Reekie [R1] which has $\Lambda \sim$ 5 cms was, in practice, found to have a reflection which required to be balanced out using a S.S.T.

§ 3.5 Cavities

It will later be shown, (3.22.2), that the sensitivity is proportional to the filling factor (η_H) of the cavity, and also to the cavity Q, or unloaded Q, Q_a.

Now
$$\frac{1}{Q_a} + \frac{1}{Q_x} = \frac{1}{Q_l} \qquad (3.5.1)$$

where Q_x and Q_l are the external Q and the loaded Q respectively. Also at critical coupling $Q_x = Q_a$. Thus it is possible to find Q_a by measuring Q_l when the cavity is critically coupled.

The following cavities were used:-

(a) H_{102} Rectangular Cavity (Fig. 3.16)

This cavity was made by soldering a strip of brass to one end of a length of waveguide [B6]. A hole in the centre of one of the narrow sides allows a sample to be situated in the region of maximum microwave magnetic field. A length of brass tube soldered over this hole acts as a waveguide beyond cut off and prevents the loss of microwave power from the cavity. Any degree of coupling can be employed by suitable choice of coupling iris and adjustment of the Variable Coupler.

The value of Q_a for this cavity was found to be ~ 4000. This rather low Q limits the sensitivity although the requirements of the frequency stabilisation system are less severe. Also, as the cavity is thick walled, it is subject to base-line drifts caused by interaction of the d.c. magnetic field with eddy currents induced by the modulation magnetic field [F4], [B6].

(b) H_{102} Plastic Cavity (Fig. 3.17)

This was cast out of Araldite CT200 with Hardner HT901 and then silvered chemically following modifications by R. C. Hutchison of the method of Dr. I. M. Firth [F5].

This cavity, having very thin walls, is not subject to the base-line drift mentioned. However, the maximum value of Q_a was found to be ~2000. An attempt was made to thicken the silver deposit on the walls by electroplating but this appeared to give no improvement in Q.

(c) H_{011} Cylindrical Cavity (Fig. 3.18)

This is similar to a cavity described by Brown [B6] who reports that, using phase sensitive detection, no improvement in sensitivity was observed over an H_{102} rectangular cavity. This was probably due to the rather crude variable coupling system of a screw moved in front of the iris and this was sensitive to vibrations.

The Variable Coupler could not be used directly with this cavity owing to the 1" length of waveguide soldered to the cylinder. However, brass strips of the same thickness as those in the Variable Coupler were soldered to the narrow waveguide sides and a 1" length of P.T.F.E. can be joined to the Variable Coupler insert (Fig. 3.18). This means that the Variable Coupler effectively extends to the coupling aperture in the side of the cylinder.

The resonant frequency of the cavity could be varied by means of a non-contact tuning plunger. An aperture of diameter 6 mm through

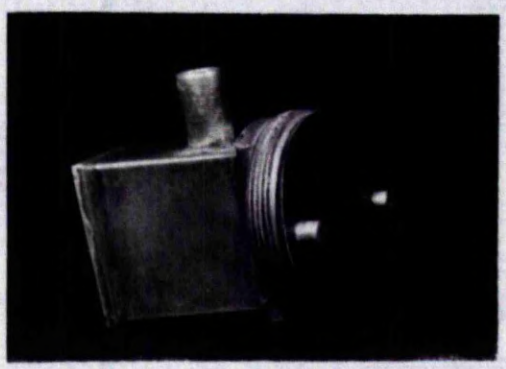

FIG 3.16 H_{102} Cavity.

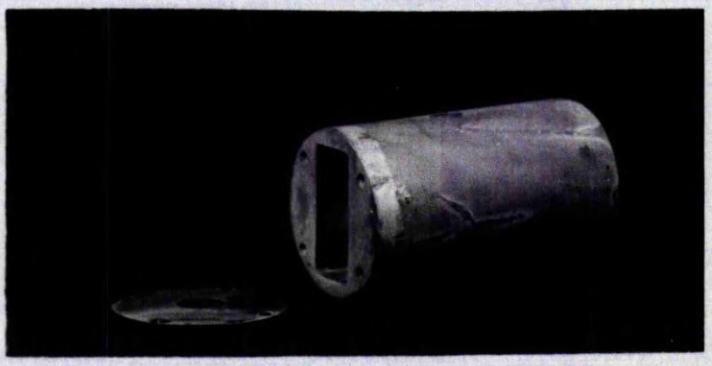

FIG 3.17 Plastic Cavity.

FIG 3.18 H_{011} Cylindrical Cavity.

this allows a sample tube to be placed in the region of maximum magnetic field i.e. along the central axis of the cylinder. A hole in the bottom of the cavity allows nitrogen at different temperatures to be blown past the sample as described in § 3.17.

This cavity has an unloaded Q ~12,000 and was used for most of the high sensitivity spectra which were recorded. It was found that, for high resolution work, in which the magnetic field modulation was 0.1-0.5 gauss, the base-line drift was unimportant.

In addition to the H_{011}, another mode occurs in this cavity but was fortunately fairly well separated from the H_{011} in frequency. The E.S.R. signal using the spurious mode is about a factor 10^3 lower than using the H_{011} mode and this can be used to identify the H_{011} mode.

(d) H_{011} Helical Cavities (Figs. 3.19 and 3.20)

The wall currents in the cylindrical part of an H_{011} cavity have no component parallel to the axis of the cavity. A cavity consisting of a closely wound coil of copper wire should therefore support the H_{011} mode. The advantages of such a cavity would be:-

(i) Suppression of undesirable modes. It is seen from the mode chart [R6] that the following modes which would be suppressed in this cavity are lower than H_{011} and could lead to spurious resonances as found in 3.5 (c):-

E_{010}, E_{110}, E_{011} and also the E_{111} which is degenerate with the H_{011}.

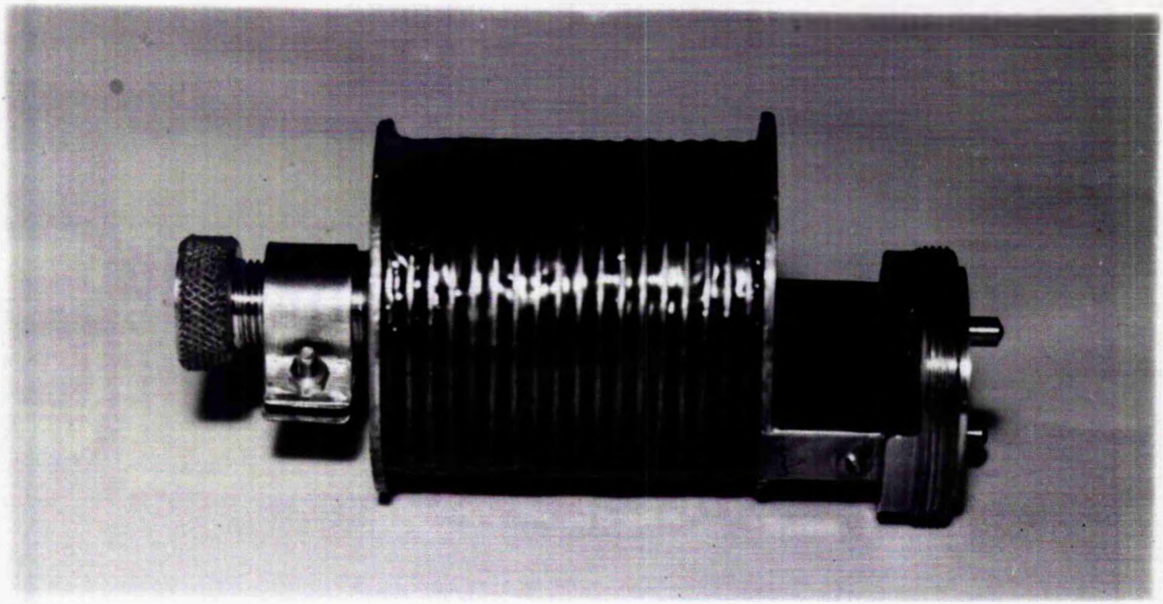

FIG 3.19 Wire Wound Cavity (12 S.W.G.).

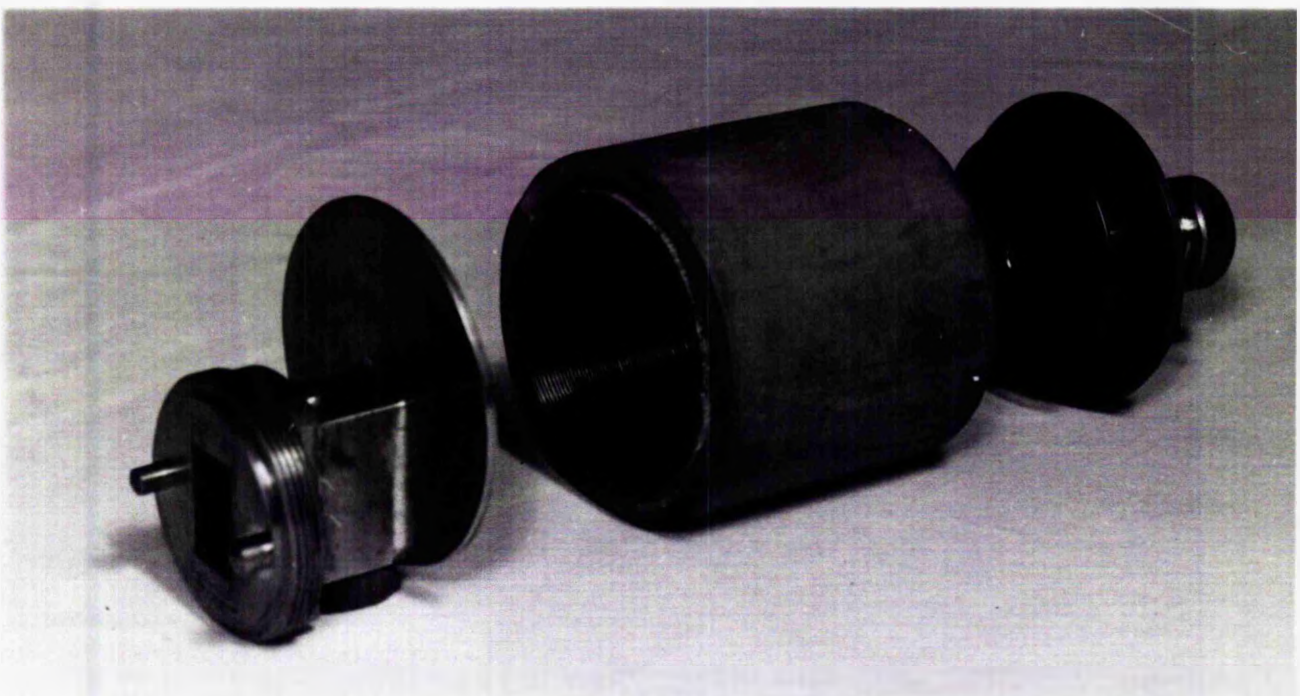

FIG 3.20 Wire Wound Cavity (18 S.W.G.).

(ii) Base-line drift should be negligible as eddy currents would virtually be eliminated.

(iii) Use in double resonance experiments (E.N.D.O.R.). As insulated wire is used in the construction of these cavities, an r.f. voltage applied between the ends of the cavity would induce an r.f. magnetic field at right angles to the d.c. magnetic field. However, this type of experiment has not been carried out.

Cavities were constructed using 12, 18 and 24 S.W.G. copper wire and 3 mm copper strip. The 12 S.W.G. cavity is shown in Fig. 3.19. In each case the wire was wound on a former and application of Araldite type 1 adhesive, with a cloth reinforcement in the 18 and 24 S.W.G. cases, produced a rigid helix. The helix of the 18 and 24 S.W.G. cavities is also supported by a wooden sleeve as shown in the exploded view of the 18 S.W.G. cavity (Fig. 3.20).

It was found that the optimum Q occurs for a diameter to length ratio smaller than the theoretical value of ~ 1.2 [R6]. This is probably due to the fact that, as the cavity is in the form of a helix, the current cannot flow such that the axial component is zero but the situation will more nearly be realised for cavities which are longer than the theoretical optimum value.

The same effect should be produced by a reduction in diameter of the wire i.e. in the pitch of the helix. In fact the 18 S.W.G. cavity

has the highest Q ($Q_a \sim 10{,}000$). For 24 S.W.G. wire the gain in Q due to a reduction in the pitch of the helix is evidently smaller than the fall in Q due to the increased resistance of the wire.

These cavities are tuned by a similar type of non-contact plunger to that used with the H_{011} cavity described in § 3.5 (c). Magnetic coupling to the waveguide is again used and, in these cavities, is effected by means of an aperture at a position mid-way between the centre and the edge of the end of the cavity. The length of waveguide projecting from the end of the cavity (Figs. 3.19 and 3.20) is adapted for use with the Variable Coupler as described for the H_{011} cavity § 3.5 (c).

The main drawback with these cavities is the (slight) microwave leakage which occurs between the turns of the helix. Any movements near the cavities cause a slight variation in coupling. This effect can be reduced by wrapping a lossy material such as sisal round the outside of the cavities which improves the variations in coupling without significantly affecting Q_l.

(e) H_{102} Cavity with Aqueous Cell

Many free radicals require to be examined in aqueous solution or in other solvents of high dielectric constants. The sample cell in these conditions should have a high magnetic filling factor (η_u) without having high dielectric losses.

In an H_{102} cavity (Fig. 3.21), the magnetic field has an antinode

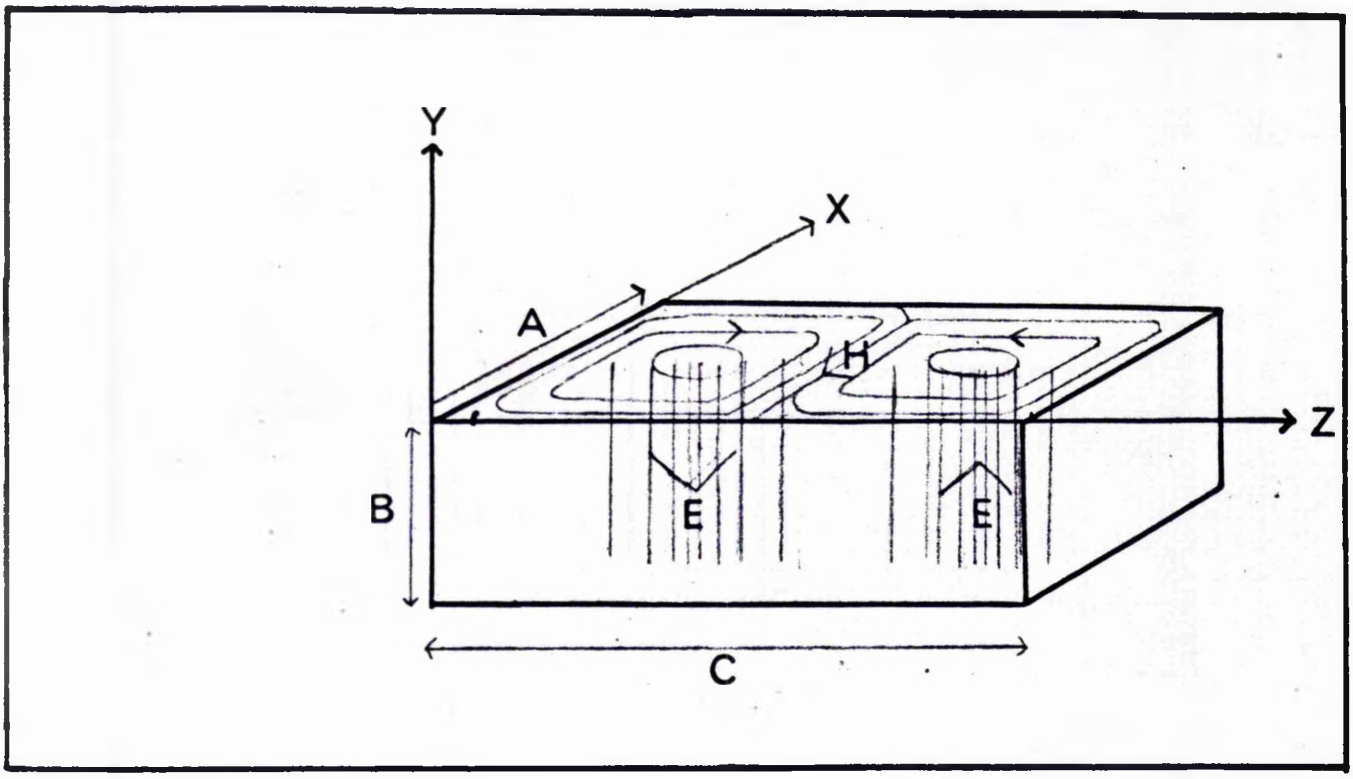

FIG 3·21 H_{102} Cavity.

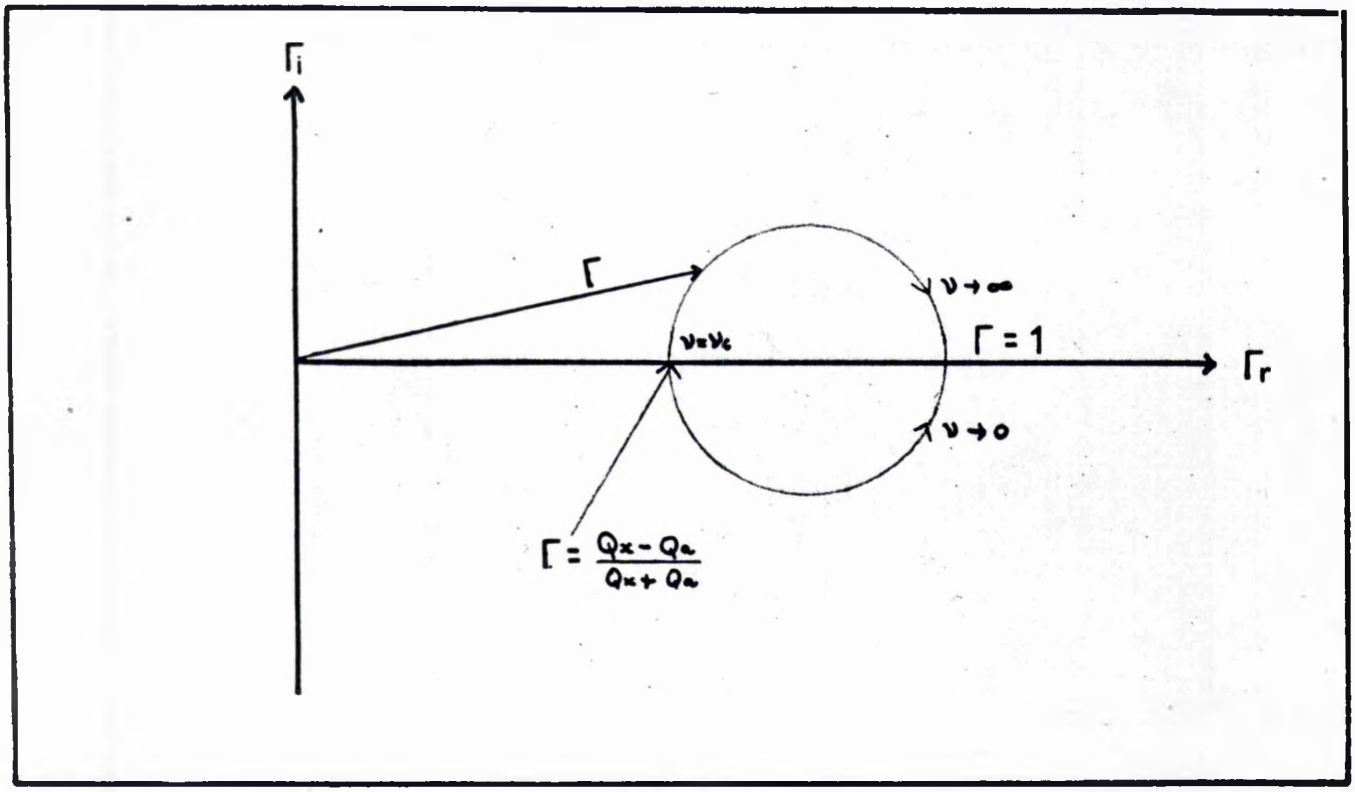

FIG 3·22 Variation Γ_i and Γ_r with frequency.
ν_c is the cavity resonant frequency.

and the electric field a node at the centre of the cavity. Thus the region of maximum magnetic filling factor, η_H , is also the region where η_E is minimum, where

$$\left.\begin{aligned}\eta_H &= \frac{\int_{\text{sample}} H^2 \, d\tau}{\int_{\text{cavity}} H^2 \, d\tau} \\ &= \frac{\int_S E^2 \, d\tau}{\int_C E^2 \, d\tau}\end{aligned}\right\} \qquad (3.5.2)$$

For aqueous or other lossy solutions, the dielectric loss is proportional to η_E , and according to Feher [F4] should be such that Q_l is reduced to two thirds of its empty cavity value.

If
$$\frac{1}{Q_a} = \frac{1}{Q_d} + \frac{1}{Q_w} \qquad (3.5.3)$$

where Q_w and Q_d represent the losses in the cavity walls and the dielectric losses in the sample respectively, (including any other dielectric losses in Q_w i.e. for the empty cavity $Q_w = Q_a$) then from (3.5.1)

$$Q_d = 2Q_w \qquad (3.5.4)$$

The value of Q_w obtained by evaluating the appropriate integrals may be inaccurate as the conductivity of the silvered brass walls of the cavity is uncertain. Also, contributions to Q_w may arise from the imperfect contact of the coupling iris with the end of the cavity.

Stoodley and others [S4], [H2], [P5] have used flat cells for aqueous solutions in order to improve sensitivity. Stoodley's calculations of optimum sensitivity involved the comparison of wall and

dielectric losses.

It has been found in practice that, using a 1 mm diameter sample tube centrally placed in an H_{102} cavity, that the dielectric loss of (3.5.4) is produced by ~ 0.01 ccs. In calculating the effects of using a flat cell, therefore, the dielectric losses are compared with this situation in which the approximation is made of considering the tube to be of square instead of circular cross section.

In calculations on a cavity containing a small lossy sample [S4], it has been shown that the "empty cavity" approximation leads to results which agree to within 2% with more accurate calculations and this is the method employed here.

Fig. 3.21 shows an H_{102} cavity of sides A, B and C. The field equations in the cavity are as follows [R6],

$$\left.\begin{aligned} H_x &= \frac{2\pi^2}{ACK^2} \sin\frac{\pi x}{A} \cos\frac{2\pi z}{C} \\ H_y &= 0 \\ H_z &= -\frac{\pi^2}{A^2K^2} \cos\frac{\pi x}{A} \sin\frac{2\pi z}{C} \\ E_x &= E_z = 0 \\ E_y &= \frac{\pi}{AK} \sin\frac{\pi x}{A} \sin\frac{2\pi z}{C} \end{aligned}\right\} \qquad (3.5.5)$$

where

$$K^2 = \left(\frac{\pi}{A}\right)^2 + \left(\frac{2\pi}{C}\right)^2 \qquad (3.5.6)$$

From (3.5.2),

$$\eta_H = \frac{\iiint_S (H_x^2 + H_z^2)\, dx\, dy\, dz}{\iiint_C (H_x^2 + H_y^2)\, dx\, dy\, dz} = \frac{I_H}{II_H} \qquad (3.5.7)$$

$$\eta_E = \frac{\iiint_S (E_y^2)\, dx\, dy\, dz}{\iiint_C (E_y)^2\, dx\, dy\, dz} = \frac{I_E}{II_E} \qquad (3.5.8)$$

On integrating it is found that,

$$II_H = \frac{8B\pi^4}{A^2K^4}\left(\frac{A}{8C} + \frac{C}{32A}\right) \qquad (3.5.9)$$

$$II_E = \frac{\pi^2 BC}{4AK^2} \qquad (3.5.10)$$

Assuming a sample of rectangular cross-section and sides 2a, 2b and 2c it is found that,

$$I_H = \frac{2b\pi^4}{A^2K^4}\left[\frac{4}{C^2}\left(a + \frac{A}{2\pi}\sin\frac{2\pi a}{A}\right)\left(c + \frac{C}{4\pi}\sin\frac{4\pi c}{C}\right)\right.$$

$$\left. + \frac{1}{A^2}\left(a - \frac{A}{2\pi}\sin\frac{2\pi a}{A}\right)\left(c - \frac{C}{4\pi}\sin\frac{4\pi c}{C}\right)\right] \qquad (3.5.11)$$

$$I_E = \frac{2\pi^2 b}{A^2K^2}\left(c - \frac{C}{4\pi}\sin\frac{4\pi c}{C}\right)\left(a + \frac{A}{2\pi}\sin\frac{2\pi a}{A}\right) \qquad (3.5.12)$$

Taking A = 2.54 cms, B = 1.27 cms, C = 4.07 cms it follows from (3.5.6) that for a frequency 9340 mc/s, $K^2 = 3.96$.

In the case of the 0.01 ccs sample with b = c = 0.05 cms, a = 0.5

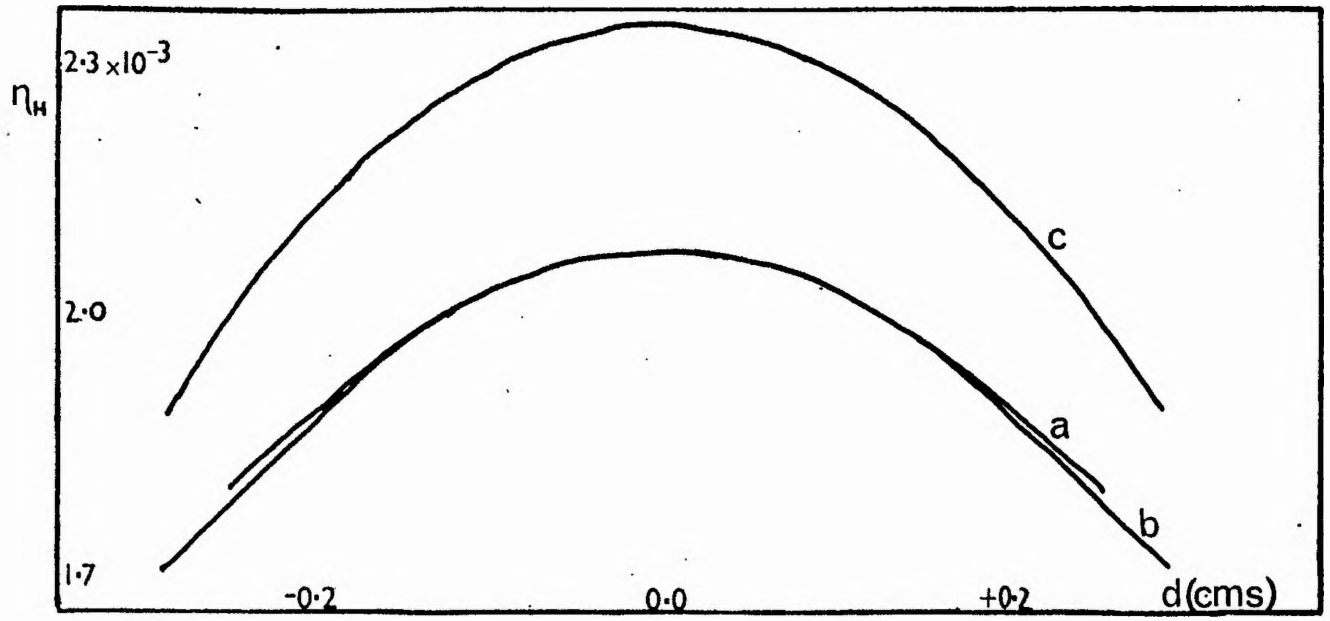

FIG 3·23 Variation of η_H for displacement of cells a, b and c from H antinode. Curve c is $\eta_H/5$.

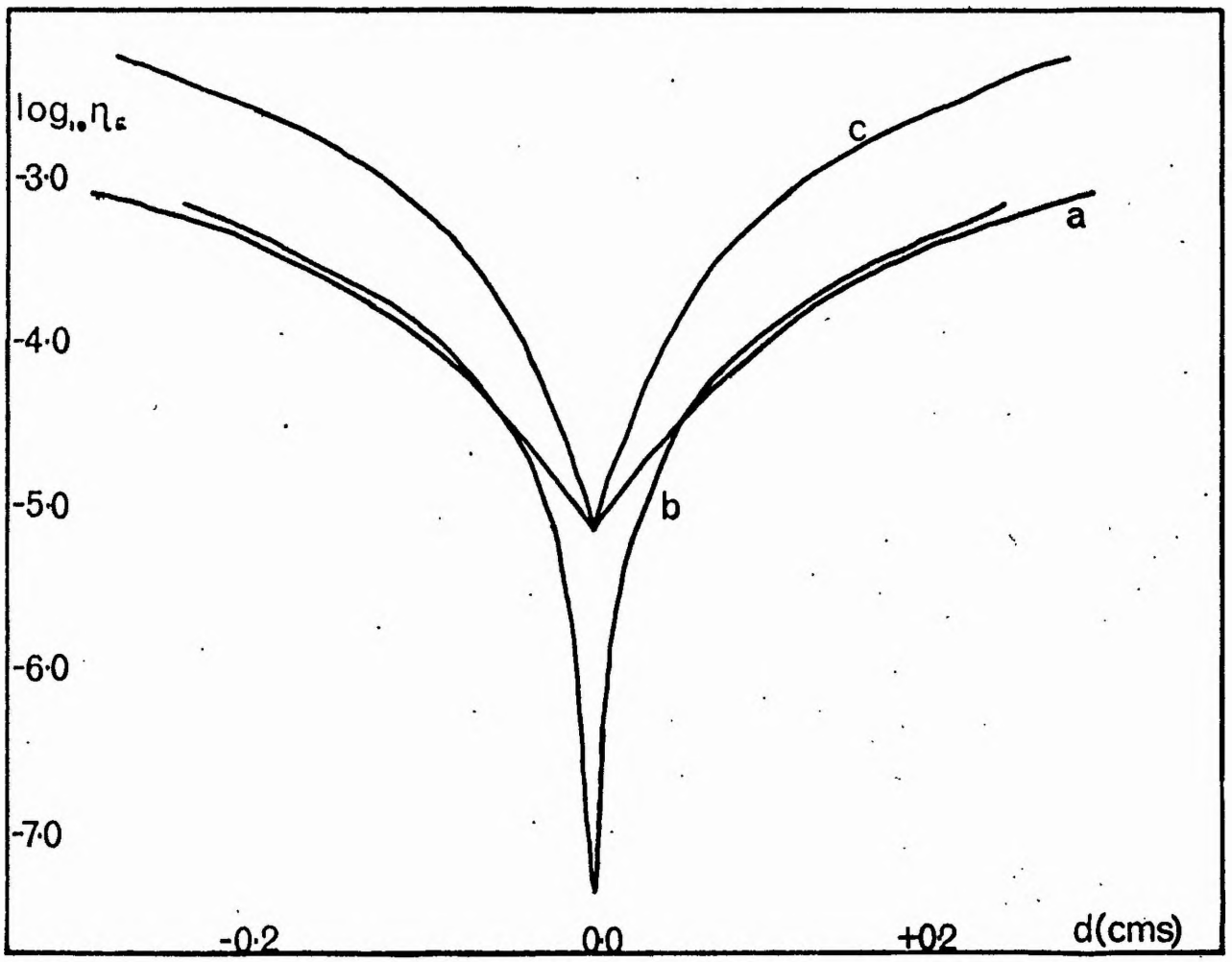

FIG 3·24 Variation of η_c for cells a, b and c.

cms, from (3.5.7-12),

$$\eta_H = 2.08 \times 10^{-3} \qquad (3.5.13)$$

$$\eta_E = 3.55 \times 10^{-5} \qquad (3.5.14)$$

Now consider a flat cell which has 2a = A, 2b = B and the same value of η_H (2.08×10^{-3}) as in (3.5.13). In this case it is found that c = 0.0035 cms and therefore from (3.5.12), $\eta_E = 2.0 \times 10^{-7}$. Thus the dielectric losses are reduced by a factor $\sim$ 200 until they are negligible compared with wall losses.

From (3.5.8, 10 and 12), 2c must be increased to $\sim$ 0.038 cms for $\eta_E = 3.55 \times 10^{-5}$ as in (3.5.14). This sample thickness is in fairly good agreement with the value $\sim$0.031 cms found by Stoodley [84] representing optimum sensitivity for a similar type of cell. The corresponding value of $\eta_H = 1.08 \times 10^{-2}$ which represents an increase by a factor $\sim$5 over (3.5.13).

The effect on η_H and η_E of a displacement (d) of the sample cell from the electric field node is shown in Figs. 3.23 and 3.24. The curves (a), (b) and (c) correspond to the three cells above respectively.

From Fig. 3.23 it is evident that η_H does not vary much with d. Thus for non-lossy solvents, the position of the sample is not critical. Curve (c) here corresponds to $\eta_H/5$.

From Fig. 3.24 it is seen that the value of d is of much greater importance in determining η_E than η_H. For the flat cells, curves (b) and (c), the cell position is more critical than is the case for (a).

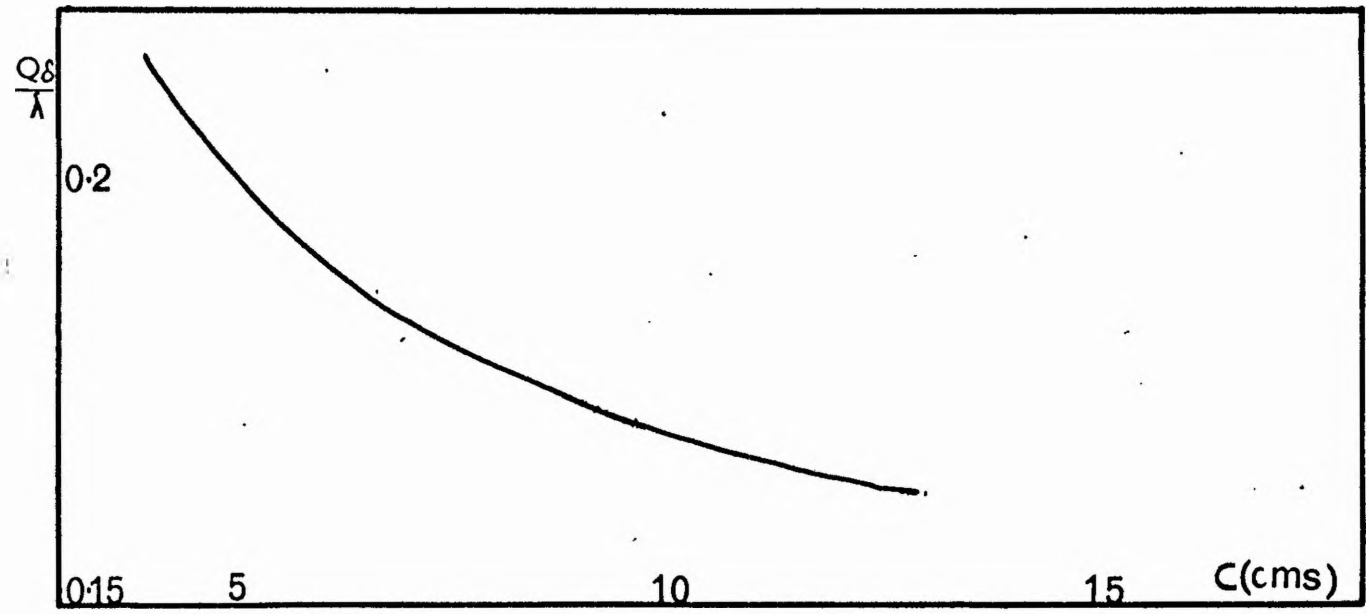

FIG 3·25 Dependence of Q on Cavity Length for H_{102} Cavity at 9340 mc/s.

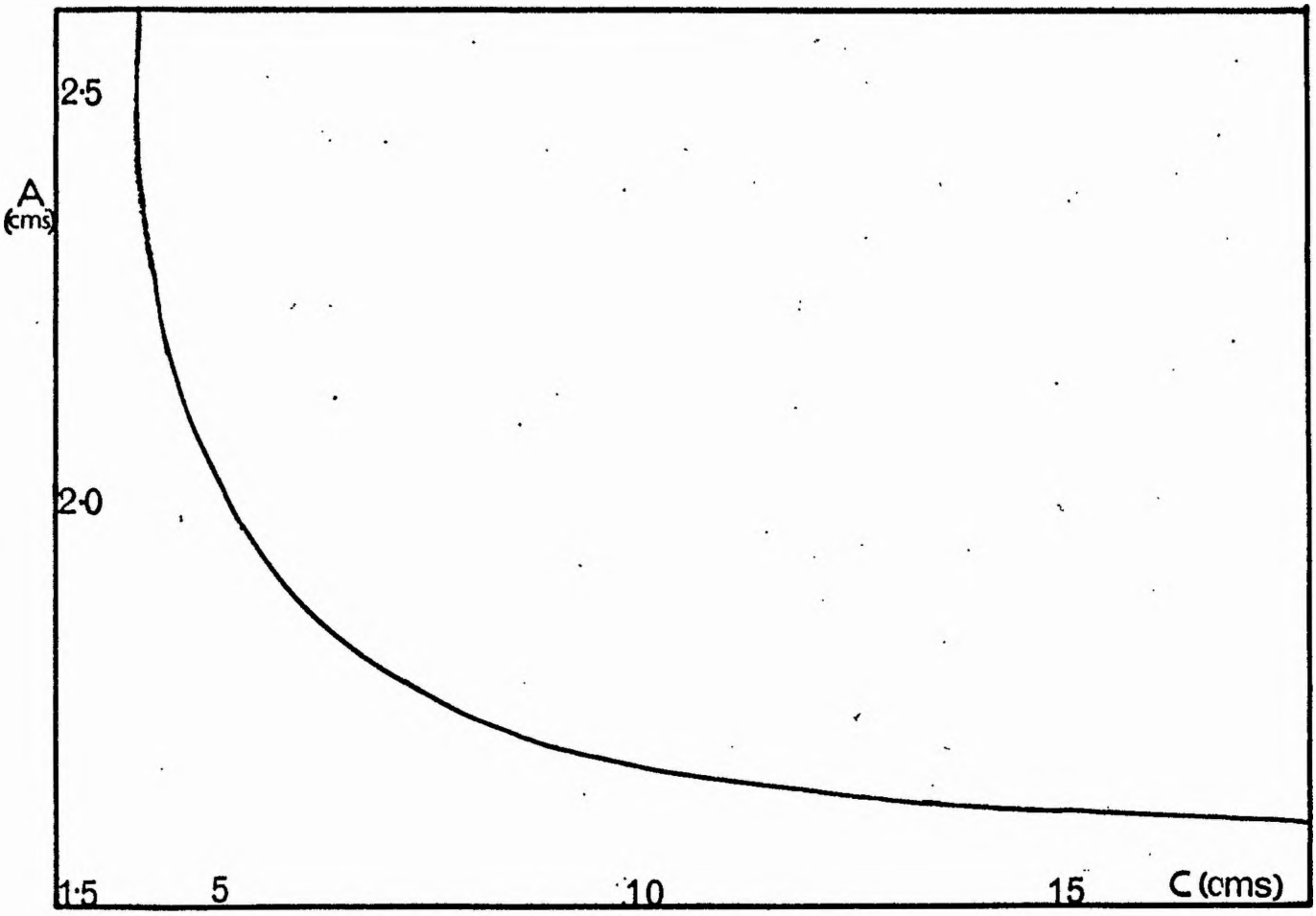

FIG 3·26 Curve relating H_{102} Cavity dimensions at 9340 mc/s.

The difficulties of making a cell of the required dimensions and of positioning it correctly would be reduced considerably if the cavity length and the cell thickness could be increased, the cavity still resonating in the H_{102} mode.

The relationship connecting the cavity dimensions and its resonant frequency are as follows,

$$\frac{4}{\lambda_{fs}^2} = \frac{1}{A^2} + \frac{4}{C^2} \qquad (3.5.15)$$

where λ_{fs} is the wavelength in free space. If A is reduced by inserting a brass strip inside the cavity, C must be increased in order that the cavity resonates at the same frequency. The relation between A and C for a frequency 9340 mc/s is shown in Fig. 3.26. It is also undesirable that there should be an appreciable reduction in Q_w on increasing C. For an H_{102} cavity, where δ is the skin depth, [R6],

$$\frac{Q_w \delta}{\lambda_{fs}} = \frac{ABC}{2} \frac{(\frac{1}{A^2} + \frac{4}{C^2})^{3/2}}{\frac{C}{A^2}(A + 2B) + \frac{4A}{C^2}(C + 2B)} \qquad (3.5.16)$$

From Fig. 3.25 it is seen that in increasing the cavity length to 10 cms the quantity $\frac{Q_w \delta}{\lambda_{fs}}$ and thus Q_w is reduced by $\sim$20%. This figure will be smaller if a significant contribution is present from the iris contact.

Two cavities were constructed of lengths 12.9 cms and 11.0 cms. Fig. 3.30 shows the shorter with an aqueous flow cell in position. It is necessary to be able to place the sample tube in the region of minimum electric field. It was thought that even for the lengthened

cavities, a mechanical control for this might be too coarse. Also a wide slit would be required in the cavity to allow for this movement. As the brass strip was brazed in position it is possible that A varies from one end of the cavity to the other i.e. the electric field node may not occur at the measured centre and this may lead to the slit being extended further in one direction to position the cell correctly.

The adjustment of the cell relative to the electric field node is made by tuning the resonant frequency of the cavity by means of a quartz rod. This alters the effective length of the cavity and shifts the position of the node.

The variation in position of the electric field node is investigated as follows. The cavity containing the empty cell (thickness $\sim$0.08 cms) shown in Fig. 3.30 is first critically coupled by means of the variable coupler. It is checked that this condition is maintained throughout the range of frequency controlled by the quartz rod tuning. With water in the cell, the magic Tee containing the cavity arm is balanced by means of the calibrated S.S.T. in the opposite arm. The V.S.W.R. resulting from dielectric loss in the aqueous sample is found as described in § 3.3 (i). Fig. 3.27 shows the V.S.W.R. as a function of the resonant frequency of the cavity and the corresponding distance of the electric field node from the cell is calculated assuming that for minimum V.S.W.R., this distance is zero.

With no sample in the cavity any dielectric losses present are

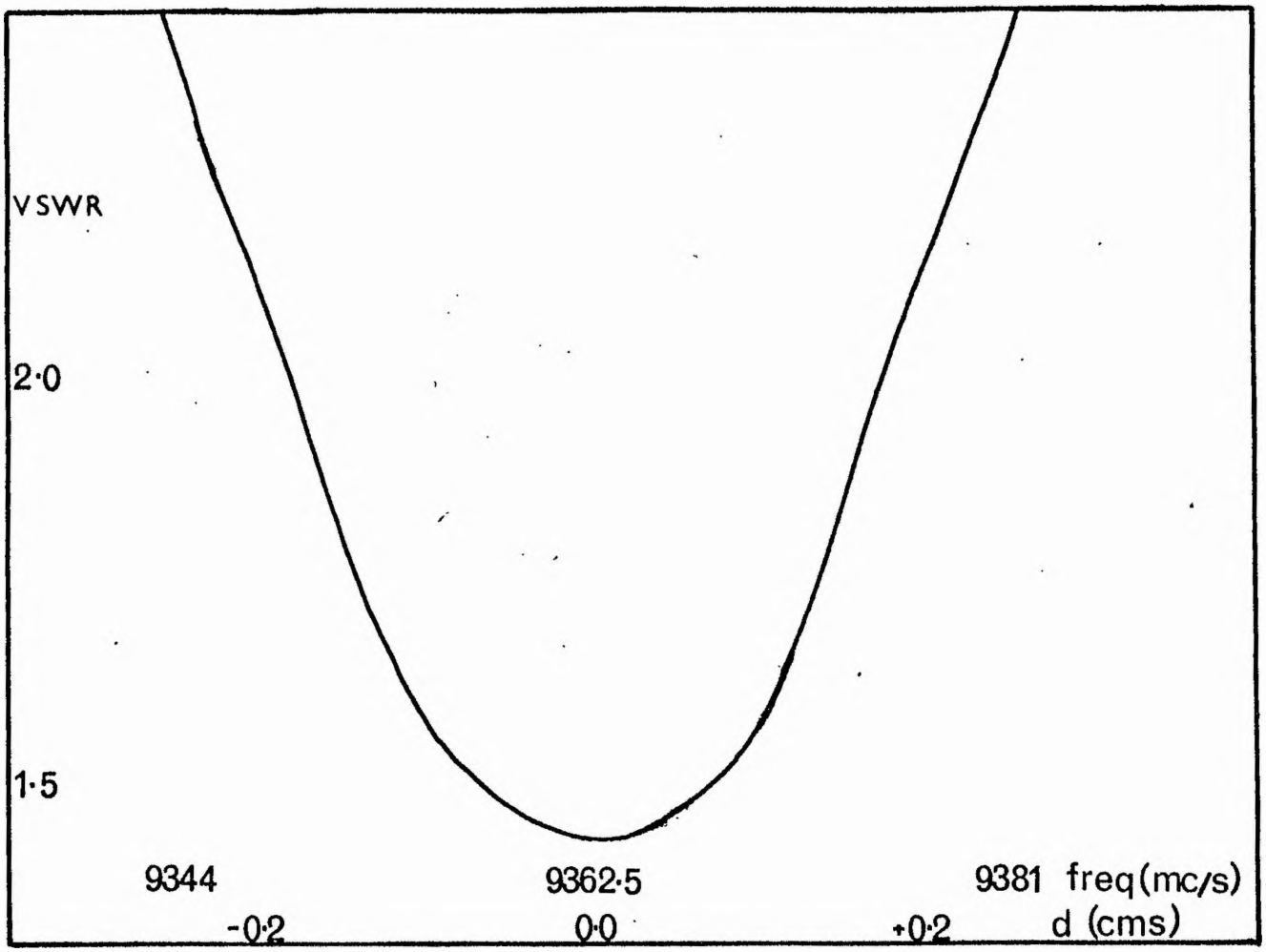

FIG 3·27 VSWR vs cavity resonant frequency and cell displacement for 0·08 cm flat cell.

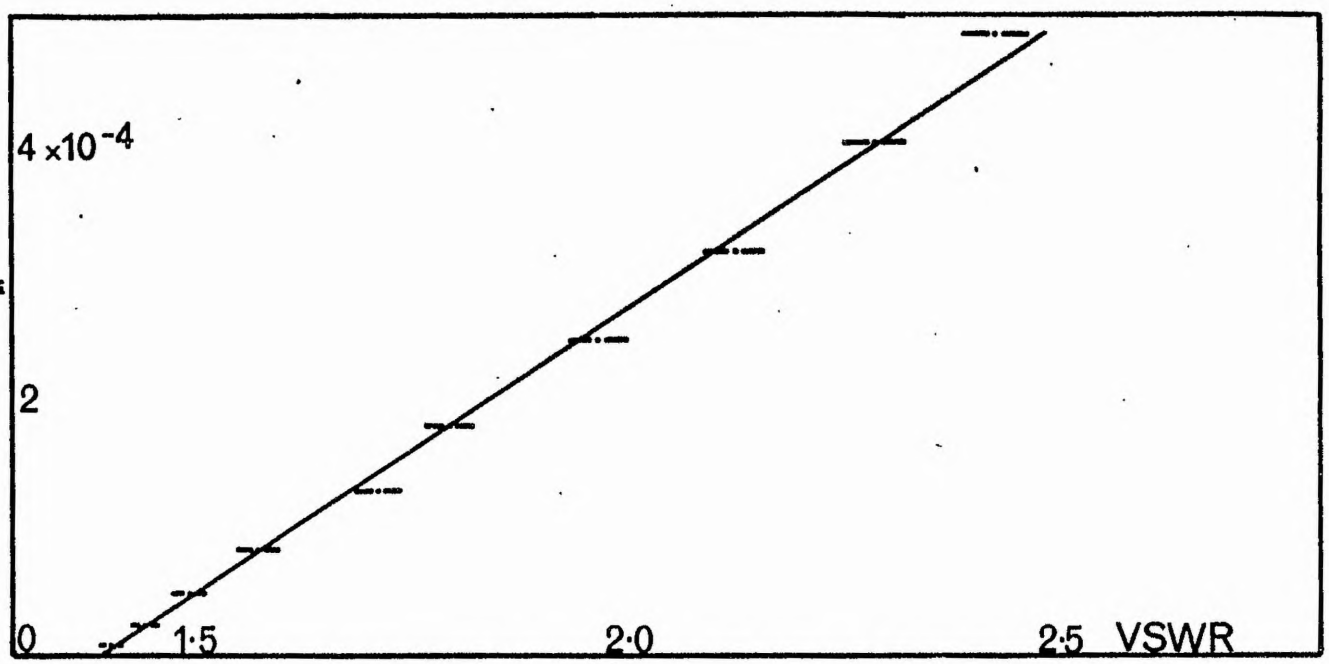

FIG 3·28 Relation between calculated and measured dielectric loss.

taken as being included in Q_w. For critical coupling, therefore, since Q_w is equal to Q_a for the empty cavity

$$Q_x = Q_w \qquad (3.5.17)$$

Now, since the coupling of the cavity and therefore Q_x remains unchanged throughout Fig. 3.27, the changes in V.S.W.R. are caused by the term in Q_d of (3.5.3).

From (3.5.3 and 17), $Q_a \leqslant Q_x$, the equality sign representing the situation where $\frac{1}{Q_d} = 0$, and otherwise the cavity is undercoupled.

$$\therefore \text{V.S.W.R.} = \frac{Q_x}{Q_a} = Q_w\left(\frac{1}{Q_w} + \frac{1}{Q_d}\right)$$

$$\therefore \text{V.S.W.R.} - 1 = \frac{Q_w}{Q_d} \qquad (3.5.18)$$

$\frac{1}{Q_d}$, and thus the V.S.W.R., is proportional to the measured dielectric loss and η_E is proportional to the calculated loss. In Fig. 3.28 η_E is plotted against V.S.W.R. and the resulting curve is linear, within the limits of experimental error, as predicted. The values of η_E and V.S.W.R. in Fig. 3.28 are related for equal distances of the cell from the E-node (from Fig. 3.27 and the equivalent curve of Fig. 3.24 for a 0.08 cm thick cell in the 11 cm cavity).

From (3.5.4 and 18), the minimum of Fig. 3.27 in the optimum sensitivity case, should correspond to a V.S.W.R. of 1.5. For any lossy sample in any cavity, then, this forms a convenient criterion for optimum sample size and it is also more accurate to couple the empty cavity

critically and then measure the V.S.W.R. when the sample is present, than it is to compare the value of Q_a in the two cases. The fact that, for the cell of Fig. 3.27, the minimum occurs at a V.S.W.R. of ~ 1.42 implies that this cell is slightly smaller than optimum.

The sample cells were made by drawing out a glass tube over a piece of copper foil of the requisite inside dimensions. The cells produced are thin walled and rather fragile. An improvement might result from the use of quartz cells which could have thicker walls without increasing dielectric losses.

The H_{102} lengthened cavities, while not offering an improvement in theoretical sensitivity over the flat cell normal length cavities, have certain advantages. The adjustment to make the E-node coincide with the cell is less critical than for normal length cavities by a factor equal to the ratio of lengths, and the manufacture of cells of the optimum dimensions is also considerably simpler. This more than compensates for the slight fall in Q predicted by Fig. 3.25.

In practice this cavity has been found to have a sensitivity which is slightly higher than the H_{011} cavity (§ 3.5 (c)). This is in agreement with Stoodley's calculation that in the optimum conditions, the sensitivity for aqueous solution in an H_{011} cavity is about two thirds that of a flat cell in an H_{102} cavity.

The lengthened H_{102} cavity would appear to have advantages in particular for the study of biological systems where larger sample

volumes are sometimes necessary.

§ 3.6 I.F. Amplifiers

The signal channel electronics consist of a Decca 30 mc/s Pre-amplifier (type 30/14/P) with a balanced input, and a Decca 30 mc/s Amplifier (type 30/18/M). The Signal I.F. Pre-amplifier output is fed to the signal input of the Phase Sensitive Detector and to the Signal I.F. Amplifier whose output is fed to one of the detection schemes of § 3.11 or 3.13. The Pre-amplifier, balanced mixer and Magic Tee (2) consists of one rigid unit which eliminates the necessity for coaxial leads.

The noise figure of the signal channel I.F. amplifiers was measured using a noise generator and was found to be optimum (~ 3 db) for maximum gain of the Pre-amplifier. This, therefore, is always operated on maximum gain (~ 55 db), care being taken to ensure that the cavity coupling is sufficiently nearly critical to avoid saturating the Pre-amplifier. The Signal I.F. Amplifier gain may be varied by applying a positive cathode bias to the second stage. Under normal conditions a gain ~ 25 db is used.

The reference channel electronics consist of a Decca 30 mc/s Amplifier (type 30/18/M) which amplifies the signal from the Reference Tee (4) and feeds it into the reference input of the P.S.D. and also into the L.O.A.F.C. unit. It was found convenient to operate the Reference I.F. Amplifier on maximum gain (~ 60 db) as its input from the Reference

crystal can be varied by means of Attenuator (3) (Fig. 3.1).

The bandwidth of the Signal I.F. Pre-amplifier is narrower than specified and also the centre frequency is displaced slightly from 30 mc/s. However sufficient overlap of the pass bands occurs to give the fairly satisfactory noise figure of 3 db.

§ 3.7 Stabilisation of Signal Klystron

(a) Necessity for Stabilisation

There are several reasons that require the Signal Klystron frequency (ν) to be stabilised to the resonant frequency of the cavity (ν_c).

(i) In a spectrometer employing a microwave bridge and I.F. amplifiers operated on high gain, any unbalance of the bridge causes the increased input to saturate the I.F. amplifiers. This unbalance occurs if the Signal Klystron is allowed to drift from the cavity resonant frequency.

(ii) In order to observe a pure absorption signal, the microwave bridge must be balanced in phase i.e. $\nu = \nu_c$, exactly. Thus a drift in frequency from the value ν_c will produce a phase unbalance in the bridge and the E.S.R. signal will contain a mixture of absorption and dispersion.

(iii) Viewed from the detuned open position, the cavity may be considered as a series L-C circuit, [G3], [G4] having resistance R_1 associated with L, and resonant at a frequency ν_c. If the cavity contains a paramagnetic sample with an effective complex r.f. susceptibility, $\chi = \chi' + j\chi''$, (where is the filling factor times the bulk susceptibility) then the impedance of the circuit is, [K3]

$$Z = R_1 + 8\pi^2\chi''\nu L + j8\pi^2\nu L\chi' + j(2\pi\nu L - \frac{1}{2\pi\nu C}) \quad (3.7.1)$$

When $\nu = \nu_c$, the imaginary part of Z is zero and thus from (3.7.1),

$$\nu_c^2 = \frac{1}{4\pi^2 LC} - \frac{\chi'}{\pi L^2 C} \quad (3.7.2)$$

Owing to the variation in χ' in passing through the E.S.R. line, it follows from (3.7.2) that there is an associated variation in the resonant frequency of the cavity. Therefore, unless the Signal Klystron is locked to ν_c during this variation, $\nu - \nu_c$ will no longer be exactly zero throughout and the observed E.S.R. signal will contain dispersion. The compensation for this dispersion is one advantage of the present type of stabilisation system over one which does not lock the Klystron to the cavity frequency. In fact the amount of dispersion involved is small unless a large number of spins is involved.

The variation in ν_c may be demonstrated by locking the klystron to ν_c and monitoring the wavemeter output on the oscilloscope while sweeping through the E.S.R. line at 50 c/s. The resulting dispersion-type curve corresponds to the klystron frequency "tracking" the variation of the cavity frequency. Fig. 3.31 shows the wavemeter output for 10^{18} spins of D.P.P.H.

(b) The Stabilisation System

The method of achieving the stabilisation of the Signal Klystron is based on the Pound system [P2] and is very similar to that used by Brown [B6].

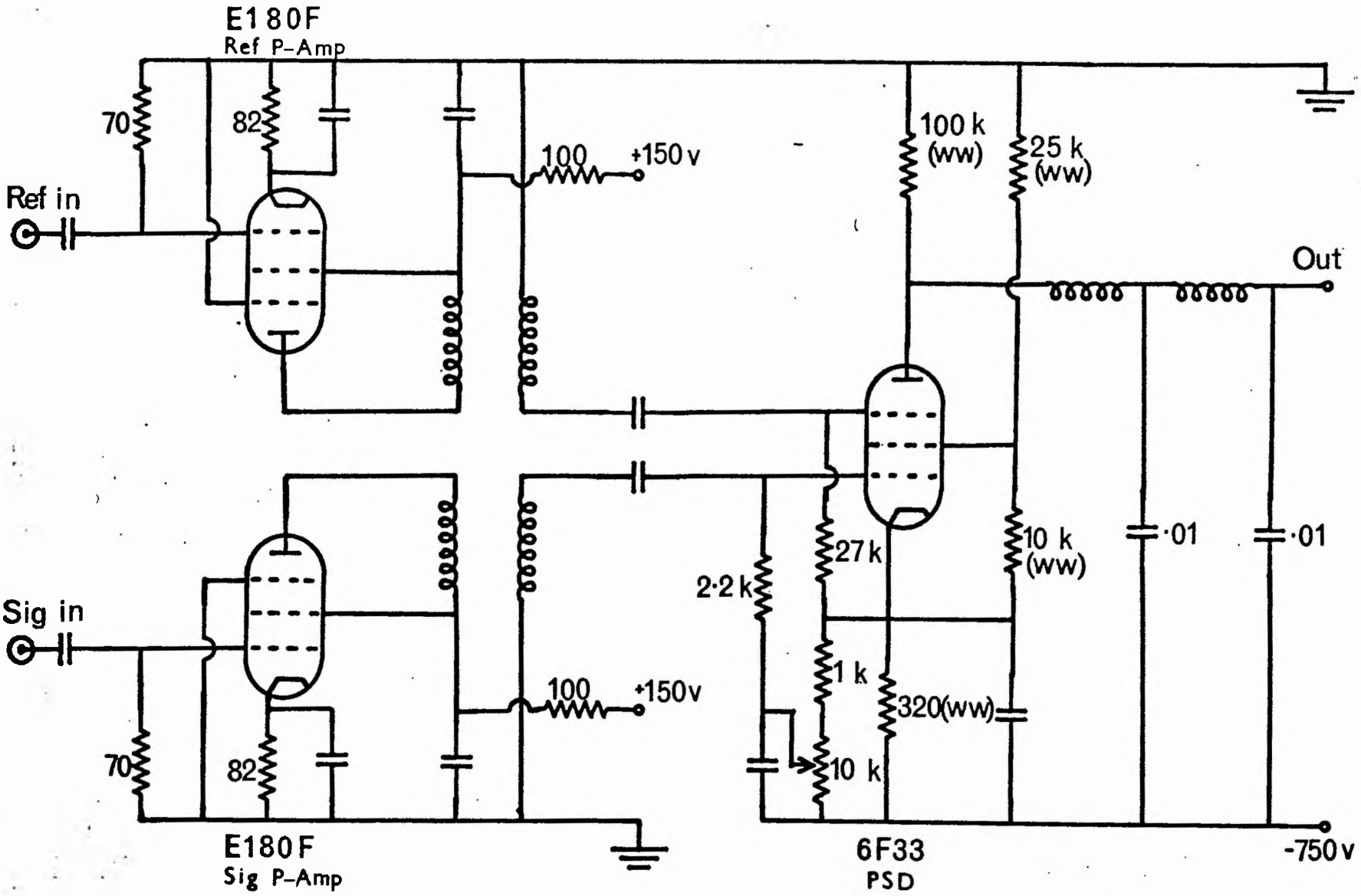

FIG 3·29 Stabilisation System for Signal Klystron

The circuit used is shown in Fig. 3.29. This consists of a Phase Sensitive Detector using a 6F33. The voltages to both reference and signal inputs of this are first pre-amplified by the E180F stages. These pre-amplifiers are supplied from the Reference I.F. Amplifier and the Signal I.F. Pre-amplifier respectively.

If the frequency drifts from the cavity frequency ν_c, an unbalance occurs of the microwave bridge in both amplitude and phase. This corresponds to a change in the real and imaginary components of the cavity reflection coefficient (Γ_r and Γ_i) according to the scheme of Fig. 3.22. In particular Γ_i changes sign as ν passes through the value ν_c. This causes a change in phase of the microwave voltage at the Balanced Mixer and therefore in the I.F. voltage at the signal input of the P.S.D. Since the reference voltage is derived from the detected microwave voltage at Tee (4), it is independent of the cavity reflection coefficient.

It has been shown [B6] that the output of the P.S.D. can be made proportional to Γ_i and thus to $(\nu - \nu_c)$ and by selecting the correct phase, this voltage when fed back to the Signal Klystron reflector, corrects the frequency drift.

A saw-tooth voltage applied to the reflector of the Signal Klystron in order to sweep through the cavity "dip" produces a P.S.D. output curve as shown in Fig. 3.32. This curve results from the correct relative phases of signal and reference P.S.D. inputs to lock on the klystron and is $\sim$200v peak to peak.

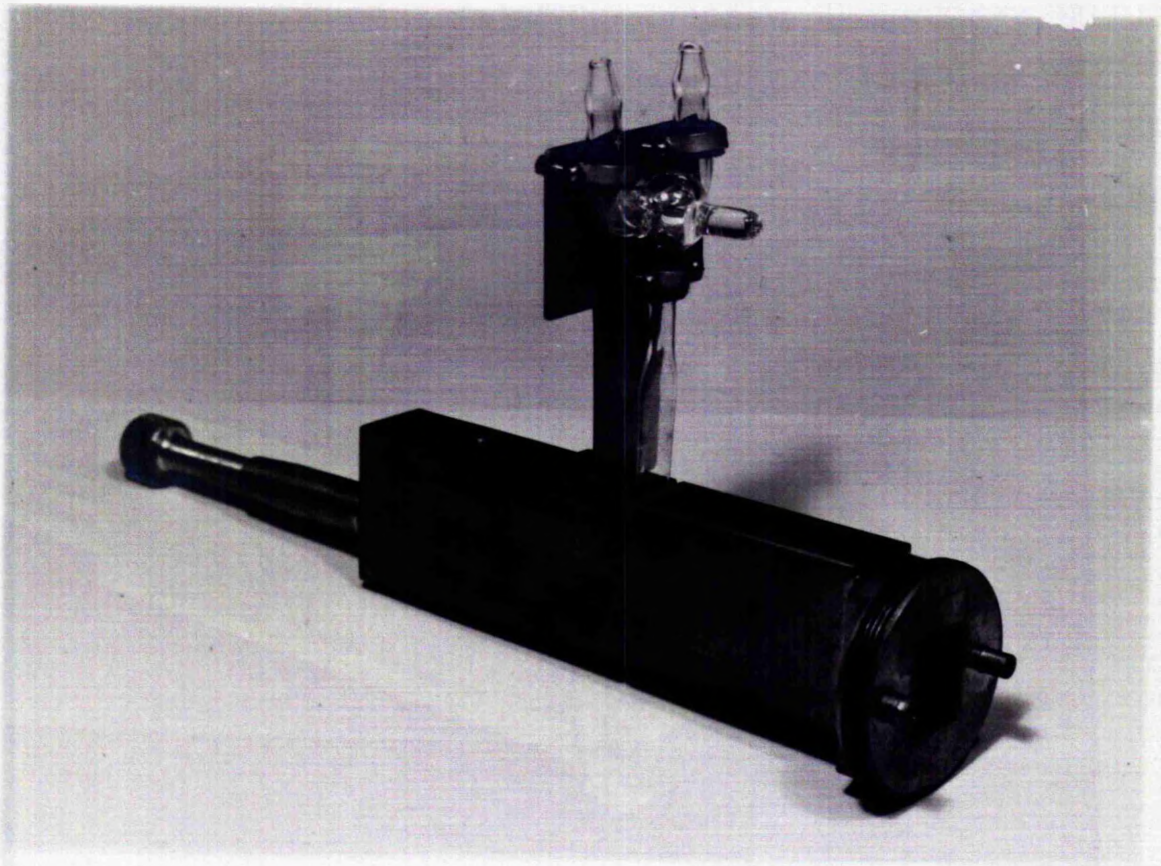

FIG 3.30 H_{102} Cavity with Aqueous Cell.

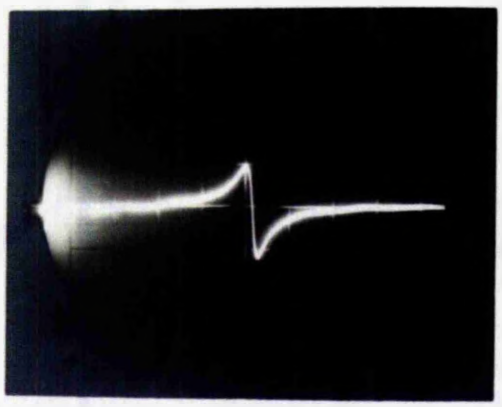

FIG 3.31 Wavemeter Output.

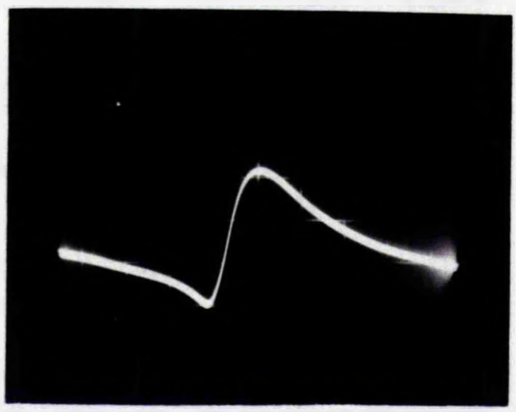

FIG 3.32 P.S.D. Output.

The procedure for setting up the stabilisation system is described in § 3.9.

E.S.R. dispersion may be displayed at the P.S.D. output (§ 3.12). The Stabilisation Ratio, S can be found by measuring the reduction in magnitude of the dispersion signal on stabilising the Signal Klystron [B6]. Measured in this way S was found to be ~ 1000.

It was found that, when no restrictions are imposed upon the bandwidth of the stabilisation loop, oscillation of about 2 Kc/s occurred. This was eliminated by reducing the bandwidth to ~500 c/s by means of an R-C filter between the P.S.D. and the Signal Klystron reflector. Attempts were made to use m-derived filters to prevent the oscillations without placing so great a restriction on the bandwidth. However, it was found that, with these filters and also with ordinary L-C filters, it is much more difficult to lock on the klystron.

§ 3.8 Local Oscillator Automatic Frequency Control (L.O.A.F.C.)

When the Signal Klystron is locked to the resonant frequency of the cavity, the Local Oscillator must be sufficiently stable in order to maintain the I.F. within the passband of the I.F. Amplifiers (~5 mc/s). In practice the L.O. (E.E. K302) is found to drift very little over a period of the order of a minute. On video presentation, therefore, no gain in signal to noise ratio is observed on stabilising the L.O.* However, for pen recordings of duration five minutes or longer,

*This is the case although the Ratio detector suppresses noise, since any noise which passes through the L.O.A.F.C. unit to the L.O. reflector and appears as L.O. noise, is later removed by the balanced mixer.

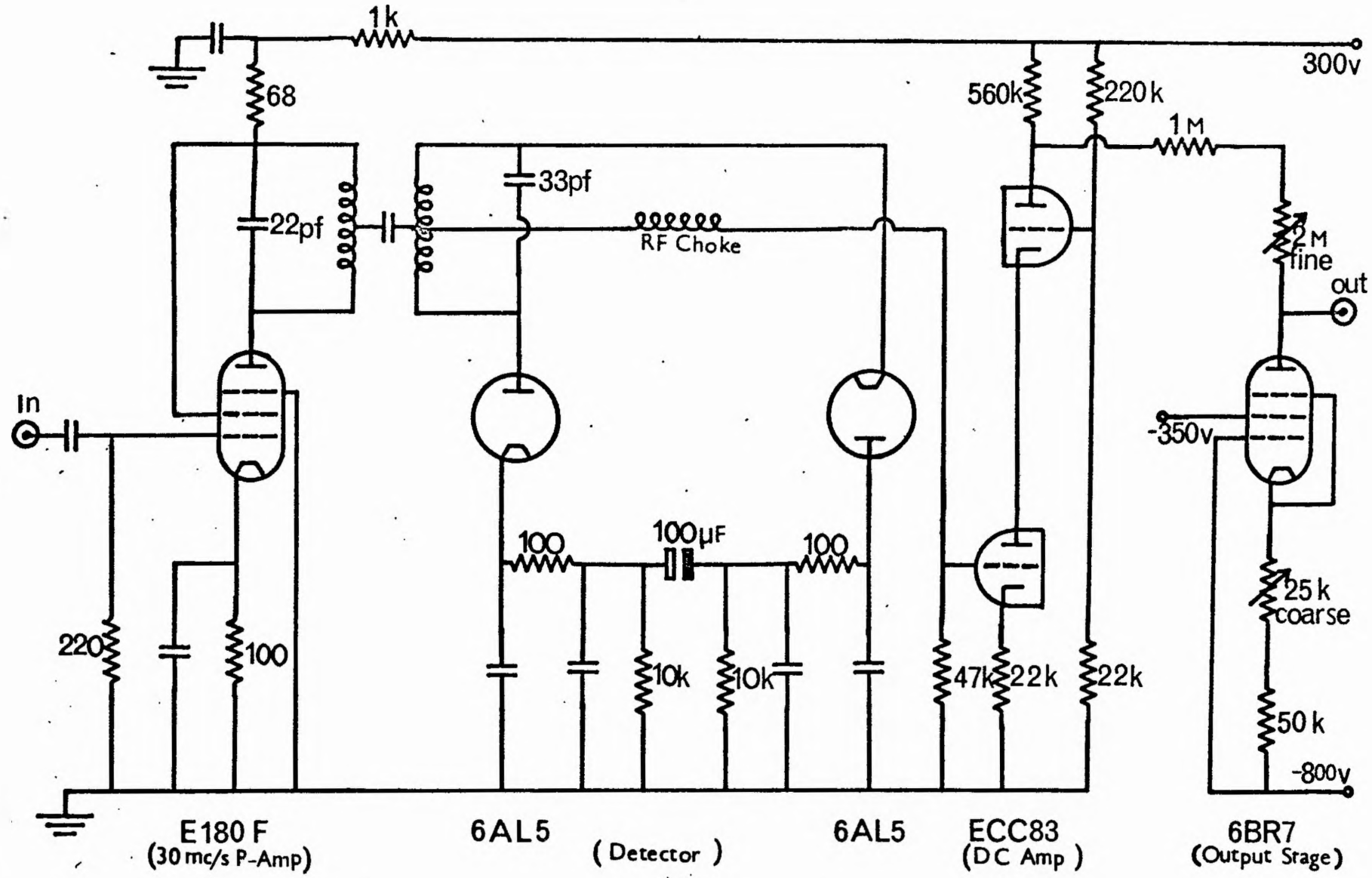

FIG 3·33 Local Oscillator Automatic Frequency Control

frequency drifts of the L.O. cause the Signal I.F. Amplifier output to vary and this results in base line drifts of the pen recording.

The circuit used is shown in Fig. 3.33. The output of the Reference I.F. Amplifier is fed into the first stage of the L.O.A.F.C. which amplifies this signal to about 10 volts. This is then detected in the following stage, a Foster-Seely Ratio Detector. The secondary of the transformer, linking the first and second stages, resonates at 30 mc/s with the 33 pf condenser across it. Thus if the I.F. drifts from 30 mc/s, the phase of the voltage across the secondary varies relative to the voltage being fed into the centre tap. The function of the 100μF electrolytic condenser is to maintain a constant voltage across itself. The result of this is to convert variations in frequency to variations in direct voltage at the output of the detector. This is amplified in the following stage, a cascode D.C. amplifier at the output of which the discriminator S-shaped curve (Fig. 3.37) measures 120v peak to peak.

Finally the output stage alters the D.C. level of this correction voltage from $\sim$ 200v at the second anode of the cascode stage to $\sim$ -500v which is the working voltage of the L.O. reflector.

§ 3.9 Procedure followed in setting up Spectrometer

In setting up the spectrometer at the beginning of a run, the following procedure was used.

The Variable Coupler is adjusted to the position where z = 0. For a cavity which has interchangeable coupling irises, an iris is selected

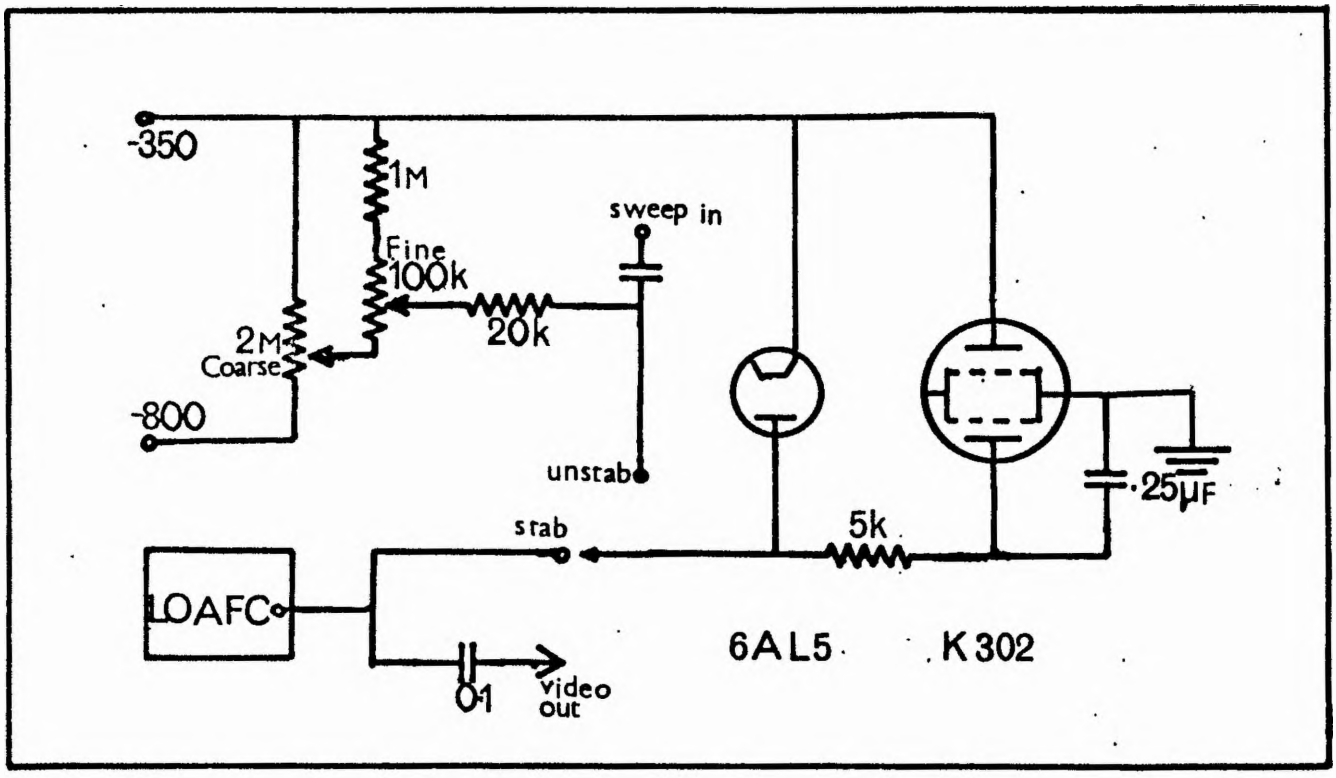

FIG 3·34 Local Oscillator Connections

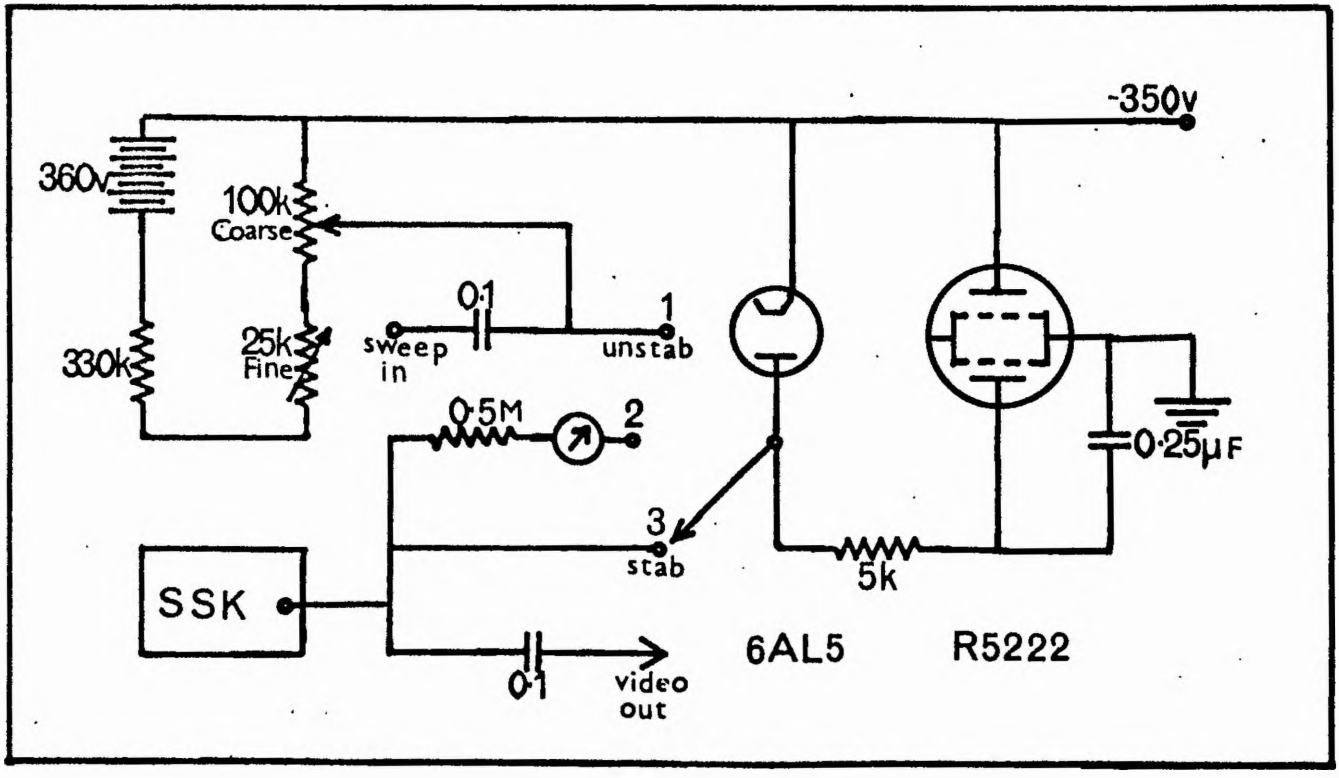

FIG 3·35 Signal Klystron Connections

which overcoupled the cavity. With the L.O. still switched off, the Signal Klystron mode is displayed by observing the output of either crystal of the Balanced Mixer on the oscilloscope, while a saw-tooth voltage is applied to the reflector via the SWEEP IN terminal of Fig. 3.35. The klystron is then tuned mechanically until the cavity dip appears after which the cavity is matched to the waveguide by adjustment of the Variable Coupler. This situation is shown in Fig. 3.38 where zero power is reflected from the cavity at its resonant frequency.

The L.O. klystron is switched on and attenuator (2) of Fig. 3.1 adjusted to give about 0.5 mA crystal current in the Balanced Mixer crystals. The L.O. is tuned mechanically and electrically until the L.O. frequency is 30 mc/s higher than that of the Signal Klystron. The L.O.A.F.C. output then has the form of Fig. 3.37 for which the Signal Klystron frequency is being swept as before. For the situation where the L.O. is operating 30 mc/s below the Signal Klystron, the slope of this curve is reversed.

The Reference I.F. Amplifier is operated on maximum gain and its second detector current is now adjusted to 0.5 mA by varying its input using Attenuator (3) (Fig. 3.1). The L.O.A.F.C. is switched to the STAB position (Fig. 3.34) and, if the second detector reading remains steady at 0.5 mA, the I.F. has been stabilised to 30 mc/s.

The P.S.D. output is now displayed and the relative phase of signal and reference voltages is adjusted by means of the Phase Shifters (1)

and (2) until the correction curve shown in Fig. 3.32 is observed. The saw-tooth sweep is now switched off and fine adjustments of the variable coupler bring the cavity sufficiently close to critical coupling to permit the use of a high gain in the Signal I.F. Amplifier. The minimum second detector reading of this amplifier is noted for fine adjustments of the Signal Klystron reflector voltage and the wavemeter is set to give a maximum reading at this frequency. The switch in Fig. 3.35 is moved to position 2 and the centre zero meter, M indicates any voltage difference between the Signal Klystron reflector and the P.S.D. output. These voltages may then be equalised by a slight adjustment of one of the Phase Shifters. The switch is then set to the STAB position (3) and, if the second detector and wavemeter continue to indicate their previous minimum and maximum readings respectively, the Signal Klystron is then locked to the cavity frequency.

The stabilisation systems of the two klystrons are independent and it is possible to reverse the order and stabilise the Signal Klystron before the L.O., although in practice, the above procedure was generally found simpler.

The functioning of the stabilisation systems is satisfactory, the spectrometer remaining stabilised for many hours without adjustment. The longest recording time used was $6\frac{1}{2}$ hours for a phenothiazine spectrum (Fig. 4.9), during which time there was no appreciable base line drift.

It has been found possible to interchange sample tubes without dis-

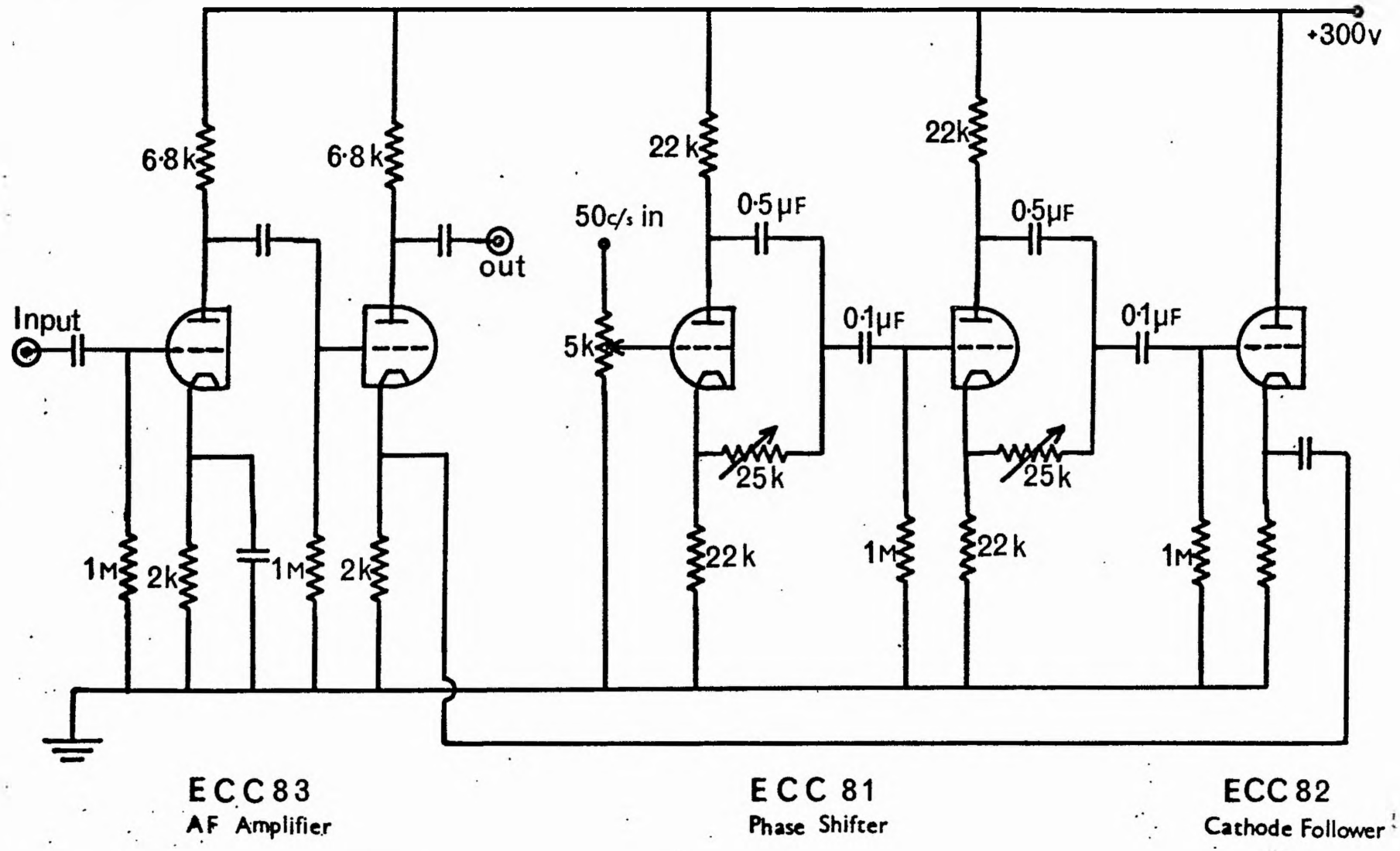

FIG 3·36 A.F. Amplifier with 50c/s Compensation

turbing the stabilisation as long as not too great a change in cavity coupling is involved in removing and replacing the tubes.

Although it consists of a considerable number of operations, the stabilisation procedure may be carried out conveniently quickly. For example, in a situation when the cavity was in place and the coupling was approximately correct, the spectrometer was set up within two minutes of switching on the power supplies.

§ 3.10 A.F. Amplifier with 50 c/s Compensation

The detected output of the Signal I.F. Amplifier in normal operation gives a signal which is too small for the most sensitive range of the oscilloscope used ($\sim$6 mv/cm).

This signal is therefore further amplified by the circuit of Fig. 3.36, the first two stages of which consist of an A.F. amplifier with a gain 40 db and an unrestricted bandwidth $\sim$30 Kc/s. The bandwidth may be reduced by means of an R-C filter at the output of the A.F. Amplifier and, normally 5 Kc/s is used.

50 c/s at the output of the Signal I.F. Amplifier is compensated by the next three stages, in which the phase of a 50 c/s signal of variable amplitude, is altered by means of a phase shifter and fed back through the cathode follower to the cathode of the second stage.

This unit is used with the video detection scheme of § 3.11.

§ 3.11 Video Display of Absorption Spectra

In order to display an absorption line, the D.C. magnetic field is modulated at 50 c/s with an amplitude larger than the line width and the

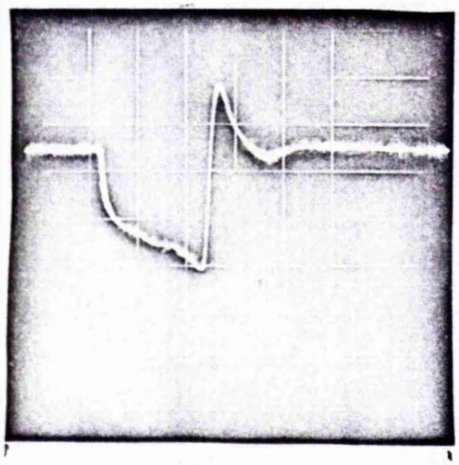

FIG 3·37 LOAFC output.

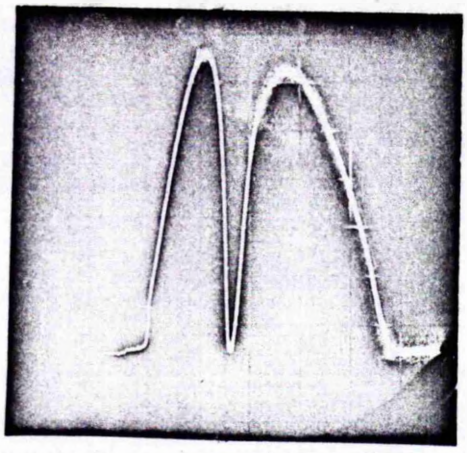

FIG 3·38 Cavity Dip.

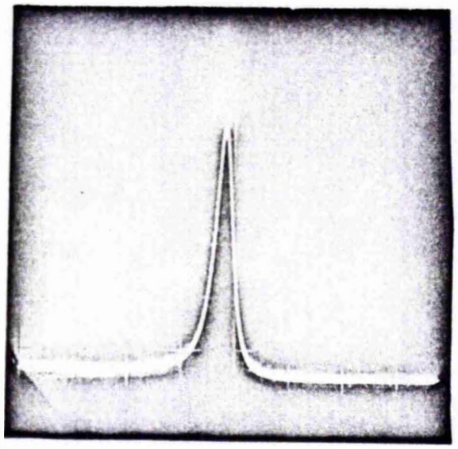

FIG 3·39 10^{16} Spins DPPH

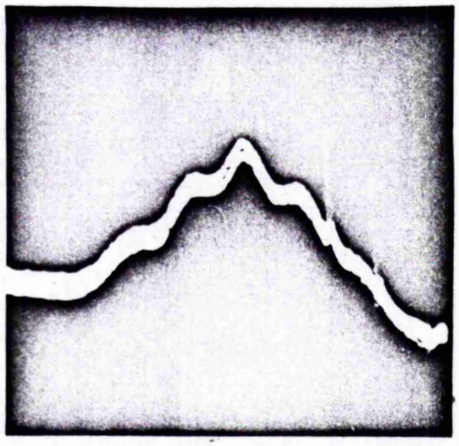

FIG 3·40 DPPH Solution.
(video)

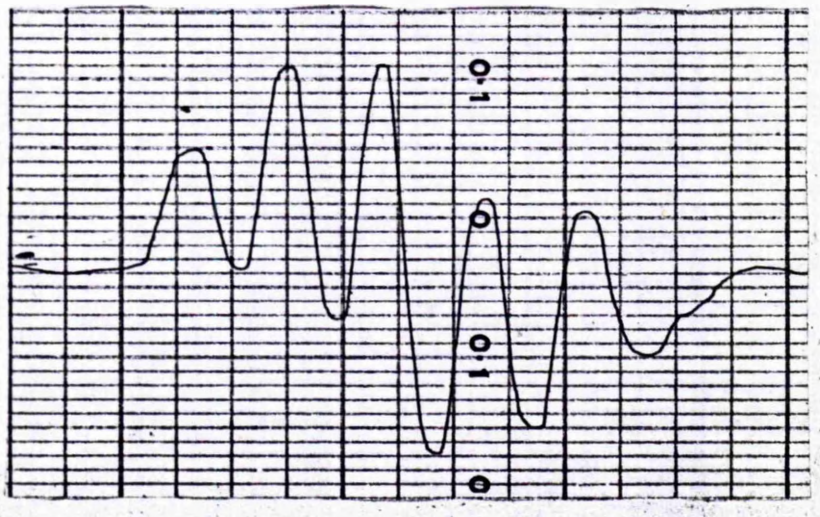

FIG 3·41

DPPH Solution.

(Pen Recording)

E.S.R. signal which appears at the output of the A.F. Amplifier is monitored on the oscilloscope.

The 50 c/s modulation is applied by means of modulation coils which are mounted on the magnet yoke of the Newport magnet (§ 3.15 (a)) but, in the case of the Mullard magnet (§ 3.15 (b)), a pair of small modulation coils mounted between the pole pieces are used.

The E.S.R. absorption line from 10^{16} spins of solid D.P.P.H. (line width ~ 2 gauss) is shown in Fig. 3.39. Fig. 3.40 represents the video spectrum of a solution of 10^{16} spins of D.P.P.H. in 0.1 cc benzene ($\sim 2 \times 10^{-4}$ M). If this is compared with Fig. 3.41 which shows the derivative of E.S.R. absorption line for the same sample using the detection scheme of § 3.13, it is evident that both sensitivity and resolution are greatly improved for the latter. In practice, therefore, for a new sample the video scheme is used to locate the resonance value of the magnetic field preliminary to recording the spectrum using the Phase Sensitive Detection scheme of § 3.13.

§ 3.12 E.S.R. Dispersion

The stabilisation system for the signal klystron, in the present spectrometer, automatically eliminates dispersion for reasons discussed in § 3.7 (a) (iii). It is therefore possible to observe dispersion only when the klystron is unstabilised.

In order to see pure dispersion at the output of the Signal I.F. Amplifier, the bridge must be unbalanced in phase but balanced in ampli-

tude [B7] i.e. the cavity is critically coupled and the klystron is detuned slightly from the cavity resonant frequency. Fig. 3.42 shows the dispersion for a sample of 10^{17} spins of D.P.P.H.

Dispersion may also be observed by displaying the output of the P.S.D. on the oscilloscope. In this case it is not necessary to ensure that the cavity is critically coupled as the P.S.D. output can be made sensitive to the phase unbalance only, by correct adjustment of the phase of the P.S.D. reference input.

As the Signal Klystron is unstabilised in both cases, the detection of dispersion is about a factor 10 less sensitive than the video detection of absorption (§ 3.11). The detection of dispersion could be made more sensitive by stabilising the Signal Klystron using a method which does not suppress dispersion. This could be done by phase locking it to a crystal or locking it to a reference cavity [N2] [M7].

§ 3.13 Phase Sensitive Detection and the 280 c/s System

A full description of the circuits of this system has already been given [B6] and as only slight modifications have been introduced into the present system, a detailed discussion need not be given here.

A tuneable Wien Bridge Oscillator provides two outputs at 280 c/s whose relative phase may be altered by means of the type of phase shifter shown in Fig. 3.36. One of these outputs provides a reference signal for the Lock in Amplifier. The other is fed into a power amplifier of the Williamson type [W5] which provides the current to drive the modulation coils. In this system the D.C. Magnetic field is modulated at 280

c/s to a depth considerably less than any hyperfine splitting it is wished to observe. If the modulation depth is too great, distortion of the line occurs [R1]. The detected signal from the I.F. amplifier is fed into the Narrow Band Amplifier (N.B.A.) whose bandwidth of $\sim$5 c/s is centred at 280 c/s. The output of the N.B.A., which is fed into the signal input of the lock in amplifier, is proportional to the slope of the E.S.R. absorption line. Thus the Pen Recorder which monitors the output of the lock in amplifier, while the D.C. magnetic field is slowly swept through the resonance value, records the derivative of the absorption line.

This detection scheme represents a gain in sensitivity of about 50 compared with the video system, when the output bandwidth of the lock in amplifier is about 0.3 c/s. Care must be taken to sweep the D.C. magnetic field sufficiently slowly to prevent distortions of the line which consist of apparent line broadening, reduction in amplitude, and shift in g-value [R1].

§ 3.14 Power Supplies

The D.C. voltages required by the electronics are all provided by stabilised power supplies. These consist of a full wave rectifier followed by an L-C filter and then a control valve (12E1 or several EL84's in parallel) across which there is a potential drop of $\sim$100 volts. The stabilised output is provided by controlling this potential drop by means of a D.C. amplifier with a balanced input which compares the

voltage at a point on a resistance chain across the output of the power supply with that at the anode of an 85A2. Any difference is fed back to the control valve.

The following power supplies were used,

(a) + 150v for the I.F. amplifiers. Separately filtered outputs for each unit prevents pick up between them.

(b) - 350v for the klystron cathodes and for the screen grid of the L.O.A.F.C. control stage.

(c) - 800v for the P.S.D. and L.O.A.F.C.

(d) + 300v for the N.B.A., Lock in Amplifier and L.O.A.F.C.

(e) + 300v for the 280 c/s oscillator and power amplifier.

The ripple on each of these was reduced to ~1 mv peak to peak. The output resistances are ~2 ohms and the Voltage Regulation better than 200.

§ 3.15 Magnets and Power Supplies

(a) Newport 7" Magnet

Initially a 7" Newport magnet with a 2" pole gap was used. The magnetic field inhomogeneity at the centre of the pole pieces is about 0.5 gauss over one inch. A 50 c/s ripple of about 2 gauss peak to peak from the Constant Current Generator (Newport type B, mark II) was reduced to ~ 0.5 gauss at the sample by applying a 50 c/s signal of correct amplitude and phase to the grids of the last stage of the Power Amplifier.

The resolution is thus limited to about 0.5-1.0 gauss. In addition the current stability, which is claimed to be 1 in 10^4 for 4% mains variation is not nearly as good, sudden changes of 1-2 gauss (i.e. ~3 in 10^4) occurring fairly frequently.

50 c/s and 280 c/s modulation are obtained using the modulation coils mounted on the magnet yoke. A slow voltage sweep, of variable amplitude and sweep rate supplied by a Bootstrap Generator is fed into the terminals of the magnet Current Generator. The slowly increasing voltage from the Bootstrap Generator causes a decreasing magnetic field. The sweep may be reset manually by short circuiting the condenser which controls the grid potential of the valve. The sweep may also be reset automatically, the condenser being shorted by means of a relay, the winding of which is in series with a neon tube. A 16μF condenser connected across the relay coil and neon charges up through a large resistance until the neon fires, triggering the relay and resetting the sweep. By varying the charging time constant, the reset time may be varied between 30 secs and 30 mins.

This automatic resetting unit makes it possible to sweep several times through a line without requiring the constant attention of the operator.

(b) Mullard Magnet (type EE1001)

In April 1964 a Mullard magnet (type EE1001), which had been installed in the same laboratory, became available and in the expectation

of improved resolution, the spectrometer was moved to its new position (Figs. 3.2 and 3.3).

In fact, the Mullard magnet was found to be superior to the Newport in all respects. A 20 K.W. 1000 c/s generator (type EE4014) provides the power, thus avoiding 50 c/s ripple and making filtering problems easier.

Magnetic field stability may be checked using a large D.P.P.H. sample on phase sensitive detection. If the peak to peak derivative amplitude (y) and the line width ($\sim$2 gauss) are known, then an approximate derivative slope $\frac{dy}{dH}$ at the centre of the line (H_o) may be estimated. If the magnetic field is kept at H_o, the pen recorder output, in addition to noise, will contain displacements δy corresponding to a field instability δH. Thus δH is given by,

$$\delta H = \frac{1}{\frac{dy}{dH}} \delta y \qquad (3.15.1)$$

The stability in this way was found to be $\sim$0.02 gauss over 10 sec and $\sim$0.04 gauss over 15 minutes i.e. $\sim$0.7 and 1.3 in 10^5 respectively. The fact that this is slightly worse than the quoted figure of 1 in 10^5 over 15 mins is probably due to the difficulty found in obtaining a sufficiently low resistance earth owing to the situation of the laboratory on top of a cliff.

The magnetic field inhomogeneity, quoted as $\pm$ 1 in 10^4 over a sphere of radius 0.6", was confirmed using (3.15.1). Also the "Wiggles"

FIG 3·42

DPPH Dispersion.

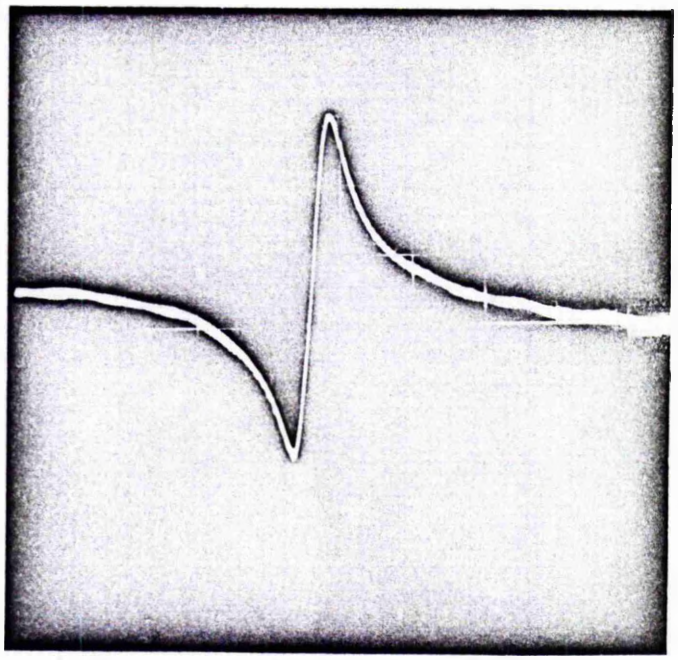

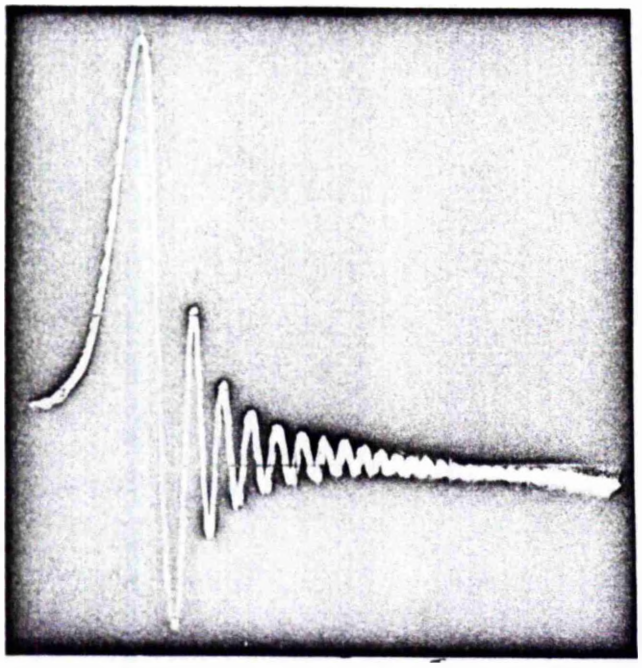

FIG 3·43 "Wiggles" (optimum)..

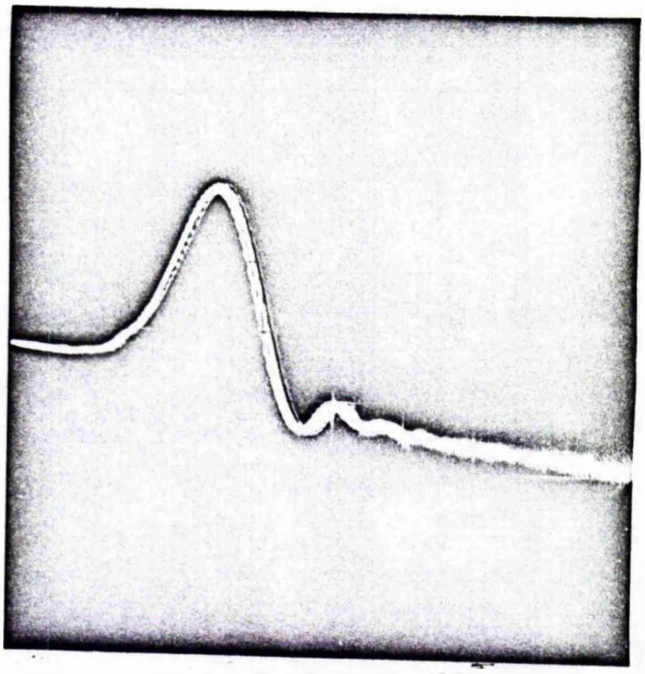

FIG 3·44 "Wiggles" (displaced 3").

obtained from the $\sim\frac{1}{2}$" long probe of a proton resonance meter (Newport magnetometer type P Mk II) at the centre of the magnet (Fig. 3.43) is comparable with that in a figure in the magnetometer handbook for an inhomogeneity of 2 in 10^5. The ringing of the N.M.R. signal is quite critically dependent upon homogeneity and Fig. 3.44 shows the signal when the probe is displaced 3" from the central position.

A water cooled resistance of 0.01 ohm in series with the magnet windings enables the current through the magnet to be measured using a potentiometer. For the free radicals which have been studied, g-values are all close to the free spin figure of 2.0023 and it was thus unnecessary to calibrate the magnet over the entire range. Calibration of the range of interest is carried out using the E.S.R. line of D.P.P.H. ($g = 2.0036$) and varying the microwave frequency. The resonance condition,

$$g\beta H = h\nu \qquad (3.15.2)$$

is then used to calibrate the potentiometer against H (Fig. 3.46).

Curve (a) here corresponds to H being increased from zero while in (b) the current has first been increased to the maximum value of 80 amps. The difference in potentiometer readings between (a) and (b) for the same H is $\sim 1\%$. This amount of hysteresis renders potentiometer readings unreliable for measurement of g-values, for which a proton resonance meter or standard E.S.R. marker of known g-value, must be used. However, as the slopes of (a) and (b) are equal to within $\sim 2\%$, the potentiometer

provides sufficient accuracy for line width measurements, as it is seldom possible to determine the line width from a spectrum to this accuracy.

§ 3.16 Sample Holders

For solutions of free radicals at a given dilution, the sensitivity depends on the sample volume. From (3.22.2) sensitivity is proportional to η_H and to Q_1.

For non-lossy solvents, e.g. benzene, the value of Q_1 should be independent of sample volume and maximum sensitivity should be obtained for a sample which fills the cavity. However, this would shift the resonant frequency of the cavity outside the range of the klystrons. Also the sample holders used are tubes which can be inserted into the cavity through an aperture in the walls. The enlargement of this aperture would lower the Q and the optimum inside diameter was found to be ~ 4 mm.

For lossy solvents with a dielectric constant up to ~ 30, e.g. acetonitrile, a tube of inside diameter 2 mm reduces the Q to about two thirds of its empty cavity value which, according to Feher, gives optimum sensitivity [F4].

For very lossy solvents, e.g. water and sulphuric acid, either the H_{102} aqueous cell cavity (§ 3.5 (e)) is used or a sample tube of inside diameter 1 mm with the H_{011} cavity of § 3.5 (c).

§ 3.17 Variable Temperature Cell

In order to study radicals at temperatures higher than room tempera-

FIG 3·45

Variable Temperature System

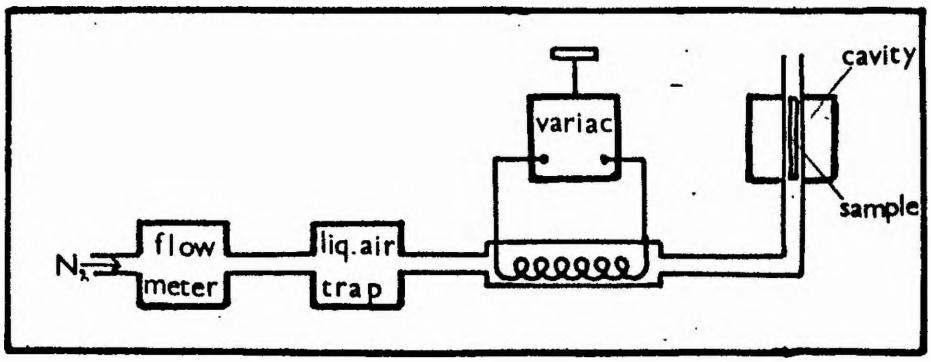

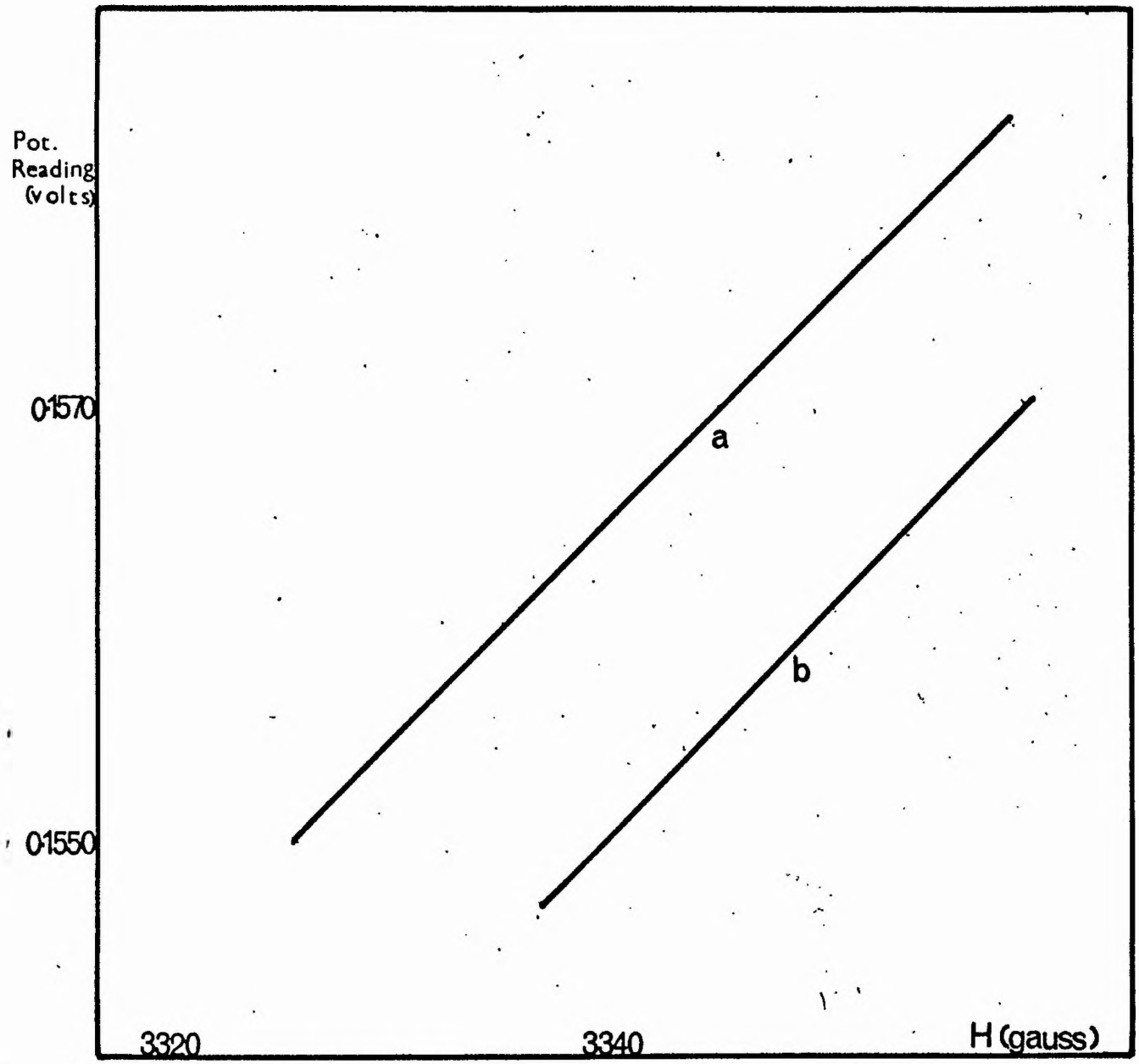

FIG 3·46 Calibration of Mullard Magnet using DPPH

ture, the apparatus shown in Fig. 3.45 is used. A coil of manganin wire, wound on an asbestos former, is placed inside a silica tube. A controlled flow of nitrogen, dried in a liquid air trap, past the coil, heats the sample to a temperature which may be varied up to 70° C by means of a variac.

§ 3.18 Flow system

It is useful to be able to examine radicals a short time after they have been formed and for this purpose the flow cell, shown in position in the H_{102} cavity (Fig. 3.26), was constructed. The two inlets are supplied from two 150 cc reservoirs containing the reacting solutions. The resulting radicals are examined $\sim$1 sec after mixing takes place.

§ 3.19 Microphonics

The laboratory in which the spectrometer is situated has a concrete floor and vibrations are not generally unduly troublesome. However, the microwave bridge is sensitive to mechanical shock and it was found that this was reduced by mounting the microwave table on sponge rubber pads. The cavity arm must necessarily be fairly long and the best arrangement here is to include a length of flexible waveguide and to clamp the cavity to the magnet.

§ 3.20 Base Line Drift

This has been found by some workers [F4], [B6] to be significant and is caused by the interaction of eddy currents, induced by the A.C. modulation, with the steady D.C. magnetic field. As this is swept, a

base line drift of the pen recorder occurs. Several cavities were constructed especially to counteract this (§ 3.5) but, using the small field modulation required for high resolution (~ 0.1 gauss), the effect was no longer troublesome. It was therefore found convenient to use the normal H_{011} cavity (§ 3.5 (c)) for most purposes.

§ 3.21 Transients

These were found to occur for switching of electrical devices in the laboratory, involving fairly large currents, and also for switching of the lathes in the workshop. The transients are reduced considerably by supplying the spectrometer from a Constant Voltage Transformer. However, the best operating conditions are at night when no switching of this form occurs.

§ 3.22 Sensitivity of Spectrometer

For a spectrometer using a Magic Tee bridge and a reflection cavity and when the detector output is linear with respect to input voltage, as is the case with a superhetrodyne system [F4],

$$\frac{\Delta V}{V} = 0.35 \frac{\Delta Q_a}{Q_a} \qquad (3.22.1)$$

where V is the microwave voltage input to the cavity and ΔV and ΔQ_a are respectively the voltage reflected from the cavity and the change in unloaded Q brought about by E.S.R. absorption.

As a result of the properties of the Magic Tee, the corresponding voltage at the detector is $\frac{\Delta V}{2}$. By comparing this voltage with the

thermal noise at the detector, the following expression is obtained for the minimum detectable number of paramagnetic centres, [B6]

$$N_{min} = \left(\frac{kT\,\Delta f}{P_o}\right)^{\frac{1}{2}} \frac{2kT}{Q_a \nu_o} \frac{V_s}{\eta_H} \frac{g\,\Delta H}{\pi^2 \beta h} \qquad (3.22.2)$$

where k is Boltzmann's constant, T is the absolute temperature, Δf is the bandwidth of the system, P_o is the power incident on the cavity, V_s is the sample volume, ΔH is the line width in gauss, g is the spectroscopic splitting factor, β is the Bohr magneton and h is Planck's constant.

Substituting in (3.22.2) for the following typical values used in the present spectrometer for the video detection scheme of § 3.11 $P_o = 15mW$, $Q_a = 6000$, $\eta_H = 0.01$, $\Delta f = 5$ kc/s, $T = 290°$ K then $N_{min} \sim 2 \times 10^{12}$ spins of line width 1 gauss.

For the detection scheme of § 3.13, the bandwidth is reduced to ~ 0.3 c/s and from (3.22.2) $N_{min} \sim 1.5 \times 10^{10}$ spins of unit line width.

However, in an actual spectrometer, additional noise is generated in the klystrons, the mixer crystals and the I.F. amplifiers. An overall noise figure (F) for the system may be defined [R7], [F4]

$$F = \frac{(G\,N_k + F_{if} + t - 1)}{G} \qquad (3.22.3)$$

where G is the conversion gain of the crystal, N_k is the noise figure at the crystal input, F_{if} the noise figure of the Signal I.F. Amplifiers and t is the noise temperature of the crystal.

For a spectrometer with a Balanced Mixer, the L.O. noise is suppressed and, according to Feher (3.22.3) becomes

$$F = \left(\frac{F_{if} + t - 1}{G}\right) \qquad (3.22.4)$$

In the case of the present spectrometer $F_{if} \sim 3$ db, $t \sim 2$ times and $G \sim 0.15$. Thus, from (3.22.4),

$$F \sim 20.$$

Now the spectrometer sensitivity, as predicted by (3.22.2), is reduced by a factor $\sqrt{F}$ and thus the expected values of the minimum detectable number of spins for video and phase sensitive detection become, respectively,

$$N_{min} = 10^{13} \text{ (video)} , \quad 8 \times 10^{10} \text{ (P.S.D.)}. \qquad (3.22.5)$$

In order to estimate the experimental sensitivity of the spectrometer, it was found more convenient to make use of standard samples of solutions of D.P.P.H. in benzene [H3] than to prepare very small samples of crystalline D.P.P.H. by allowing solutions to evaporate [B6], [F4].

In benzene solution D.P.P.H. has five hyperfine components of intensity ratios 1:3:5:3:1, each of which has line width ~ 10 gauss [H3], [U1]. Thus the signal to noise ratio for the outermost components will be a factor ~ 65 times lower than for crystalline D.P.P.H., line width ~ 2 gauss.

Using ~ 0.1 ccs samples, it was found that a solution $\sim 10^{-4}$ M/l gives a signal to noise ratio ~ 2 for video detection and a solution

$\sim 10^{-5}$ M/l gives a signal to noise ratio ~ 3 using phase sensitive detection with a magnetic modulation amplitude ~ 3 gauss. Extrapolating to unit signal to noise ratio, the minimum detectable number of spins in the two cases for unit line width, is $\sim 5 \times 10^{13}$ and $\sim 10^{12}$ respectively.

Comparing these figures with (3.22.5), it is seen that they are respectively factors of ~5 and ~12 higher than anticipated.

It would appear that, in general, for superhetrodyne spectrometers this actual sensitivity tends to be lower than the calculated value especially at higher microwave powers. Hirshon and Fraenkel [H2] report a sensitivity which is a factor of almost 100 lower than calculated. Brown [B6], using a very noisy I.F. amplifier, found a sensitivity ~6 times lower than expected for Phase Sensitive Detection and no improvement was noted on reducing F_{if}. Feher has found that, for powers below 10^{-3} W, the sensitivity agrees fairly well with theory but above this power he concludes that instabilities in the required Magic Tee balance (of better than 40 db) begin to contribute to noise which lowers the sensitivity.

These noise components will be included in the term GN_k in (3.22.3). Also Signal Klystron noise is not eliminated by a balanced mixer and thus the term GN_k, containing components from these two sources, should be included in (3.22.4). It was noted that, towards the end of the life of a Signal Klystron, the observed sensitivity fell owing to increased

klystron noise.

An improvement in sensitivity might, therefore, result from the use of a system which compensates for Signal Klystron noise.

A superhetrodyne spectrometer using transmission cavities in which the microwave carrier noise was suppressed [M7] gave a sensitivity $\sim 3 \times 10^{10}$ spins of unit line width which was near the calculated value. Also a spectrometer suppressing carrier noise by use of a bimodal cavity is capable of a similar sensitivity [T1].

The Decca superhetrodyne spectrometer which is based upon the D.S.I.R. recommendation [D1] suppresses Signal Klystron noise by phase locking the Signal Klystron to a crystal but, by means of an additional stabilisation system, allows the Signal Klystron to be locked to the cavity.

It appears, therefore, that a reduction in Signal Klystron noise should lead to an improvement in the sensitivity of the present spectrometer.

Further suggestions for improvements to the spectrometer are made in Chapter 9.

FIG 4·1

Phenothiazine.

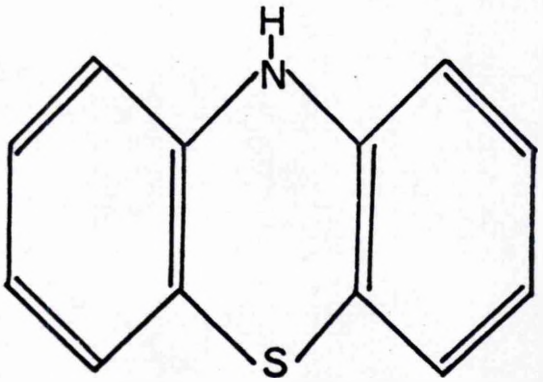

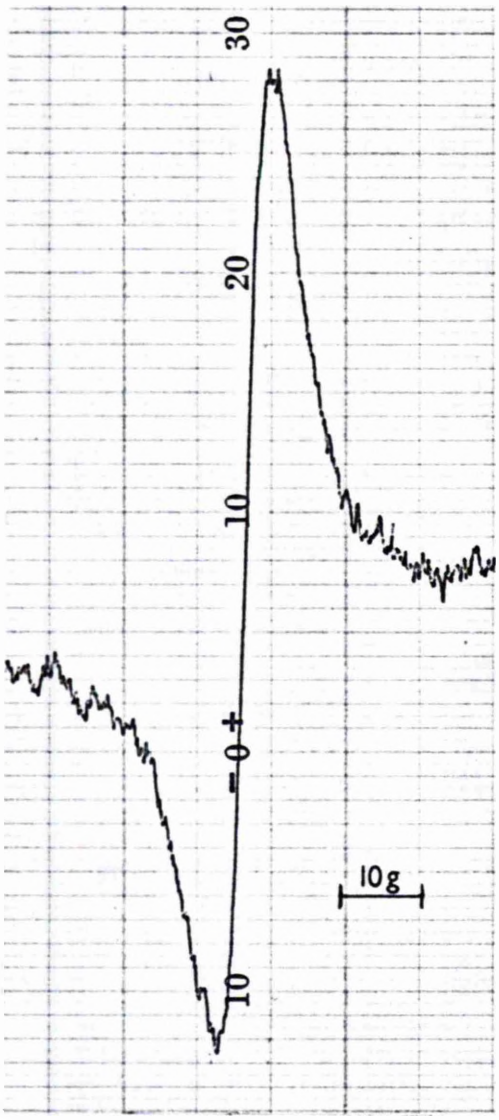

FIG 4·2

The ''Green Product''

CHAPTER 4

PHENOTHIAZINE

§ 4.1 Introduction

The molecular structure of phenothiazine (PTZ) is shown in Fig. 4.1. PTZ is used in the production of certain dyestuffs, and several of its derivatives, for example Chlorpromazine (§ 5.3) have been used as tranquillisers in mental diseases [G7].

PTZ has a fairly low ionisation potential (about 6.7 eV) [L1], and is therefore expected to be a fairly good electron donor, and to form paramagnetic complexes with electron acceptors of high electron affinity. Also oxidation to the $[PTZ]^+$ ion should be relatively easy.

§ 4.2 Phenothiazine perchlorate

A sample of $PTZClO_4$, which is a greenish powder, was supplied by Dr. R. Foster. It is found to be paramagnetic, containing about 0.1-0.5% radical content in the solid state. The E.S.R. line obtained is without hyperfine structure, as is to be expected from a collection of randomly orientated spins, and has a line width about 7 gauss.

In an ionising solution such as Acetonitrile the radical content increases to almost 100%, and on dilution the spectrum has the form of Fig. 4.3 for a 10^{-3} M solution. This compound is assumed to dissociate in solution.

$$PTZClO_4 \rightleftharpoons PTZ^+ + ClO_4^- \qquad (4.2.1)$$

Dilution to a concentration of 10^{-4} M provides no improvement in resolution.

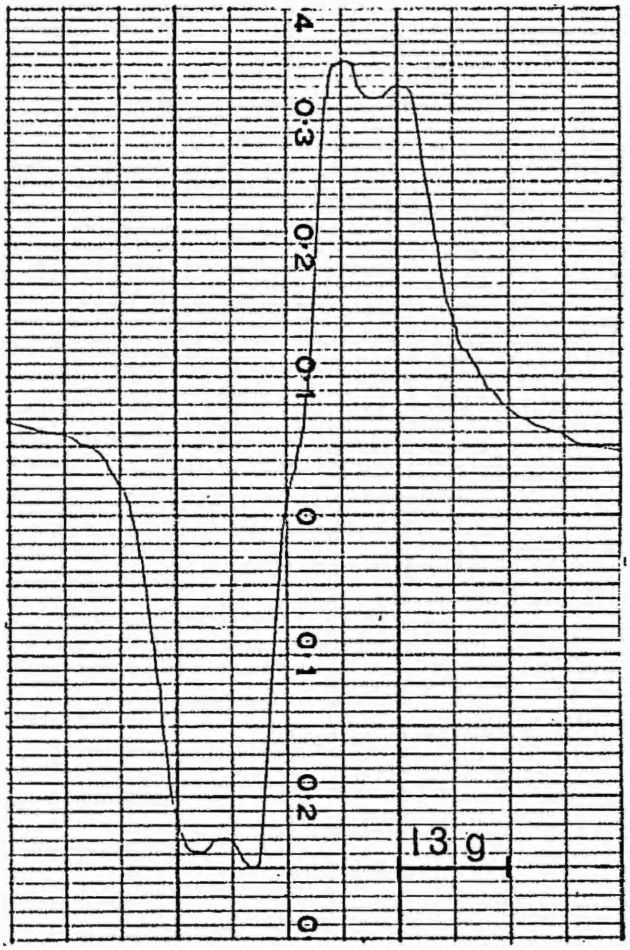

FIG 4·3 $PTZClO_4$

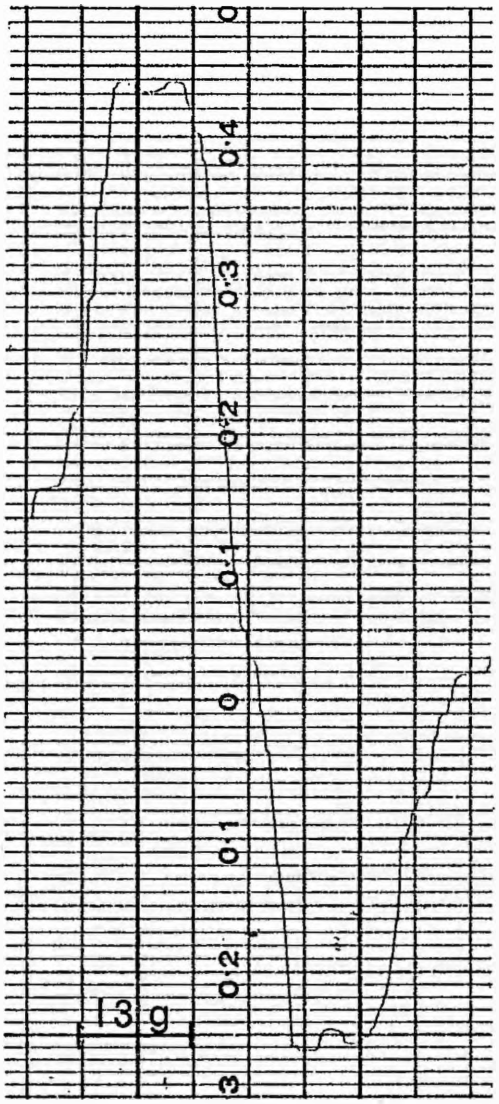

FIG 4·4 $PTZ\text{-}I_2$

§ 4.3 PTZ-iodine and PTZ-lead tetra-acetate

PTZ reacts with iodine in an ionising solution of Acetonitrile and gives rise to a dark green paramagnetic complex (Fig. 4.4). The similarity of Figs. 4.4 and 4.3 suggests that, again, the PTZ positive ion is involved.

$$2PTZ + I_2 \rightleftharpoons 2[PTZ]^+ + 2I^- \qquad (4.3.1)$$

In this case also resolution is not improved by dilution.

A similar spectrum to Figs. 4.3 and 4.4 is found when PTZ is oxidised by means of lead tetra-acetate in a solution of acetic acid.

§ 4.4 The "Green Product"

When 2, 3-Dicyanobenzoquinone (DCNQ) is added to a solution of PTZ in Acetonitrile, an immediate dark green colour results. Foster, who has termed this complex the "Green Product", has postulated, on the basis of optical absorption work [F7], the existence of a free radical for this complex of a similar nature to $PTZClO_4$.

The "Green Product" is found to be strongly paramagnetic, but the spectrum of a dilute acetonitrile solution (Fig. 4.2) shows no hyperfine structure. Thus the radical involved may be of a different nature to those of Figs. 4.3 and 4.4.

The spectrum of this complex appears to be fairly similar for excess concentrations of both donor and acceptor, and thus it seems unlikely that the resolution is limited by an electron exchange process of the form of § 2.3 (k). The removal of dissolved oxygen has not been

attempted for this complex and it is possible that the mechanism of § 2.3 (j) inhibits the resolution of hyperfine structure.

§ 4.5 Complexes of PTZ with other organic acceptors

On the addition of Tetracyanoethylene (TCNE) to an acetonitrile solution of PTZ a dark green colour results immediately, and this is again associated with a paramagnetic complex. The E.S.R. line has a form similar to Fig. 4.2, but is slightly less intense. A complex is formed between PTZ and chloranil, of which the E.S.R. signal has the same form as Fig. 4.2, but is weaker than for DCNQ or TCNE. A solution in acetonitrile of PTZ with s-trinitrobenzene (TNB) slowly turns green, but in this case shows no paramagnetism.

§ 4.6 Discussion of PTZ complexes

It appears that two distinct types of PTZ spectra occur. This is explained if it is assumed that the spectra of the form of Fig. 4.3 involve the PTZ^+ ion, while complexes with organic acceptors, which have an E.S.R. spectrum of the form of Fig. 4.2, do not dissociate in solution.

In the case of the organic acceptors, the E.S.R. spectrum is assumed to be characteristic of the complex as a whole rather than of the constituent parts. If the latter were true, two overlapping spectra would be expected. In the case of the TCNE complex, for example, one of these would be the highly characteristic spectrum of Fig. 7.13.

The decrease in radical content from TCNE to TNB can be explained

by considering the electron affinities of the acceptors. TCNE, Chloranil and TNB have, relative to I_2, electron affinities of 1.1 eV, 0.8 eV and 0.0 eV respectively [B9]. DCNQ, however, has an electron affinity approximately equal to and probably slightly lower than that of TCNE [B10]. Thus it is unexpected that the radical content for DCNQ-PTZ is slightly greater than for the TCNE complex. This difference, however, is small and may perhaps be explained by the rather old TCNE sample used. There does, however, appear to be a correlation between electron affinity of the acceptor and radical content.

This correlation has been observed for complexes of acceptors with tetramethylp-phenylenediamine (TMPD) by Brown [B6]. A similar reduction in radical content has been noted for complexes of TCNE with donors of increasing ionisation potential by Slough [S5].

The PTZ complexes with organic donors, then, are assumed to possess a dative ground state as postulated by Bijl, Kainer and Rose-Innes [B14] and to be biradicals.

The very considerable difference in the paramagnetic properties of PTZ complexes with TNB and I_2, is not consistent with the equal electron affinities noted above. (Bately and Lyons [B9] state that this difference is 0.06 ± 0.13 eV.) Briegleb [B10] has noted that iodine is a σ-acceptor and,as such,it should not be made the basis of a scale of electron affinities for π-acceptors [M9] [M10] which form a different type of complex. The electron affinities calculated on this basis are

0.8-1.0 eV too high which may explain why the PTZ-I_2 complex is paramagnetic while the PTZ-TNB complex is not.

§ 4.7 PTZ in Alkaline Solution

Heinekin et al [H4] have reported that solutions of certain PTZ dyes to which a pellet of NaOH is added are paramagnetic, and exhibit complex hyperfine structure characterised by a primary three line spectrum rather than the four lines which have been observed in acid solutions [L2] [C1] [C2], and § 4.8.

PTZ itself is basic, and when alkali is added to a solution of PTZ in ethyl alcohol,no E.S.R. signal is observed. (Heinekin et al in fact used the crude dyes in the form of the zinc double chloride salts.)

If a solution of PTZ in sulphuric acid is diluted with water and sufficient KOH added to ensure that the solution is strongly alkaline, the E.S.R. spectrum of Fig. 4.5 is observed.

This spectrum obviously contains four lines rather than the three which would be expected if the formation of the radical involved the removal of the proton attached to the nitrogen atom [H4]. It will be seen in § 4.8 that a similar four line spectrum is observed in H_2SO_4 solution. Therefore,the removal of the proton does not appear to be related merely to pH but apparently depends upon the nature of the initial compound of PTZ or the PTZ derivative, which is treated with alkali.

§ 4.8 PTZ in Concentrated Sulphuric Acid

(a) Aromatic hydrocarbons in H_2SO_4

The E.S.R. spectra have been studied of several aromatic hydrocarbons in concentrated sulphuric acid solution [W6], [K2], [C3]. Although reservations have been put forward [M11], it is generally accepted [S6] that this produces the cation. The E.S.R. and C.T. spectra of the positive ions generated in this manner usually bear a fairly close resemblance to the spectra of radical anions [K4].

(b) Low Resolution Spectrum

PTZ dissolves immediately in concentrated sulphuric acid (specific gravity 1.8) to give a light green solution which is characterised by a strong E.S.R. signal [L1] [C1] [C2] [G6]. The low resolution spectrum obtained using the Newport magnet (§ 3.15 (a)) is shown in Fig. 4.6.

This spectrum consists of four main lines whose ratio of intensities approximates to 1:2:2:1. Fig. 4.8 shows the hyperfine splitting of the energy levels in a magnetic field for varying relative magnitudes of the hyperfine splitting parameters of the spin Hamiltonian (2.1.4), corresponding to the N^{14} nucleus ($I = 1$) and the proton ($I = \frac{1}{2}$) bonded to it. These parameters will be referred to as α and β respectively. Evidently the above four line spectrum may be explained by assigning approximately equal values to α and β (about 6.7 gauss).

On closer examination, it appears that the four components are not equally spaced as should be the situation for $\alpha = \beta$, but that the central

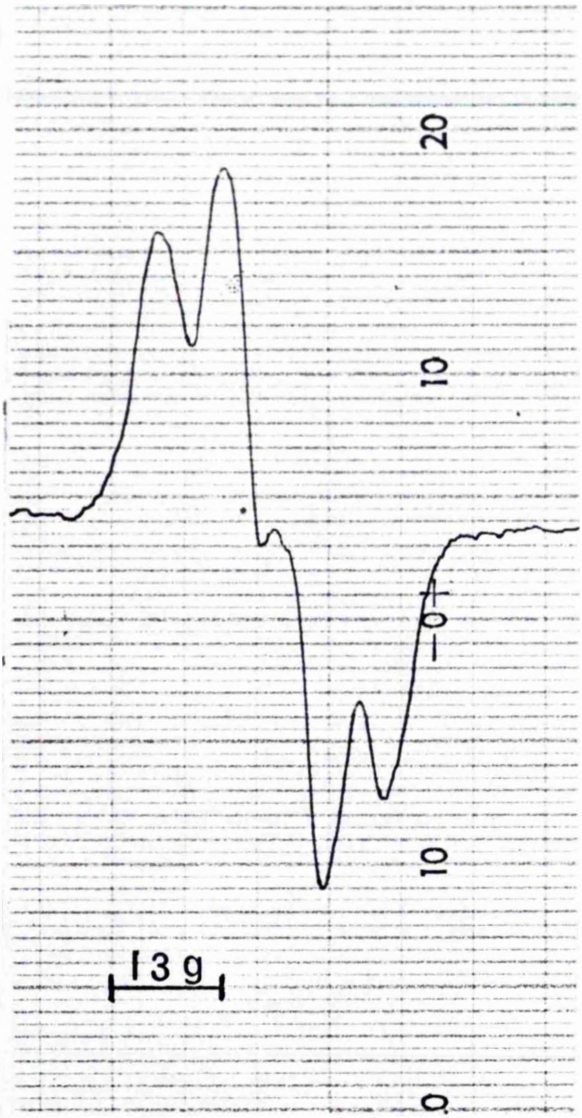

FIG 4·5 PTZ in Alkaline Solution.

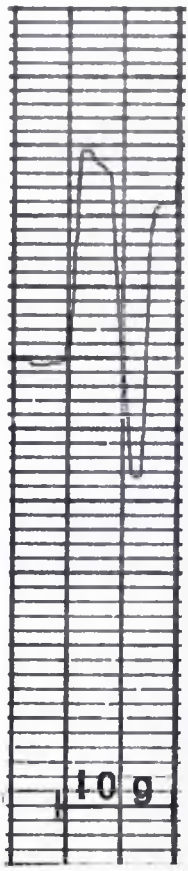

FIG 4·6

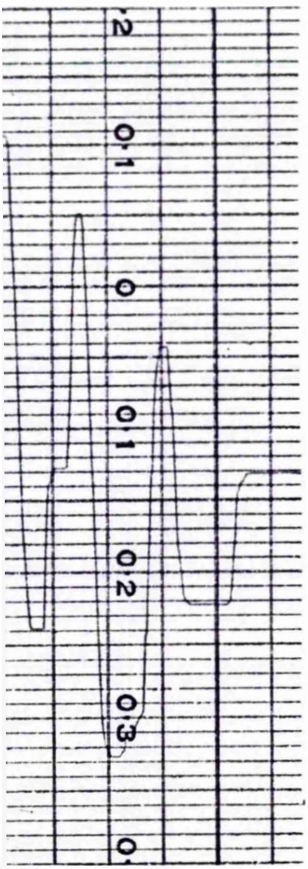

PT Z in H_2SO_4

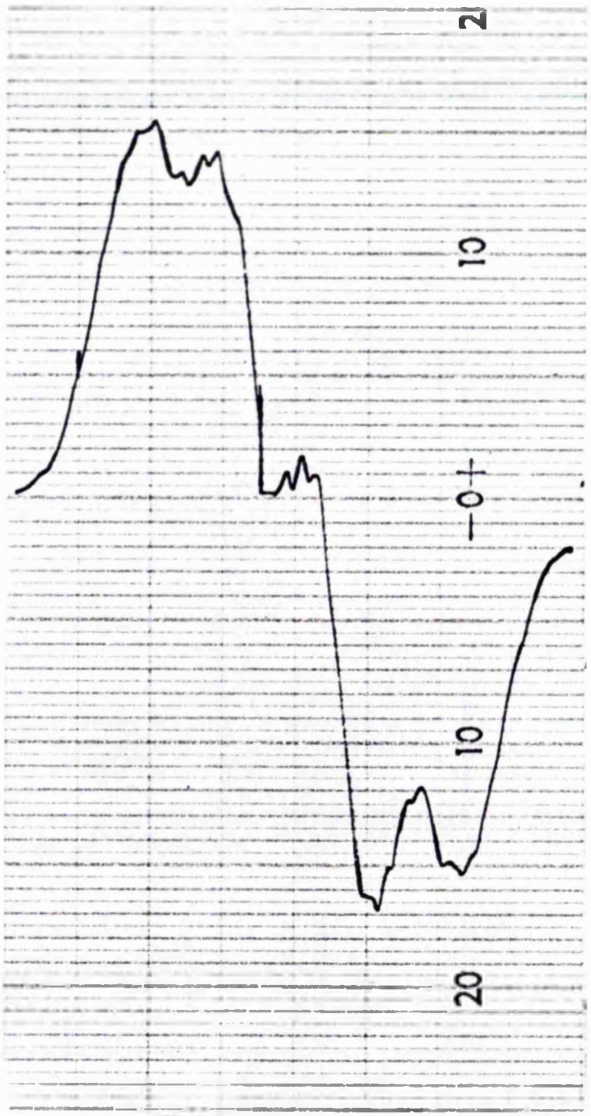

FIG 4·7 Analogue Computer Simulation.

two lines are closer together than the average separation. Fig. 4.8 shows that if $\beta > \alpha$, but not to such an extent that more than four of the six lines are resolved, then the separation of the central two lines will be less than average. Relative to the centre of the spectrum, the six lines occur at positions

$$\alpha + \beta/2;\ \beta/2;\ \alpha - \beta/2;\ \beta/2 - \alpha;\ -\beta/2;\ -\alpha - \beta/2. \quad (4.8.1)$$

Therefore $\alpha < 6.7$ gauss, and $\beta > 6.7$ gauss.

(c) Reaction with H_2SO_4

The fact that the E.S.R. spectrum may be explained by approximately equal interactions of the unpaired electron with the N^{14} nucleus and its associated proton, makes unlikely the suggestion of Croisignani et al [C1] that a neutral radical is formed by removal of this proton. It seems probable that the reaction is similar to that proposed for N-methyl PTZ [C2] and is as follows:

$$2PTZ + 3H_2SO_4 \rightarrow 2[PTZ]^+ + 2HSO_4^- + SO_2 + 2H_2O.$$

Therefore, as in § 4.2 and § 4.3 the positive ion appears to be involved.

(d) Equivalence of the positive ion spectra

The spectrum of Fig. 4.3 shows some signs of hyperfine splitting and it is possible that this is equivalent to Fig. 4.6 apart from a greater line width.

Using the PACE TR48 Analogue computer a four line spectrum with intensities 1:2:2:1 has been synthesised for different line widths. As

a crude approximation, a Gaussian line shape is assumed (the actual line shape is complicated by the existence of unresolved hyperfine components). This method will be described in detail in § 7.10.

The simulated spectrum of Fig. 4.7 shows a similarity to Fig. 4.3 which allows the possibility that both Figs. 4.3 and 4.6 arise from the $[PTZ]^+$ ion with different line widths in the two cases.

(e) The high resolution spectrum

With the higher resolution available with the Mullard magnet (§ 3.15 (b)), it is seen that many more lines are now visible (Fig. 4.9)*. In order to limit noise, the bandwidth was, on one occasion, reduced to 0.03 c/s and six hours was taken to sweep through the spectrum using a 280 c/s modulation of 0.1 gauss. Although the slowest pen recorder paper speed of one sixth of an inch per minute was used, this recording occupies about seven feet of paper. The measurements made from this spectrum have been given greatest weight in the following interpretation (§ 4.8 (f)) of the hyperfine splitting parameters. However, for ease of reproduction the spectrum of Fig. 4.9 is a one and a half hour recording for which an output bandwidth of 0.1 c/s was used. Half of the six hour recording is shown in Figs. 4.10, 4.11 and 4.12 as a basis for comparison with simulated spectra.

(f) Interpretation of Fig. 4.9*

The interpretation of this spectrum is rendered more difficult by its asymmetry, which is caused by an increase in line width with magnetic

*See page 163.

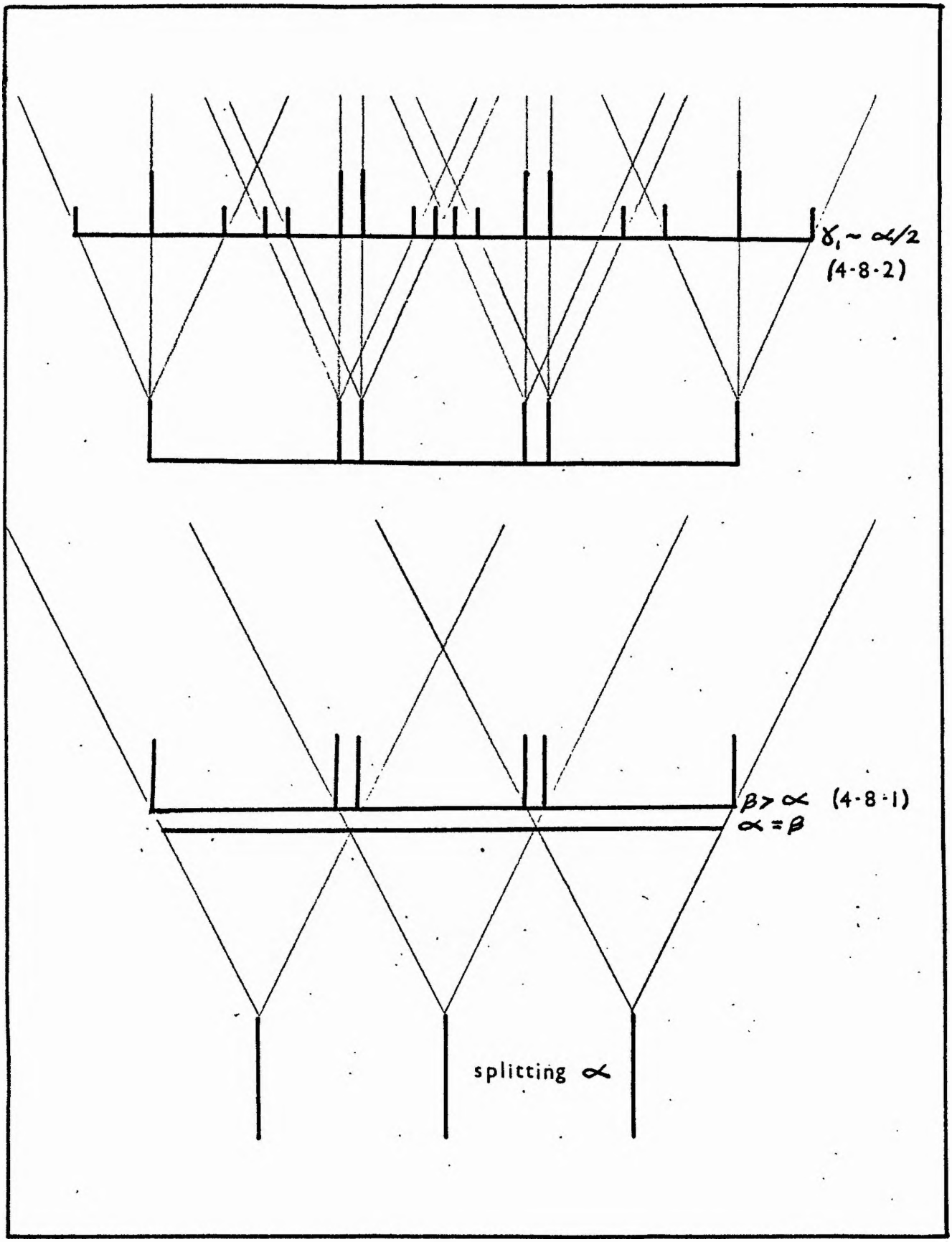

FIG 4·8 Hyperfine Splittings for PTZ.

field. The spectrum is seen to be composed of nine main groups of lines, the last two at the higher magnetic field end being unresolved. Apart from the Nitrogen nucleus and its associated proton, the splittings (α and β) of which determine the low resolution spectrum and of which the approximate values were estimated in § 4.8 (b), further hyperfine splittings can arise from interactions of the electron spin with the four pairs of equivalent ring protons. The hyperfine splitting parameters in the spin Hamiltonian (§ 2.1) of these are taken to be γ_1, γ_2, γ_3 and γ_4 in decreasing magnitude, each representing a pair of equivalent protons and thus corresponding to a splitting of 1:2:1. At this stage it is not possible to associate any of these parameters with a particular position in the molecule.

Fig. 4.8 shows the further splitting of the six lines of (4.8.1) which account for the low resolution spectrum, by one pair of equivalent protons (splitting parameter γ_1). It appears that the only situation for which nine groups of lines could occur, corresponds to $\gamma_1 \doteq \frac{\alpha}{2}, \frac{\beta}{2}$. Also the approximately equal spacing between groups excludes the possibility that any of γ_2, γ_3, γ_4 are as great as γ_1. Thus, including γ_1, (4.8.1) is extended to eighteen lines in nine groups, of which the positions relative to the centre of the spectrum and their intensities are as follows:

Group	I, line	(1), position	$\alpha + \beta/2 + \gamma_1$,	intensity x 1
	II	(2)	$\alpha + \beta/2$	x 2
		(3)	$\alpha + \beta/2 - \gamma_1$	x 1
	III	(4)	$\beta/2 + \gamma_1$	x 1
		(5)	$\alpha - \beta/2 + \gamma_1$	x 1
	IV	(6)	$\beta/2$	x 2
		(7)	$\alpha - \beta/2$	x 2
		(8)	$\beta/2 - \gamma_1$	x 1
	V	(9)	$\alpha - \beta/2 - \gamma_1$	x 1
		(10)	$-\alpha + \beta/2 + \gamma_1$	x 1
		(11)	$-\beta/2 + \gamma_1$	x 1
	Etc.			

(4.8.2)

The spectrum is symmetrical about group V and about lines 9 and 10. The lines of intensity 2 correspond to the original six lines of (4.8.1).

The only two resolved groups which each contain a single one of the eighteen lines above are I and II, and thus if lines (1) and (2) correspond to the central hyperfine components of groups I and II, their separation gives γ_1, which is found to be 2.4 gauss. If the next largest parameter, γ_2 were approximately equal to γ_1, a system of eleven groups of lines would be predicted, with an intensity ratio 1:4:8:9:15:16:15:9:8:4:1, and the system of nine groups of lines is not predicted unless $\gamma_2 < \gamma_1/2$. From an examination of the individual lines in the

various groups, it is evident that they are of approximately equal spacing. Also, the manner in which the hyperfine components of groups I and II, each of which is derived from a single line of (4.8.2), appear to increase regularly in intensity towards the centre of the group, suggests that there exists a simple integral relationship connecting γ_2, γ_3, and γ_4. In attempting to assess the possible values of γ_2, γ_3 and γ_4 the outer side of group I may be considered, as this is unaffected by overlapping lines from neighbouring groups. The intensity ratios calculated below apply to each of the eighteen lines of (4.8.2).

An insufficient number of lines is predicted if γ_3 and γ_4 are both unresolved. The possible integral ratios of γ_2, γ_3 and γ_4, consistent with $\gamma_2 < \gamma_1/2$, are

(i) γ_4 unresolved, $\gamma_2 = \gamma_3$ = smallest observed splitting $\doteqdot$ 0.5 gauss. This is rejected as again too few lines are predicted.

(ii) γ_4 unresolved, $\gamma_2 = 2\gamma_3$, with $\gamma_3 \doteqdot$ 0.5 gauss. This predicts 1:2:3:4:3:2:1.

(iii) γ_4 unresolved, $\gamma_2 = 3\gamma_3$. This must be rejected, as in this case γ_2 is greater than $\gamma_1/2$.

(iv) $\gamma_2 = \gamma_3 = \gamma_4 \doteqdot$ 0.5 gauss. This predicts 1:6:15:20:15:6:1.

(v) $\gamma_2 = \gamma_3 = 2\gamma_4$, with $\gamma_4 \doteqdot$ 0.5 gauss. This predicts 1:2:5:8:10:12:10:8:5:2:1.

(vi) $\gamma_2 = 2\gamma_3 = 2\gamma_4$, with $\gamma_4 \doteqdot$ 0.5 gauss. This predicts 1:4:8:12:14:12:8:4:1.

Now, the approximate peak to peak derivative intensity ratios of the outer side of group I in Fig. 4.9 is 1:6:13:22:25. When the experimental intensities are compared with the above predicted ratios, (vi) agrees quite well, although the outermost line in the experimental spectrum is slightly too weak. If this line were due to a C^{13} splitting, the ratios of (ii) would also be a reasonably good approximation, although no evidence exists of other C^{13} splittings still further out, which might then be expected. This is discussed further in § 6.4. On the assumption that either (ii) or (vi) may be valid, the separations of the hyperfine components of group I are measured. (The position of a hyperfine line is assumed to occur midway between the positions of maximum and minimum slope.) If $\gamma_2 = 2\gamma_3$ is exactly true for (ii) or $\gamma_2 = 2\gamma_3 = 2\gamma_4$ for (vi), then the spacings between adjacent lines should be equal. By similar arguments to that used in § 4.8 (b) to show that $\beta > \alpha$, the slight departures from equal spacing in the two cases enables the following estimations of hyperfine splitting parameters to be made:

$$\text{for (ii)} \quad \begin{aligned} \gamma_2 &= 1.05 \text{ gauss} \\ \gamma_3 &= 0.51 \text{ gauss} \\ \gamma_4 &= 0 \end{aligned} \qquad (4.8.3)$$

$$\text{for (vi)} \quad \begin{aligned} \gamma_2 &= 1.07 \text{ gauss} \\ \gamma_3 &= 0.49 \text{ gauss} \\ \gamma_4 &= 0.49 \text{ gauss} \end{aligned} \qquad (4.8.4)$$

In fact, in the latter case, if γ_3 is not exactly equal to γ_4 no displace-

ment of the hyperfine components is predicted, and the assignment should be $\frac{\gamma_3 + \gamma_4}{2} = 0.49$ gauss.

Thus approximate values of α and β are now known, γ_1 is known fairly accurately, and two possible sets of values of γ_2, γ_3 and γ_4 have been calculated. A more accurate estimation of α and β must now be made, after which the complete spectrum may be reconstructed, and the relative merits of (4.8.3) and (4.8.4) considered further.

Group IV contains two lines of (4.8.2) which are separated by $\beta-\alpha$. The intensities of the hyperfine components of this group increase towards the centre of the group, where they have about the greatest magnitude in the spectrum. This suggests that $\beta-\alpha$ is approximately an integral multiple of the smallest splitting parameter γ_3. The symmetry of group IV about two hyperfine components indicates that this multiple is an odd integer, i.e. $\beta-\alpha = \gamma_3$ or $\beta-\alpha = 3\gamma_3$.

The difference between β and α cannot be greater than $3\gamma_3$ as the central lines of the group would not then have the greatest intensity.

The same intensity distribution should occur for group VI, but here the increased hyperfine line width reduces the resolution, and the observed intensity of the hyperfine components. The condition of symmetry about the two central lines of group VI does not appear quite so obvious as in group IV.

In order to examine the possible values of $(\beta - \alpha)$, each of the

eighteen lines of (4.8.2) are now assigned to a particular hyperfine component in the spectrum, the assignment taking slightly different forms for $\beta - \alpha = \gamma_3$ and $3\gamma_3$. No ambiguity exists about lines (1) and (2) of (4.8.2) as these must occur at the components of greatest intensity of groups I and II respectively, and these have already been used to determine γ_1.

The positioning of the group IV lines, (6) and (7), is also obvious for $\beta - \alpha = \gamma_3$ and $3\gamma_3$ as they must be symmetrical about the two central components of the group. As γ_1 is known, the lines (3), (4), (5), (8) and (9) may be located, and the same process on the high magnetic field half of the spectrum determines lines (10) to (16). The last two are unresolved. The assignments in the two cases are shown in Fig. 4.9.

By measuring the separations between appropriate lines of (4.8.2), it is possible to obtain ten values of γ_1, nine for α and five for β, and these values must all be consistent. The following values and standard deviations are found.

<u>For $\beta - \alpha = \gamma_3$</u>

$$\begin{aligned} \alpha &= 6.48 \pm 0.07 \text{ gauss} \\ \beta &= 7.03 \pm 0.08 \text{ gauss} \\ \gamma_1 &= 2.38 \pm 0.06 \text{ gauss} \end{aligned} \qquad (4.8.5)$$

<u>For $\beta - \alpha = 3\gamma_3$</u>

$$\begin{aligned} \alpha &= 5.93 \pm 0.07 \text{ gauss} \\ \beta &= 7.51 \pm 0.07 \text{ gauss} \\ \gamma_1 &= 2.41 \pm 0.06 \text{ gauss} \end{aligned} \qquad (4.8.6)$$

The standard deviations here refer to the ratio of the parameters, and the corresponding errors in γ_2 and γ_3 of (4.8.3) and (4.8.4) are 0.02 and 0.01 gauss respectively. The actual error in converting to gauss is 2% (§ 3.15 (b)).

The possibility of $\beta - \alpha = 2\gamma_3$ has already been rejected, and it is further noted that a self consistent assignment of lines could be made for this case, only if group V contained an additional line.

Four possibilities now exist for the splitting parameters, i.e. either (4.8.5) or (4.8.6) determines α, β and γ_1 which define the eighteen lines of (4.8.2), while either (4.8.3) or (4.8.4) determines γ_2, γ_3 and γ_4, which further split each of these eighteen lines.

In each of the four cases, therefore, the spectrum may be reconstructed as in Fig. 4.10(b), which shows half the reconstructed spectrum (which is symmetrical) when the parameters are determined by (4.8.3) and (4.8.5) together with the better resolved half of the experimental spectrum (Fig. 4.10(a)).

It is now necessary to consider which of the above four possibilities best describes the experimental spectrum. The respective merits of (4.8.3) and (4.8.4) have already been mentioned, and no further evidence is available until the digital computer spectrum simulations are discussed in § 4.9.

It was shown from the low resolution spectrum (§ 4.8 (b)) that $\beta > \alpha$. An examination of sixteen spectra indicates that the ratio of α to β is

0.91 ± 0.01. (4.8.5) predicts $\alpha/\beta = 0.923 \pm 0.015$ and is therefore in agreement, but (4.8.6) predicts $\alpha/\beta = 0.790 \pm 0.014$ which is well outside the experimental error. However, the low resolution spectrum, while approximating to a four line structure contains many unresolved lines, and these comparisons may, therefore, not be very significant.

Barton and Fraenkel [B8] have noted that when a nitrogen atom is bonded to a proton and to two carbon atoms, as in this case, the ratio of N^{14} splitting to proton splitting, i.e. α/β, is 0.94 unless a high unpaired electron density occurs on the N^{14} atom. (It will be seen in § 6.4 that $\rho_n \doteq 0.2$ and thus presumably cannot be considered to be unduly high.) This provides additional evidence in favour of (4.8.5).

In the assignment of lines (12) and (13) of (4.8.2) to group VI, Fig. 4.9 shows that (4.8.5) requires a different pair of components to be chosen as the central pair about which the group should be symmetrical than is the case for (4.8.6). The latter assignment appears slightly more probable although the progressive line width variation makes the former quite possible.

The results of spectrum simulations in § 4.9 will provide further evidence. At this stage any one of the four interpretations is still possible although the evidence favours (4.8.5) together with (4.8.4). In fact, it will be shown in § 4.9 that (4.8.6) is incorrect and in § 6.4 (b) that (4.8.3) is incorrect and therefore Fig. 4.9 is described by the following parameters

$$\alpha = 6.48 \text{ gauss}, \quad \beta = 7.03 \text{ gauss}$$
$$\gamma_1 = 2.38 \text{ gauss}, \quad \gamma_2 = 1.07 \text{ gauss} \qquad (4.8.7)$$
$$\gamma_3 = 0.49 \text{ gauss}, \quad \gamma_4 = 0.49 \text{ gauss}$$

(g) Summary of the evidence for the interpretation

(i) From the molecular symmetry only six hyperfine splitting parameters are involved (α, β, γ_1, γ_2, γ_3 and γ_4).

(ii) Low resolution 1:2:2:1 spectrum suggest $\alpha = \beta$ with $\beta > \alpha$.

(iii) On high resolution, nine approximately equally spaced groups of lines are observed which indicates that the highest splitting parameter of the pairs of ring protons, $\gamma_1 \doteq \alpha/2$ and the eighteen lines of (4.8.2) are predicted by α, β and γ_1. Also none of γ_2, γ_3 and γ_4 are $> \gamma_1/2$.

(iv) Lines (1) and (2) of (4.8.2) are the only ones in groups I and II and their separation gives γ_1.

(v) The eighteen lines of (4.8.2) are further split by γ_2, γ_3 and γ_4 by an intensity ratio 1:2:1 in each case. This suggests that most of the hyperfine components at the positions of (4.8.2) will be of above average intensity.

(vi) The intensity distributions in groups I and II require an integral relation among γ_2, γ_3 and γ_4 and the distribution in groups IV and VI requires that $\beta - \alpha$ = n times the lowest observed splitting where n = 1 or 3.

(vii) It follows from (v), that an assignment of the lines of (4.8.2)

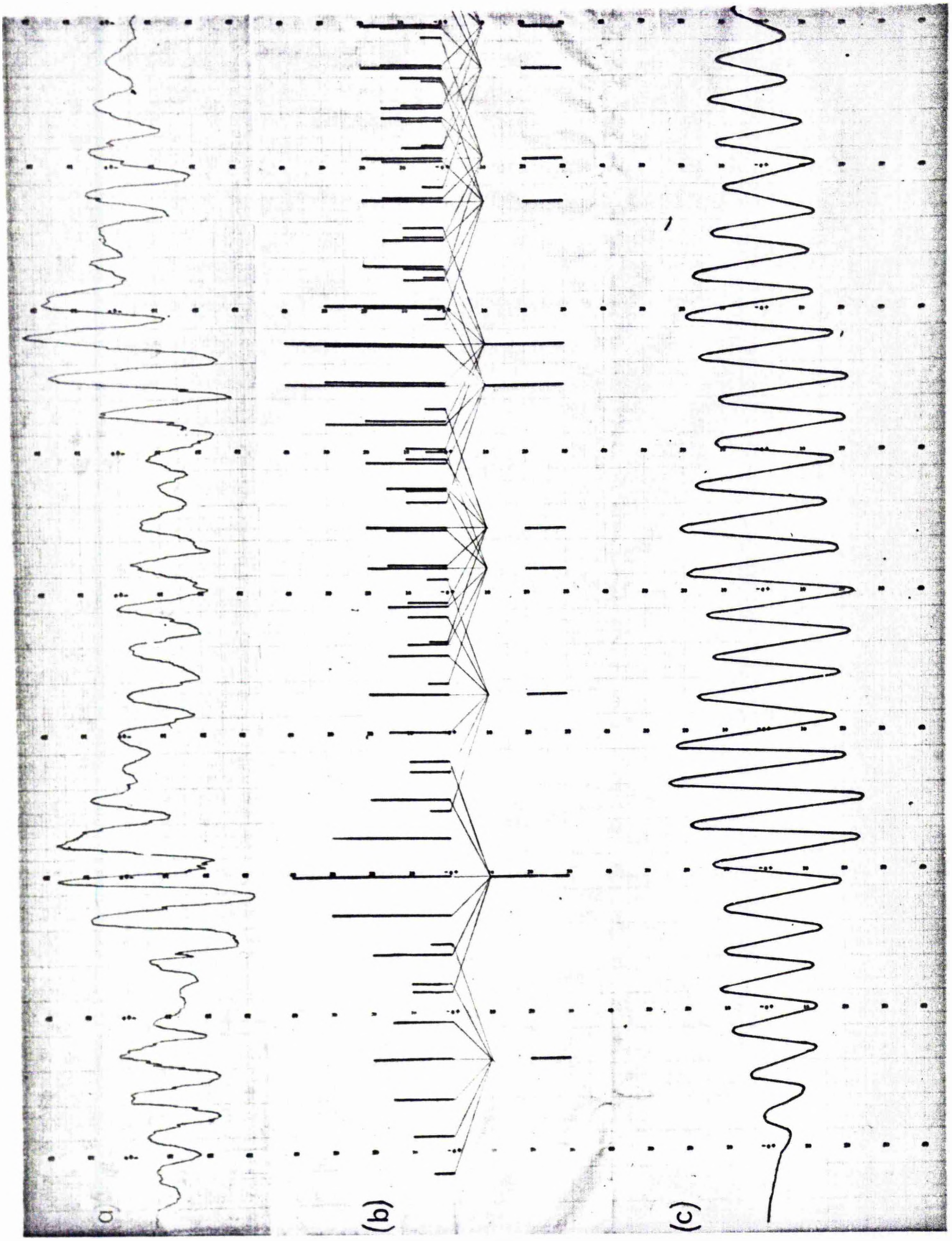

FIG 4·10 PTZ , Reconstruction, & Sim. Spec. of Gagnaire.

may be made to individual components of the spectrum. The separations of these lines must be consistent, in which case accurate values of α, β and γ_1 are obtained.

§ 4.9 Simulation of PTZ Spectrum

The reconstruction of the PTZ spectrum of Fig. 4.10(b) gives the calculated positions of the individual hyperfine lines when the hyperfine splitting parameters of the spin Hamiltonian are determined by (4.8.3) and (4.8.5). If the hyperfine components were unbroadened it would be possible unequivocally to check the position of each against the positions in Fig. 4.9 and decide whether the spectrum had been correctly interpreted.

However when the resolution is not complete the comparison of this type of reconstruction with the experimental spectrum is not so straightforward. It is difficult, for example, to judge whether two adjacent lines are too close together to be resolved, and if so, exactly what form the sum of their derivatives will take.

In § 7.10 a method will be described whereby simple E.S.R. spectra may be simulated using an analogue computer. However, the simulation of a complicated spectrum involving many hyperfine lines is a more suitable problem for a digital computer and several programs for the simulation of E.S.R. spectra have been described in the literature [G5] [S7] [S8]. Of these,only one [S7] is suitable for spectra containing hyperfine lines, but this does not allow the incorporation of a line

width variation. A Fortran program which can include a variation of line width in the synthesised spectrum, was written by the author for use with the IBM 1620 computer. A print out of this program is shown in Appendix I.

The positions, P(N), and intensities, FACP(N), of the 270 lines in the reconstructions of the PTZ spectrum (e.g. Fig. 4.10(b)) may be defined by means of five hyperfine splitting parameters. The magnitudes of the splitting produced by these parameters (PA(I) etc.) and the distribution of intensities predicted by each (FC(I) etc.) are read in as data. The smallest of the parameters accounts for either four or two equivalent protons ($\gamma_3 = \gamma_1$ and $\gamma_4 = 0$ respectively) by taking the intensity distribution, FE(I), as 1:4:6:4:1 or 0:1:2:1:0 in the two cases. The line-width parameters, which are also read in as data, are used to calculate Lorentzian and Gaussian line shapes (FL and FG) each of which occupies 60 locations. The Gaussian spectrum, for example, is compiled in a 1000 location store (SPEC) by adding a multiple of FG at each of the 270 positions. For the N^{th} line, for example, FG is multiplied by FACP(N) and is added into the 60 locations of SPEC centred about P(N). It is also possible to use other line shapes besides Gaussian and Lorentzian.

The type of variation of line width with I_z, as observed in PTZ, is included by the use of four line-width parameters, A(I), which define four functions for each of FL and FG. These four line widths correspond roughly to the four lines of the low resolution PTZ spectrum. At the

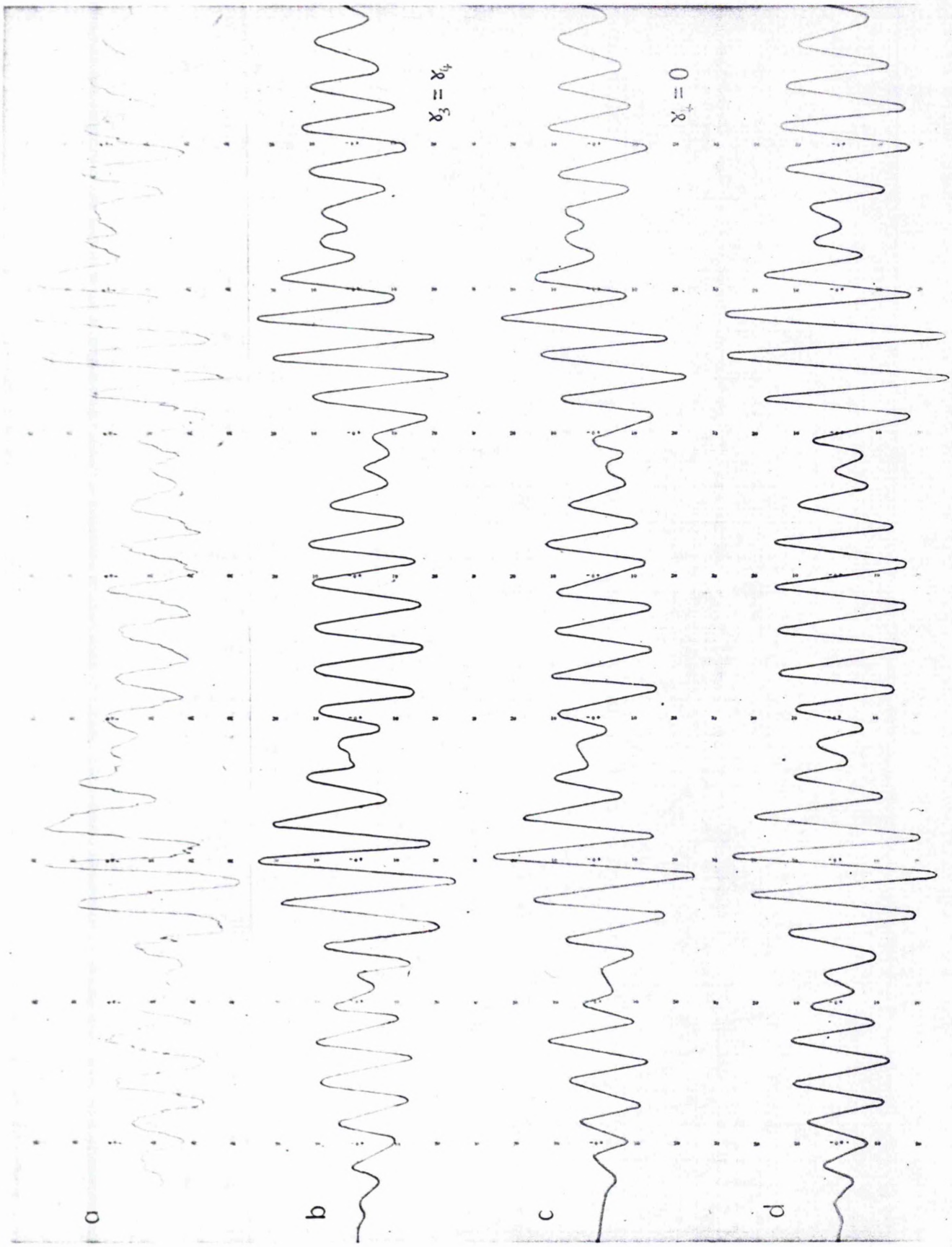

FIG 4·11 PTZ & Sim. Spectra for (4·8·5)

same time as P(N) and FACP(N), an additional function NCH(N) is compiled, which determines the allocation of one of the four values of FL or FG to that particular line (N). In this manner, the changes in line width are not abrupt and a considerable overlap of lines of the two types occurs at the appropriate position of each change in line-width parameter.

Using this program it is now possible to simulate spectra corresponding to the four situations represented by (4.8.3) to (4.8.6). For the purposes of comparison with the experimental spectrum, it is more convenient to consider only the better resolved half of the spectrum. If complete agreement is obtained for this half, then the hyperfine splitting parameters may be considered to account entirely for the actual unpaired electron distribution in the PTZ molecule. If, in this case, the other half of the simulated spectrum is not in full agreement with the corresponding part of Fig. 4.9, the discrepancies will be due entirely to the use of incorrect line-width parameters.

Some of the spectra which have been simulated using this program are shown in Figs. 4.10, 4.11 and 4.12, below the experimentally observed spectrum in each case. Fig. 4.11(b) and (c) and 4.12(b) and (c) show the simulated spectra for the four sets of hyperfine splitting parameters determined by (4.8.3) to (4.8.6) for a Lorentzian line shape. Evidently both Figs. 4.11(b) and (c) represent considerably closer agreement with Fig. 4.11(a) than do Figs. 4.12(b) and (c). This adds fairly conclusive evidence that (4.8.5) is correct rather than (4.8.6).

Fig. 4.12(b) is the result of a systematic variation of hyperfine

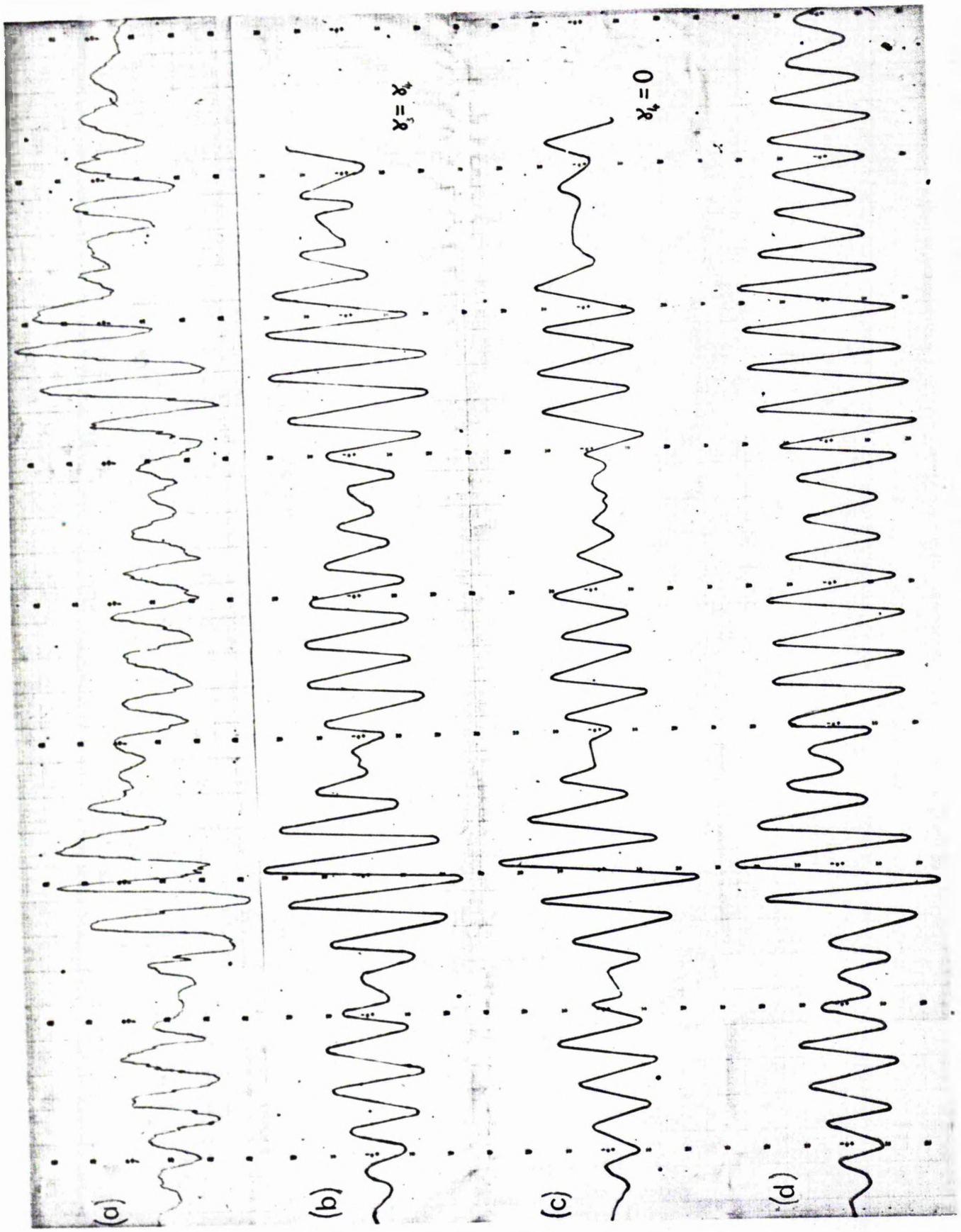

FIG 4·12 PTZ & Sim. Spectra for (4·8·6)

splitting parameters and line-width parameters, in the course of which about 25 spectra were simulated in an unsuccessful attempt to predict the correct ratio of intensities, particularly within group IV. The attempt is even less successful in Fig. 4.13(c) although the reason for the smaller actual magnitude of group IV lines is that the line-width parameters used here are the same as those used in Figs. 4.11(b) and (c), while Fig. 4.12(b) employs the line-width parameters which predict the correct actual magnitude of the central two lines in group IV.

Fig. 4.11(d) shows the spectrum, using a Gaussian lineshape, for the same values of the parameters as Fig. 4.11(b). Slight differences occur between these two spectra although both agree reasonably well with Fig. 4.11(a).

Fig. 4.12(d) shows the effect of reducing γ_1 by 2% and increasing α by 2% from the values of Fig. 4.12(b) until the overlapping components from different groups are no longer "out of phase" and therefore the division of the spectrum into groups is not so obvious.

The computer program was altered to permit a continuous linear variation of line-width throughout the spectrum. In this program, the line-width parameter and also the line shape function is calculated afresh for each line in the spectrum. This increases the amount of machine time required to compile a spectrum from about three minutes to about twenty minutes without resulting in a significant improvement.

Gagnaire et al [G6] have obtained a high resolution PTZ spectrum

in H_2SO_4, their interpretation of which led to a set of hyperfine splitting parameters which disagree with all of the possible combinations discussed here. Fig. 4.10(c) shows the Lorentzian spectrum predicted by their parameters, which evidently bears little resemblance to the experimental spectrum.

The IBM 1620 computer became available only shortly before the end of 1964 and, as neither a card reader and plotter nor a digital to analogue converter is at present available, all spectra require to be plotted by hand. This has left time to carry out a fairly exhaustive variation of parameters only for Fig. 4.12(b) and (c) which shows conclusively that (4.8.6) is incorrect. The only parameters varied for the spectra of (4.8.5), i.e. those of Fig. 4.11, are the line-width parameters. The hyperfine splitting parameters have been used exactly as calculated in (4.8.3), (4.8.4) and (4.8.5).

§ 4.10 Hyperfine Line Width of PTZ in H_2SO_4

The progressive increase in line width of the hyperfine components with increasing magnetic field has already been noted as causing additional difficulties in the interpretation of the PTZ spectrum. The mechanisms which cause this line broadening will now be investigated.

From the time dependent part of the microcrystalline Hamiltonian (2.2.3), it has been shown (§ 2.3 (g)) that, for a correlation time which is sufficiently long, significant contributions can arise to the spin lattice and transverse relaxation times (T_1 and T_2' respectively).

Evidently these relaxation times involve the nuclear orientation (2.3.6) and (2.3.7) and thus a variation in line width with I_z is predicted. Both T_1 and T_2' involve the term ($\Delta g\beta H + bI_z$) and a shorter relaxation time is predicted for negative than for positive I_z. This agrees in sign with the observed variation for PTZ, where the line width is greater at the higher magnetic field end of the spectrum.

In the case of the Cu^{++} ion in aqueous solution, knowing the values of Δg and b (2.2.4), McConnel was able to perform an order of magnitude estimation of T_1 and T_2', using values of τ_c based upon 3A° and 15A° as the limiting values of the effective radii of the microcrystal [M1].

The H_2SO_4 molecule has a similar dipole moment to H_2O and, as the basis of an order of magnitude estimation, it seems reasonable to assume a similar extent of solvent polarization in the vicinity of a charged cation, and to use the same value for the maximum radius of the microcrystal (15A°) in the case of PTZ in H_2SO_4. The minimum value is taken to be 3A°, although for PTZ this is probably unnecessarily low.

For PTZ it is not possible to follow the above procedure as both Δg and b are unknown. It is possible, however, to estimate the line widths of the hyperfine components at different parts of the spectrum and relate these to an effective value of I_z.

The approximate line-width in the different groups is estimated by the help of the spectrum simulation method of § 4.9. The parameters

of (4.8.7) are used and the line width parameters are varied until the correct magnitude of lines occurs at the centre of the group under consideration.

The value of an effective nuclear spin (I_{eff}) is required, the z component of which will characterise the position of each of the nine groups. It seems reasonable to neglect the contribution of those nuclei which correspond to the splitting parameters smaller than γ_1 as no obvious changes in line width occur within the groups.

In assigning the effective nuclear spin, it is not sufficient to take

$$I_{eff} = \sum_i I_i \qquad (4.10.1)$$

where the sum is taken over the nuclei which give rise to the splittings α, β and γ_1, as this takes no account of the different magnitudes of the splitting parameters. If a weighting factor W is considered, proportional to the hyperfine splitting, I_{eff} is then written

$$I_{eff} = \sum_i W_i I_i . \qquad (4.10.2)$$

The splitting parameter $\alpha \fallingdotseq \beta \fallingdotseq 2\gamma$ and, if W_α is chosen to be unity, then $W_\beta = 1$, $W_\gamma = \frac{1}{2}$ and $I_{eff} = 2$. The possible values of $I_{z(eff)}$ predict a nine line spectrum of equal spacing which corresponds roughly to the nine groups of the PTZ spectrum. The fact that $I_{eff} = 2$ predicts nine lines of equal intensity, while $\alpha \fallingdotseq \beta \fallingdotseq 2\gamma_1$, gives rise to a distribution of intensities 1:2:3:4:4:4:3:2:1 shows that this crude approximation of

attempting to describe the spectrum by one effective nuclear spin, accounts for the position of lines only. The estimated line widths of the different groups and the corresponding values of $I_{z(eff)}$ are as follows.

Group	I	II	III	IV	V	VI	VII	VIII	IX
$I_{z(eff)}$	+ 2	+ 3/2	+ 1	+ ½	0	- ½	- 1	- 3/2	- 2
Line width (gauss)	0.18	0.20	0.25	0.28	0.33	0.36	0.43	>0.6	>0.6

(4.10.3)

Equations (2.3.6) and (2.3.7) may be written in the form

$$\left(\frac{1}{T_1}\right)^{\frac{1}{2}} = k_1(\Delta g\beta H + bI_z) \qquad (4.10.4)$$

$$\left(\frac{1}{T_2}\right)\left(\frac{1}{\tan^{-1}\frac{2\tau_c}{T_2}}\right)^{\frac{1}{2}} = k_2(\Delta g\beta H + bI_z) \qquad (4.10.5)$$

where k_1 and k_2 are independent of T_1 and T_2'. These equations assume that the approximations of McConnel in omitting terms from (2.2.3) are justified and that there are no significant contributions to T_1 through spin orbit coupling and to T_2' through dipolar or exchange interactions with other paramagnetic ions.

The two situations are now considered where the observed line widths of (4.10.3), expressed in terms of $\frac{1}{T_2}$, are determined by (i) T_1 and (ii) T_2'.

(i) $T_2 = T_1$. $\frac{1}{T_1}$ is plotted against $I_{z(eff)}$ and a straight line graph should result from (4.10.4). The slope of this and its intercept with

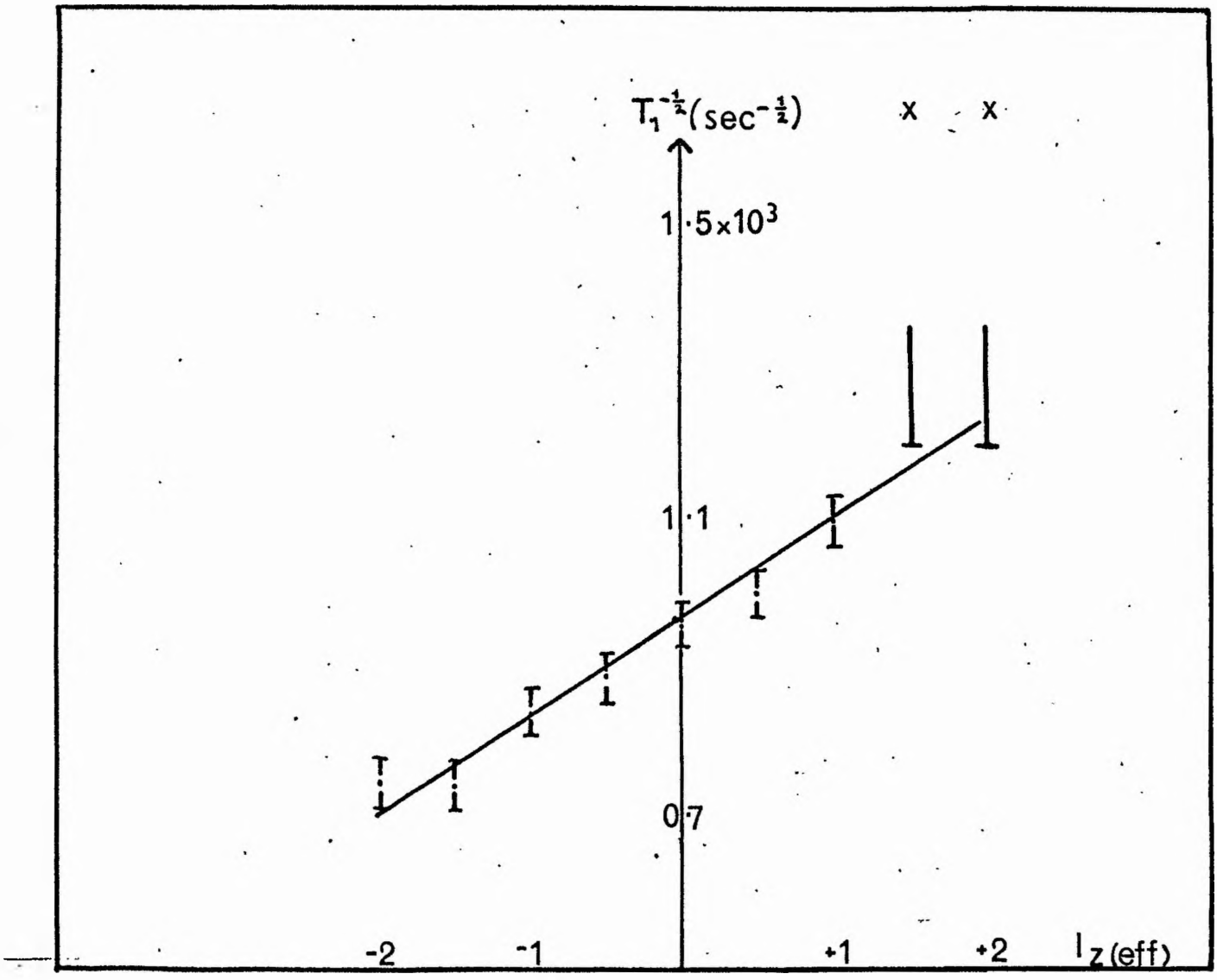

FIG 4·13 $T_1^{-\frac{1}{2}}$ vs $I_{z(eff)}$ for PTZ at 17°C

the $I_{z(eff)}$ axis should give values for b and Δg respectively. A plot of this nature using the estimated line widths from (4.10.3) is shown in Fig. 4.13.

This graph is a fairly good approximation to a straight line as would be anticipated from the theory although fairly large errors are involved in estimating the line widths. This curve corresponds to the lower value of a (i.e. 3A°) and from it Δg and b are found to be about 0.05 and 0.001 cm^{-1} respectively. For a = 15A° the ordinates of all the points in Fig. 4.13 are multiplied by a constant factor and Δg and b become about 0.55 and 0.025 cm^{-1}.

(ii) $T_2 = T_2'$. In this situation the following results are obtained

$$a = 3A°, \qquad \Delta g \fallingdotseq 0.06, \qquad b \fallingdotseq 0.001 \text{ cm}^{-1}$$

$$a = 15A°, \qquad \Delta g \fallingdotseq 0.005, \qquad b \fallingdotseq 0.0001 \text{ cm}^{-1}$$

Thus for $T_2 = T_1$ much higher values of Δg and b are predicted when the larger correlation time is used than for $T_2 = T_2'$. However, when the smaller τ_c is used the predicted values are comparable in the two cases.

Unfortunately no data are available concerning the values of Δg and b for PTZ. However the g value of PTZ in H_2SO_4 was measured using a D.P.P.H. marker and found to be 2.0047 ± 0.0002. Since g is within 0.003 of the value for a free spin, it is unlikely that Δg is much greater than 0.003 and only the lowest predicted value of Δg(i.e. 0.005) would appear to be possible. (A typical example of an organic radical, D.P.P.H. has $\Delta g \fallingdotseq 0.001$ [H7] and irradiated glycollic acid has $\Delta g \fallingdotseq 0.003$ [A5].)

The hyperfine splitting corresponding to unit difference in I_z is about 7 gauss (i.e. about 0.0006 cm^{-1}) and again the case of $T_2 = T_2'$ and r = 15A°, which predicts the lowest value of b ($\sim$0.0001 cm^{-1}), is the only one where b is of a feasible order of magnitude.

If therefore the McConnel theory is applicable to PTZ in H_2SO_4, then the line width of the hyperfine components must result from a transverse relaxation time, and the effective microcrystal radius must be at least 15A° and probably more.

The approximation that the 3rd, 4th and 5th terms of (2.2.3) are negligible assumes that $\Delta g\beta H \gg b$, to justify the omission of terms in b^2 compared with terms in $(\Delta g\beta H)^2$ and $\Delta g\beta Hb$. Here the ratio between $\Delta g\beta H$ and b is about 10, which is probably not sufficiently great to justify fully this approximation.

A more likely reason for disagreement with the theory is the incomplete resolution of the spectrum which, Rogers and Pake [R9] have noted, would conflict with the initial assumptions. The overlapping of adjacent lines would conflict with assumptions also in the more advanced theory of Kivelson [K5]. The procedure in the latter case would involve fitting line widths to a quadratic equation in I_z which would require a more accurate line width determination than that of (4.10.3).

§ 4.11 Temperature Variation of Line Width

As the lines of groups VIII and IX are unresolved, the corresponding points on Fig. 4.13 are uncertain, and the lower limits of these points

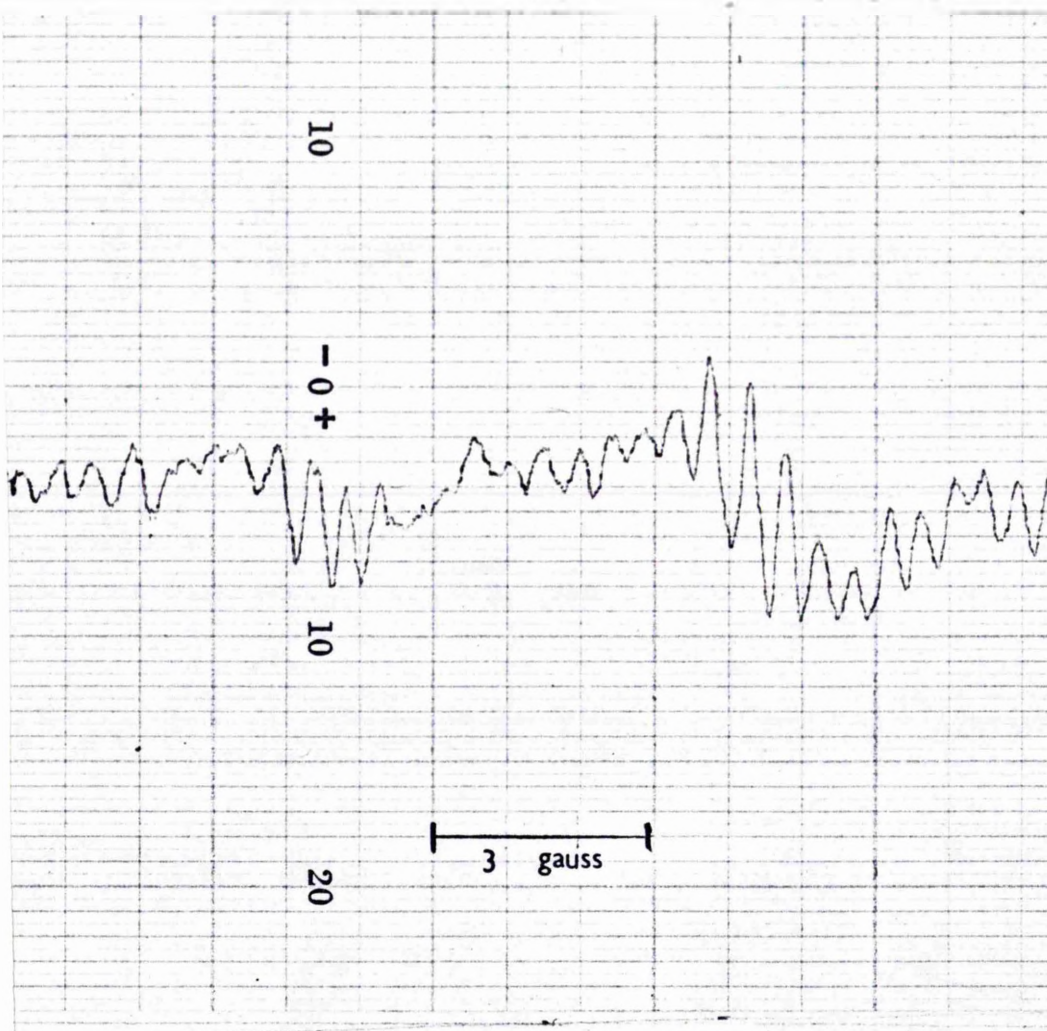

FIG 4·14 PTZ at 36°C.

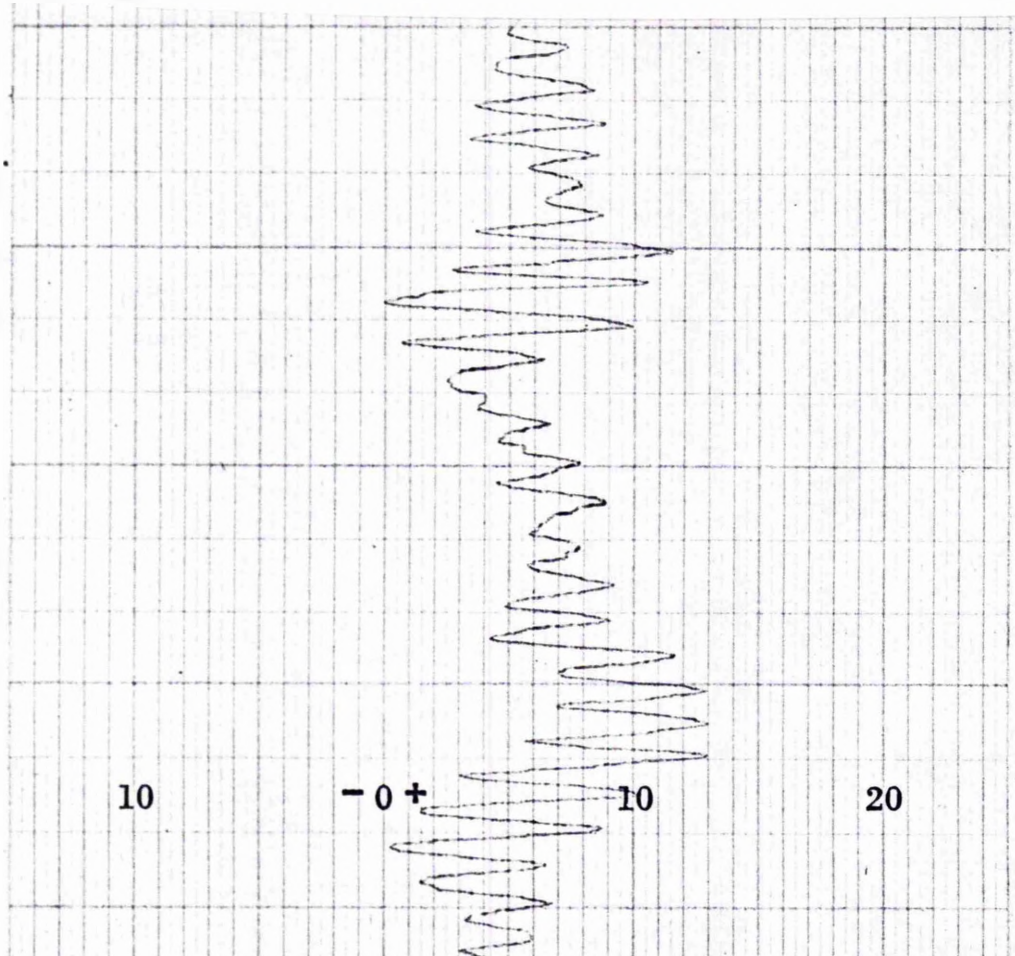
10
- 0 +
10
20

are determined by the minimum line width for which they will remain unresolved.

From the expressions for $\frac{1}{T_1}$ and $\frac{1}{T_2}$, (2.3.6) and (2.3.7), derived from the microcrystalline model, it appears that a reduction in line width would be effected by reducing τ_c as a result of raising the temperature and, therefore, lowering the viscosity.

PTZ spectra have been recorded using the variable temperature cell of § 3.17 at 36°C and 45°C and, as expected, the hyperfine components are now resolved in groups VIII and IX. The recording at 36°C is shown in Fig. 4.14, from which it is evident that, although the line width variation with I_z still occurs, the spectrum now appears to be symmetrical, and corresponding lines in groups I and IX and also in II and VIII may now be identified. By raising the temperature to 36° and 45°, from (2.2.5), τ_c is reduced by factors of 2.3 and 2.8 respectively. Therefore, if the line width were determined by (2.3.6) or (2.3.7), reductions in line width by the same factors would occur. This is evidently not so for groups I and II where there is no significant reduction in line width, which suggests that the width of the hyperfine components at this end of the spectrum is determined by another mechanism.

For groups VIII and IX the estimated line widths at 36° is approximately 0.40 gauss and 0.43 gauss respectively. Substitution of the appropriate values of η and T into (4.10.4) indicates that the previous room temperature line widths were approximately 1.0 gauss, which

certainly implies that these groups were not resolved at 17°C, but,on the other hand,the corresponding points (x) on Fig. 4.13 would lie at $T_2^{-\frac{1}{2}}$ = 1.65×10^{3} $sec^{-\frac{1}{2}}$ i.e. well off the straight line. This,therefore,represents a further disagreement with McConnel's theory.

§ 4.12 The line width of group I and group II lines

If the line width of groups I and II lines at room temperature is determined by collision broadening (2.3.3), then δH should increase with temperature (§ 2.3 (c)). If in (2.3.4) W is assumed to remain constant with increasing temperature, then at 45°C the line width should increase to 0.35 gauss, while if W is assumed to be proportional to η, the line width would increase to about 10 gauss at 45°C. In fact the line width at 45°C appears to be less than 0.25 gauss and,therefore,the line width at room temperature evidently does not result from collision broadening.

On the other hand, it has been shown in § 4.11 that, on raising the temperature, the reduction in line width of group I and II lines, predicted by the Microcrystalline Model, does not occur either. The observed line width of about 0.2 gauss should not result from dipolar broadening (§ 2.3 (e)) at the concentrations used ($\sim 10^{-3}$ M). Under the experimental conditions the magnetic field inhomogeneity and modulation depth should not broaden the lines to this extent. In addition, reduction of the microwave power at the cavity (typically 10-15 mW) does not indicate the presence of saturation broadening. Therefore,resolution

should not be inhibited by apparatus broadening (§ 2.4). Removal of dissolved oxygen also appears to have little effect.

The possibility exists that at room temperature the line width is determined by microcrystalline relaxation processes but on raising the temperature the reduction in line width predicted by this effect is accompanied by increased collision broadening. Thus, at the two temperatures the line widths are approximately equal.

FIG 5·1
DMPTZ.

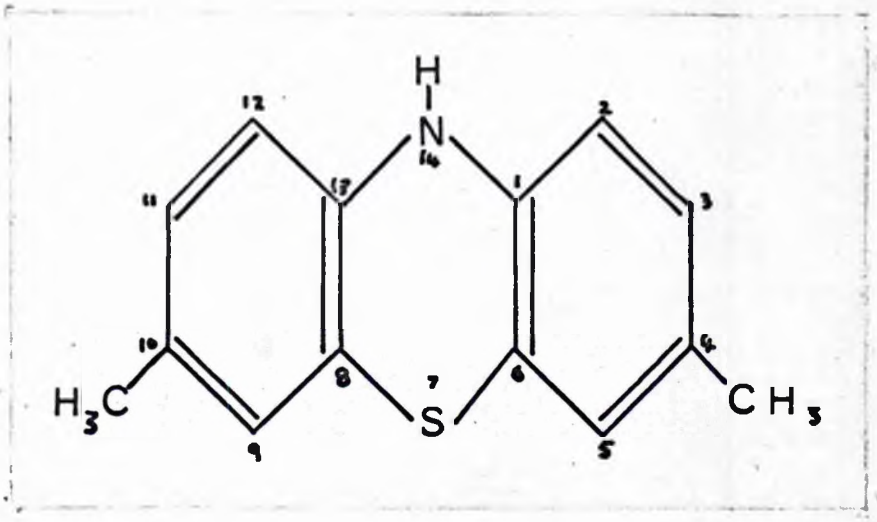

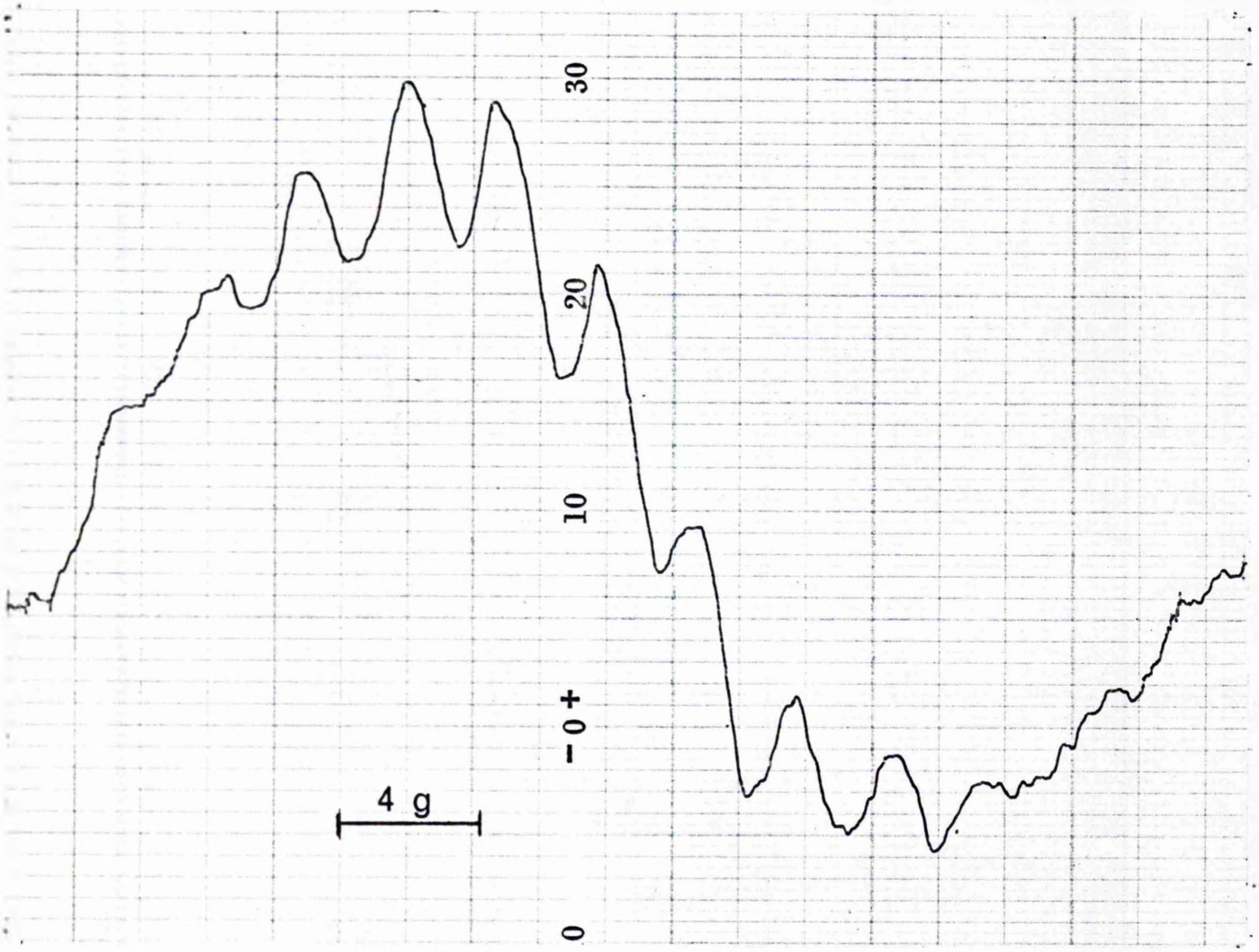

FIG 5·2 DMPTZ in H_2SO_4.

CHAPTER 5

DERIVATIVES OF PHENOTHIAZINE

§ 5.1 4,10-Dimethylphenothiazine (DMPTZ)

The molecular structure of this substance is shown in Fig. 5.1 which also indicates the system which has been adopted in numbering the positions in the molecule. This differs from that used by Billon [B11] which, in turn, differs from notations that have been used to number phenazine [S9] and thianthrene [K6]. In subsequent molecular orbital calculations (Chapter 6) it is more convenient to assign numbers also to the four ring carbon atoms which do not have an attached proton.

DMPTZ dissolves immediately in concentrated H_2SO_4 to give a dark red solution which, as in the case of the parent PTZ, is strongly paramagnetic. The low resolution spectrum of a 2×10^{-3} M solution is shown in Fig. 5.2. This is considerably different from that of PTZ itself (Figs. 4.6 and 4.9). Unfortunately the sample had deteriorated before the Mullard magnet became available, and therefore a high resolution spectrum has not been obtained.

Billon [B12] has studied the positive ion of DMPTZ which he generated electrochemically in acetonitrile solution. The spectrum which he obtained appears to be very similar in form to Fig. 5.2, although the spacing between lines in Fig. 5.2 is about 3.2 gauss compared with about 3.6 gauss in Billon's spectrum.

While not offering an interpretation of this spectrum, Billon

suggests that the interaction of the unpaired electron with methyl protons by the mechanism of hyperconjugation leads to higher hyperfine splitting parameters (of similar magnitude to the N^{14} splitting) than would result from interactions with ring protons by σ-π configuration interaction. These mechanisms (2.5.10) and (2.5.8) are, in fact, generally believed to lead to splittings of similar magnitudes.

Billon's suggestion of equal hyperfine splitting parameters for the N^{14} nucleus, its adjoining proton and the six equivalent methyl protons, predicts a ten line spectrum with a ratio of intensities

$$1:8:29:63:85:85:63:29:8:1 \qquad (5.1.1)$$

As this is symmetrical about two equal central lines, it cannot account for the experimental spectrum, which appears to contain eleven components. Also, assuming that the N^{14} splitting has a similar value as in PTZ, the above spectrum would extend over about 60 gauss instead of about 30 gauss.

On the assumption (which is supported by the H.M.O. results of § 6.5) that the substitution of methyl groups in the 4 and 10 positions of PTZ does not result in a large change in the distribution of unpaired electron densities, then in the nomenclature of § 4.8, it is likely that α and β for DMPTZ have values similar to those for PTZ. Also, if each of the methyl protons gives rise to a hyperfine splitting whose magnitude is about half of α, a thirteen line spectrum results with an intensity distribution

1:6:17:32:47:58:62:58:47:32:17:6:1 (5.1.2)

The experimental spectrum (Fig. 5.2) agrees quite well with this distribution except that the outer two lines are not observed. These, however, could easily be masked by noise.

The following interpretation is therefore offered for DMPTZ:

$$\begin{aligned} \alpha &\doteq 6.5 \text{ gauss} \\ \beta &\doteq 6.5 \text{ gauss} \\ \gamma_1 &\doteq 3.2 \text{ gauss} \end{aligned} \qquad (5.1.3)$$

Experimental evidence suggests that these figures may be slightly higher for the electrochemically produced cation [B12].

The fact that the hyperfine splitting by the methyl protons attached to the 4 and 10 positions is approximately equal to γ_1 in § 4.8 (f), suggests that, for PTZ, γ_1 refers to the sites 4 and 10.

Molecular orbital calculations on DMPTZ are carried out in § 6.5 where further evidence supports the interpretation (5.1.3).

§ 5.2 4-Methylphenothiazine (MPTZ)

Although this derivative was not available, Billon [B12] has published a spectrum of the electrochemically generated positive ion in acetonitrile solution, for which he offers no interpretation. The spectrum appears to contain eleven lines with an approximate intensity ratio

1.5:4:8:11:13:14:13:9:7:4:1 (5.2.1)

The spacing is about 3.5 gauss.

If, as may be the case for 4,10-dimethylphenothiazine, the spectrum is explained by hyperfine splittings of about 7 gauss of the N^{14} nucleus and the proton bonded to it, and of about 3.5 gauss with the methyl protons, ten lines would result.

If the interaction of an unpaired electron with a single ring proton also leads to a 3.5 gauss splitting an eleven line spectrum is predicted whose intensity ratio

1:4:8:12:15:16:15:12:8:4:1 (5.2.2)

is consistent with the above approximate experimental spectrum (5.2.1).

It appears likely that this ring proton is in the 10 position unless the methyl group bonded to the ring carbon 4 causes a large change in π electron distribution. Some evidence to support this hypothesis will be found in § 6.6, where a molecular orbital calculation on MPTZ is carried out.

§ 5.3 Chlorpromazine (CPZ)

(a) The E.S.R. Spectrum of CPZ in H_2SO_4

The molecular structure of 3,chloro N,dimethylaminopropylphenothiazine or chlorpromazine (CPZ) is shown in Fig. 5.4. This and other similar phenothiazine derivatives have been used as tranquillisers in mental diseases [G7]. The positive ion is obtained by dissolving CPZ in concentrated H_2SO_4, as in the case of PTZ. The solution slowly develops a light red colour with this compound, and is strongly paramagnetic. The E.S.R. spectrum, which is slightly better resolved than that

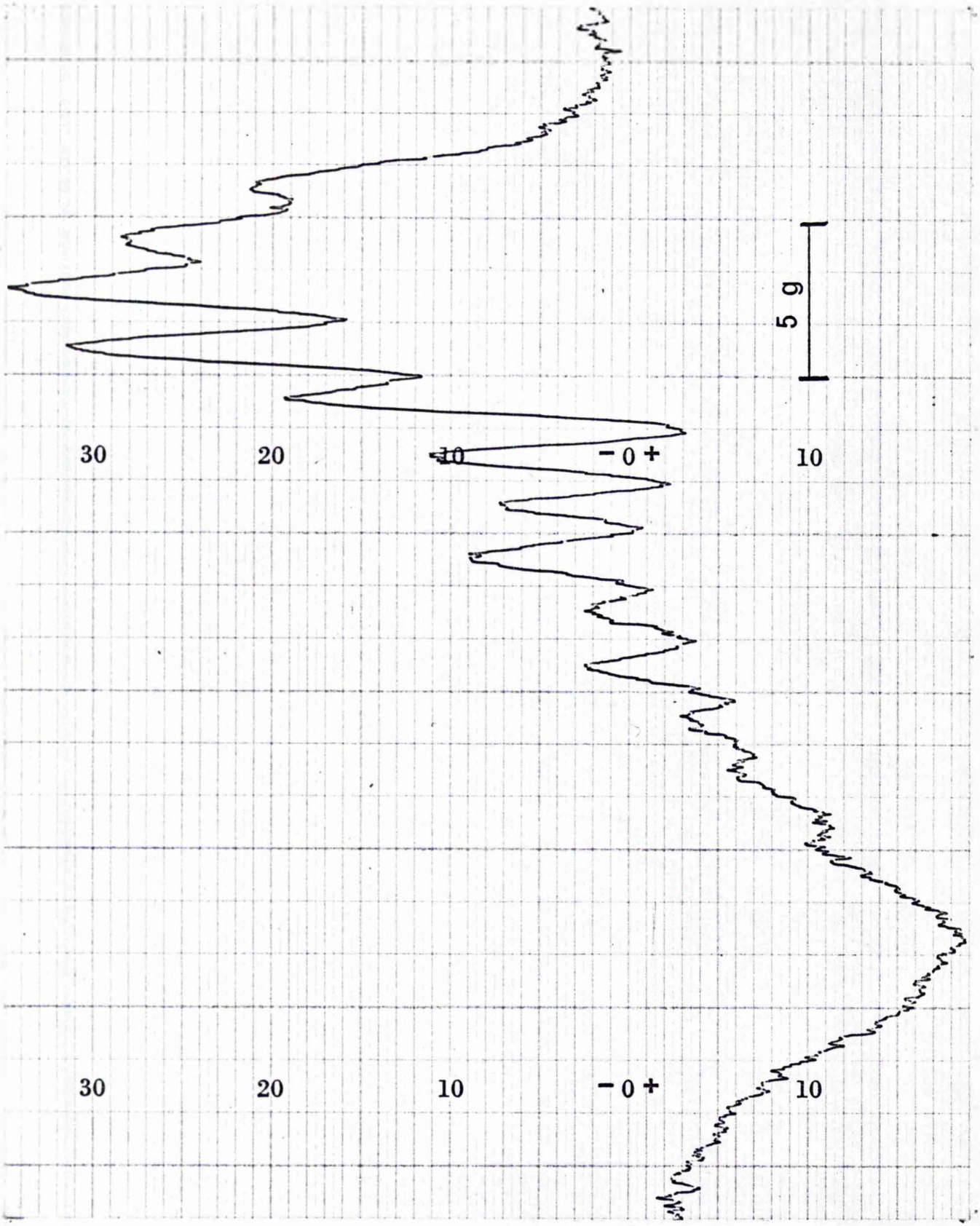

FIG 5·3 CPZ at 17°C

of Piette and Forrest [P4], is shown in Fig. 5.3. For recording conditions under which hyperfine splittings down to 0.1 gauss should be resolved, no additional hyperfine structure has been observed. The removal of dissolved oxygen also appears to have no effect on the resolution.

It is clear that, as in the case of PTZ, there is a progressive change in line width with I_z. Here, however, the splitting of the hyperfine components observed is about 1.8 gauss, while for PTZ the splitting is about 0.5 gauss, and the line width at the high magnetic field end of the PTZ spectrum is almost certainly less than 1.2 gauss. It is, therefore, rather unexpected that the hyperfine structure at the high magnetic field end of the CPZ spectrum should be completely broadened out.

This asymmetry, and the fact that only about twelve lines are resolved, creates difficulties in the interpretation of the spectrum. If the spectrum were completely resolved, however, interactions of the free electron with two N^{14} nuclei ($I = 1$), nineteen protons ($I = \frac{1}{2}$) and one Cl nucleus ($I = 3/2$) would result in about 55,000 lines in all.

Apart from the variation of line width with I_z, the spectrum should be symmetrical about its centre. Therefore, the peak to peak derivative amplitudes of the partly resolved components and the separations of adjacent components should also show this symmetry about the centre. By measuring these quantities it should be possible to locate

FIG 5·4

Chlorpromazine.

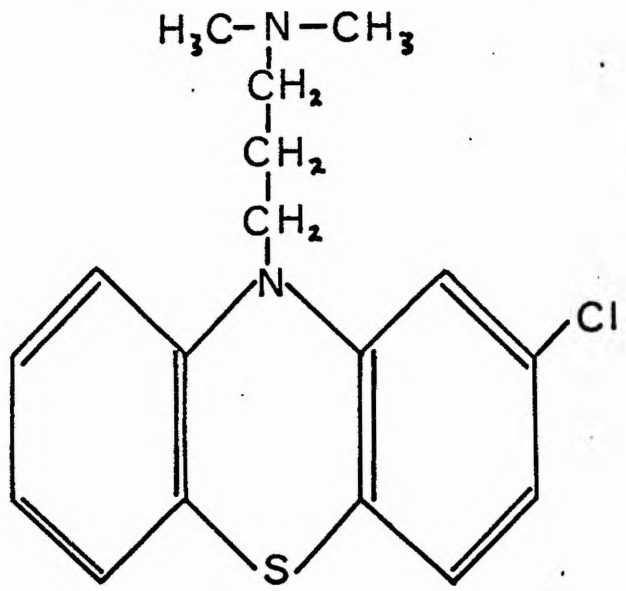

Line No.	1	2	3	4	5	6	7	8	9	10	11	12
Approx. Intensity	1·0	2·0	4·1	3·7	4·9	3·8	2·2	2·9	1·3	1·8	0·7	0·3
Separation (gauss)		1·87	1·70	1·96	1·73	1·78	1·65	1·77	1·66	1·99	1·72	1·90
Sep n from Sim. Spec.		1·89	1·71	1·93	1·68	1·76	1·67	1·76	1·68	1·93	1·71	1·89

FIG 5·5 Measurements from FIG 5·3.

the position of the centre of the spectrum, and thus to decide how many of these partly resolved lines it contains.

The data considered here are taken from three spectra, one of which is a four hour recording, and the measurements from which are given the greatest weight. These measurements are shown in Fig. 5.5.

From Fig. 5.3 it appears unlikely that more than sixteen hyperfine lines occur in all. The total width of the spectrum is such that, if there are less than about fourteen of them, Fig. 5.3 must consist of two spectra which partially overlap. One of these spectra contains the resolved components, and the other, which has a lower g value, consists of a broad unresolved line.

In an attempt to decide how many hyperfine lines the CPZ spectrum contains in addition to the twelve resolved components, the separations between lines (9) and (10) and between (3) and (4) (Fig. 5.5) appear to be much larger than the average spacing. The fact that a spectrum must be symmetrical about its centre, together with these above average spacings, eliminates all possible systems except those containing twelve, eighteen, or over twenty lines. It was noted above that the number of lines is unlikely to exceed sixteen which excludes the possibility that a system of over twenty lines is involved and makes very improbable the eighteen line system. Also, in the latter system, the two central lines should be of equal intensity, or owing to the variation in line width with I_z, line (10) should be less intense than line (9).

In fact the opposite is the case.

If the twelve line system is the correct one, the conditions which require to be satisfied are much more stringent than for a larger number of lines, as all twelve are resolved. Thus it is required that five pairs of separations of adjacent lines and six intensity ratios of pairs of adjacent lines must all be satisfied, making, in all, eleven conditions each of which appears to be satisfied within the limits of experimental error. Therefore the resolved structure of the spectrum of Fig. 5.3 appears to be explained by assuming a twelve line system.

(b) Suggested interpretation for a twelve line spectrum

With the rather scanty data available, it is obviously not possible to arrive at a complete interpretation of the spectrum, and an estimation of all the hyperfine splitting parameters. However, as PTZ itself has been examined, some clue exists as to the probable unpaired electron distribution. In PTZ the N nucleus and its adjoining proton account for the largest splitting parameters. Therefore, in CPZ, these seem likely to be associated with the ring nitrogen atom, and also possibly with the nearest CH_2 group of the side chain.

Alternatively it is possible that the N nucleus of the side chain accounts for the greatest hyperfine splitting. In this case, however, a further splitting would probably be due to six equivalent methyl protons and one or more pairs of equivalent protons from the CH_2 groups. Any combination of these leads to a spectrum which contains an odd

number of lines. In fact, if a significant splitting by an N^{14} nucleus ($I = 1$) occurs, an even number of lines is not predicted unless a significant splitting is produced also, either by an odd number of protons, or by the Cl nucleus ($I = 3/2$), but not by both. The latter splitting is unlikely to be resolved owing to the low magnetic moment of the Cl nucleus.

In accordance with the nomenclature of § 4.8, the N^{14} atoms of the ring and chain have splitting parameters α_1 and α_2 respectively. γ_1, γ_2, etc refer to splittings by pairs of equivalent protons and β_1, β_2, etc. to single proton splittings. More than one of these may arise if the presence of the Cl atom affects the symmetry of the unpaired electron distribution.

A ratio of parameters which appears to predict a distribution of intensities fairly close to that of Fig. 5.5 is

$$\alpha_1 = \gamma_1 = 2\gamma_2 = 2\beta_1 \qquad (5.3.1)$$

which predicts a spectrum with relative intensities

$$1:3:6:10:13:15:15:13:10:6:3:1 \qquad (5.3.2)$$

Two alternatives to (5.3.1) predict similar intensities to (5.3.2)

(i) γ_1 or γ_2 is replaced by α_2

(ii) The pairs of protons corresponding to γ_1 and γ_2 may not, in fact, be exactly equivalent, owing to an asymmetry of unpaired electron density caused by the presence of the Cl atom in the 3 position (Fig. 5.4).

The extent of (ii) will be considered in § 6.7 where some molecular orbital calculations on CPZ are made.

If (5.3.1) is approximately correct, the CPZ spectrum must contain a broad unresolved line in addition to the twelve line spectrum. This hypothesis could be tested by examining CPZ at a different microwave frequency. If two separate spectra with different g values are involved, it is expected that the form of the overall spectrum would be significantly different.

This unresolved line could be due to the presence of an additional unpaired electron associated with the nitrogen atom of the side chain. This would imply that, in H_2SO_4, CPZ exists as a doubly charged ion $[CPZ]^{++}$, which would be a biradical. In order that two separate E.S.R. lines should occur, the amount of intramolecular exchange would require to be quite small.

(c) Simulation of twelve line CPZ spectrum

A reconstruction of the CPZ spectrum similar to that of Fig. 4.10(b) for PTZ, may be made from (5.3.1). If the possibilities (i) and (ii) of § 5.3 (b) are ignored, the original twelve lines may, by a systematic variation of the ratio of the parameters in (5.3.1), become twelve groups of lines whose separations may be adjusted to agree with the spacing noted in Fig. 5.5.

Thus the following values are found for the parameters,

$$\begin{aligned} \alpha_1 &= 3.4 \text{ gauss}, & \gamma_1 &= 3.8 \text{ gauss} \\ \gamma_2 &= 2.05 \text{ gauss}, & \beta_1 &= 1.45 \text{ gauss} \end{aligned} \qquad (5.3.3)$$

This final set of parameters is now used to simulate the CPZ

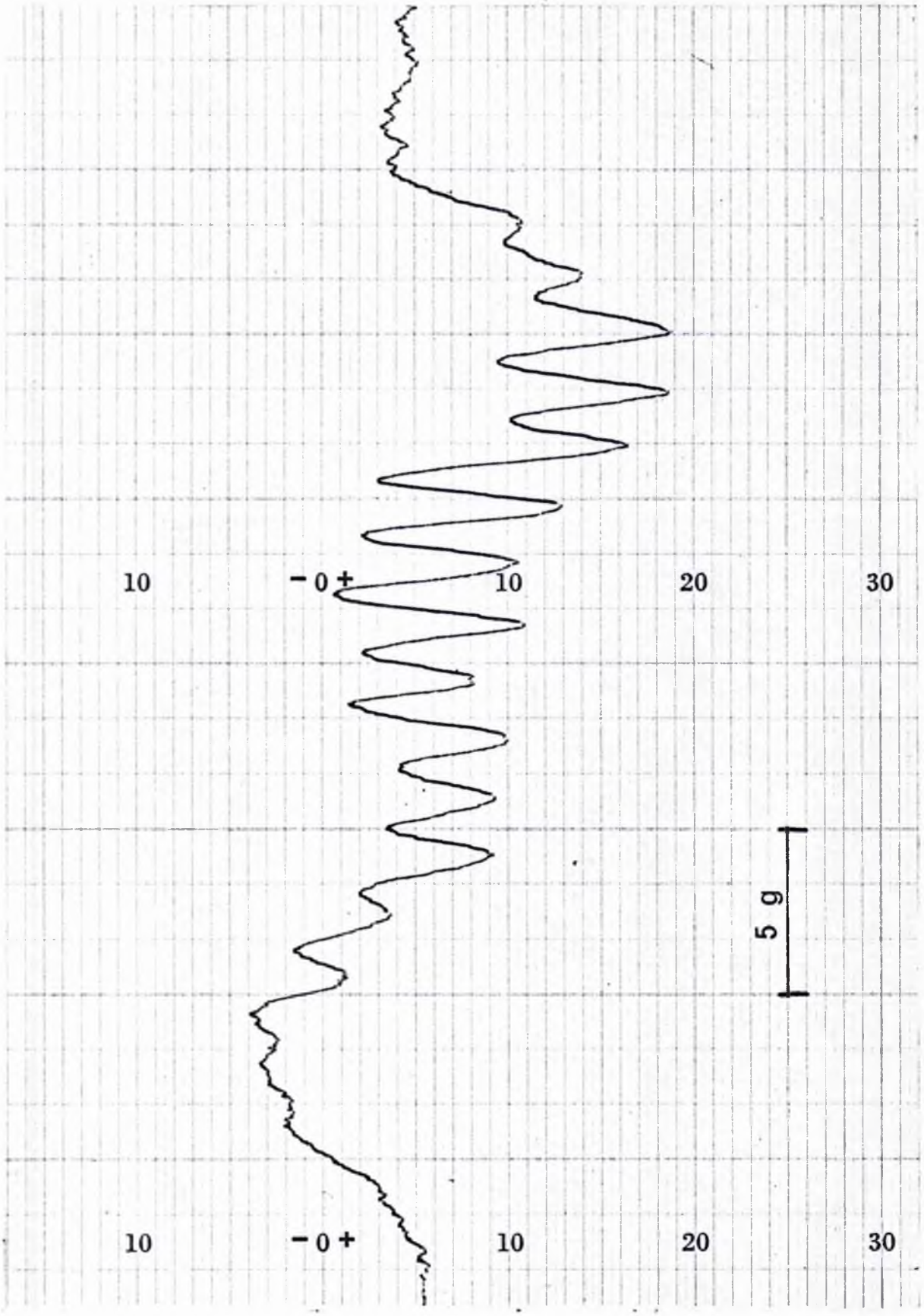

FIG 5·6 CPZ at 60°C.

spectrum in a method similar to that of § 4.9. The separations of adjacent components measured from the simulated spectrum are shown in Fig. 5.5, and evidently agree fairly well with the experimental spacings.

(d) Line width of CPZ lines

As was noted in § 5.3 (a), the observed spacing of about 1.8 gauss of the lines of Fig. 5.3, together with the magnitude of PTZ line widths (§ 4.10), makes the extent of the variation in CPZ line width unexpected. This variation appears to be very approximately linear with respect to magnetic field, and the line width ranges from about 0.7 gauss to 2.0 gauss. The increased line widths compared with PTZ may be due to the larger molecule and hence to the larger microcrystal radius. If a reduction in line width occurred when the temperature was raised, it might be expected that each of the lines of Fig. 5.3 would be further split into several hyperfine lines.

(e) CPZ spectrum at higher temperatures

The spectrum obtained at a temperature of 60°C is shown in Fig. 5.6. From this it appears that the lines of Fig. 5.3 are not further split, but that additional lines appear at the high magnetic field end of the spectrum. This now consists of sixteen lines, and therefore appears, at first sight, to invalidate the possibility that the room temperature spectrum contains twelve lines.

However, an examination of the spacings between adjacent lines shows that the separation of lines (9) and (10) is no longer so much

greater than that of (7) and (8) as it was previously (Fig. 5.5). This was the main factor which formerly eliminated the possibility of a sixteen line system rather than a twelve line one. Also, apart from the fact that sixteen lines appear to be resolved, the spacings between components are fairly consistent with a sixteen line spectrum. When the temperature is reduced again the spectrum reverts to the form of Fig. 5.3.

This change from a twelve to a sixteen line spectrum appears to occur at about 30°C-40°C. Above these temperatures the resolution at the high magnetic field end improves continually up to the highest temperature used, 70°C.

If the same factors considered in arriving at the hyperfine splitting parameters of (5.3.1) are taken into account, a possible explanation of the sixteen line spectrum employs the same parameters as (5.3.1) but in an approximate ratio

$$\alpha_1 = 2\gamma_1 = 4\gamma_2 = 4\beta_1 \qquad (5.3.4)$$

The lines predicted by (5.3.4) have relative intensities

$$1:3:5:7:8:8:8:8:8:8:8:8:7:5:3:1 \qquad (5.3.5)$$

which appears to account reasonably well for Fig. 5.6, as departures from equality in (5.3.4) should cause a greater reduction in the central lines (intensity 7 and 8 in (5.3.5)) than in the outer lines.

The values of the hyperfine splitting parameters are therefore:

$$\alpha_1 = 7.0 \text{ gauss}, \quad \gamma_1 = 3.5 \text{ gauss}, \quad \gamma_2 = 1.7 \text{ gauss} = \beta_1 .$$

FIG 5·7

Decomposition

Products of CPZ

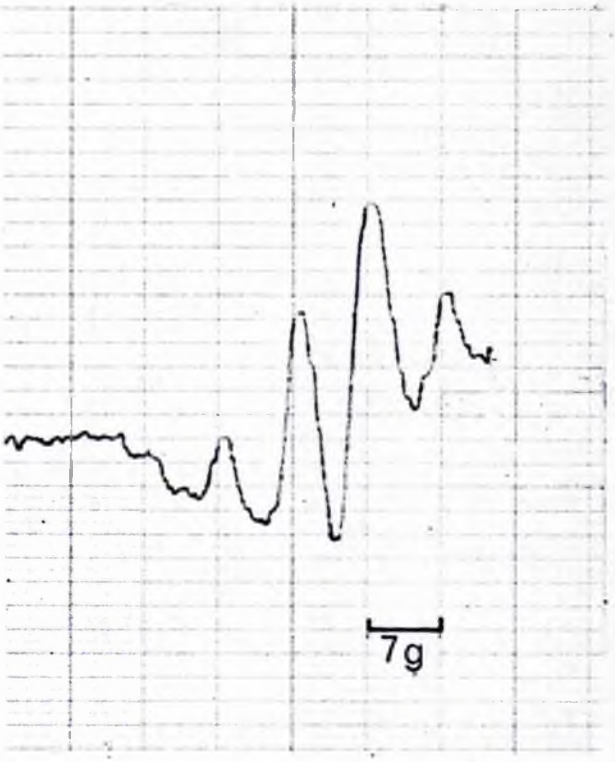

FIG 5·8 Promazine at 60°C.

The protons to which γ_1, γ_2 and β_1 refer are not necessarily the same as in (5.3.1).

From measurements on the activation energy of CPZ, Gutmann [G7] has found that CPZ undergoes a transition between 28°C and 32°C. At temperatures below this, the side chain is thought to be folded over the ring structure, while above the transition temperature the chain may be straightened out. Although the temperature at which the E.S.R. spectrum changes its form may be slightly higher than 30°C, it appears likely that the two changes correspond to the same transition.

A possible mechanism whereby the folding over of the chain could cause an appreciable change in unpaired electron distribution, involves steric effects. The planarity of the ring structure could thus be affected, a bending perhaps occurring about the N-S axis. This would alter the π electron density at the ring carbon atoms and the unpaired electron interaction with the protons of the CH_2 group would also be affected.

After a sample tube containing CPZ has been heated in a bunsen flame for a few seconds, the E.S.R. signal is considerably weaker. The spectrum obtained is shown in Fig. 5.7. This has a four line form similar to the PTZ spectrum of Fig. 4.6. The CPZ molecule evidently breaks down under these conditions into products which are mainly non paramagnetic, but one of which is probably PTZ or a derivative with a similar E.S.R. spectrum.

§ 5.4 Promazine

A sample of promazine was kindly made specially by Dr. R. Foster, who, however, expressed some doubts as to its purity. Any change of hyperfine structure from CPZ may be attributed to the effects of the chlorine atom in the 3 position of Fig. 5.4.

The E.S.R. spectrum obtained is shown in Fig. 5.8, which, indeed, is seen to differ from Fig. 5.3. However, the lack of structure does not enable any further conclusions to be drawn concerning the effects of this substitution of the Cl atom.

The resolution of Fig. 5.3 is not improved when dissolved oxygen is removed and the sample is heated up to 75°C, or when the solution is diluted with water.

The lack of observed structure conflicts with the findings of Piette and Forrest [P4], who have published a spectrum of promazine in H_2SO_4, which has a complicated hyperfine structure. The basic splitting of this appears to be about 0.5 gauss, and should have been resolved in the present situation.

CHAPTER 6

MOLECULAR ORBITAL CALCULATIONS

§ 6.1 Molecular Orbital Theory and Hyperfine Splittings

From a knowledge of the hyperfine splitting parameters of the spin Hamiltonian (2.1.1) obtained from an E.S.R. spectrum, it is possible to arrive at a value for the unpaired electron density at atoms in the molecule which have a nuclear spin or at carbon atoms bonded to a ring proton or methyl group. These spin densities may be calculated, using the McConnel relation (2.5.8) or one of (2.5.10), (2.5.11) or (2.5.12) which relate hyperfine splittings with unpaired electron densities. The positions in the molecule which do not give rise to hyperfine splittings will, in general, have non zero unpaired electron densities, about which no further information is available using E.S.R. without resorting to the substitution of isotopes which possess nuclear magnetic moments.

Calculations employing the Hückel Molecular Orbital (HMO) theory [H5], or one of the many variations [W7] [P6] [M5] which attempt to compensate for the crudity of some of the assumptions, will yield a set of eigenvalues and eigenfunctions for the molecular orbitals. The coefficients of these eigenfunctions may be used to predict the electron density at each of the atoms in the molecule. However, particularly if the molecule contains atoms other than carbon and hydrogen, the values of parameters which require to be chosen empirically, and the nature of some of the assumptions in the Hückel theory, make the results of such

calculations uncertain. The predicted unpaired electron densities may be fitted to the values calculated from hyperfine splittings by a variation of parameters within limits determined by previous successful M.O. calculations on other molecules. If a good agreement of spin densities is obtained for the atoms which give rise to hyperfine splittings, then the assumption may be made that a reasonably correct electron distribution is predicted at the other atoms also.

If the value of Q = -23.7 gauss is used in the McConnel relation (2.5.8), Barton and Fraenkel [B8] have calculated that $Q_{nh}^{h} = -33.7$ gauss in the notation of § 2.5 (c). In the case of PTZ, the unpaired spin density on the nitrogen atom (ρ_n) of Fig. 4.1, is therefore as shown in Fig. 6.2(a). The spin densities at pairs of equivalent ring protons, calculated from the hyperfine splitting parameters γ_1, γ_2, etc. of (4.8.7), are also shown in Fig. 6.2(a), although the assignment of these values of ρ to particular pairs of protons is not possible. From a consideration of DMPTZ and MPTZ in § 5.1 and § 5.2, it seems likely that the figure of 0.102 refers to the positions 4 and 10 of Fig. 4.1 and therefore ρ_4 (and ρ_{10}) is taken as 0.102.

§ 6.2 Application of HMO Method to PTZ

The HMO method is well known and a full account has been given by Streitweiser [S10]. In the calculation, by the variational method, of the energy (ϵ) corresponding to the molecular orbitals, it is necessary to find the roots of the characteristic equation which is derived from

the secular determinant.

$$\begin{vmatrix} \alpha_1-\epsilon & \beta_{12} & \cdots & \beta_{1n} \\ \beta_{21} & \alpha_2-\epsilon & \cdots & \beta_{2n} \\ \vdots & & & \\ \beta_{n1} & \beta_{n2} & \cdots & \alpha_n-\epsilon \end{vmatrix} = 0 \qquad (6.2.1)$$

when α_r is the coulomb integral for the r^{th} atom, and, if only carbon atoms are involved, all values of α_r are taken to be equal ($= \alpha$). β_{ij} is the bond integral between atoms i and j and is taken to be zero, unless atoms i and j are bonded, in which case for carbon-carbon bonds,

$$\beta_{ij} = \beta_{ji} = \beta \qquad (6.2.2)$$

The n values of ϵ obtained, give the energies of the orbitals. If

$$x = \frac{\alpha - \epsilon}{\beta} \qquad (6.2.3)$$

then, for an unsaturated chain of n carbon atoms numbered consecutively, the n eigenvalues (x_i) of the matrix

$$\begin{bmatrix} 0 & 1 & & & & \\ 1 & 0 & 1 & & & \\ & 1 & \ddots & & & \\ & & & 1 & & \\ & & & 1 & 0 & 1 \\ & & & & 1 & 0 \end{bmatrix} \qquad (6.2.4)$$

give n equations of the form

$$x_i = \frac{\alpha - \epsilon_i}{\beta} \qquad (6.2.5)$$

FIG 6·1

Matrix for PTZ.

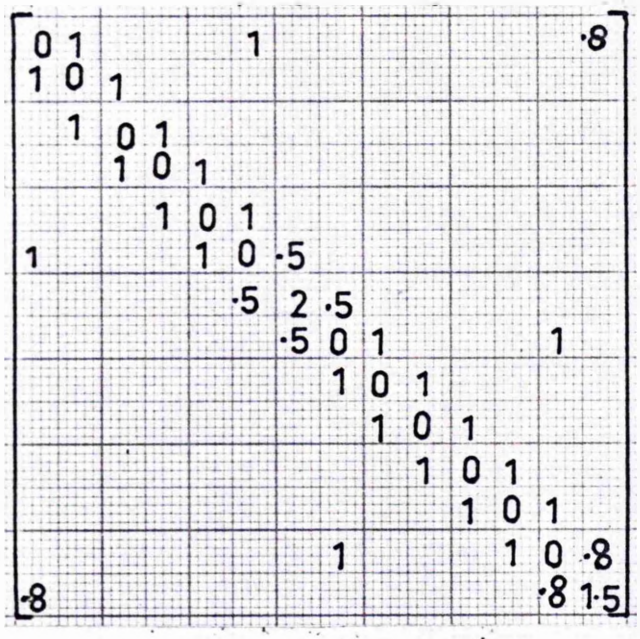

		P_2	P_3	P_4	P_5	P_n	$X_{8.}$	Error %
a	Expt.	·046	·022	·102	·022	·210	/	/
	From HMO h_s k_{c-s}							
b	0 0·9	·016	·081	·008	·088	·068	-0·435	4 6
c	0·9 0·9	·014	·070	·029	·055	·122	+0·185	3 1
d	1·5 0·9	·019	·063	·049	·032	·163	+0·325	2 0
e	1·5 0·5	·042	·033	·088	·001	·215	+0·510	1 8
f	2·0 0·5	·052	·026	·101	·000	·232	+0·544	10·4

FIG 6·2 HMO Results for PTZ.

Thus the values of ϵ are related in units of the bond integral to the energy of a carbon 2p orbital.

Finally, if atom X is not carbon, then

$$\alpha_x = \alpha + h_x\beta$$

and $$\beta_{x-c} = k_{c-x}\beta \qquad (6.2.6)$$

The matrix for PTZ is set up as shown in Fig. 6.1 which corresponds to the numbering of atoms shown in Fig. 5.1. The values taken here for h_n and k_{c-n} (1.5 and 0.8 respectively) are fairly well established [S10], but for sulphur some doubt exists. h_s is taken by Kreevoy [K7] as 0.0 and k_{c-s} as 1.0. This value of k_{c-s} is probably too high, and that of h_s too low.

§ 6.3 Fortran Program for eigenvalues and eigenfunctions

Originally, an iterative method was used in order to find the eigenvalues and eigenfunctions of the matrix of Fig. 6.1 and a Fortran program was written for the IBM 1620 computer for this purpose. Unfortunately, this matrix appears to contain some degenerate eigenvalues which inhibit the convergence of the wave functions in this method.

A print-out of the Fortran program which was used finally, is shown in Appendix II. This program uses the Jacobi methodof reducing the matrix to diagonal form by a unitary transformation and was written with the assistance of Mr. J. M. S. Hutchison. Each time round the loop determined by "GO TO 6", the largest pair of non diagonal elements, A(I,J) and A(J,I) are put equal to zero, and the elements of rows I and

J and columns I and J of A and U are altered accordingly. When the non diagonal elements have all been reduced below the level determined by LIMIT, usually 10^{-5}, the program transfers out of this loop. The eigenvalues are printed out from the now diagonal matrix A and the eigenfunctions from the unitary matrix U.

This program has been found to work very well, taking about six minutes to reduce the non diagonal elements of the 14 x 14 PTZ matrix below 10^{-5}. For matrices of higher order, the approximate times taken for this degree of convergence are: 16 x 16 - 10 minutes, 18 x 18 - 16 minutes, 22 x 22 - 28 minutes, 23 x 23 - 32 minutes. The length of the program, therefore, appears to be proportional to about the third or fourth power of the order of the matrix.

The program was originally intended to deal with matrices of any order, but the FORMAT statement which was required to read in the matrix was rather inconvenient, and it has been found simpler to use a FORMAT statement which reads in one row of the matrix per card. In this way, although it is necessary to compile a new object deck for each new order of matrix, only one card in the Fortran program need be changed. When the calculation is extended to a derivative of a molecule which has been dealt with already, considerable time is saved by duplication, in punching the rather large number of data cards required to read in the new matrix.

§ 6.4 Calculations on PTZ

(a) Variation of Sulphur Coulomb and Bond integrals

Initially, values of $h_n = 1.5$, $k_{c-n} = 0.8$, $h_s = 0.0$, $k_{c-s} = 0.9$, were assumed and the matrix is then as shown in Fig. 6.1.

As mentioned previously, the unpaired electron densities predicted by the molecular orbital calculation should agree with the values obtained from the hyperfine splitting parameters, in Fig. 6.2(a).

It may be seen from Fig. 6.2(b) that the spin densities calculated from the above N and S parameters show no similarity to the experimental values and ρ_n, in particular, is about a factor of three too low.

With $k_{c-s} = 0.9$, h_s was next increased, in steps of 0.3, to 1.5. From Fig. 6.2(c) and (d), it is seen that the value of ρ_n becomes increasingly closer to 0.210. However, the spin densities at the ring carbon atoms show little resemblance to Fig. 6.2(a) and none is nearly as great as 0.102.

For values of $k_{c-s} = 0.6$, 0.5 and 0.4, h_s was varied to try to obtain the best fit to Fig. 6.2(a). Fig. 6.2(e) shows reasonably good agreement, and Fig. 6.2(f) is even better. The mean percentage error in the best fit of the unpaired electron densities, in each case, to Fig. 6.2(a), excluding ρ_5 (see § 6.4 (b)), is shown in Fig. 6.2.

(b) E.S.R. spectrum of PTZ

It was noted in § 4.8 (f), that γ_4 could be zero only if the outermost hyperfine component of Fig. 4.9 arises from a C^{13} splitting. As

the unpaired electron densities of Fig. 6.2(a) may now be assigned to definite positions in the molecule, it is possible to calculate the possible C^{13} splittings from (2.5.11) and, therefore, to check this possibility.

The splitting caused by a C^{13} atom in position 4 or 10 of Fig. 4.1 is thus found to be about 3.3 gauss. This is greater than the separation (about 2.2 gauss) between the largest hyperfine component of group I and the outermost component. Therefore, if this outermost component were due to the presence of C^{13} atoms in a different position in the molecule, another component which is at least equally intense, is expected another 1.1 gauss further out.

The fact that $\rho_5 \neq 0$, i.e. that the unpaired electron density at positions 5 and 9 in Fig. 4.1 is zero, appears to favour the interpretation that $\gamma_4 = 0$ and to conflict with the above evidence. If it were the case that $\gamma_4 = 0$, then all the experimental unpaired electron densities of Fig. 6.2(a) are in reasonable agreement with Fig. 6.2(f). However, the simple HMO theory is unable to predict negative unpaired electron densities as these are simply taken to be the squares of coefficients. Therefore, it is possible that $\rho_5 = -0.022$ and this could be checked by using a more advanced molecular orbital calculation such as that of McLachlan for the addition of configuration interaction [M5].

(c) Value of ρ_1

From (2.5.12), the splitting of an N^{14} nucleus involves the unpaired

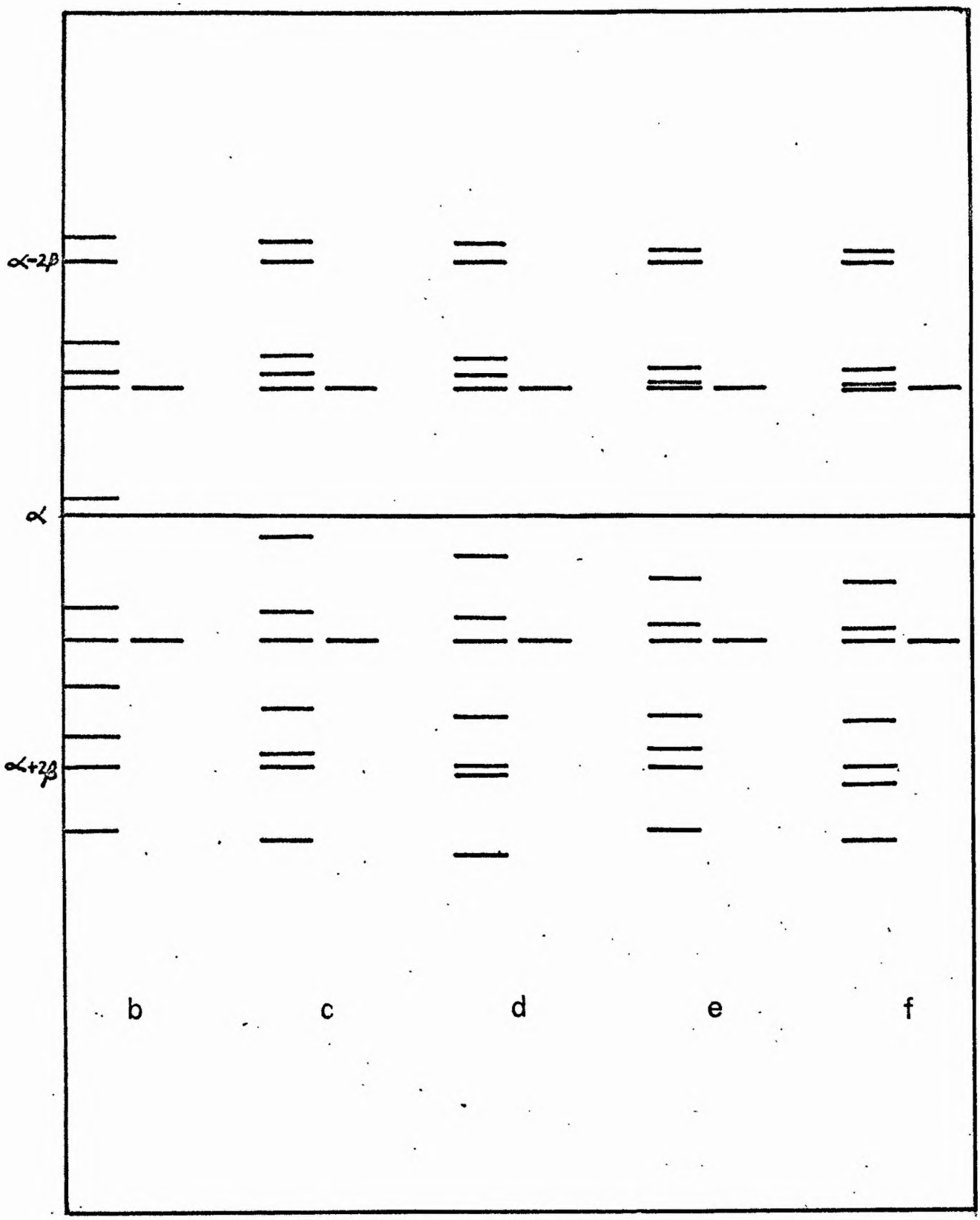

FIG 6·3 PTZ Eigenvalues.

electron density at the carbon atoms to which it is bonded (ρ_1) in addition to that at the N^{14} atom (ρ_n). The value of ρ_1 for Fig. 6.2(f) is 0.082. The numerical values obtained by Barton and Fraenkel [B8] are substituted into (2.5.12) which becomes

$$28.4\rho_n + 5.2\rho_1 = 6.5 \text{ gauss} \qquad (6.4.1)$$

Now $\rho_n = 0.210$ experimentally, and therefore ρ_1 is found to be 0.10 which compares with the value of 0.082 from the HMO calculation. However, the significance of this result is not very great as a 5% error in ρ_n will give rise to an error of about 40% in ρ_1.

(d) PTZ eigenvalues and eigenfunctions

The energy eigenvalues of the orbital containing the unpaired electron are shown in Fig. 6.2 for each of the situations (b) to (f). Here x represents, in units of β, the amount that the energy of the orbital is less than a carbon 2p orbital. For Fig. 6.2(a), $x = -0.135$ and, if this calculation were correct, the highest filled orbital of PTZ would be an antibonding orbital. Karreman [K8] states that this is the case for both PTZ (for which $x = -0.210$ for this orbital) and CPZ. However, he gives no further details of his calculations. In all the other cases, (c) to (f), the unpaired electron appears to be contained in a bonding orbital.

The eigenvalues of all the orbitals are shown for cases (b) to (f) in Fig. 6.3. Evidently the other energy levels show variations in energy also, although no other level changes by quite such a large

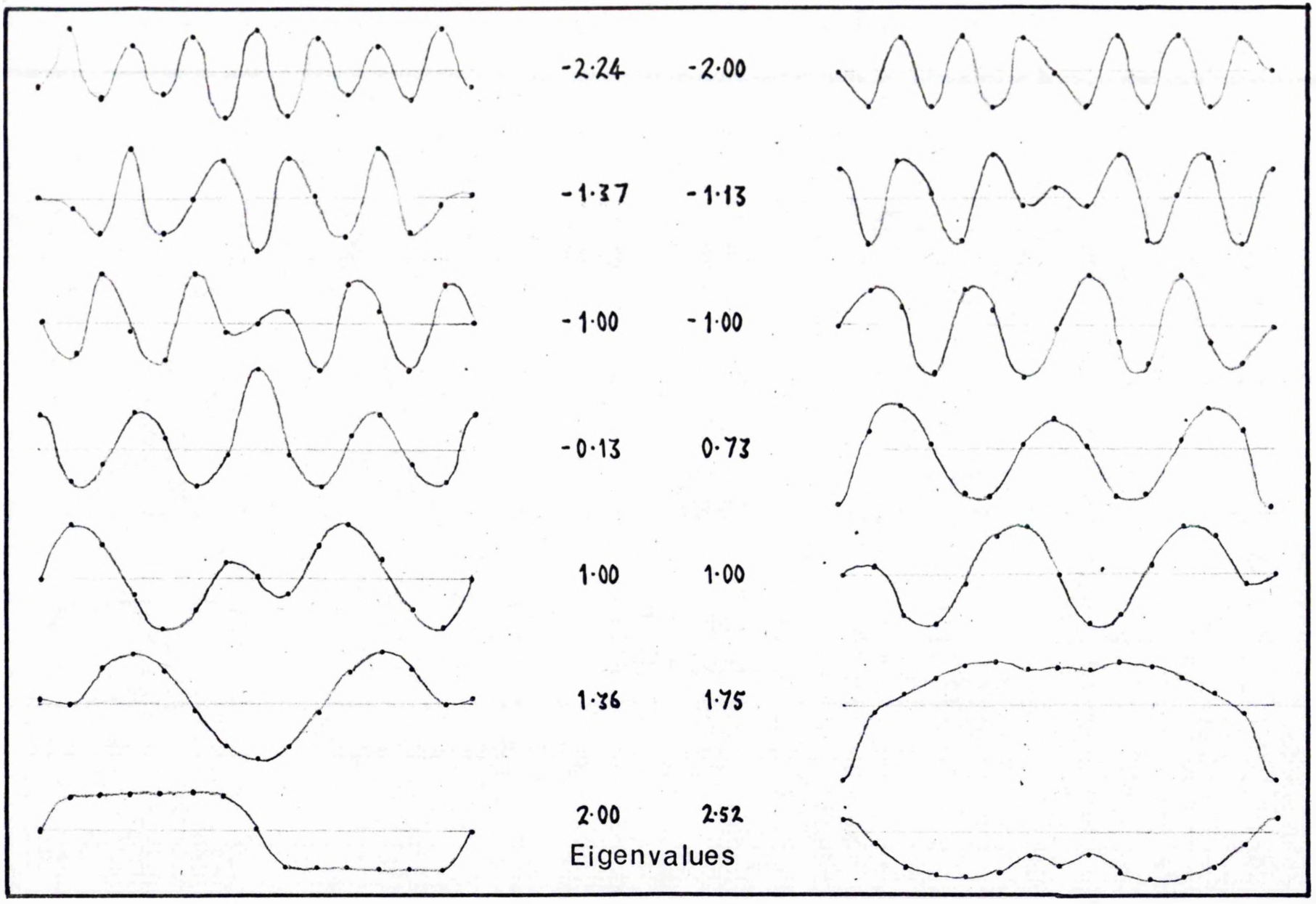

FIG 6·4 Plot of Eigenfunctions.

extent.

Some idea of the nature of the eigenfunctions is seen in Fig. 6.4, where the coefficients of the eigenfunctions corresponding to Fig. 6.2 (b) are plotted, beginning and ending with the nitrogen atom. As expected, the eigenfunctions which correspond to the highest energies have the greatest number of alternations in sign of the coefficients.

(e) Variation of α

In the HMO theory, all the coulomb integrals for carbon atoms are taken to be equal i.e. $\alpha_r = \alpha$. Jaffé [J2] noted that, in naphthalene, the two carbon atoms which are not bonded to a ring proton are slightly more electronegative than the remainder, and he compensated for this by assigning $\alpha_r = \alpha + 0.12\beta$ for these positions.

A similar situation exists for PTZ, in that atoms 1, 6, 8 and 13 are more electronegative than other carbon atoms. When α_r is put equal to $\alpha + 0.1\beta$ the following spin densities are predicted,

$$\rho_n = 0.246,\ \rho_2 = 0.054,\ \rho_3 = 0.022,\ \rho_4 = 0.103,\ \rho_5 = 0.001 \qquad (6.4.2)$$

The mean error for (6.4.2) is 8.3% compared with 10.4% for Fig. 6.2(f).

The electronegativity of these sites may be accounted for by use of the Auxiliary Inductive Parameter. For a carbon atom bonded to a heteroatom X the value of h_c is taken to be

$$h_c = \delta h_x \qquad (6.4.3)$$

where the value of δ recommended by Streitweiser [S10] for approximate

work is 0.1. For PTZ, the value of α_r for positions 1 and 13 is $\alpha + 0.15\beta$, and for positions 6 and 8 is $\alpha + 0.2\beta$. Now, the following spin densities are predicted,

$$\rho_n = 0.255,\ \rho_2 = 0.059,\ \rho_3 = 0.018,\ \rho_4 = 0.103,\ \rho_5 = 0.003 \qquad (6.4.4)$$

The mean error is 16.5% which is considerably worse than for Fig. 6.2(f). Evidently the value of δ used here is too high, as the values of h_c which lead to (6.4.2), correspond roughly to $\delta \fallingdotseq 0.05$.

An attempt to improve upon the compensation for electronegativity by using the ω technique [S11] has not proved to be successful, although only one cycle has been tried.

§ 6.5 Molecular Orbital Calculations on DMPTZ

(a) Conjugation Model

In this method, the attachment of the methyl group to a carbon atom in the π system is represented as

$$C - Y - Z \qquad (6.5.1)$$

where Y represents the methyl carbon atom, and Z the methyl protons. Values of h_c, h_y, h_z, k_{c-y}, k_{y-z} have to be assigned and are taken respectively as 0.0, 0.0, 2.8, 0.7, -0.3 [S11]. The other parameters have the values used in Fig. 6.2(f). Corresponding to the notation of Fig. 6.2, the following results are obtained:

$$\rho_n = 0.227,\ \rho_2 = 0.052,\ \rho_3 = 0.027,\ \rho_4 = 0.100,\ \rho_5 = 0.000 \qquad (6.5.2)$$

If $Q_{nh}^{\ h}$ = -33.7 gauss and Q' in (2.5.10) = 28 gauss, the values of ρ_n

and ρ_4 predicted by (5.1.3) are approximately 0.20 and 0.115 respectively, which are in fairly good agreement with (6.5.2). The value of ρ_2 predicts a hyperfine splitting of about 1.2 gauss which is probably sufficiently close to half the methyl proton splitting to alter the thirteen line spectrum to one of twenty-seven lines which are spaced at about 1.6 gauss instead of about 3.2 gauss. The value of ρ_2 appears to be overestimated for PTZ in Fig. 6.2(f) and, if the same is the case here, (6.5.2) and (5.1.3) may be considered compatible.

It would be very useful, however, to have a high resolution spectrum of DMPTZ which would allow the estimation of further splitting parameters and a more accurate estimation of those of (5.1.3).

By a systematic variation of the values of h_y, k_{c-y}, etc., an attempt could then be made to fit the unpaired electron densities of (6.5.2) to the experimental data by a method similar to that of § 6.4 (a).

(b) Heteroatom Model

For this method, the methyl group is considered to be a heteroatom X which contributes a pair of π electrons. The value of h_x is taken to be 2.0 and k_{c-x} to be 0.7 [S11]. The predicted unpaired electron densities are found to be

$$\rho_n = 0.212,\ \rho_2 = 0.051,\ \rho_3 = 0.034,\ \rho_4 = 0.099,\ \rho_5 = 0.004 \qquad (6.5.3)$$

This agrees well with (6.5.2) and the mean error between the two sets

of data, calculated as in § 6.4 (a) is only 8.3%. If the values of the parameters used in the two calculations were exactly correct, (6.5.2) and (6.5.3) should be identical. However, considerable doubt exists as to the correct value of these parameters, particularly in the conjugative model if allowance is not made for overlap. The small extent of the difference between these results provides confirmation of the accuracy of the values of the parameters recommended by Streitweiser for use with the HMO method.

§ 6.6 Calculation on MPTZ

An approximate interpretation of the MPTZ spectrum of Billon [B11] was given in § 5.2 from which

$$\rho_n \doteqdot 0.21,\ \rho_4 \doteqdot 0.13,\ \rho_r \doteqdot 0.13 \qquad (6.6.1)$$

where ρ_4 and ρ_r are the unpaired electron densities at the positions 4 and r, and r is probably 10.

Using the heteroatom method (§ 6.5 (b)), the calculation may easily be performed for MPTZ by reducing the order of the DMPTZ 16 x 16 matrix by one. This effectively removes the methyl group from the 10 position. The following results are obtained,

$$\rho_4 = 0.118,\ \rho_{10} = 0.082;\quad \rho_2 = 0.056,\ \rho_{12} = 0.047;$$
$$\rho_3 = 0.044,\ \rho_{11} = 0.019;\quad \rho_5 = 0.006,\ \rho_9 = 0.004;$$
$$\rho_n = 0.218. \qquad (6.6.2)$$

In this case, the values of ρ do not correspond to pairs of equiva-

lent atoms, and a certain asymmetry between the pairs 4 and 10, 2 and 12, 3 and 11, 5 and 9 is now observed.

The values of ρ_n, ρ_4 and ρ_{10} are very approximately in agreement with (6.6.1), but ρ_2, ρ_{12} and ρ_3 have probably been overestimated slightly. The values of these in (6.6.2) would otherwise probably result in a larger number of lines than the eleven of (5.2.2) and the spacing between them would be about half the observed spacing (cf § 6.5 (a)).

§ 6.7 Chlorpromazine and Promazine

The situation for CPZ is complicated by the fact that the two interpretations (5.3.1) and (5.3.4) have been obtained for different temperatures. In both of these, three protons have hyperfine splitting parameters of about 1.7 gauss and if these are ring protons, $\rho \doteq 0.07$. For promazine, the lack of resolved structure affords the information only that the spectrum differs from CPZ. Therefore, the substitution of a Cl atom probably has the effect,

(a) that the unpaired electron distribution alters sufficiently for one of a pair of ring protons, which are equivalent for promazine, to have $\rho = 0.07$ for CPZ, and the other proton to have a different value,

(b) that $\rho_3 = \rho_{11} = 0.07$ for CPZ and for promazine, and the change in E.S.R. spectrum is caused by the fact that the Cl nucleus leads to a small splitting compared with a proton, or

(c) that $\rho_3 > \rho_{11}$ for CPZ and, neither the Cl atom nor the proton, gives rise to a significant splitting but that $\rho_3 = \rho_{11}$ in promazine and both

these protons have an appreciable splitting.

Initially, the M.O. calculation assumed $k_{c-c} = 1$ for the bonds of the side chain and that the parameters for the methyl groups are unchanged from those used in § 6.5 (b). Values of $h_{cl} = 2.0$ and $k_{c-cl} = 0.2$ [S11] are also used. This model assumes that all C-C bonds are equivalent, but the aliphatic chain is not a conjugated system, and therefore the predicted unpaired electron densities outside the ring system are ignored. It is found that $\rho_4 = 0.088$ and $\rho_{10} = 0.080$, but no other single ring carbon has an unpaired spin density about 0.07. Also $\rho_3 = 0.030$ and $\rho_{11} = 0.026$, and these are not the next largest spin densities. The effect of increasing k_{c-cl} to 0.8 causes a greater discrepancy between ρ_4 and ρ_{10} ($\rho_4 = .109$, $\rho_{10} = .070$) but still none of situations (a), (b) or (c) above can be explained.

The effect of putting $k_{c-c} = 0$, for the side chain, with $k_{c-cl} = 0.2$, is to reduce the unpaired spin density on the carbon atoms of this side chain to zero, with the exception of the atom adjacent to the nitrogen atom of the ring system. However, the electron densities at ring carbon atoms still do not account for either (a) or (b) above. The case (c), on the other hand, is now possible. The largest spin densities of ring carbon atoms, apart from ρ_4 and ρ_{10} are now $\rho_3 = 0.051$ and $\rho_{11} = 0.041$ for CPZ, and for promazine both are 0.044. This difference between ρ_3 and ρ_{11} will be emphasised if higher values of k_{c-cl} are used.

It is noted that, in these three calculations, ρ_n is respectively 0.150, 0.135, 0.112, all of which are considerably lower than the value for PTZ. This, therefore, allows the possibility that (5.1.3), which predicts $\rho_n \doteq 0.11$, could be correct.

§ 6.8 Phenoxathiine

The molecular structure of phenoxathiine (PXT) is equivalent to Fig. 4.1, apart from the replacement of the NH group by an oxygen atom. Lamotte et al [L3] have examined the E.S.R. spectrum of a solution of this in concentrated H_2SO_4. They explain this spectrum by assigning hyperfine splitting parameters to the four pairs of equivalent ring protons as follows;

$$\gamma_1 = 2.4 \text{ gauss}, \quad \gamma_2 = 1.2 \text{ gauss}, \qquad \gamma_3 = 0.6 \text{ gauss}, \quad \gamma_4 = 0.3 \text{ gauss}. \tag{6.8.1}$$

From these with Q = -23.7 gauss in (2.5.8) the corresponding unpaired electron densities are:-

$$0.101,\ 0.051,\ 0.025,\ 0.013 \tag{6.8.2}$$

The values of $h_s = 2.0$ and $k_{c-s} = 0.5$, which have been used in the HMO calculations on PTZ and derivatives, may now be checked by performing an HMO calculation on PXT, using these same values of h_s and k_{c-s}. The values recommended for h_o and k_{c-o} are 2.0 and 0.8 respectively [S11].

A good fit of unpaired electron densities to (6.8.2) has been found for $h_o = 2.0$ and $k_{c-o} = 0.7$ which leads to

$$\rho_2 = 0.0265,\ \rho_3 = 0.052,\ \rho_4 = 0.101,\ \rho_5 = 0.000 \quad (6.8.3)$$

The failure to predict a non zero value of ρ_5 here may be attributed to reasons similar to those in the case of PTZ (§ 6.4 (b)). Excluding ρ_5, the mean deviation for the values of (6.8.3) from those of (6.8.2) is only 2.6%. This, therefore, provides evidence to support the values of h_s and k_{c-s} which have been used in the other HMO calculations of this chapter.

§ 6.9 Thianthrene

The molecular structure of thianthrene is again similar to Fig. 4.1, but in this case the NH group is replaced by a second sulphur atom.

The E.S.R. spectrum of thianthrene in concentrated H_2SO_4 has been observed by several workers [H6], [F8], [S12]. The spectrum appears to be explained by a hyperfine splitting of about 1.5 gauss due to four equivalent protons, and an unresolved splitting due to the other four. The larger splitting is thought by Shine [S13] to correspond to positions 3, 4, 10, 11.

The probable unpaired electron densities for the two groups of protons are, therefore, $\sim$0.06 and $\sim$0.02 from (2.5.8).

An HMO calculation, using the same values of h_s and k_{c-s} as before, predicts 0.086 and 0.004 respectively and, although the first figure is somewhat high, this represents quite good agreement with experiment, as the slight discrepancy could be explained by a slightly greater angle about the S-S bond than is the case for PTZ about the N-S bond [S11].

The values of $h_s = 2.0$ and $k_{c-s} = 0.5$ are, therefore, again seen to be reasonably successful in predicting a realistic unpaired electron distribution.

Donor	λ max (mμ) *	I_D (eV) **	ε max	ESR	
				in Acetone	in Ethanol
Phenanthrene	-	8.1	-	No	No
Naphthalene	~470	8.2	1440**	No	No
Anilene	~470	7.7	$\sim 10^3$*	No	No
Anthracene	~470	7.3	$\sim 10^3$*	See § 6.3	No

*Measurements of M.W. [M2]

**Measurements of Briegleb [B13]

FIG. 7.1 Optical and ESR Characteristics of Group II donors with TNB

CHAPTER 7

COMPLEXES OF 1,3,5-TRINITROBENZENE WITH DONORS

§ 7.1 Introduction

The optical absorption spectra of some complexes of 1,3,5-Trinitrobenzene (TNB) with donors have been studied by Miller and Wynne-Jones (henceforth referred to as M.W.), who find two distinct groups of complexes which are characterised by different spectra [M2].

The donors of Group I consist of the amines, pyridene, etc., and may be considered to be Onium donors. Group II consists of aromatic hydrocarbons, which are π donors. The donors of these two types donate electrons from non bonding and bonding molecular orbitals respectively [M9] [M10].

This chapter attempts to relate the E.S.R. spectra of a number of complexes of these types with their optical absorption spectra. Group II will here be considered first.

§ 7.2 Optical absorption spectra of Group II

Group II donors all exhibit similar behaviour optically, giving rise to complexes which appear almost instantaneously, and which have an absorption band at about 470 mμ with an extinction coefficient about 10^3. Also, no further absorption bands appear subsequently. The spectral changes of these complexes are consistent with Mullikan's and Brackman's 1:1 complexes whose spectra are characteristic of the complex as a whole. The donors used are listed in Fig. 7.1. Although

values of λ_{max} and ε_{max} are not listed for phenathrene, it has been shown to form a similar type of complex with TNB as the other donors mentioned [B13].

§ 7.3 E.S.R. of Group I

The results of E.S.R. measurements on some Group II complexes is shown in Fig. 7.1.

In the case in which E.S.R. was observed, with anthracene, the line width is about 25 gauss and the radical content is less than 0.001%. This could easily be due to slight impurities in the reagents.

With this possible exception, the absence of E.S.R. in these complexes is consistent with the concept of Bijl, Kainer and Rose-Innes [B14], of non paramagnetic 1:1 molecular complexes which have a singlet ground state and a triplet excited state separated by an energy much greater than kT. This situation arises when either of the conditions of the acceptor having a high electron affinity (E_A), and the donor having a low ionisation potential (I_D) are not satisfied, as for TNB, where E is only 1.8 ± 0.13 eV [B9], and the values of I_D for the donors are shown in Fig. 7.1. The fact that anthracene has the lowest value of I_D is, presumably, not very significant, since, if this complex has appreciably more ionic character, the optical absorption measurements would also be expected to differ from those of other donors.

Also, a complex of TNB with phenothiazine (PTZ) was found to be non paramagnetic. PTZ is expected to act as a π donor [M9] and, having a considerably lower ionisation potential (~6.7 eV) [L1], it should give

Donor	Solvent	Reaction (1)	D_{570}/D_{470} Reaction (2)	Whether 3 line ESR spectrum	Radical Content %
DEA.	EtOH	✓	.44-.49	Yes	0.5-2.0
	Acetone	✓	.44-.49	Yes	0.5-2.0
	DEA, Benzene	✓	.05	Yes	~ 0.1
	MeCN, DME	-	-	Yes	~ 0.5
PPD	EtOH	✓	0.3	Yes	~ 1.0
	Acetone	-	-	Yes	~ 1.0
	PPD	✓	-	Yes	~ 0.1
	PPD+H_2O	✓	-	Yes	~ 0.5
TEA.	EtOH	✓	0.4	Yes	~ 0.02
	Benzene	✓	0.1	-	-
CXA.	EtOH	✓	0.3*	Probably	~ 0.005
Pyridene	Pyridene	✓	0.52*	No	~ 0.01
NH_3	water	✓	0.01	-	-
NaOH	water	✓	-	-	-
	EtOH	-	-	No	~ 0.1
Acetone	Acetone	?	0.5	-	-

*See § 7.4

FIG. 7.2 Optical and ESR behaviour of Group I complexes

rise to a complex with TNB which has more ionic character than anthracene - TNB.

§ 7.4 Optical Absorption Spectra of Group I complexes

Group I donors form complexes with TNB which show an absorption band at about 470 mμ, as do Group II complexes, but usually at a rate which is measurable [A4] and with an extinction coefficient about 10^4. Certain of these donors then undergo a secondary reaction more slowly ($\sim\frac{1}{2}$ hour) which results in an absorption band at 570 mμ. The donors of this group, their behaviour in the primary reaction, and the ratio of the optical densities at 570 mμ and 470 mμ for those donors which undergo the secondary reaction (D_{570}/D_{470}), are listed in Fig. 7.2. Unfortunately, exact values of the extinction coefficients are not available.

The value for cyclohexylamine (CXA) of 0.3 for D_{570}/D_{470} was not found to be reproducible, and using purified CXA no absorption at 570 mμ was found [M2].

The reaction in the case of pyridene proceeds more slowly [M2] than for the amines.

§§ 7.5 E.S.R. Spectra of Group I complexes

Several of the Group I donors give rise to complexes which are paramagnetic, and the E.S.R. behaviour of these is summarised in Fig. 7.2. The E.S.R. spectra of the various complexes are now considered in detail.

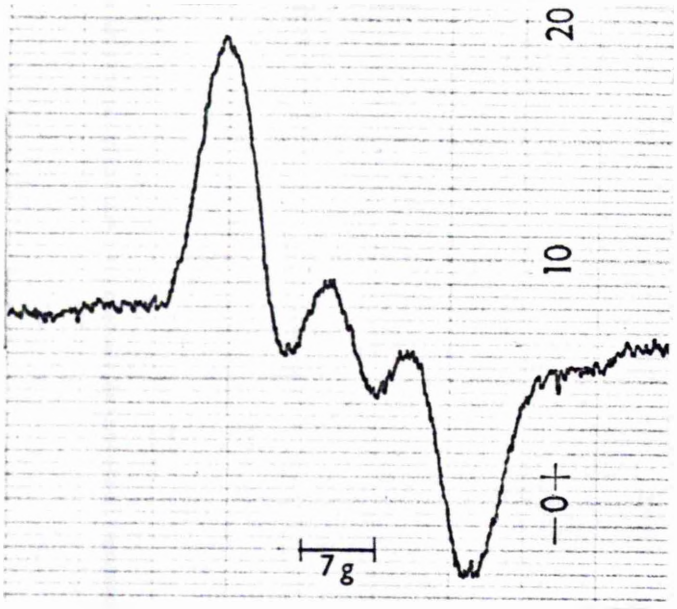

FIG 7·3 DEA–TNB

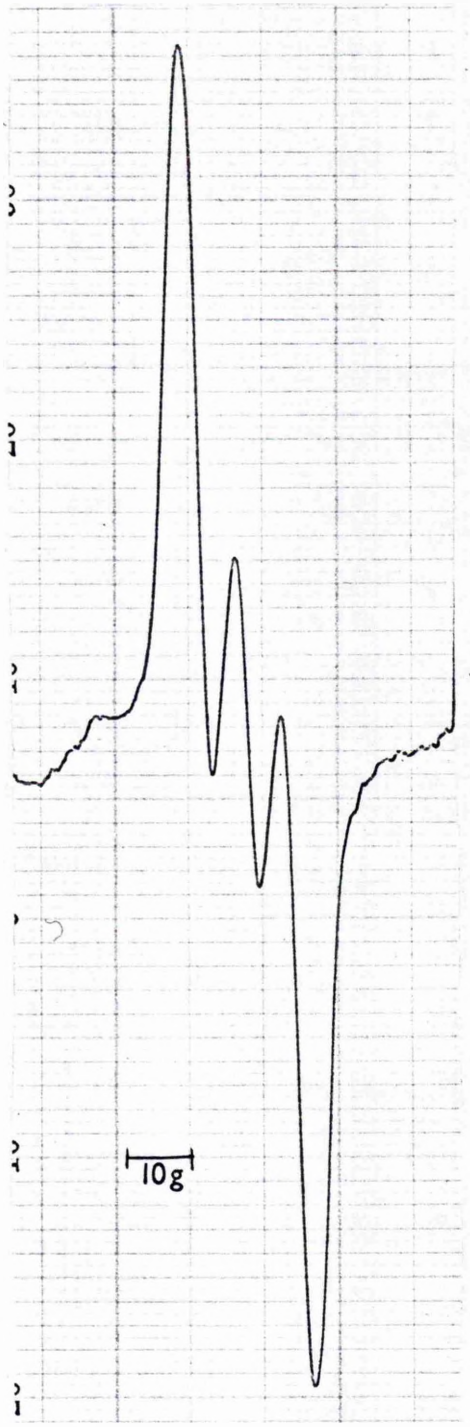

FIG 7·4 PPD–TNB

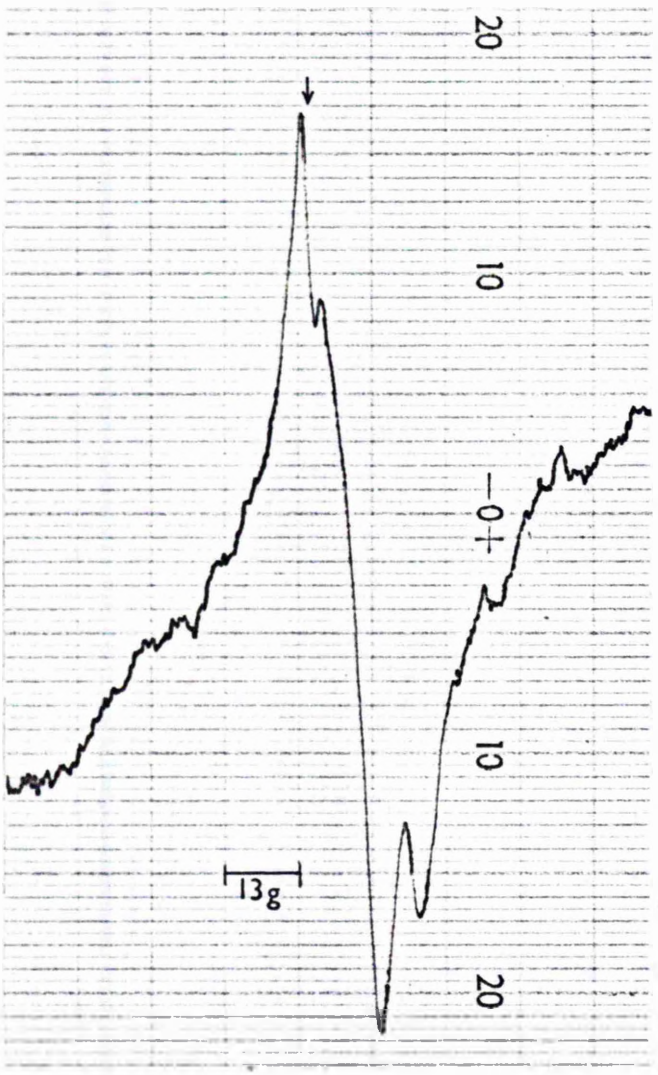

FIG 7·5 NaOH–TNB

(a) Diethylamine - TNB

When a solution of TNB in ethanol or acetone is added to diethylamine (DEA) a dark red colour appears almost immediately. The reaction, however, has been found to take place at a measurable rate [M2] [A4]. The colour then becomes gradually lighter red corresponding to the second reaction described by M.W.

The solution of the resulting complex, in these ionising solvents, shows a fairly strong E.S.R. absorption. It will be shown below that this probably corresponds to the latter reaction. The spectrum of DEA and TNB in ethanol is shown in Fig. 7.3 which appears to consist of three hyperfine components of equal intensity, the resolution of which is incomplete. An indication of the approximate splitting (8.5 gauss) and line width (7.5 gauss) is obtained using the method which will be described in § 7.10.

Dilution of these solutions down to the minimum concentration for which the signal is discernable, provides no improvement in resolution and no evidence of further hyperfine splitting.

The % radical content does not appear to be very reproducible and may vary between 0.5% and 3% in conditions which seem to be identical.

In non polar solvents such as DEA, an E.S.R. line is observed, similar to Fig. 7.3, with an intensity about a tenth that in ionising solvents. This is in agreement with the values of D_{570}/D_{470} for the two cases (Fig. 7.2).

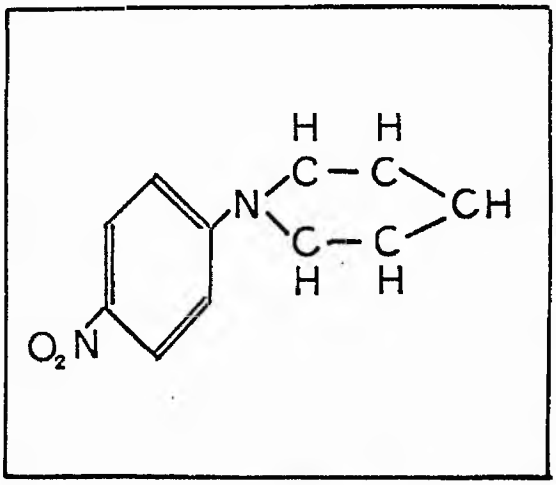

FIG 7·6 Piperidene

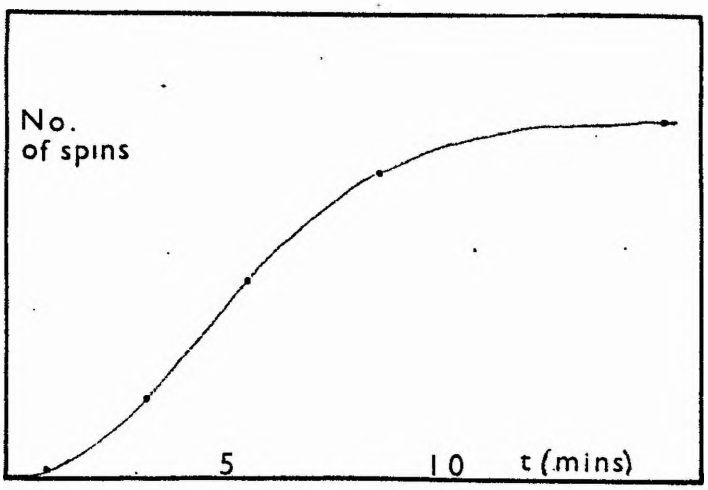

FIG 7·7 Reaction DEA–TNB

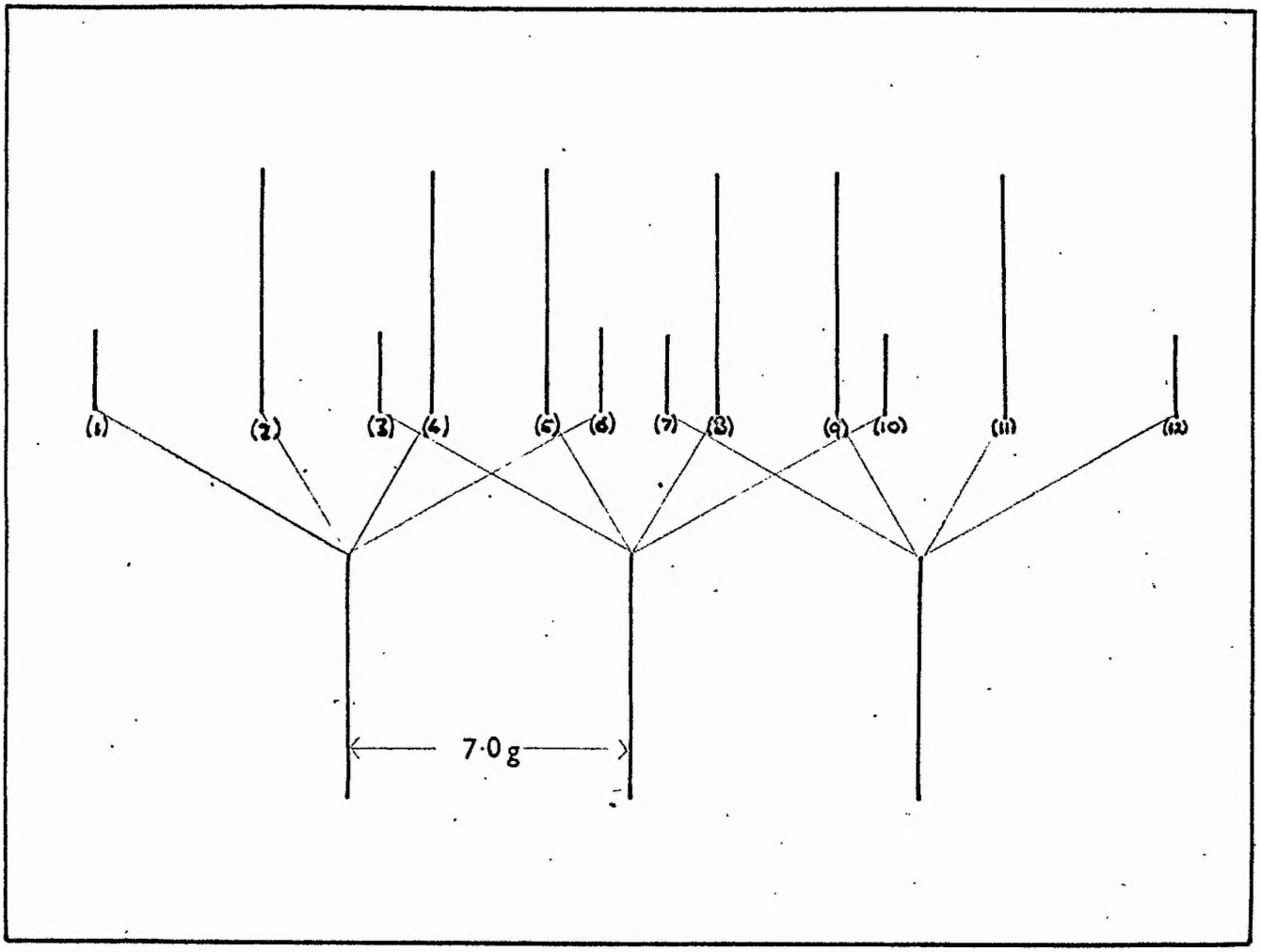

FIG 7·8 Splittings for Na–TNB Complex.

An attempt was made to relate the variation with time of the number of spins present, with the colour changes of M.W., in order to decide if the radical is characteristic of the second reaction. No E.S.R. signal was seen using the flow cell described in § 3.18 and observing within 1 sec., the results of mixing solutions of TNB in ethanol with DEA.

As a means of observing the results of this reaction at times longer than 1 sec after mixing, a small TNB crystal was dropped into a sample tube which extended into the cavity and contained a solution of DEA in ethanol. The E.S.R. signal was displayed on the pen recorder as the magnetic field was swept through the resonance value. The sample holder used was the quartz tube described in § 8.2 which has a small E.S.R. signal as a result of U.V. irradiation. This forms a convenient "marker" against which the intensity of the TNB - DEA E.S.R. signal may be measured. The variation with time of the E.S.R. signal is shown in Fig. 7.7. From the rate of increase of the E.S.R. signal, it appears that the second reaction and the 570 mμ absorption band corresponds to the paramagnetic complex of Fig. 7.3.

The nature of this complex is discussed in § 7.7.

(b) Piperidene - TNB

The molecular structure of piperidene (PPD) is shown in Fig. 7.6 and the E.S.R. characteristics of the complex in Fig. 7.4, which is evidently very similar to that of DEA. The hyperfine splitting is

again about 8.5 gauss in ethanol and the line width is about 7.5 gauss. The radical content is approximately the same as for DEA in ethanol and in acetone, which agrees with the ratio of D_{570}/D_{470} in the two cases.

The E.S.R. behaviour of the complex in non polar solvents, e.g. PPD, is similar to the DEA complex. This disagrees with M.W., who report that $D_{570}/D_{470} = 0$ under these conditions.

(c) Triethylamine - TNB

This complex is very weakly paramagnetic in ethanol or acetone solutions with hyperfine splitting and line width similar to Fig. 7.3 and 7.4. In non polar solvents no E.S R. is observed.

This result comprises one of the largest discrepancies from the optical measurements of M.W., who find D_{570}/D_{470} greater than for PPD.

(d) Cyclohexylamine (CXA) - TNB

The E.S.R. line observed here, with ethanol as the solvent, is very weak, and has similar total line width to the donors (a), (b) and (c) of this section. The very low signal to noise ratio makes it difficult to be certain if this line also is split into three hyperfine components, although this appears likely.

(e) Pyridene - TNB

For this complex in acetone as solvent a very weak E.S.R. line is observed of line width about 25 gauss and without resolved hyperfine structure. The difference from the DEA- TNB complex which has a similar

value of D_{570}/D_{470} is very marked and, as noted in § 7.4, the reaction rate differs. In preparing this complex, the colour turns a light red in a similar manner to Group II complexes rather than turning dark red and then fading to a lighter colour, as do the previous donors of this group. From qualitative observations the extinction coefficient appears similar to group II complexes, rather than those of Group I.

(f) NaOH - TNB

When a solution of TNB in acetone is mixed with an aqueous solution of NaOH, a reddish colour results, and a very weak E.S.R. signal appears, which fades in about an hour.

A considerably stronger E.S.R. signal is obtained using ethanol as solvent. In this case, the solution turns red and, after about half an hour, a yellowish-red non paramagnetic precipitate forms. The E.S.R. spectrum (Fig. 7.5) differs from Fig. 7.3. The arrow in Fig. 7.5 indicates the "marker" due to the quartz sample holder (§ 8.2).

(g) Acetone - TNB

According to M.W., a solution of TNB in acetone develops an absorption band at 570 mμ, and D_{570}/D_{470} rises to 0.5 in eight weeks. The extinction coefficient is not given, but this must be very low. No E.S.R. is observed in this case.

§ 7.6 Possible equivalence of TNB - DEA with other TNB complexes

Before proceeding to a discussion on the probable nature of the radicals involved in complexes of TNB with Group I donors, it is of

interest to consider whether these complexes are similar to some paramagnetic TNB complexes with different types of donor.

It will be shown in § 7.10 that the spectra of Fig. 7.3 and 7.4 may be attributed to three lines of equal intensity and with hyperfine splittings of about 8.5 gauss. This splitting seems likely to be due to a single N^{14} nucleus (I = 1).

A similar three line structure has been observed for photo-induced radicals, resulting from a complex of TNB with tetrahydrofuran (THF) [L4]. A further splitting by three equivalent protons and two equivalent N^{14} nuclei [W9] has also been noted. However, the magnitude of the primary splitting (13.0 gauss) is too large to allow the possibility that the same radical is involved.

Ward [W8] has found, for complexes of TNB with alkali metals, that again the largest hyperfine splitting parameter (7.0 gauss) is due to a single N^{14} nucleus. A splitting of 4.1 gauss, due to three equivalent protons, is also observed. The question arises, whether the similar N^{14} splitting for the Group I complexes means that, as suggested by Wynne-Jones [W10], these radicals are equivalent apart from line widths. A reconstruction of the E.S.R. spectrum of Wards Na-TNB complex is shown in Fig. 7.8. If the line width were about 2 gauss, an eight line spectrum would probably result [C4], and only lines (3), (6), (7) and (10) would be unresolved. If the line width were increased to about 4 gauss and the small outer lines (1) and (12) were neglected, it would appear likely that a four line spectrum would result, with an approximate inten-

sity ratio 1:2:2:1. In this case lines (2) and (4) etc., would be resolved, while (4) and (5) would not. A further increase in line width does not predict a system of three equal lines, and this excludes the possibility of equivalence of this radical with Group I - TNB complexes.

The TNB anion has been generated electrochemically [G10], and in this case the three N^{14} nuclei are equivalent, with a hyperfine splitting of about 2.2 gauss. The Group I complexes with TNB therefore cannot involve $[TNB]^{\cdot\cdot}$.

§ 7.7 Discussion of the form of Group I complexes

The suggestion has been made by M.W. that the following scheme is involved in the formation of Group I complexes,

$$A + D \rightleftharpoons \underset{(\text{outer})}{AD} \rightleftharpoons \underset{(\text{inner})}{A^-D^+} \underset{\text{solvent}}{\overset{\text{polar}}{\rightleftharpoons}} A^-_{\text{solv.}} + D^+_{\text{solv.}} \qquad (7.7.1)$$

The first reaction, which occurs also with Group II donors, is explained as forming the outer complex of Mullikan [M10], and the rate of the second reaction is determined by the height of the potential barrier in the formation of the inner complex. The observed radical would be explained by $A^{\cdot\cdot}$ in the final stage, or the ion pair of the inner complex in non polar solvents. This situation is represented by I of Fig. 7.9.

However, it was noted in § 7.6 that $[TNB]^{\cdot\cdot}$ contains three equivalent nitrogen atoms, and therefore structure I cannot explain the three line spectra of Figs. 7.3 and 7.4.

The reaction of (7.7.1) does not, it seems, proceed to the final

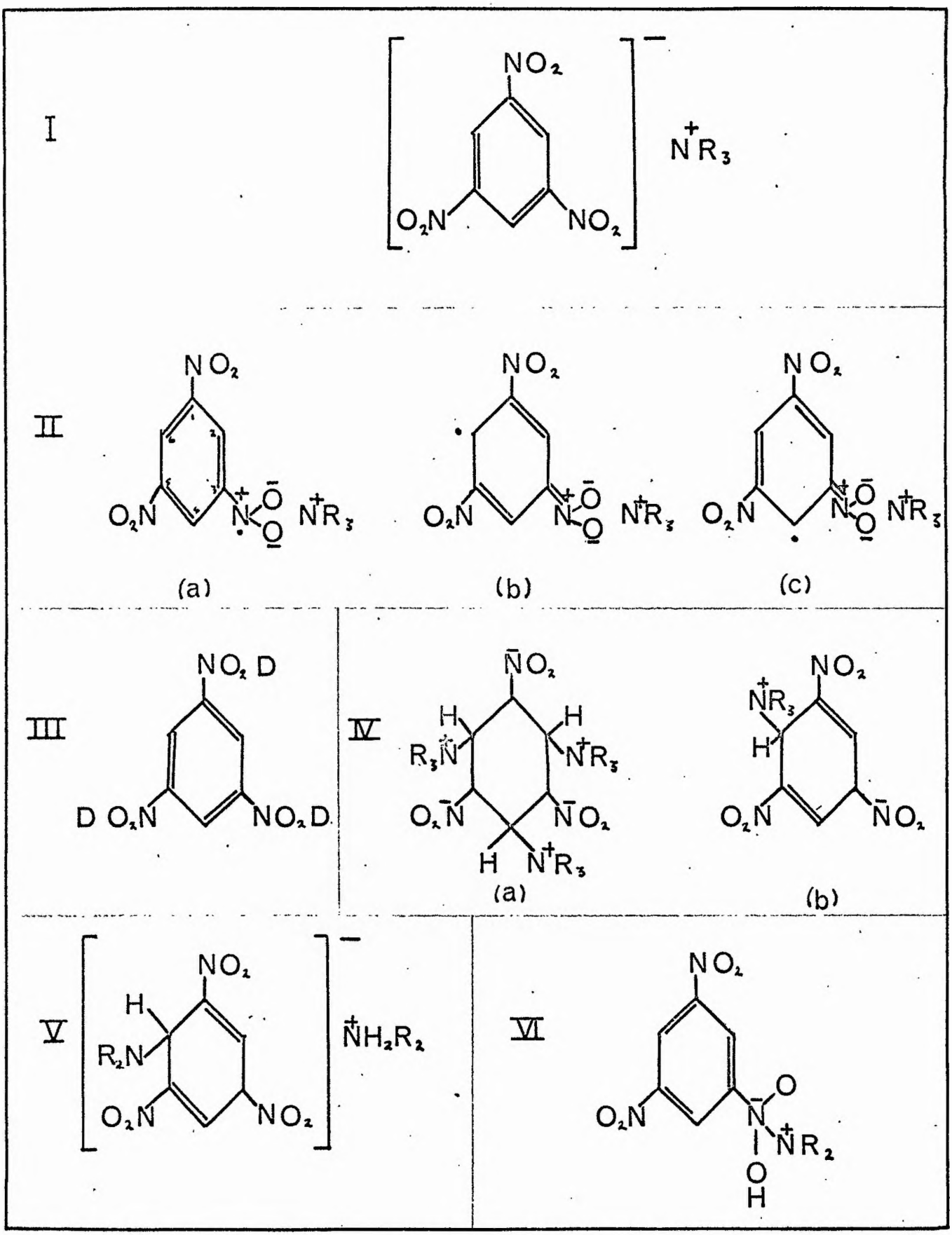

FIG 7·9 Possible forms of the TNB–Group I Complexes.

stage, and furthermore, the configuration of the inner complex must be consistent with the higher unpaired spin density at one nitrogen atom than at the other two.

The radical involved has been shown in § 7.7 to differ from the Na-TNB complex, which may be attributed to resonance among the structures (a), (b) and (c) of Fig. 7.9II in a manner similar to that described for the Nitrobenzene-Na complex [G8].

The optically induced radicals of TNB with THF have been attributed [L4] to a radical involving three separate spin systems of the form III (Fig. 7.9). Ward [W9] considers that, for this radical also, the form II is more likely than III.

It appears quite probable, therefore, that the TNB complexes with group I donors also, involve a similar resonance among the structures of II but the differences in the E.S.R. spectra in the three cases arise from differences in the proportions λ_a, λ_b and λ_c in which the eigenfunctions ϕ_a, ϕ_b and ϕ_c are present.

The ground state wavefunction for II, ψ_N, may be written

$$\psi_N = \lambda_a\phi_a + \lambda_b\phi_b + \lambda_c\phi_c \qquad (7.7.2)$$

Then, in order that the three ring protons are equivalent, as is the case for both Na-TNB and optically-induced radicals,

$$2\lambda_b = \lambda_c \qquad (7.7.3)$$

since there are two ortho positions and only one para position.

The value of λ_b is equal to the spin density on the ring carbon

atom at position 6, which from McConnel's relation (2.5.8), with Q = -28.0 gauss, and a^h as the experimental proton splitting, is in the two cases

$$\begin{aligned} \lambda_b \text{ (Na)} &= 0.146 \\ \lambda_b \text{ (opt)} &= 0.111 \end{aligned} \qquad (7.7.4)$$

As TNB is an odd alternant molecule, negative unpaired spin densities are predicted at the ring carbons 1 and 5, arising from cross terms in the eigenfunctions ϕ_b and ϕ_c. However, as the experimental splittings by the nitrogen nuclei of the nitro groups in these positions in the optically induced radicals is only 0.23 gauss [W9], this spin density will be neglected. Therefore, from (7.7.3)

$$\lambda_a = 1 - 3\lambda_b$$

and so from (7.7.4)

$$\begin{aligned} \lambda_a \text{ (Na)} &= 0.562 \\ \lambda_a \text{ (opt)} &= 0.667 \end{aligned}$$

and the ratio of these values of λ_a is 0.84. The corresponding ratio of N^{14} splittings a^n (Na): a^n (opt) is 0.54, and the difference between these ratios implies that the change in a^n involves a redistribution of spin density within the nitro group, as well as a change in the total nitro group spin density (λ_a).

λ_a is equal to the sum of unpaired spin densities on the nitrogen atom (ρ_n^π), on the two nitro group oxygen atoms (ρ_o^π) and on the ring carbon atom to which the nitro group is attached (ρ_o^π) although, as ,

with sites 1 and 5, the value of ρ_c^π will probably be negligible at this site [R2]. Therefore

$$\lambda_a \doteq \rho_n^\pi + 2\rho_o^\pi \qquad (7.7.5)$$

The probable numerical values are substituted into (2.5.13) [R2], which becomes (in gauss)

$$a^n = (99 \pm 10)\rho_n^\pi - (71 \pm 11)\rho_o^\pi \qquad (7.7.6)$$

Solving equations (7.7.5) and (7.7.6) in the case of the Na-TNB radicals gives

$$\rho_n^\pi = 0.20 \pm .04, \quad \rho_o^\pi = 0.18 \pm .03$$

and for optically-induced radicals

$$\rho_n^\pi = 0.31 \pm .04, \quad \rho_o^\pi = 0.18 \pm .03 .$$

Thus it appears that the value of ρ_o^π remains constant for these two radicals while the variations in a^n are caused by changes in ρ_n^π.

It is interesting to speculate whether, in the case of the TNB - Group I radicals, ρ_o^π still remains 0.18 ± 0.03, assuming that these radicals also are explained by the structures of Fig. 7.9 II. Substituting this value together with $a^n = 8.5 \pm 0.5$ gauss in (7.7.5), (7.7.6) and (2.5.8), a predicted ring proton splitting of 3.9 ± 0.8 gauss is obtained, assuming that, as in the other two types of TNB radicals, the protons are equivalent.

If the system of hyperfine lines which results from these values of a^n and a^h is considered for large line widths as in § 7.6, a spec-

trum consisting of three equal lines similar to Fig. 7.3 appears to be predicted for 3.1 gauss $< a^h <$ 4.0 gauss. Thus, although there is no evidence that for this type of radical ρ_o^π again has the same value, the results of this conjucture predict a spectrum which is consistent with experiment.

Several other configurations are possible for the Group I - TNB radicals. It has been suggested that 4:1 [F10], 3:1 [F11], 2:1 [A4] and 1:1 [M2] complexes are formed. Foster [F11] proposed that different complexes are involved for "small" amine molecules (IVa), including DEA, and for "bulky" amines (IVb), which presumably would include piperidene. However, the similarity of the E.S.R. spectra of these two complexes suggests that they have the same form, which could not be IVa owing to the non-equivalence of nitro groups.

A structure similar to IVb which involves a 2:1 complex (V) is considered by Briegleb to be most likely [B13]. However, in this the amine is of the form NHR_2 which resembles DEA, but differs from PPD (Fig. 7.6). The only other form mentioned by Briegleb, which could be consistent with the E.S.R. spectrum, is VI which was one of the earliest structures proposed [B14]. This suffers from the same criticism as V that the amine must be of the form NHR_2. If the transfer of the proton does not take place, this structure becomes that of II (a).

Of all the possible forms considered either II or IVb appears to offer the most likely structure for these Group I complexes.

§ 7.8 Mechanisms of Line Broadening

In both Na-TNB and optically induced TNB radicals, hyperfine splittings by ring protons have been observed, and these are expected for Group I - TNB radicals also (§ 7.7). The more likely mechanisms of line broadening were therefore investigated.

On reducing the Signal Klystron power at the cavity to < 1 mW, no improvement in resolution is observed, implying that power saturation of the line does not inhibit resolution.

Lagercrantz and Yhland [L4] and also Ward [W8], [W9] have found improved resolution for the other TNB radicals, following the removal of dissolved oxygen.

The following degassing procedures were tried.

(a) The pressure over the sample was reduced, using a water pump, several times, between which the vessel was rinsed out with nitrogen. The sample was sealed in a nitrogen atmosphere.

(b) The sample was frozen and evacuated to about 1 mm mercury for about an hour, during which the vessel was rinsed out several times with nitrogen, and the sample was again sealed in a nitrogen atmosphere.

Neither (a) nor (b) improved the resolution, from which it may be concluded that the lines are not significantly broadened by the presence of dissolved oxygen.

The presence of free TNB in solution could cause line broadening by a process similar to the electron exchange reaction of § 2.3 (k) and

no other mechanism of § 2.3 or 2.4 appears to predict a line width of the magnitude which is found. Nothing, however, has been done to check this hypothesis.

§ 7.9 Effect of solvent on a^n

The N^{14} splitting of nitro groups involves two terms of opposite sign and comparable magnitude [R2], which are proportional to the spin densities on the N and O atoms respectively. It follows that a small change in distribution of spin density in the nitro group, owing to an alteration in the configuration of solvent molecules in the vicinity, may cause an appreciable change in a^n. This has been noted for alkali metal complexes with nitrobenzene and dinitrobenzenes [G9].

For the DEA - TNB complex the value of a^n for acetone solutions appears to be slightly but consistently lower than for ethanol solutions although no large variations have been observed for solutions of higher dielectric constant (acetonitrile and dimethoxyethane). Thus the solvent appears to have only a slight effect on a^n.

§ 7.10 Simulation of Fig. 7.3

The spectrum of Fig. 7.3 is simulated by adding the derivatives of three Gaussian lines of equal amplitude and adjusting the ratio of hyperfine splitting to line width until the resulting curve resembles Fig. 7.3 as closely as possible.

The Gaussian line shape function, g(H) is given by,

$$g(H) = \exp[-(\Delta H)^2/2\sigma^2] \qquad (7.10.1)$$

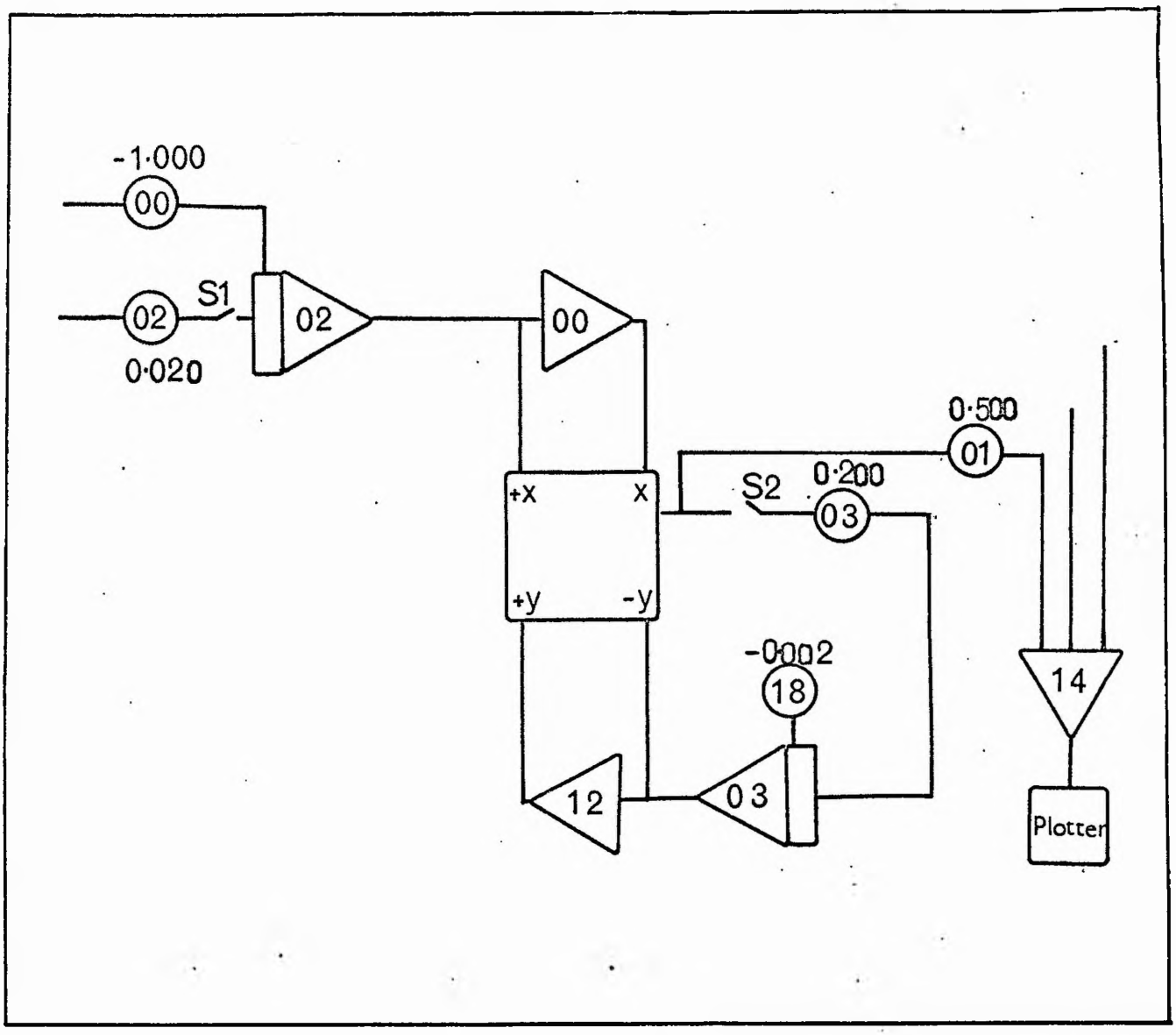

FIG 7·10 Flow Diagram

where ΔH is the difference in magnetic field from the resonance value and σ is the line width measured from peak to peak of the derivative, $g'(H)$. (7.10.1) may be expressed in differential form,

$$g'(H) = -1/\sigma^2 \, (\Delta H) \, g(H) \qquad (7.10.2)$$

which was solved using an E.A.I. PACE TR48 analogue computer. The flow diagram for (7.10.2) is shown in Fig. 7.10. The second and third lines are initiated by means of comparitors and the three are added by means of summing amplifier 14.

The constituent lines, and their sum which approximates to Figs. 7.3 and 7.4, are shown in Figs. 7.11(a) and (b) respectively.

The estimation of the position of the individual lines in a spectrum whose resolution is not complete, such as Fig. 7.3, tends to be inaccurate, and comparison with Fig. 7.11 facilitates this estimation. Also, the line widths of the partly resolved lines of which the spectrum is composed, may be calculated by this method. The hyperfine splittings and line widths of § 7.5 have, in fact, been obtained using Fig. 7.11. As the actual line shape is probably complicated by the presence of unresolved structure, the approximation of assuming a Gaussian line shape is unlikely to be a good one. Line widths calculated by this method, therefore, are likely to be overestimated.

The appearance of straight line sections in Fig. 7.11, particularly around the peaks, is due to the switching characteristics of the

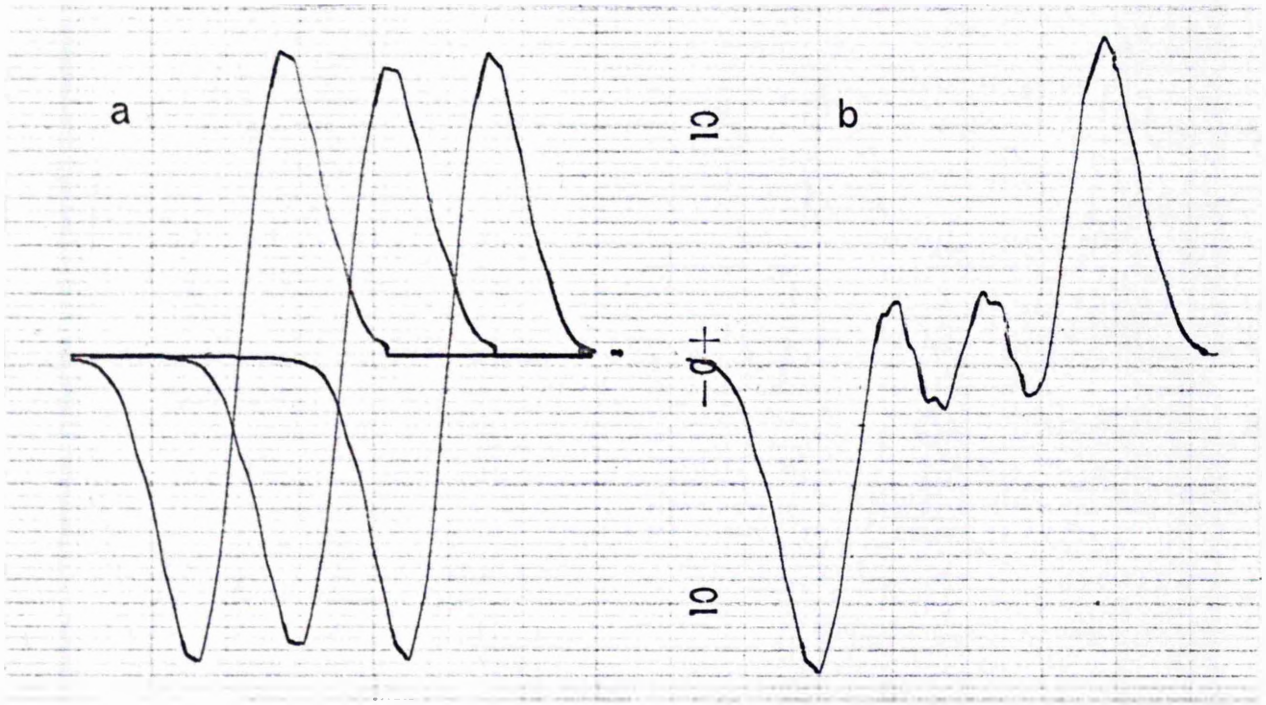

FIG 7·11 Simulation of Fig 7·3

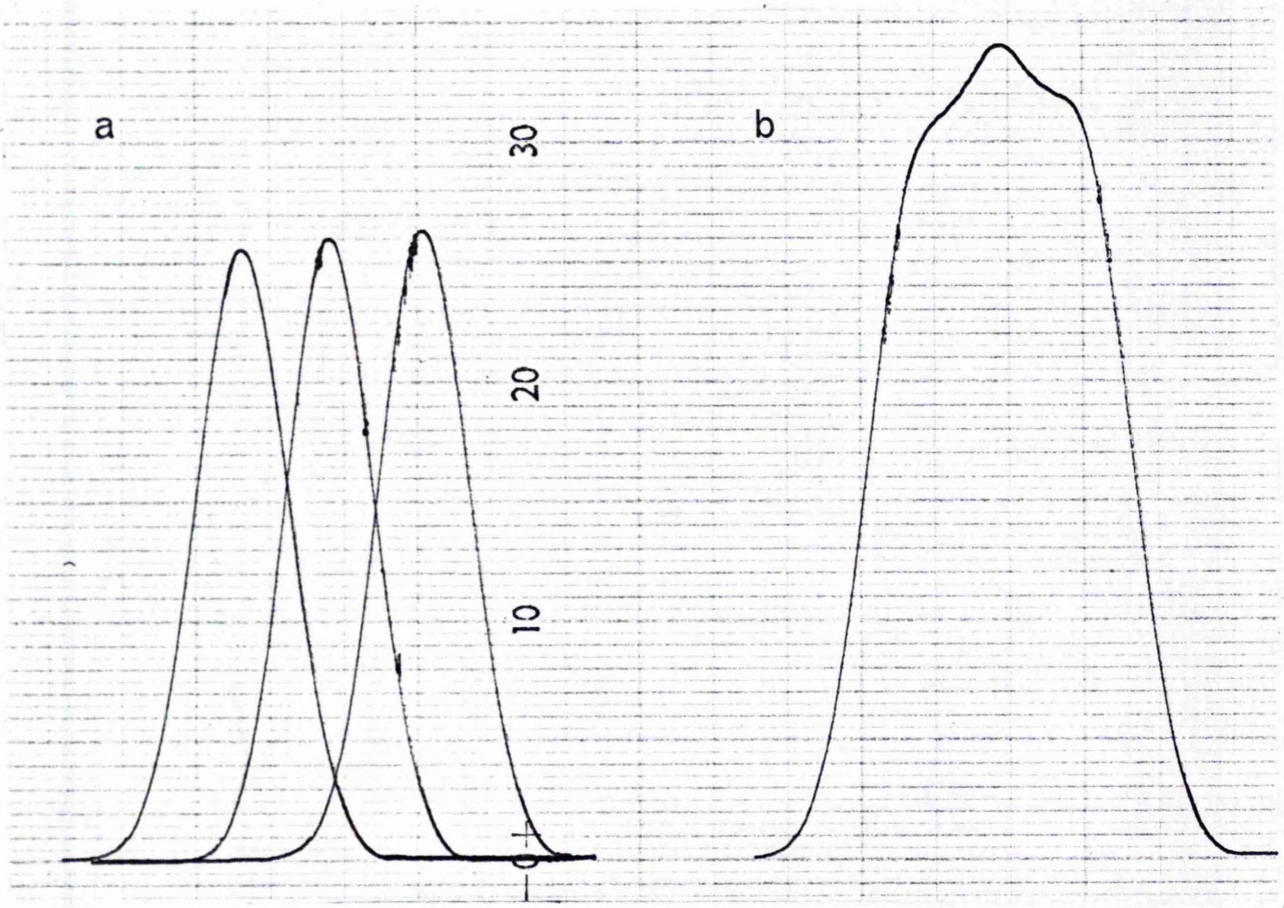

FIG 7·12 Integrals of Fig 7·11

diodes in the quarter square multipliers. This also causes the apparent further structure in Fig. 7.11(b).

The slight differences in amplitude of the curves are due to the fact that the setting of potentiometer 03 is rather critical. It was also found necessary to impose a small positive bias to integrator 03 in order that the solution should start in the correct direction.

Figs. 7.12(a) and (b) represent the integrals of Figs. 7.11(a) and (b) respectively. The undifferentiated line is obtained at the output of integrator 03 of Fig. 7.10. A comparison of Figs. 7.11(a) and 7.12(a) shows the improvement in resolution obtained by recording the derivatives of E.S.R. spectra.

§ 7.11 Nature of NaOH-TNB complex

The only member of the Group I donors to give rise to a paramagnetic complex with TNB, apart from those which exhibit a second optical absorption band, is NaOH (§ 7.5 (f)). Although the spectrum (Fig. 7.5) is not well resolved, it appears that the free radical involved differs from those of Figs. 7.3 and 7.4.

Fig. 7.5 could result from the same spectrum as TNB-Na where the line width is still greater than that considered in § 7.6 and the only larger lines resolved are (2) and (4) and also (9) and (11).

The reason for the asymmetry of this line is not obvious.

§ 7.12 Complex of PPD with TCNE

In order to determine the behaviour of Group I donors with acceptors

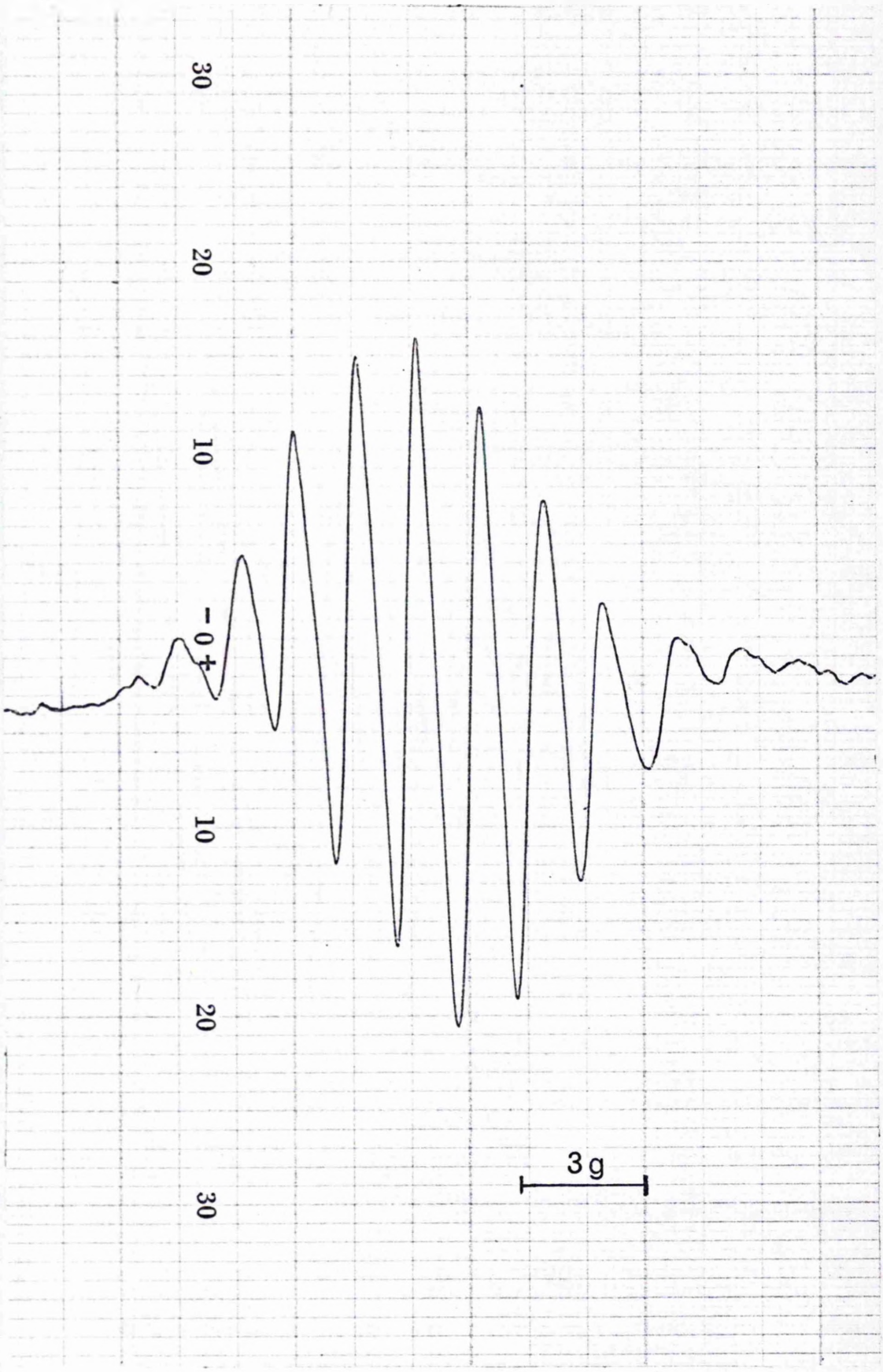

FIG 7·13 PPD-TCNE

which have a higher electron affinity than TNB, a complex was formed between PPD and TCNE which has an electron affinity of 2.8 $\pm$ 0.1eV compared to the value of 1.8 $\pm$ 0.1 for TNB [B9].

TCNE dissolves in PPD to give a reddish solution and a strong E.S.R. line is observed. On dilution the nine line spectrum of Fig. 7.13 is obtained of which the intensity ratio is in good agreement with the ratio for the $[TCNE]^-$ ion predicted by equal splittings by four equivalent nitrogen nuclei.

Theoretical	1: 4 : 10 : 16 :19: 16 : 10: 4 : 1
Estimated from Fig. 7.13	1.6:4.9:11.8:16.4:19:16.4:8.8:4.7:1.3

The observed splitting of 1.6 $\pm$ 0.2 gauss is also in agreement with that of a complex of Na-TCNE [B6], [P7].

The fact that even in a non ionising solvent (PPD), the $[TCNE]^-$ ion is observed, implies the formation of an ion pair involving the transfer of an electron from PPD to TCNE.

§ 7.13 Conclusion

There appears to be a certain degree of correlation between the appearance of the 570 mμ absorption band and of E.S.R. With the exception of TNB - PPD with PPD as solvent (and this could have contained traces of water), no donor for which $D_{570}/D_{470} = 0$ exhibits an E.S.R. spectrum of the form of Fig. 7.3.

On the other hand for pyridene and also for acetone, neither of which is an amine, the value of D_{570}/D_{470} eventually reached about 0.5,

although for acetone this took eight weeks, and E.S.R. of the form of Fig. 7.3 was not observed in either case. The extinction coefficients for these complexes appear to be lower than for amines as donors, and the E.S.R. behaviour may depend upon an absorption band at 570 mμ and a high extinction coefficient.

The only other serious discrepancy is the TEA complex which has a considerably lower radical content than expected.

The lack of resolution is probably due to the rather low radical content which leaves a high concentration of TNB in non radical form. Improvement of this resolution and a knowledge of the ring proton splittings should make it easier to decide which, if any, of the proposed structures of § 7.7 explains the form of these complexes of trinitrobenzene with Group I donors.

FIG 8·1

DMPD ; Chloranil.

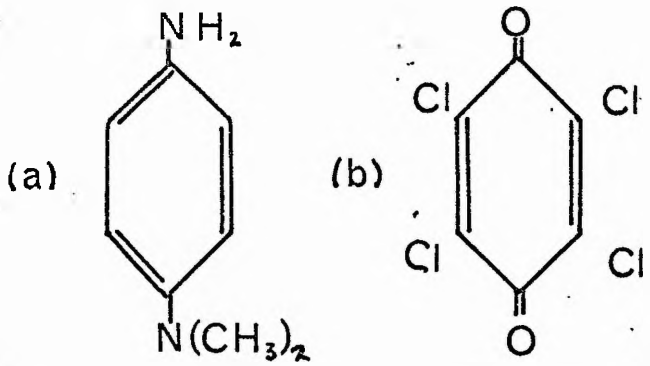

FIG 8·2

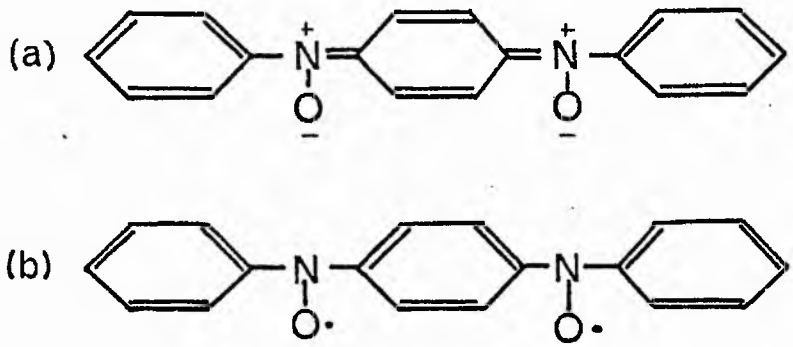

FIG 8·3

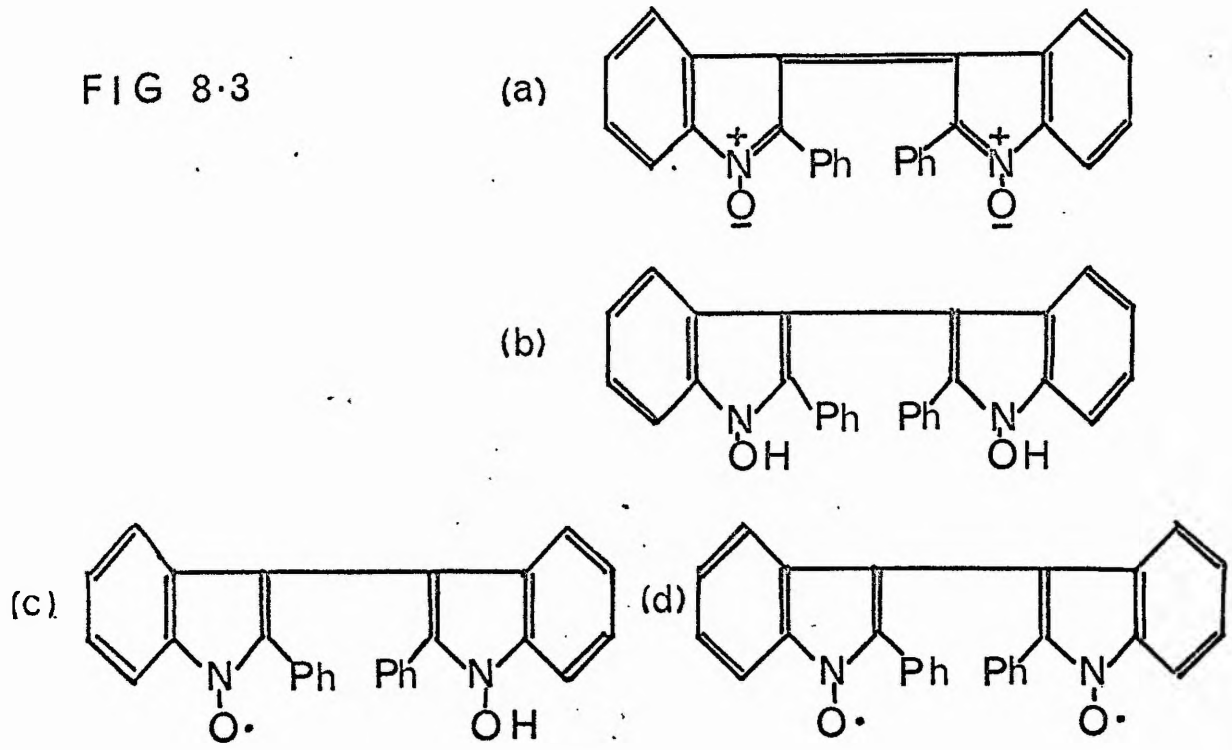

CHAPTER 8

ADDITIONAL E.S.R. EXPERIMENTS

§ 8.1 Complex of Dimethyl p-phenylenediamine (DMPD) and chloranil

Brown has described the E.S.R. spectra of complexes of tetramethyl p-phenylenediamine (TMPD) with chloranil, bromanil and iodanil in which he has observed some hyperfine structure [B6].

The complex of chloranil with DMPD (Fig. 8.1(a) and (b) respectively) in acetonitrile solution, is paramagnetic but unfortunately, at the time of this experiment, the spectrometer stabilisation system was not functioning well. Neither the video display of the E.S.R. line, nor the rather poor pen recordings which were obtained, show any hyperfine structure. The line width (about 25 gauss) is comparable to that of Brown's TMPD complexes.

Foster [F7] has noted that the optical absorption spectrum of this complex depends upon which constituent is in excess, but no such difference has been observed in the E.S.R. spectrum.

DMPD is evidently very unstable as, despite being kept under vacuum and in the dark, the sample had deteriorated by the time that higher sensitivity was available. The products of this decomposition are, in fact, paramagnetic, but the solution in benzene shows no hyperfine structure.

§ 8.2 Radicals produced by U.V. irradiation

It was intended to examine the E.S.R. properties of U.V. irradiated

polymethylmethacrylate and other related polymers for Dr. J. R. McCallum. The medium pressure U.V. lamp, however, does not give a large output at a wavelength of 2537A° or below, which appears to be necessary for the creation of radicals in these polymers.

Although the irradiation of the polymers led to no conclusive results, a fairly weak E.S.R. line of line width about 2.5 gauss has been observed, associated with the quartz sample tube. Cleaning the tube with chromic acid does not reduce the intensity of this line. The removal of a layer of quartz from the inner and outer surfaces of the tube by means of hydrofluoric acid, also has no effect. The E.S.R. line is therefore due to some trapped radicals within the quartz.

This sample tube has been found useful in estimating the change in radical content during a reaction (§ 7.5 (a)). No explanation is offered for the cause of this E.S.R. line which does not occur prior to irradiation.

§§ 8.3 Nitroxide Radicals

Two samples, Fig. 8.2(a) and the reduction product of Fig. 8.3(a) were obtained from Dr. A. Forrester of Aberdeen.

The nitroxide Fig. 8.2(a) is found to be non paramagnetic in the solid state and also in the following ionising solvents: acetonitrile, dimethylformamide, dimethylsulphoxide, water. Therefore, less than 10^{-3} % of this nitroxide occurs in the biradical form of Fig. 8.2(b).

A sample of the reduction product of Fig. 8.3(a), which was

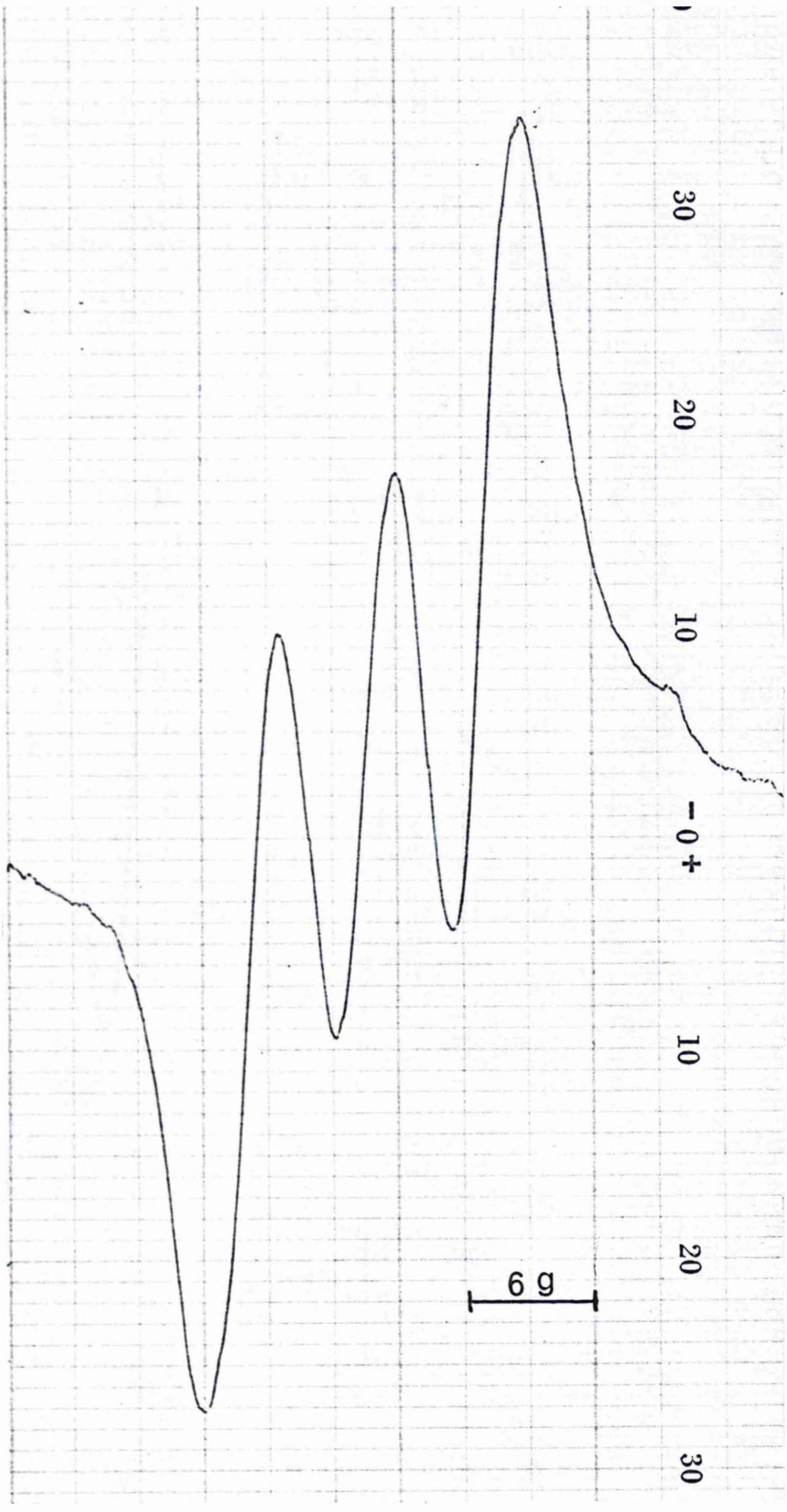

FIG 8·4 ESR Spectrum of Fig 8·3 .

assumed to have the form shown in Fig. 8.3(b) [F9], is in fact found to be strongly paramagnetic, and, in polycrystalline form, has a line width of about 11 gauss. In polar and non polar solvents, the spectrum has the form of Fig. 8.4. The radical may be explained by the partial oxidation to Fig. 8.3(c) which would lead to a three line spectrum by the interaction of the unpaired electron with the N^{14} nucleus (I = 1). As the radical content is at least 50%, this oxidation must occur to quite a large extent. It is also possible that oxidation to the biradical Fig. 8.3(d) occurs.

The spectrum of Fig. 8.4 is unchanged when the solution is diluted to a concentration of 5×10^{-5} M and no proton splittings are resolved. The removal of dissolved oxygen, however, has not been attempted.

CHAPTER 9

CONCLUSIONS AND RECOMMENDATIONS FOR THE FUTURE

The interpretation of the phenothiazine spectrum has been fairly conclusively confirmed by the spectrum simulation of § 4.9. The hyperfine splitting parameters agree reasonably well with the values calculated from Molecular Orbital theory. Agreement has also been obtained between calculated and observed unpaired electron densities for some phenothiazine derivatives.

However, the line width estimation of § 4.10 is not very accurate, and this could be improved by making a slight modification to the spectrometer, which would allow the recording of the second derivative of the E.S.R. absorption. A measurement of the line widths at the low magnetic field end of the spectrum for a range of temperatures between 17°C and 36°C, would allow the checking of the hypothesis of § 4.12.

If the room temperature E.S.R. spectrum of chlorpromazine in concentrated sulphuric acid were examined at Q band frequencies, the interpretation of § 5.3 (b) could be checked.

A correlation between the optical behaviour and the E.S.R. spectra of s-trinitrobenzene complexes was noted in Chapter 7, and two suggestions were put forward as to the possible structure of these complexes.

Although the spectrometer has a sensitivity of about 10^{12} spins of unit line width, this is not as good as the figure attained by some

commercial spectrometers. As was mentioned in § 3.22, an improvement might result from the use of a stabilisation system which phase locks the signal klystron to a harmonic of a quartz crystal, while still maintaining the facility of adjusting this frequency to the cavity resonant frequency [D1]. An additional improvement in signal to noise ratio would result from the use of a continuous averaging device, several of which are now available commercially [D2], and it is intended to purchase one of these in the near future.

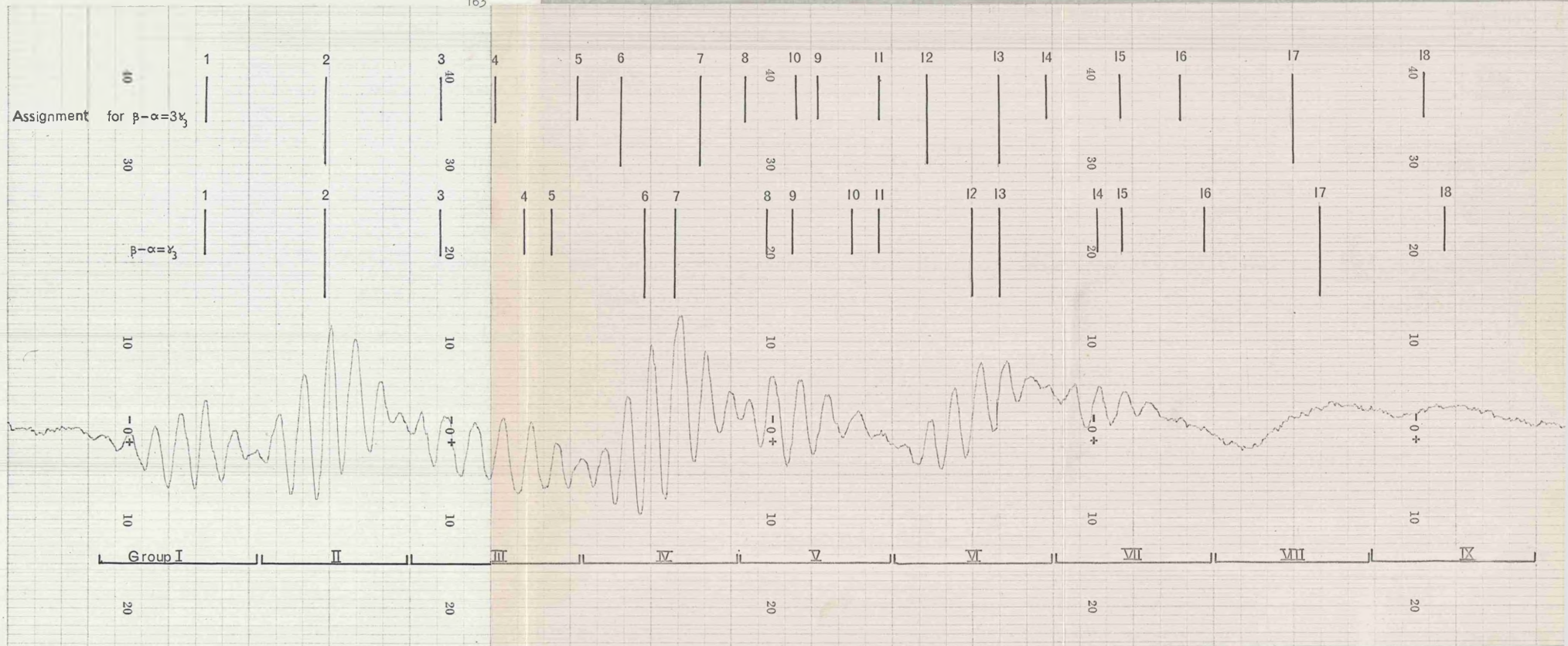

FIG 4·9 High Resolution PTZ Spectrum (17°C).

APPENDIX I

```
**      SIMULATION  OF  SPECTRUM      D. RORKE
        DIMENSIONP(270),FACP(270),SPEC(1000),SPECL(1000),A(4)
       1,PA(3),PB(2),PC(3),PD(3),PE(5),FC(3),FD(3),FE(5),NCH(270)
       2,FL(60,4),FG(60,4)
        READ1,(PA(I),PC(I),PD(I),FC(I),FD(I),I=1,3),(PB(I),I=1,2),
       1(PE(J),FE(J),J=1,5),CEN
    1  FORMAT(10F5.0)
        READ8,(A(I),I=1,4)
    8  FORMAT(4F5.2)
        IF(NT-1)11,11,10
   10   PE(5)=0.0
   15   FE(1)=0.0
        FE(2)=1.0
        FE(3)=2.0
        FE(4)=1.0
        FE(5)=0.0
   11   CONTINUE
        DO4M=1,4
        B=A(M)
        DO4J=1,60
        JY=J-30
        Y=JY
        FL(J,M)=-1.1*B*Y/(3.*B*B+Y*Y)**2.
    4   FG(J,M)=-Y*EXPF(-Y*Y*0.5/(B*B))/(B*B)
        PRINT7,A,PA(3),PB(2),PC(3),PD(3),PE(5)
    7   FORMAT(29H1 LINEWIDTH  PARAMETERS  ARE ,4F6.2,/
       131H  INTERACTION   CONSTANTS  ARE ,5F8.0)
        DO3I=1,1000
        SPECL(I)=0.0
    3   SPEC(I)=0.0
        N=0
        DO2M=1,3
        DO2L=1,2
        DO2K=1,3
        DO2J=1,3
        DO2I=1,5
        N=N+1
        NCH(N)=M+L-1
        P(N)=PA(M)+PB(L)+PC(K)+PD(J)+PE(I)+CEN
    2   FACP(N)=FC(K)*FD(J)*FE(I)
        DO6N=1,270
```

```
      NP=P(N)
      NB=NCH(N)
      DO6J=1,60
      IY=NP-30+J
      SPECL(IY)=SPECL(IY)+FL(J,NB)*FACP(N)
    6 SPEC(IY)=SPEC(IY)+FG(J,NB)*FACP(N)
      S=0.0
      SG=0.0
      DO20I=200,290
      IF(SPECL(I)-S)21,21,22
   22 S=SPECL(I)
   21 CONTINUE
      IF(SPEC(I)-SG)20,20,24
   24 SG=SPEC(I)
   20 CONTINUE
      DO25I=1,1000
      SPECL(I)=SPECL(I)*2.5/S
      SPEC(I)=SPEC(I)*2.5/SG
   25 CONTINUE
      PRINT9,SPECL
    9 FORMAT(38H  SIMULATED  LORENTZIAN  SPECTRUM  IS ,(/15F8.3))
      PRINT5,SPEC
    5 FORMAT(38H  SIMULATED  GAUSSIAN    SPECTRUM  IS ,(/15F8.3))
   26 CONTINUE
      CALL EXIT
      END
```

APPENDIX II

```
CC     PHENOTHIAZINE MOLECULAR ORBITAL CALCULATION D RORKE
       DIMENSIONA(24,24),U(24,24),AM(24,24),B(24)
      1,FJ(24)
       READ1,N,LIMIT,NMAX
     1 FORMAT(I2,I2,I5)
       Q=.1**LIMIT
       READ2,((AM(I,J),I=1,N),J=1,N)
     2 FORMAT(14F3.1)
       READ62,(FJ(I),I=1,N)
    62 FORMAT(10F6.3)
       DO41I=1,N
       DO41J=1,N
       IF(AM(I,J)-AM(J,I))16,41,16
    16 TYPE18,I,J
    18 FORMAT(22H  MATRIX NOT SYMMETRIC/15H CHECK ELEMENT
      1 I2,2X,I2)
       GOTO19
    41 CONTINUE
    24 NH=N
    50 DO15I=1,NH
       DO17J=1,NH
       A(I,J)=AM(I,J)
    17 U(I,J)=0.
    15 U(I,I)=1.
       NT=0
     6 AMAX=0.
       DO5K=2,NH
       M=K-1
       DO5L=1,M
       IF(ABSF(A(K,L))-AMAX)5,4,3
     3 AMAX=ABSF(A(K,L))
     4 I=K
       J=L
     5 CONTINUE
       IF(NT-NMAX)20,7,7
    20 IF(AMAX-Q)7,7,23
    23 D=(A(I,I)-A(J,J))/(2.*A(I,J))
       E=SQRTF(D*D+1.)
       IF(D)22,22,21
    21 E=-E
```

```
22 E=1./(E-D)
   X=1./SQRTF(E*E+1.)
   Y=E*X
   ALPHA=2.*A(I,J)*Y*(D*Y+X)
   A(I,I)=A(I,I)-ALPHA
   A(J,J)=A(J,J)+ALPHA
   A(I,J)=0.
   A(J,I)=0.
   DO8K=1,NH
   IF(K-I)9,10,9
 9 IF(K-J)11,10,11
11 V=X*A(K,I)-Y*A(K,J)
   A(K,J)=Y*A(K,I)+X*A(K,J)
   A(K,I)=V
   A(I,K)=A(K,I)
   A(J,K)=A(K,J)
10 V=X*U(K,I)-Y*U(K,J)
   U(K,J)=Y*U(K,I)+X*U(K,J)
 8 U(K,I)=V
   NT=NT+1
   GOTO6
 7 DO12J=1,NH
   B(J)=A(J,J)
12 PRINT13,A(J,J),(U(I,J),I=1,NH)
13 FORMAT(14H  EIGENVALUE =F12.6,19H WITH EIGENFUNCTION
  1 /(10F11.6))
   PRINT14,NT,AMAX
14 FORMAT(8H AT THE I5,39H TH ROUND, THE LARGEST NON-DIAGONAL
  1/14H   ELEMENT IS E10.4)
43 CONTINUE
19 STOP
   END
```

REFERENCES

A1 Abragam A. and Pryce M. H. L.: Proc. Roy. Soc., 205, 135 (1951)
A2 Anderson P. W. and Weiss P. R.: Rev. Mod. Phys., 25, 269 (1953)
A3 Al'tshuler S. A. and Kosyrev B. M.: Electron Paramagnetic Resonance, (Acad. Press 1964)
A4 Allen C. R., Brook A. J. and Caldin E. F.: J. Chem. Soc., 1961, 2171
A5 Atherton N. M. and Whiffin D. H.: Mol. Phys., 3, 1, 103 (1960)

B1 Bleaney B. and Stevens K. W. H.: Rep. Prog. Phys., 16, 108 (1953)
B2 Bowers K. D. and Owen J.: Ibid 18, 304 (1955)
B3 Bloembergen N., Purcell E. M. and Pound R. V.: Phys. Rev., 73, 679 (1948)
B4 Bleaney B. and Penrose R. P.: Proc. Phys. Soc., 60, 83 (1948)
B5 Bijl D.: Thesis, Leiden 1950
B6 Brown I. M.: Thesis, St. Andrews 1961
B7 Bloembergen N., Purcell E. M. and Pound R. V.: Phys. Rev., 73, 679 (1948)
B8 Barton B. L. Fraenkel G. K.: J. Chem. Phys., 41, 1445 (1964)
B9 Bateley M. and Lyons L. E.: Nature 196, 573 (1962)
B10 Briegleb G.:Angew. Chem. (Int. Ed.) 3, 617 (1964)
B11 Billon J. P.: Ann. de Chimie 183, 1962
B12 Billon J. P.: Comptes Rendus 253, 1593 (1961)
B13 Briegleb G.: Electronen Donator Acceptor Komplexe (Springer Verlag 1961)
B14 Bijl D., Kainer H. and Rose-Innes A. C.: J. Chem. Phys., 30, 765 (1959)
B15 Brewin A. and Turner E. E.: J. Chem. Soc., 1928, 332

C1 Croisignani E. et al: Inst. Lombardo A95, 535 (1961)
C2 Croisignani E. et al: Bull. Colloq. Ampere 1961, 153
C3 Carrington A. and Dos Santos-Veiga J.: Mol. Phys., 5, 285 (1962)
C4 Chu T. L. et al: J. Phys. Chem., 57, 504 (1953)

D1 D.S.I.R. Panel on E.S.R., report 1962
D2 Digital Memory Oscilloscope, (Northern Scientific) and Computer of Average Transients, (Technical Measurements Corp.)

F1 Freed J. H., Rieger P. H. and Fraenkel G. K.: J. Chem. Phy., 37, 1881 (1962)
F2 Freed J. H. and Fraenkel G. K.: Ibid, 39, 326 (1963)
F3 Fermi E.: Zeit. Phy., 60, 320 (1930)
F4 Feher G.: Bell Syst. Tech. J., 36, 449 (1957)

F5 Firth I. M.: J. Sc. Instr., 39, 131 (1962)
F6 Fraenkel G. K. and Venkaterman B.: J. Chem. Phys., 24, 737 (1956)
F7 Foster R.: Private Communication
F8 Fava A., Sogo P. B. and Calvin M.: J.A.C.S., 79, 1078 (1957)
F9 Forrester A.: Private Communication
F10 Foster R., Hammick D. L. and Wardley A. A.: J. Chem. Soc., 1953, 3818
F11 Foster R.: Ibid, 1959, 3508

G1 Gordon J. P.: Rev. Sc. Instr., 32, 661 (1961)
G2 Ginzton E. L.: Microwave Measurements (McGraw-Hill 1957) p. 232
G3 Ibid, p. 400
G4 Goldsborough J. P. and Mandel M.: Rev. Sc. Instr., 31, 1044 (1960)
G5 Glarum S. H. and Snyder L. C.: J. Chem. Phys., 36, 2989 (1962)
G6 Gagnaire D. et al: Comptes Rendus, 255, 1441 (1962)
G7 Gutmann F. and Netschey A.: J. Chem. Phys., 36, 2355 (1962)
G8 Geske D. H. and Maki A. H.: J.A.C.S., 82, 2671 (1960)
G9 Gendel J., Freed J. H. and Fraenkel G. K.: J. Chem. Phys., 37, 2832 (1962)
G10 Glarum S. H. and Marshall J. H.: Ibid, 41, 2182 (1964)

H1 Hausser K. H.: Colloq. Amp. (Pisa) 1960
H2 Hirshon J. M. and Fraenkel G. K.: Rev. Sc. Instr., 26, 34 (1955)
H3 Henning J. C. M.: Ibid, 32, 35 (1961)
H4 Heinekin F. W., Bruin M. and Bruin F.: J. Chem. Phys., 37, 1480 (1962)
H5 Hückel E.: Zeit. Physik, 70, 204 (1931)
H6 Hirshon J. M., Gardner D. M. and Fraenkel G. K.: J.A.C.S., 75, 4115 (1953)
H7 Hutchison C. A., Pastor R. C. and Kowalsky A. G.: J. Chem. Phys., 20, 534 (1952)

I1 Ingram D. J. E.: Spectroscopy at Radio and Microwave Frequencies (Butterworth, 1955)
I2 Ingram D. J. E.: Free Radicals (Butterworth 1958)

J1 Jarrett H. S.: J. Chem. Phys., 25, 1289 (1956)
J2 Jaffe H. H.: Ibid, 20, 778 (1952)

K1 Karplus M. and Fraenkel G. K.: J. Chem. Phys., 35, 1312 (1961)
K2 Kommandeur J.: Mol. Phys., 4, 509 (1961)
K3 Kopferman H.: Nuclear Moments (Acad. Press 1958)

K4 Kon H. and Blois M. S.: J. Chem. Phys., 28, 743 (1958)
K5 Kivelson D.: Ibid, 33, 1094 (1960)
K6 Kaiser E. T. and Eargle D. H.: Ibid, 39, 1353 (1963)
K7 Kreevoy M. M.: J.A.C.S., 80, 5543 (1958)
K8 Karreman G. et al: Science 130, 1191 (1959)

L1 Lyons L. E. and Mackie J. E.: Nature, 197, 589 (1963)
L2 Lanzi G. et al: Bull Colloq. Ampere 1960, 274
L3 Lamotte B. et al: Comptes Rendus, 255, 1508 (1962)
L4 Lagercrantz C. and Yhland M.: Acta Chem. Scand., 16, 1043, 1799 (1962)

M1 McConnel H.: J. Chem. Phys., 25, 709 (1956)
M2 Miller R. E. and Wynne-Jones W. F. K.: J. Chem. Soc., 1959 2375
M3 McConnel H.: J. Chem. Phys., 24, 764 (1956)
M4 McClure D. S.: Ibid, 20, 682 (1952)
M5 McLachlan A. D.: Mol. Phys. 3, 233 (1960)
M6 Microwave Engineers' Handbook 1964
M7 Melkopf A. F. and Smidt J.: Rev. Sc. Instr., 32, 1421 (1961)
M8 McLachlan A. D.: Mol. Phys., 1, 233 (1958)
M9 Mullikan R. S.: J. Phys. Chem., 56, 801 (1952)
M10 Mullikan R. S.: J.A.C.S. 74, 811 (1952)
M11 MacLean C. and van der Waals J. H.: J. Chem. Phys., 27, 827 (1957)

N1 North A. M.: Collision Theory of Chemical Reactions in Liquids, (Methuen, 1964)
N2 Narath A. and Gwinn W. D.: Rev. Sc. Instr., 33, 79 (1962)

P1 Pryce M. H. L.: Proc. Phys. Soc., 63, 25 (1950)
P2 Pound R. V.: Rev. Sc., Instr., 17, 490 (1946)
P3 Pake G. E.: Paramagnetic Resonance (Benjamin Inc. 1962)
P4 Piette L. H. and Forrest I. S.: Biochim. Biophys. Acta 57, 419 (1962)
P5 Piette L. H. et al: Free Radicals in Biological Systems (Acad. Press)
P6 Pariser R. and Parr R. G.: J. Chem. Phys. 21, 466, 767 (1953)
P7 Phillips W., Rowell J. C. and Weissman S. I.: Ibid, 33, 626 (1960)

R1 Reekie D.: Thesis, St. Andrews 1965
R2 Rieger P. H. and Fraenkel G. K.: J. Chem. Phys., 39, 609 (1963)
R3 Radiation Lab. Series (McGraw-Hill 1948) 11, 527
R4 Roberts S. and von Hippel A.: J. App. Ph., 17 610, (1946)
R5 Ramo S. and Whinnery J. R.: Fields and Waves in Modern Radio (Wiley 1944)
R6 Radiation Lab. Series (McGraw-Hill) 11, Chap. 5

R7 Ibid 15 Chap. 7
R8 Ibid 16 P.10
R9 Rogers R. N. and Pake G. E. : J. Chem. Phys., 33, 1107 (1960)

S1 Schreurs J. W. H.,Blomgren G. E. and Fraenkel G. K.:J. Chem: Phys. 32, 1861 (1960)
S2 Strauss H. L. and Fraenkel G. K.: Ibid 35, 1738 (1961)
S3 Slater J. C.: Microwave Electronics (Van Nostrand 1950)
S4 Stoodley L. G.: J. Elec. and Cont.,14, 531 (1963)
S5 Slough W.: Trans. Far. Soc., 59, 2445 (1963)
S6 Schmidt U.: Angew. Chem.(Int. Ed.) 3,602 (1964)
S7 Stone E. W. and Maki A. H.: J. Chem. Phys., 38, 1999 (1963)
S8 Snyder L. C. and Kornegay R. L.: Bull. Am. Phys. Soc.,9,101 (1964)
S9 Stone E. W. and Maki A. H.: J. Chem. Phys., 39, 1635 (1963)
S10 Streitweiser A.: Molecular Orbital Theory (Wiley)
S11 Sappenfield D. S. and Kreevoy.: Tetrahedron 19,Suppl.2,157 (1963)
S12 Shine H. J. and Piette L. H.: J. A. C. S., 84, 4798 (1962)
S13 Shine H. J. et al : J. Chem. Phys., 38, 569 (1963)

T1 Teaney D. T. et al : Rev. Sc. Instr., 32, 721 (1961)

U1 Ueda H., Kuri Z. and Shida S.: J. Chem. Phys., 36, 1676 (1962)

V1 Van Vleck J. H. and Weisskopf V. F.: Rev. Mod. Phys.,17,227 (1945)

W1 Ward R. L. and Weissman S. I.: J. A. C. S.,76, 3612 (1954)
W2 Ward R. L. and Weissman S. I.: Ibid, 79, 2086 (1957)
W3 Weissman S. I. et al : J. Chem. Phys., 21, 2227 (1953)
W4 Weissman S.I. : Ibid, 25, 890 (1956)
W5 Williamson D. T. N.: Wireless World, 55, 282 (1949)
W6 Weissman S. I. and De Boer E.: J. Chem. Phys.,26,963 (1957)
W7 Wheland G. W. and Mann D. E.: Ibid, 17, 264 (1949)
W8 Ward R. L.: J. A. C. S., 83, 1296 (1961)
W9 Ward R. L.: J. Chem. Phys., 38, 2588 (1963)
W10 Wynne-Jones W. F. K.: Nature, 186, 149 (1960)

Y1 Yariv A. and Klapp F. P.: Rev. Sc. Instr., 30, 684 (1959)

Z1 Zavoisky Y. K.: J. Phys. U.S.S.R., 9, 245 (1945)

ACKNOWLEDGEMENTS

I should like to record my sincere thanks to:-

Professor J. F. Allen, F.R.S. : for his encouragement and for allowing me the facilities of Edgecliffe Research Laboratory.

Dr. D. Bijl, F.R.S.E. : for suggesting the topic and for his helpful supervision and advice.

Dr. R. Foster, Chemistry Department, Queen's College, Dundee : for supplying many of the samples.

Professor R. B. Dingle : for the use of the PACE TR48 Analogue Computer.

The Computing Laboratory : for the use of the IBM1620 Digital Computer.

The following members of the Radiospectroscopy Group:

Dr. I. M. Firth, Messrs. I. D. Campbell, J. M. S. Hutchison, R. C. Hutchison, H. van Mal and D. Reekie : for helpful discussions.

Messrs. J. Gerrard and J. Spark : for assistance with the photography.

Mr. F. Akerboom : for his competent glassblowing.

Messrs. J. McNab and M. Bird : for fabricating some waveguide components.

Mr. H. Cairns : for the loan of some equipment.

Mrs. J. E. F. Rorke, M.A. : for translations of French and German articles and for preparing many of the diagrams.

Mrs. M. R. Cunningham : for her efficient typing.

The Department of Scientific and Industrial Research and the University of St. Andrews : for the award of maintenance grants.